

Ionic Liquids for Main Group Catalysis



By

Lucy Christabel Brown, MChem

Presented to the School of Chemistry and Chemical
Engineering

The Queen's University of Belfast

in fulfilment

of the requirements

for the degree of

Doctor of Philosophy

The Queen's University of Belfast

September 2019

ACKNOWLEDGEMENTS

Firstly, I would like to thank Dr Gosia Swadźba-Kwaśny for giving me the opportunity to pursue this research and for her constant support throughout my work. Her motivation, dedication and expertise has been a constant inspiration. I am grateful for your time, mentorship, guidance and constant encouragement.

I would also like to thank Professor John Holbrey for many insightful comments and support during my work. Also for his patience and confidence as I struggled through syntheses of deuterated materials up until the moment the taxi left for the airport. I would also like to thank Dr Leila Moura for guidance in the lab, inspiring Schlenk line designs and support in every aspect of my work as I learned to be a researcher. I hope introducing you to underwater hockey may go some way to repaying my debt. Additionally I would like to thank Dr James Hogg for his mentorship, help and creative ideas over the course of this research.

I am also grateful to Dr Nimal Gunaratne for many useful conversations on synthesis. I would like to thank Dr Karolina Matuszek for productive collaborative work from Poland and in Belfast and for providing reaction data. I would also like to thank Ruairi O'Donnell and Dr Nancy Artioli for assistance with the safe use of hydrogen.

My sincere thanks go to Deborah for her help in so many aspects of my time at QUILL, not least in planning the MSDG meeting in which she took her time to guide us through and made a success of despite simultaneously coordinating other events. Thank you also for the pens. I am grateful too to the technical staff at QUILL and QUB. In particular I would like to thank Richard Murphy for his help with NMR spectroscopy.

My time in Belfast has been a brilliant period of my life and for this I am hugely indebted to so many people including James, Mark, Leila, Emily, Keith, Nicki, Rachel, Alice, Anne, Yoan, Jeni, Gareth, Eoghain, Oli, Natasha and Marty for their friendship and support. I would also like to thank the members of QUB underwater hockey for welcoming me and giving me a life outside of the lab.

Finally I would like to thank my Mum, Dad, brother Ed, my partner Richard and the Grannies for their constant support, encouragement and patience during my research.

ABSTRACT

Lewis acidic ionic liquids, in particular chloroaluminate systems, have been found to be very effective catalysts for reactions such as Diels-Alder and Friedel-Crafts, and made their way to pilot and industrial processes, including oligomerisation of olefins (DifasolTM by IFP) and refinery alkylations (IonikylationTM by PetroChina and ISOALKYTM by Chevron).¹ Despite their popularity, this archetypal group of catalysts faces two key challenges: the use of an expensive organic cation which plays no role in the catalytic process and placing the Lewis acidic function on the chloroaluminate anion, which does not allow for further modification of catalytic activity.

The first of the two shortcomings has been addressed in the Swadźba-Kwaśny group through the development of liquid coordination complexes (LCCs),² eutectic mixtures formed of an organic donor and a metal halide. The work reported here begins with the development of LCCs containing a breadth of halometallate species, synthesised by combining AlCl₃, GaCl₃, InCl₃, SbCl₃, SnCl₄, SnCl₂, ZnCl₂ or TiCl₄ with either trioctylphosphine (P₈₈₈) or trioctylphosphine oxide (P₈₈₈O), through study of their speciation and quantification of their acidity using Gutmann acceptor numbers (Chapter 2).³

The second drawback of chloroaluminate ionic liquids (Lewis acidity placed in the chloroaluminate anion) was addressed by developing borenium ionic liquids, with Lewis superacidic borenium cation.⁴ These first generation borenium ionic liquids maintained the chlorometallate anion combined with borenium cation. This work takes the borenium ionic liquids further, delivering metal-free systems with one, well-defined acidity centre in the cations (Chapter 3). These metal-free borenium ionic liquids were subsequently combined with sterically-hindered phosphines, such as tris(*tert*-butyl)phosphine, and some had the capability for H₂ splitting, acting as the first reported ionic liquids frustrated Lewis pairs (IL-FLPs). This was achieved by the combination of a catechol ligand, adding steric bulk to the borenium cation, the introduction of long-chain ligands to lower the melting point, and the use of non-coordinating anions to prevent their involvement in the reaction.

Another strand of the FLP work explored the potential for “traditional” ionic liquids as solvents for FLP reactions (Chapter 5). A classic hydrogen activating FLP, tris(pentafluorophenyl) borane (BCF) and tris(*tert*-butyl) phosphine (P^{*t*}Bu₃), was dissolved in a non-coordinating ionic liquid [C₁₀mim][NTf₂] and the addition of H₂ showed that the FLP in ionic liquid was capable of activating H₂. Further to this, the movement of the FLP components in ionic liquid was found to be restricted in comparison to in molecular solvents. This promoted the lifetime of the reactive precursor, the encounter complex. A fundamental

study into a weakly-bound BCF/phosphine encounter complexes in both benzene and [C₁₀mim][NTf₂] by neutron scattering was carried out and this is described in Chapter 4.⁵ The results of the neutron scattering suggested an interatomic P-B distance of ~8 Å which agrees with molecular dynamics simulations in the literature.⁶ A pre-requisite for this study was the synthesis of deuterated phosphines *via* a Grignard synthesis, also described in Chapter 4.

TABLE OF CONTENTS

1	Introduction	1
1.1	Defining Acidity	1
1.1.1	Historical Perspective	1
1.1.2	Lewis Acidity	2
1.1.3	Quantification Methods	4
1.1.4	Superacidity	7
1.2	The Boron Group and Borocations	8
1.2.1	Elements of the Boron Group	8
1.2.2	Borocations	9
1.3	Lewis Acidic Ionic Liquids	17
1.3.1	Historical Context	17
1.3.2	Chlorometallate Ionic Liquids	18
1.3.3	Liquid Coordination Complexes (LCCs)	25
1.3.4	Ionic Liquids with Cationic Lewis Acids	30
1.4	Motivation for This Work	34
2	Liquid Coordination Complexes	36
2.1	Experimental	36
2.1.1	Materials and Methods	36
2.1.2	Synthesis of LCCs	36
2.1.3	Gutmann Acceptor Number Measurements	37
2.1.4	General Procedure for the Diels-Alder Reaction	38
2.2	Synthetic Plan and Approach to Study Speciation	38
2.3	Aluminium-Based Liquid Coordination Complexes	42
2.4	Gallium-Based Liquid Coordination Complexes	45
2.5	Indium-Based Liquid Coordination Complexes	47
2.6	Antimony-Based Liquid Coordination Complexes	48
2.7	Tin-Based Liquid Coordination Complexes	51
2.7.1	Tin(II)-Based Liquid Coordination Complexes	51
2.7.2	Tin(IV)-Based Liquid Coordination Complexes	53
2.8	Titanium-Based Liquid Coordination Complexes	55
2.9	Zinc-Based Liquid Coordination Complexes	58
2.10	Summary of Liquid Coordination Complex Speciation	59
2.11	Lewis Acidity Determination using a Spectroscopic Probe	61
2.11.1	Lewis Acidity of Metal Halides	62

2.11.2	Lewis Acidity of LCCs.....	65
2.12	Lewis Acidity Determination Using a Model Reaction	69
2.13	Conclusions	71
3	Borenium Ionic Liquids.....	73
3.1	Experimental	73
3.1.1	Materials and Methods	73
3.1.2	Purification of Catechol.....	74
3.1.3	Synthesis of B-chlorocatechol Borane, BcatCl	74
3.1.4	Synthesis of B-catechol Triflate, BcatOTf.....	74
3.1.5	General Procedure for the Synthesis of Boron Complexes.....	75
3.1.6	General Procedure for the Synthesis of Borenium Ionic Liquids with Chlorometallate Anions.....	75
3.1.7	General Procedure for the Synthesis of Borenium Ionic Liquids with Chloride Free Anions	75
3.1.8	Synthesis of Bistriflimidic Acid	76
3.1.9	Synthesis of [BCl ₂ (mim)][NTf ₂] from HNTf ₂	76
3.1.10	Synthesis of Silver Bistriflimide	76
3.1.11	Synthesis of [BCl ₂ (mim)][NTf ₂] from AgNTf ₂	77
3.1.12	Gutmann Acceptor Number Measurements	77
3.1.13	Differential Scanning Calorimetry Measurements.....	77
3.2	Boron Complexes	77
3.3	Ionic Liquid Synthesis.....	87
3.3.1	Chlorometallate Anions.....	87
3.3.2	Chloride-Free Anions	88
3.4	Conclusions	122
4	Frustrated Lewis Pairs in Ionic Liquids	124
4.1	Introduction to Frustrated Lewis Pairs	124
4.1.1	Concept of Frustrated Lewis Pairs and Metal-Free H ₂ Activation.....	124
4.1.2	Encounter Complexes.....	125
4.2	Experimental	129
4.2.1	General	129
4.2.2	Preparation of Bromomesitylene- d ₁₁	130
4.2.3	Preparation of Trimesitylphosphine- d ₃₃	130
4.2.4	Preparation of Tri(tert-butyl)phosphine- d ₂₇	130
4.3	Deuterated Phosphine Synthesis	131
4.3.1	Justification – Contrast for Neutron Scattering Studies	131

4.3.2	Synthesis of Deuterated Phosphines.....	132
4.4	Neutron Scattering.....	144
4.5	Conclusions	148
5	Frustrated Lewis Pairs in/as Ionic Liquids	149
5.1	Experimental	149
5.1.1	Materials and Methods	149
5.1.2	Preparations of Solutions in Benzene-d ₆	149
5.1.3	Preparations of Solutions in [C ₁₀ mim][NTf ₂].....	149
5.1.4	Hydrogenation of B(C ₆ F ₅) ₃ and P ^t Bu ₃ Dissolved in Benzene-d ₆	150
5.1.5	Hydrogenation of B(C ₆ F ₅) ₃ and P ^t Bu ₃ Dissolved in [C ₁₀ mim][NTf ₂]	150
5.1.6	Synthesis of [BCl ₂ mim][M ₂ Cl ₇]	150
5.1.7	Combination of bases with [BCl ₂ mim][M ₂ Cl ₇].....	151
5.1.8	Synthesis of [Bcat(P ₈₈₈)] [NTf ₂] with 1 eq. of P ^t Bu ₃	151
5.2	Frustrated Lewis pairs in inert ionic liquids.....	151
5.3	Hydrogenation of FLPs in inert ionic liquids.....	157
5.4	Development of Ionic Liquid FLPs.....	158
5.4.1	First Generation Borenium Ionic Liquids as FLP Components	158
5.4.2	Second Generation Borenium Ionic Liquids as FLP Components.....	162
5.5	Conclusions	170
6	Summary and Conclusions	171
7	Bibliography	173
	Appendix A	186
	Appendix B.....	188

LIST OF FIGURES

Figure 1. The reaction of boron trichloride and ammonia.	3
Figure 2. Crotonaldehyde sensor molecule developed by Childs et al.	6
Figure 3. The three classically described borocations, divided by their coordination number. R represents a monoanionic group and L is a 2-electron donor ligand.	10
Figure 4. The development of borenium cations <i>via</i> boracycles from the first recorded borenium cation (a) in 1970, ⁶⁹ the introduction of five-membered borocycle (b) in 1985, ⁷⁶ an arylated analogue (c) by Cowley <i>et al.</i> ,.....	15
Figure 5. The structure of anions a) boron tetrafluoride, b) tetrakis(pentafluorophenyl)borate, c) triflate, [OTf] ⁻ , and d) bistriflimide, [NTf ₂] ⁻	16
Figure 6. The concentration of anionic species in the system [C ₂ mim]Cl-AlCl ₃ at 200 °C, calculated from a thermodynamic model. (adapted from)	19
Figure 7. Phase diagrams of NaCl-AlCl ₃ and 1-ethyl-3-methyl imidazolium chloride-AlCl ₃	19
Figure 8. Gutmann acceptor number values recorded for ionic liquids [C ₈ mim]Cl-MCl _x (where M = Al ^{III} , Ga ^{III} , In ^{III} , Zn ^{II} and Sn ^{II}) plotted against molar fraction. (adapted from ^{21,105,106})...	22
Figure 9. ISOALKY process plant scheme illustrating the refit which is currently underway. ¹¹³	24
Figure 10. Phase diagram of the ZnCl ₂ mixture showing melting point as a function of urea concentration.	26
Figure 11. ²⁷ Al NMR spectra showing speciation in (<i>left</i>) AcA-AlCl ₃ χ_{AlCl_3} = 0.5 and 0.6, and (<i>right</i>) L-AlCl ₃ χ_{AlCl_3} = 0.5.	28
Figure 12. The structure of the solvate ionic liquid [Li(G3)][NTf ₂].	31
Figure 13. <i>Left</i> ¹¹ B NMR spectra of neat borenium ILs with DMSO-d ₆ lock (composition given on spectra); <i>right</i> Gutmann acceptor number values measured for borenium ILs of a general formula L-BCl ₃ -nMCl ₃ , for four different ligands (L), two metals (M) and n = 1–3. (Adapted from ⁴).....	33
Figure 14. Gutmann acceptor number measurements, showing a) multiple P ₂₂₂ O peaks for the sample P ₂₂₂ O and AlCl ₃ as 0.375 mol dm ⁻³ solution in 1,2- dichloroethane and b) a single P ₂₂₂ O peak for the sample P ₂₂₂ O and GaCl ₃ as 0.375 mol dm ⁻³ solution in 1,2-dichloroethane.	38
Figure 15. Comparison between ²⁷ Al (a,b,c and d) and ³¹ P (e,f,g and h) NMR spectra of (a,e) P888O-AlCl ₃ , χ_{AlCl_3} = 0.50, (b,f) P888O- AlCl ₃ , χ_{AlCl_3} = 0.60, (c,g) P888-AlCl ₃ , χ_{AlCl_3} = 0.50, and (d,h) P888-AlCl ₃ , χ_{AlCl_3} = 0.60.....	43

Figure 16. ^{31}P NMR spectra of L-GaCl_3 where $\text{L} = \text{P}_{888}\text{O}$ (left) or P_{888} (right) with compositions (a) $\chi_{\text{GaCl}_3} = 0.50$, (b) $\chi_{\text{GaCl}_3} = 0.60$, (c) $\chi_{\text{GaCl}_3} = 0.67$, and (d) $\chi_{\text{GaCl}_3} = 0.75$. (* denotes artefact)	45
Figure 17. Crystal structures of (<i>left</i>) $\text{SbCl}_3(\text{PMe}_3)$ in a polymeric chain, (<i>centre</i>) in the dimeric $[\text{SbCl}_3(\text{PPh}_3)]$ and (<i>right</i>) in dimeric $[\text{SbCl}_3(\text{PCy}_3)]$. ¹⁵⁸	49
Figure 18. Changes to ^{31}P NMR spectra of $\text{P}_{888}\text{-SbCl}_3$, $\chi_{\text{SbCl}_3} = 0.50$ from a) immediately after synthesis, b) after two days under inert conditions and c) after six months under inert conditions.	50
Figure 19. ^{31}P NMR spectra of $\text{P}_{888}\text{O-SbCl}_3$ $\chi_{\text{SbCl}_3} = 0.50$ (top) and $\chi_{\text{SbCl}_3} = 0.60$ (bottom).	50
Figure 20. Sn(II) LCC NMR spectra of L-SnCl_2 LCCs at $\chi_{\text{SnCl}_2} = 0.50$ a) ^{119}Sn NMR spectrum of $\text{P}_{888}\text{-SnCl}_2$, b) ^{119}Sn NMR spectrum of $\text{P}_{888}\text{O-SnCl}_2$, c) ^{31}P NMR spectrum of $\text{P}_{888}\text{-SnCl}_2$, and d) ^{31}P NMR spectrum of $\text{P}_{888}\text{O-SnCl}_2$	52
Figure 21. ^{31}P NMR spectra of $\text{P}_{888}\text{-SnCl}_4$ at $\chi_{\text{SnCl}_4} = 0.50$	53
Figure 22. Tin(IV) LCC NMR spectra of $\text{P}_{888}\text{O-SnCl}_4$ LCCs a) ^{119}Sn NMR spectrum of $\text{P}_{888}\text{O-SnCl}_4$ at $\chi_{\text{SnCl}_4} = 0.50$, b) ^{119}Sn NMR spectrum of $\text{P}_{888}\text{O-SnCl}_4$ at $\chi_{\text{SnCl}_4} = 0.60$, c) ^{31}P NMR spectrum of $\text{P}_{888}\text{O-SnCl}_4$ at $\chi_{\text{SnCl}_4} = 0.50$, and d) ^{31}P NMR spectrum of $\text{P}_{888}\text{O-SnCl}_4$ at $\chi_{\text{SnCl}_4} = 0.60$	55
Figure 23. ^{31}P NMR spectra for L-TiCl_4 LCCs a) $\text{P}_{888}\text{-TiCl}_4$ at $\chi_{\text{TiCl}_4} = 0.50$, b) $\text{P}_{888}\text{-TiCl}_4$ at $\chi_{\text{TiCl}_4} = 0.60$ c) $\text{P}_{888}\text{O-TiCl}_4$ at $\chi_{\text{TiCl}_4} = 0.50$	56
Figure 24. The proposed structure of $[\text{Ti}_2\text{Cl}_8\text{PR}_3]$	57
Figure 25. The structure of the equimolar combination of ZnCl_2 and P^iBu_3 as determined by crystallography.	58
Figure 26. ^{31}P NMR spectra for L-ZnCl_2 LCCs a) $\text{P}_{888}\text{-ZnCl}_2$ at $\chi_{\text{ZnCl}_2} = 0.50$, b) $\text{P}_{888}\text{O-ZnCl}_2$ at $\chi_{\text{ZnCl}_2} = 0.50$ c) $\text{P}_{888}\text{O-ZnCl}_2$ at $\chi_{\text{ZnCl}_2} = 0.60$	59
Figure 27. Comparison of relative Lewis acidities reported by Kobayashi <i>et al.</i> ,	65
Figure 28. Comparison of ANs for metal halides (recorded in 1,2-dichloroethane), with ANs for all LCCs for $\text{MCl}_x\text{-L}$ for all values of χ_{MCl_x} recorded. $\text{L} = \text{P}_{888}\text{O}$ (top) and $\text{L} = \text{P}_{888}$ (bottom).	66
Figure 29. Catalytic performance in terms of conversion and stereoselectivity for LCCs with a general formula $\text{MCl}_x\text{-P}_{888}\text{O}$ $\chi_{\text{MCl}_x} = 0.5$ (results provided by Dr Matuszek).	70
Figure 30. Dienophile conversion rates in the model Diels-Alder reaction catalysed by LCCs with the general formula $\text{MCl}_x\text{-P}_{888}\text{O}$ $\chi_{\text{MCl}_x} = 0.5$, plotted against the Gutmann acceptor numbers of each LCC.	71
Figure 31. ^{11}B NMR spectrum showing the presence of both B-chlorocatecholborane and $[\text{B}_2\text{Cat}_3]$ forming in similar proportions.	79

Figure 32. Donor ligands included in this work: l-r methylimidazole, triethylamine, tri(<i>tert</i> -butyl phosphine), trioctylphosphine and trioctylphosphine oxide	79
Figure 33. The adducts formed from the combination of [BcatCl] with a ligand (L) where L is (l-r) methylimidazole, triethylamine, tri- <i>tert</i> -butyl phosphine, trioctylphosphine and trioctylphosphine oxide	82
Figure 34. The ^{11}B NMR spectrum of a) BcatCl, compared to spectra of [BcatClL] adducts, where L is: b) methylimidazole, c) triethylamine, d) tri- <i>tert</i> -butyl phosphine, e) trioctylphosphine and f) trioctylphosphine oxide (samples dissolved in DCM).....	82
Figure 35. The ^1H NMR spectra of adduct [BcatCl(mim)] in DCM with a DMSO- d_6 capillary.	83
Figure 36. The appearance of the product of reaction of [BcatCl(mim)] with MeNTf.....	84
Figure 37. NMR spectra of [BcatCl(P ₈₈₈)] and starting materials: ^{31}P NMR spectra of a) P ₈₈₈ (neat with a DMSO- d_6 capillary) and b) [BcatCl(P ₈₈₈)] in C ₆ D ₆ ; ^{11}B NMR spectra of c) [BcatCl] (in DCM with a DMSO- d_6 capillary) and d) [BcatCl(P ₈₈₈)] in C ₆ D ₆	85
Figure 38. NMR spectra of [BcatCl(P ₈₈₈ O)] and starting materials: ^{31}P NMR spectra of a) P ₈₈₈ O (recorded in CDCl ₃) and b) [BcatCl(P ₈₈₈ O)] in C ₆ D ₆ ; ^{11}B NMR spectra of c) [BcatCl] in DCM with a DMSO- d_6 capillary and d) [BcatCl(P ₈₈₈ O)] in C ₆ D ₆	86
Figure 39. ^{11}B NMR spectrum for the salt [Bcat(P ^t Bu ₃)] [Ga ₃ Cl ₁₀] in deuterated benzene and (inset) the ionic liquid [Bcat(P ^t Bu ₃)] [Ga ₃ Cl ₁₀].	87
Figure 40. The structures of the triflate, [OTf] ⁻ (left) and bistriflimide, [NTf ₂] ⁻ (right) anions.	88
Figure 41. The ^{19}F NMR spectrum of [BcatL(OTf)] adducts, where L is: a) trioctylphosphine, b) trioctylphosphine oxide c) triethylamine, d) tri- <i>tert</i> -butyl phosphine (samples recorded neat at 350 K with a DMSO- d_6 capillary).	92
Figure 42. ^{11}B NMR spectrum for (top) [Bcat(OTf)(P ₈₈₈)] and (bottom) [Bcat(OTf)(P ₈₈₈ O)], at room temperature.	93
Figure 43. Comparison of ^{31}P NMR spectra of liquids with the general formula [Bcat(OTf)L], where L= (left) P ₈₈₈ and (right) P ₈₈₈ O, at 300 and 350 K.	94
Figure 44. ^{13}C NMR spectrum for [Bcat(OTf)(P ₈₈₈ O)] indicating the generation of [TMS(P ₈₈₈ O)(OTf)].	95
Figure 45. The ^{11}B NMR spectra for (left) [Bcat(P ₈₈₈)] [OTf] and (right) [Bcat(P ₈₈₈ O)] [OTf], at a range of temperatures.	96
Figure 46. The ^{11}B NMR spectra for (left) [Bcat(N ₂₂₂)(OTf)] and (right) [Bcat(P ^t Bu ₃)(OTf)] at temperatures from 340 to 360 K.....	97
Figure 47. ^{31}P NMR spectrum for [Bcat(OTf)(P ^t Bu ₃)] at 360 K.....	98
Figure 48. Comparison of ^1H NMR spectra of a) [BCl ₃ (mim)] b) the reaction mixture of [BCl ₃ (mim)] and HNTf ₂ , after stirring for 15 h at 60 °C <i>in vacuo</i> , and c) the product following	

stirring for three days at 60 °C <i>in vacuo</i> . The starting material peaks are highlighted in blue, while the product peaks are highlighted in green.	102
Figure 49. ¹ H NMR spectra showing a) the starting material [BCl ₃ (mim)] in DCM and the products of the reaction mixture of silver bistriflimide and [BCl ₃ (mim)] in DCM with a DMSO-d ₆ capillary, over four days (b-e).	103
Figure 50. The ¹¹ B NMR spectrum of (top) the starting material [BCl ₃ (mim)] (in CDCl ₃) and (bottom) [BCl ₃ (NTf ₂)(mim)] from silver bistriflimide (in DCM with a DMSO-d ₆ capillary).	104
Figure 51. ¹ H NMR spectra of starting material, [BCl ₃ (mim)] (top, in chloroform) and the product of reaction with methyl bistriflimide (bottom, neat with a DMSO capillary). * marks solvent peak.	105
Figure 52. ¹¹ B NMR spectrum of (top) [BCl ₃ (mim)] in CDCl ₃ and (bottom) the product of the reaction of [BCl ₃ (mim)] with MeNTf ₂ (solventless, with DMSO capillary).	106
Figure 53. The ¹¹ B NMR spectra for [Bcat(NTf ₂)(N ₂₂₂)] and at increasing temperatures from 300 to 360 K (26.85 to 86.85 °C), and again at 300 K following cooling. Insert shows the emergence of peak at 21 ppm over this temperature range.	111
Figure 54. The ¹⁹ F NMR spectrum for [Bcat(NTf ₂)(N ₂₂₂)].	112
Figure 55. The ¹¹ B NMR spectra for [Bcat(NTf ₂)(P ^t Bu ₃)] and at increasing temperatures from 300 to 350 K (26.85 to 76.85 °C) and again at 300 K following cooling. Insert shows the emergence of peak at 26.79 ppm over this temperature range.	113
Figure 56. The ³¹ P NMR spectra and for [Bcat(NTf ₂)(P ^t Bu ₃)] and at increasing temperatures from 300 to 350 K (26.85 to 76.85 °C).	114
Figure 57. ¹⁹ F NMR spectra for [Bcat(NTf ₂)(P ^t Bu ₃)] at increasing temperatures from 300 to 350 K (26.85 to 76.85 °C)	115
Figure 58. The ¹¹ B NMR spectra for [Bcat(NTf ₂)(P ₈₈₈)] and at increasing temperatures from 300 to 360 K (26.85 to 86.85 °C) and again at 300 K following cooling.	116
Figure 59. NMR spectra of [Bcat(NTf ₂)(P ₈₈₈)] at 300 K: ³¹ P (left) and ¹⁹ F (right)	117
Figure 60. The ¹¹ B NMR spectra for [Bcat(NTf ₂)(P ₈₈₈ O)] at increasing temperatures from 300 to 350 K (26.85 to 76.85 °C) and again at 300 K following cooling, inset showing formation of peaks at 28.20 and 22.64 ppm over this temperature range.	118
Figure 61. NMR spectra of [Bcat(NTf ₂)(P ₈₈₈ O)]: ³¹ P at 300 K (left); ¹⁹ F at 300 K (top right) and ¹⁹ F at 350 K (bottom right).	119
Figure 62. Free energy profile for the activation of dihydrogen by an FLP (adapted from ²¹⁷)	126
Figure 63. Geometry-optimised structures of transition states for iPr ₃ SnOTf/DABCO FLPs with different triflate positions. Orbital overlap structures show the non-bonding orbitals	

$\sigma(\text{H}_2)$, empty p-orbital on Sn, and a O^* orbital from OTf are given below (adapted from ²²²)	128
Figure 64. Comparison of peaks at full width half-height as a function of temperature (T) of the signals due to the ortho-Me of PMes_3 (240 mM) and para-F of BCF (15 mM) in (a) isolated species and (b) as a mixture. ²²³	129
Figure 65. The structure of trimesityl phosphine (left 2D, right 3D).	132
Figure 66. ^{31}P NMR spectrum showing the formation of the side product $\text{Mes}_2\text{P-PMes}_2$ (at -31 ppm) and PMes_3 (at -37 ppm) with a ratio of 66:33 of side-product: desired product....	133
Figure 67. Structure of 1,1,2,2-tetrakis(2,4,6-trimethylphenyl)diphosphine as obtained from single crystal X-ray diffraction.	134
Figure 68. ^{31}P NMR spectrum showing PMes_3 .	136
Figure 69. ^{31}P NMR spectrum showing the formation of $\text{PMes}_3\text{-d}_{33}$ (at -37 ppm) and the side product $\text{Mes}_2\text{P-PMes}_2$ (at -31 ppm).	137
Figure 70. Side products generated in the synthesis of P^tBu_3 .	139
Figure 71. Comparison of mono-substituted intermediate species.	139
Figure 72. A comparison of ^{31}P spectra a) with and b) without copper(I) iodide and lithium bromide at a 5% mol ratio.	141
Figure 73. ^{13}C and ^{31}P NMR spectra of tri-tert-butyl phosphine- d_{27} in C_6D_6 (solvent peak in ^{13}C at 128 ppm).	144
Figure 74. Comparison of the small $\text{P}^t\text{Bu}_3 \cdots \text{BCF}$ correlation in the EPSR model of the experimental data with the larger radial distribution functions (RDFs) between BCF and benzene (black), P^tBu_3 and benzene (blue) and the benzene-benzene self-correlation (red).	146
Figure 75. The plot of the P-B pair partial radial correlation function (blue) between P^tBu_3 and BCF in benzene (1:1:70), averaged from two independent data-driven simulation models (purple and magenta data points), and compared to the equivalent correlation from DFT simulation of P^tBu_3 and BCF in toluene (red line). ⁶ Correlation distances corresponding to the range of 'solvent-separated' pairs (6–9 Å) are indicated by the shaded region.	147
Figure 76. Spectra of the FLP, BCF/ P^tBu_3 , and its components, in $[\text{C}_{10}\text{mim}][\text{NTf}_2]$ (a) ^{19}F NMR spectrum of BCF, (b) ^{31}P NMR spectrum of P^tBu_3 , (c) ^{19}F NMR spectrum of BCF/ P^tBu_3 and (d) ^{31}P NMR spectrum of BCF/ P^tBu_3 .	153
Figure 77. Computationally derived square functions ($S(q)$) (which is a function of X-ray scattering intensity against concentration and atom type) for (left) molecular solvents and (right) ionic liquids graphs developed by Araque <i>et al.</i> based on computational derivations from Kashyap <i>et al.</i> ^{266,270-273}	155
Figure 78. The structure of the room temperature ionic liquid $[\text{C}_{10}\text{mim}][\text{NTf}_2]$.	155

Figure 79. Representations of cage and jump movements for the solute methane in the ionic liquid 1-butyl-1-methylpyrrolidinium bistriflimide, illustrating the different movements through each domain of the ionic liquid. ²⁶⁵	156
Figure 80. Setup for H ₂ saturation experiments.	157
Figure 81. Fragments of ¹ H NMR spectra of the FLP solutions in benzene (top) and [C10mim][NTf ₂] (bottom) after saturation with H ₂ , showing signals from split H ₂ molecule.	158
Figure 82. Structures of (clockwise from top right): N,N diisopropyl ethyl amine; 2,2,4,6 tetramethyl piperidine; proton sponge (1,8-bis(dimethylamino)naphthalene) and triphenyl phosphine.....	159
Figure 83. Comparison of ¹¹ B NMR spectra illustrating the change of boron environment from a) [BCl ₂ (mim)][M ₂ Cl ₇] on the addition of a 0.5 mol equivalents of a base b) diisopropyl ethylamine, c) tetramethyl piperidine, d) triphenyl phosphine and e) 0.1 mol equivalents of proton sponge. (left M = Al; right M = Ga)	160
Figure 84. Comparison of ²⁷ Al NMR spectra illustrating the change of boron environment from a) neat [BCl ₂ (mim)][Al ₂ Cl ₇] upon the addition of a 0.5 mol equivalents of a base b) diisopropyl ethylamine, c) tetramethyl piperidine, d) triphenyl phosphine and e) 0.1 mol equivalents of proton sponge.....	160
Figure 85. The ³¹ P spectrum of [BCl ₂ (mim)][Al ₂ Cl ₇] with PPh ₃	161
Figure 86. ¹¹ B NMR spectra (in benzene) showing the effect of increasing concentration of metal halide on the system [BcatCl(P ^t Bu ₃)] where a) $\chi_{\text{AlCl}_3} = 0$, b) $\chi_{\text{AlCl}_3} = 0.5$ and a) $\chi_{\text{AlCl}_3} = 0.67$	164
Figure 87. ³¹ P NMR spectra (in benzene) showing the effect of increasing concentration of metal halide on the system [BcatCl(P ^t Bu ₃)] where a) $\chi_{\text{AlCl}_3} = 0$, b) $\chi_{\text{AlCl}_3} = 0.5$ and a) $\chi_{\text{AlCl}_3} = 0.67$	165
Figure 88. ¹ H NMR spectra showing the effect of adding H ₂ to [Bcat(P ^t Bu ₃)][Ga ₃ Cl ₁₀]/ P ^t Bu ₃ , where a) is before exposure to H ₂ and b) is following H ₂ exposure.....	166
Figure 89. The liquid [Bcat(P ₈₈₈)] [NTf ₂] with one equivalent of P ^t Bu ₃	167
Figure 90. ¹¹ B NMR spectra of a) the Lewis acidic ionic liquid [Bcat(P ₈₈₈)] [NTf ₂] and b) [Bcat(P ₈₈₈)] [NTf ₂] with 1 eq. of P ^t Bu ₃ and ³¹ P NMR spectra of c) the Lewis acidic ionic liquid [Bcat(P ₈₈₈)] [NTf ₂] and d) [Bcat(P ₈₈₈)] [NTf ₂] with 1 eq. of P ^t Bu ₃	168
Figure 91. ¹ H NMR spectra in C ₆ D ₆ of a) the Lewis acidic ionic liquid [Bcat(P ₈₈₈)] [NTf ₂] with 1 eq. of P ^t Bu ₃ and b) the sample following exposure the 1 bar of H ₂ overnight.	169
Figure 92. ³¹ P NMR spectra in C ₆ D ₆ showing a) the Lewis acidic ionic liquid [Bcat(P ₈₈₈)] [NTf ₂] with 1 eq. of P ^t Bu ₃ and b) the sample following exposure the 1 bar of H ₂ overnight.....	169

Figure 93. The ^{13}C NMR spectrum of $[\text{Bcat}(\text{OTf})\text{L}]$ adducts, where L is: a), triethylamine b) tri- <i>tert</i> -butyl phosphine c) trioctylphosphine d) trioctylphosphine oxide (samples recorded neat at 300 K with a DMSO- d_6 capillary).	186
Figure 94. The ^1H NMR spectrum of $[\text{Bcat}(\text{OTf})\text{L}]$ adducts, where L is: a), triethylamine b) tri- <i>tert</i> -butyl phosphine c) trioctylphosphine d) trioctylphosphine oxide (samples recorded neat at 300 K with a DMSO- d_6 capillary).	186
Figure 95. The ^{13}C NMR spectrum of $[\text{Bcat}(\text{NTf}_2)\text{L}]$ adducts, where L is: a), triethylamine b) tri- <i>tert</i> -butyl phosphine c) trioctylphosphine d) trioctylphosphine oxide (samples recorded neat at 300 K with a DMSO- d_6 capillary).	187
Figure 96. The ^1H NMR spectrum of $[\text{Bcat}(\text{NTf}_2)\text{L}]$ adducts, where L is: a), triethylamine b) tri- <i>tert</i> -butyl phosphine c) trioctylphosphine d) trioctylphosphine oxide (samples recorded neat at 300 K with a DMSO- d_6 capillary).	187
Figure 97. DSC plot for $[\text{Bcat}(\text{OTf})(\text{N}_{222})$	188
Figure 98. DSC plot for $[\text{Bcat}(\text{OTf})(\text{P}^t\text{Bu}_3)$	188
Figure 99. DSC plot for $[\text{Bcat}(\text{OTf})(\text{P}_{888})$	189
Figure 100. DSC plot for $[\text{Bcat}(\text{OTf})(\text{P}_{888}\text{O})$	189
Figure 101. DSC plot for $[\text{Bcat}(\text{NTf}_2)(\text{N}_{222})$	190
Figure 102. DSC plot for $[\text{Bcat}(\text{NTf}_2)(\text{P}^t\text{Bu}_3)$	190
Figure 103. DSC plot for $[\text{Bcat}(\text{NTf}_2)(\text{P}_{888})$	191
Figure 104. DSC plot for $[\text{Bcat}(\text{NTf}_2)(\text{P}_{888}\text{O})$	191

LIST OF SCHEMES

Scheme 1. Adduct formation between $P_{222}O$ and a Lewis acid.....	4
Scheme 2. The structure of the borinium cation $[B(Mes)_2]^+$ and the products of arylation–deoxygenation of CO_2	11
Scheme 3. Borenium synthesis <i>via</i> B-X bond heterolysis.....	12
Scheme 4. The major equilibria present in borenium halometallate mixtures on the formation of $[BY_2L][AlCl_4]$	13
Scheme 5. Borenium synthesis <i>via</i> non-reversible bond heterolysis.	13
Scheme 6. The formation of a tricoordinate boron cation <i>via</i> reversible bond heterolysis....	14
Scheme 7. The enantiomerically pure borenium catalyst for the Diels-Alder reaction developed by Hayashi <i>et al.</i> and the “masked” borenium resting state.	14
Scheme 8. The formation of a borenium cation <i>via</i> the coordination of an electrophile.	15
Scheme 9. Reaction between Lewis acidic $[Al_2Cl_7]^-$ with a Lewis base, L.	20
Scheme 10. Synthesis of a borenium ionic liquid. ⁶⁹	31
Scheme 11. Diels Alder reaction between cyclopentadiene to ethyl acrylate.....	34
Scheme 12. Model Diels-Alder reaction between cyclopentadiene (CPD) and ethyl acrylate (EA) used in this study.	69
Scheme 13. The formation of the B-catecholboron complex.	78
Scheme 14. Mechanism for the redistribution of $[PR_3BcatCl]$ in the presence of $BcatCl$. ¹⁸⁵	81
Scheme 15. The products of the combination of $[BX_3(mim)]$ with TMSOTf, forming a tetracoordinate boron adduct <i>via</i> halide abstraction (top) and the formation of boron tritriflate <i>via</i> a postulated ligand scrambling pathway (bottom).	90
Scheme 16. The formation of $[BCl_2(mim)][NTf_2]$ using bistriflimidic acid as the halide abstracting agent.....	101
Scheme 17. The formation of $[BCl_2(mim)][NTf_2]$ using silver bistriflimide as the halide abstracting agent.....	103
Scheme 18. The formation of $[BCl_2(mim)][NTf_2]$ using methyl bistriflimide as the halide abstracting agent.....	104
Scheme 19. The main products of the reaction between catechol boron complex and methyl bistriflimide.	107
Scheme 20. The first FLP reaction reported by Stephan <i>et al.</i> in 2006. ²¹⁰	124

Scheme 21. Representation of the orbital interactions in substrate cleavage (E-E') by i) a transition metal and ii) an FLP.	125
Scheme 22. The reaction of the FLP (Mes) ₂ PCH ₂ CH ₂ B(C ₆ F ₅) ₂ with a dihydrogen molecule <i>via</i> a dimeric intermolecular pathway, which has been shown to be preferred to the intramolecular pathway. (adapted from ²²¹).....	127
Scheme 23. The synthesis of trimesityl phosphine <i>via</i> a Grignard intermediate.	133
Scheme 24. Proposed pathways for the synthesis of Pmes ₃ and Mes ₂ P-Pmes ₂ <i>via</i> kinetic and thermodynamic pathways.....	135
Scheme 25. Synthesis of deuterated trimesityl phosphine.	136
Scheme 26. P ^t Bu ₃ as a catalyst in cross coupling reactions.	138
Scheme 27. The synthesis of deuterated tri- <i>tert</i> -butyl phosphine.	143
Scheme 28. The products observed in-situ from the reaction of 1,8-Bis(dimethylamino)naphthalene with a catechol borenium (Bcat) with a triethyl amine adduct.(Adapted from ⁷²).....	162
Scheme 29. The activation of H ₂ by [CatB(P ^t Bu ₃)] [AlCl ₄]/ P ^t Bu ₃ and the subsequent equilibrium which forms and the products of disproportionation. (Adapted from ¹⁹⁰)	163
Scheme 30. The appearance before and after hydrogen activation of [Bcat(P ^t Bu ₃)] [Ga ₃ Cl ₁₀]/ P ^t Bu ₃	166
Scheme 31. The appearance before and after hydrogen activation of [Bcat(P ₈₈₈)(P ^t Bu ₃)] [NTf ₂]	168

LIST OF TABLES

Table 1. Physical descriptions of LCCs synthesised in this work.....	40
Table 2. The appearance of spectra from a range of heteronuclear NMR spectra.	41
Table 3. ^{31}P NMR chemical shifts for all compositions which formed homogeneous liquids. Also given are the change in chemical shift of the ligand in the LCC.....	42
Table 4. Comparison of NMR spectroscopic data for tin(II) complexes with oxide ligands.	52
Table 5. The relative speciations of different LCCs with the formula $\text{MCl}_x\text{-P}_{888}\text{O}$	60
Table 6. The relative speciations of different LCCs with the formula $\text{MCl}_x\text{-P}_{888}$	61
Table 7. Gutmann acceptor numbers recorded for metal halides, in 1,2 dichloroethane, and LCCs, recorded as neat liquids.	62
Table 8. Comparison between metal halide Gutmann AN measurements in diethyl ether ²⁵ and in 1,2-dichloroethane.....	63
Table 9. Physical appearances of systems formed from the combination of boron complexes with the general formula $[\text{BcatCIL}]$ and TMSOTf , along with ^{19}F NMR signals for each sample, recorded neat at 350 K.	91
Table 10. AN values for all $[\text{Bcat}(\text{OTf})\text{L}]$ liquids (measured at 300 K) shown with the $\delta^{31}\text{P}$ resonances recorded (in ppm) measured for solutions of these liquids containing 1, 2 and 3 mol% P_{222}O (referenced to $\delta^{31}\text{P}$, H_3PO_4 85% = 0 ppm).	99
Table 11 Physical appearances of systems formed from the combination of boron complexes with the general formula $[\text{BcatCIL}]$ and MeNTf_2	107
Table 12. Chemical shifts and relative integrations of ^{19}F NMR spectra for compositions $[\text{Bcat}(\text{NTf}_2)\text{L}]$	108
Table 13. Chemical shifts and relative integrations of ^{11}B NMR spectra for compositions $[\text{Bcat}(\text{NTf}_2)\text{L}]$	109
Table 14. Chemical shifts and relative integrations of ^{31}P NMR spectra for phosphorus containing compositions $[\text{Bcat}(\text{NTf}_2)\text{L}]$	110
Table 15. AN values for all $[\text{Bcat}(\text{NTf}_2)\text{L}]$ liquids at 300 K shown with the $\delta^{31}\text{P}$ resonances recorded (in ppm) measured for solutions of these liquids containing 1, 2 and 3 mol% P_{222}O (referenced to $\delta^{31}\text{P}$, H_3PO_4 85% = 0 ppm).	121
Table 16. The results of thin layer chromatography of the crude product containing both PMes_3 and $\text{Mes}_2\text{P-PMes}_2$	134
Table 17. The detected side and by- products from the synthesis of tri- <i>tert</i> -butyl phosphine (in benzene).....	142

Table 18. ^{19}F and ^{31}P NMR signals of solutions of the BCF/ $\text{P}^{\text{t}}\text{Bu}_3$ FLP and its individual components in benzene- d_6 and in an ionic liquid, $[\text{C10mim}][\text{NTf}_2]$ at a concentration of 160 mmol.....	152
--	-----

LIST OF EQUATIONS

Equation 1.....	5
Equation 2.....	7
Equation 3.....	7
Equation 4.....	18
Equation 5.....	18
Equation 6.....	21
Equation 7.....	27
Equation 8.....	27
Equation 9.....	27
Equation 10.....	32
Equation 11.....	43
Equation 12.....	43
Equation 13.....	46
Equation 14.....	47
Equation 15.....	47
Equation 16.....	48
Equation 17.....	49
Equation 18.....	50
Equation 19.....	52
Equation 20.....	53
Equation 21.....	53
Equation 22.....	55
Equation 23.....	56
Equation 24.....	56
Equation 25.....	56
Equation 26.....	57
Equation 27.....	58

Equation 28.....	59
Equation 29.....	63
Equation 30.....	64
Equation 31.....	67
Equation 32.....	67
Equation 33.....	67
Equation 34.....	67
Equation 35.....	68
Equation 36.....	68
Equation 37.....	78
Equation 38.....	84
Equation 39.....	86
Equation 40.....	87
Equation 41.....	94
Equation 42.....	95
Equation 43.....	97
Equation 44.....	98
Equation 45.....	99
Equation 46.....	100
Equation 47.....	100
Equation 48.....	100
Equation 49.....	100
Equation 50.....	112
Equation 51.....	112
Equation 52.....	115
Equation 53.....	115
Equation 54.....	117
Equation 55.....	117
Equation 56.....	120

Equation 57.....	120
Equation 58.....	121
Equation 59.....	121
Equation 60.....	122
Equation 61.....	122
Equation 62.....	165

ABBREVIATIONS

AcA - Acetamide
AN – Gutmann acceptor number
BeatCl – B-Chlorocatechol borane (2-chloro-1,3,2-benzodioxaborole)
[C_nmim]⁺ – 1-Alkyl-3-methylimidazolium cation
C_n – A hydrocarbon chain consisting of *n* carbon atoms
CSD – Cambridge Structural Database
DABCO - 1,4diazabicyclo[2.2.2]octane
DCM – Dichloromethane
DFT – Density Functional Theory
DMA - N,N -dimethylacetamide
DMF – Dimethyl Formamide
DMSO – Dimethylsulphoxide
DSC – Differential Scanning Calorimetry
Eq – Equivalent
FIA – Fluoride ion affinity
FLPs – Frustrated Lewis pairs
HIA – Hydride ion affinity
HSAB – Hard soft acid base
HOMO – Highest occupied molecular orbital
[Him]⁺ – Protonated imidazolium cation
IL – Ionic liquid
IR - Infrared
LCC – Liquid coordination complex
LMCT – Ligand Metal Charge Transfer
LUMO – Lowest unoccupied molecular orbital
MeCN - Acetonitrile
Mes – Mesitylene (2,4,6-trimethylbenzene)
Mim – Methylimidazolium
NMA - N-methylacetamide
NHC – *N*-Heterocyclic carbene
NMR – Nuclear magnetic resonance
[NTf₂]⁻ – Bistriflimide (Bis(trifluoromethylsulfonyl)imide) anion
[OTf]⁻ – Trifluoromethanesulfonate anion
P₂₂₂O – Triethylphosphine oxide
PMP - 1,2,2,6,6-pentamethylpiperidine
SCILL – Solid catalyst with ionic liquid layer
SILP – Supported ionic liquid phase
SUr - Thiourea
TGA – Thermogravimetric analysis
THF – Tetrahydrofuran
TMP -2,2,6,6-tetramethylpiperidine
Ur - Urea
X - Halide
χ_A – Molar fraction of A

PUBLICATIONS ARISING FROM THIS WORK

Published

- 1) J. M. Hogg, L. C. Brown, K. Matuszek, P. Latos, A. Chrobok and M. Swadźba-Kwaśny, *Liquid coordination complexes of Lewis acidic metal chlorides: Lewis acidity and insights into speciation*, Dalton Trans., 2017, **46**, 11561–11574. (cover)
- 2) L. C. Brown, J. M. Hogg and M. Swadźba-Kwaśny, *Lewis Acidic Ionic Liquids*, Top. Curr. Chem., 2017, **375**, 1-40.
- 3) L. Moura, L. C. Brown, M. Blesic and J. D. Holbrey, *LCST Phase Behavior and Complexation with Water of an Ionic Liquid Incorporating the 5-Phenyltetrazolate Anion*, ChemPhysChem, 2017, **18**, 3384–3389.
- 4) L.C. Brown, J.M. Hogg, M. Gilmore, L. Moura, S. Imberti, S. Gärtner, H.Q.N. Gunaratne, R.J. O'Donnell, N. Artioli, J.D. Holbrey and M. Swadźba-Kwaśny, *Frustrated Lewis pairs in ionic liquids and molecular solvents – a neutron scattering and NMR study of encounter complexes*, Chem. Commun., 2018, **54**, 8689-8692. (cover)
- 5) P. Latos, A. Culkin, N. Barteczko, S. Boncel, S. Jurczyk, L. C. Brown, P. Nockemann, A. Chrobok and M. Swadźba-Kwaśny, *Water-Tolerant Trifloaluminate Ionic Liquids: New and Unique Lewis Acidic Catalysts for the Synthesis of Chromane*, Front. Chem., 2018, **6**, 2010–2015.

Submitted

- 1) L.C. Brown, J.M. Hogg, S. Youngs, J. Tellam, H. Q. N. Gunaratne, Y. Delavoux, J.D. Holbrey and M. Swadźba-Kwaśny, *The synthesis of deuterium-labelled tri-tert-butyl phosphine*, 2019, submitted
- 2) L.C. Brown, A. McGrogan, R.J. O'Donnell, N. Artioli, J.D. Holbrey and M. Swadźba-Kwaśny, *Chloride-free borenium ionic liquids and their use as ionic liquid frustrated Lewis pairs*, 2019, in preparation



1 INTRODUCTION

This introduction provides an overview of the conceptualisation of Lewis acidity and methods of its quantification. Further on, the uses of Lewis acids, particularly in ionic liquids, as catalysts are outlined briefly to provide a wider context of this work.

1.1 Defining Acidity

1.1.1 *Historical Perspective*

Acids were well known as natural substances long before their chemistry began to be understood. They were observed to have sour tastes, accounting for their being named from the Latin word *acidus* meaning sour, and to affect the colour of plant materials, like litmus.⁷ Among his multitudinous contributions to the burgeoning study of chemistry, Lavoisier made the first attempt to categorise acids that we might recognise today. The scientific community in this period sought to identify each property of a chemical as arising from a single isolatable substance. Seeking a unifying component which provided the property of acidity, Lavoisier began to study oxygen. By reacting elements with oxygen and dissolving them in water he created acidic solutions. This led him to the conclusion that it was oxygen which was responsible for acidity and as such he named it from the Greek for “acid-former”. This theory, while accurate for elements such as nitrogen and sulfur, does not account for the formation of basic solutions of many metal oxides and relied on Lavoisier’s unproven assertion that HCl contained oxygen.

Following Lavoisier’s death in the French revolution, Davy proved the absence of oxygen in the hydrohalic acids. The 19th century scientific community abandoned the quest for a unifying element causing acidity, and Davy stated that “acidity does not depend upon any particular elementary substance, but upon peculiar arrangement of various substances.”⁸ Although Davy was unable to form a principle from his observation, the work paved the way for a hydrogen theory, with the core belief that “an acid must be a hydrogen compound, but not all hydrogen compounds are acids”. This led to Arrhenius’ proposal that an acid is a compound which dissociates in water to give H^+ ions, whereas a base dissociates to give OH^- . In collaboration with Ostwald, Arrhenius studied the physical chemistry of solutions of acids in water. Whereas organic substrates had normal osmotic pressures in water, inorganic substrates behaved as though they were more concentrated in water than their formula would suggest. Arrhenius and Ostwald realised that this was indicative of their dissociation into ions, and used conductivity

measurements to show that acids such as HCl and HNO₃ were completely dissociated in water.⁷ Limiting their theory to the dissociation of H⁺ and OH⁻, they proposed a simple system for the direct comparison of acids and bases from conductivity measurements. Focused exclusively on molecules dissolved in water, their definition excluded solutions such as HCl in ether, and failed to rationalise reactions such as NH₃ and BF₃.

A 1905 publication by Franklin expanded Arrhenius' work through interrogating acid-base interactions in liquid ammonia and discovering that the formation of NH₂⁻ and NH₄⁺ anions was analogous to the formation of protons and hydroxide ions in water. He sought to create a parallel field of research into "ammonolysis" to characterise the behaviour of salts in ammonia. However, the work of Germann in 1925 went a step further, generalising the observations of solvent effects across aprotic solvents.⁹ Writing about solvent autoionisation, he classified the positive species as the solvonium (or lyonium) ions and negative species as solvate (or lyate) anions; the change in concentration of these species determined the relative acidity or basicity of the resultant solution. The main charge against this definition was that it was too broad to be of general use and did not provide mechanistic insight.⁸

These, now obsolete definitions, rely on a wealth of molecular entities which can be considered "acidic" under a variety of interrelated and cumulative statements. Such definitions are entirely dependent on the species produced, such as hydroxide anions and protons, and the identification of such species by techniques such as conductivity measurements. The next phase in the conceptualisation of acidity began in 1923, with theories that shifted the focus from particular species to identifying chemical reactivity patterns that were resulting from a shared phenomenon of acidity/basicity. The first of the two theories which underpin modern scientific understanding stemmed from independent work of the Danish and British scientists Brønsted and Lowry, who simultaneously proposed an acid-base theory centred around the process of protonation, whereby an acid is a species which donates H⁺, while a base accepts a proton in a reaction. Whilst this theory bears the hallmarks of those before it, it focuses on the process of the chemical reaction rather than the matter produced.¹⁰ For example, while a hydroxide ion is typically a very strong base in many reactions, in some solvents and amongst other strong bases it may not be called a Brønsted-Lowry base. The second of the two modern definitions, provided by Lewis, lies in the heart of this work, and is discussed in detail in the next section.

1.1.2 Lewis Acidity

In his book, *Valence and the Structure of Atoms and Molecules*, G. N. Lewis proposed a new definition for acids as those substances which can "employ an electron lone pair from another molecule in completing the stable group of one of its own atoms",¹¹ which was a significantly

broader definition than Brønsted and Lowry took. Lewis justified this approach, differing from other proton-centric definitions, stating that "to restrict the group of acids to those substances that contain hydrogen interferes as seriously with the systematic understanding of chemistry as would the restriction of the term oxidizing agent to substances containing oxygen."¹²

A Lewis acid is classically described as an electron pair acceptor, which encompasses the reactions involving Brønsted acids and further expands to include species such as metals, which have a LUMO accessible by a Lewis base. Notably, whereas in Brønsted definition proton is a 'medium' of acidity, in Lewis definition proton is an acid in its own right. Lewis bases here are the converse, species which donate a pair of electrons. A classic illustration of this is the interaction between boron trichloride and ammonia (Figure 1), where the lone pair on the nitrogen of the ammonia donates into the empty orbital of the boron, forming a Lewis acid-base adduct. By the same token, Brønsted acids, such as HCl, become Lewis adducts of a Lewis acid, H^+ , and a Lewis base, Cl^- .

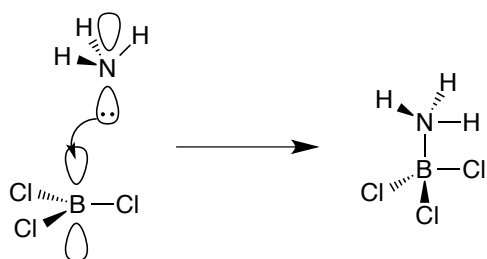


Figure 1. The reaction of boron trichloride and ammonia.

The scope Lewis acids is very broad, encompassing the proton, boranes and aluminium chloride, as well as metal centres in organometallic structures where ligands are Lewis bases donating into the *d*-orbitals of the Lewis acidic metal. For practical purposes, a qualitative approach to understanding the nature of the range of Lewis acidic entities was developed in the 1960s by Pearson,¹³⁻¹⁵ who described the relative reactivities of species through four terms: hard, soft, acid and base (HSAB). A hard species would be small, with high charge states and not be easily polarised, whilst a soft species would be large, with low charge states and easily polarised. With these two definitions came the recognition that a soft acid, such as platinum, would bind most strongly to a soft base, such bromide or iodide, whilst a hard acid, such as boron trifluoride would bind most strongly to a hard base, such as ammonia. These qualitative descriptions essentially demonstrate the principles of formation of covalent *vs.* ionic bonds (soft *vs.* hard, respectively).

The HSAB theory is now used as an approximation by chemists when discussing reactivity on a colloquial level. However, molecular orbital theory has developed to provide a quantitative

measurement of orbital interaction and energy, this has replaced the more qualitative explanation provided by the HSAB theory.

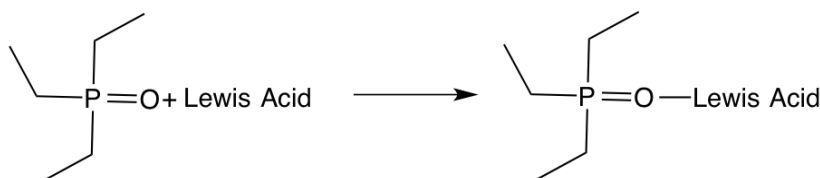
1.1.3 Quantification Methods

Quantification of Lewis acidity is inherently a challenge, as there is no ‘medium of acidity’, such as H^+ . The strength of the acid-base interaction depends on both the acid as the base, and more precisely on the shape and energy of the frontier molecular orbitals (HOMO of the base and LUMO of the acid), in addition to any steric hindrance around the reactive centre. This can be typified by the interaction between ammonia and boron trichloride (Figure 1), which is stronger than interaction between ammonia and boron trifluoride. However, CO forms a stronger adduct with BF_3 than with BCl_3 .¹⁶ This means that there is inherent difficulty in quantifying Lewis acidity, in which the scale of acidity strength is always probe-dependent. Despite this, a number of Lewis acidity scales have been developed for various practical purposes, typically using a probe molecule and quantifying the strength of the interaction between the probe and the acid.

1.1.3.1 Gutmann Acceptor Number

The classical Gutmann acceptor number (AN) approach uses ^{31}P NMR spectroscopy to determine the strength of donor/acceptor interactions between a sample and triethylphosphine oxide ($P_{222}O$), used as a ^{31}P NMR spectroscopic probe (Scheme 1).

Scheme 1. Adduct formation between $P_{222}O$ and a Lewis acid.



Initially, Gutmann used this technique to evaluate the acceptor properties of molecular solvents, however it was subsequently expanded to Lewis acidic solutions.^{17,18} It has been widely used in the measurement of Lewis acidity of ionic liquids.¹⁹⁻²¹ The measurement involves the dissolution of the probe in the liquid of interest and the coordination of the oxygen in the phosphine oxides induces a shift in the ^{31}P NMR chemical shift. Across a range of three known concentrations of probe, the chemical shift is extrapolated to infinite dilution (δ_{inf}) and the infinite dilution of $P_{222}O$ in hexane ($\Delta\delta_{inf}$) is used to normalise the value. Equation 1 is then used to calculate AN values.

$$AN = 2.348 \times \Delta\delta_{inf}$$

Equation 1

The range of AN is arbitrarily defined for hexane as AN = 0 and SbCl₅, 2 M solution in 1,2-dichloroethane as AN = 100, with species giving ANs above 100 being classed as superacids. A higher AN value indicates greater donation of electron density from the oxygen atom to the acidic species, reducing the electron density around the ³¹P centre and giving a higher chemical shift. The selection of P₂₂₂O as the probe is advantageous in the context of NMR spectroscopy, as the ³¹P nucleus has excellent sensitivity, is naturally 100% abundant and has spin ½ giving clear spectra, in addition to P₂₂₂O having good solubility across a wide range of solvents. It also has structural advantages, being simultaneously sensitive, as its short ethyl chains provide low steric hindrance and make the molecule strongly donating, giving greater sensitivity to the ³¹P chemical shift. At the same time, P₂₂₂O is robust because the ethyl chains provide protection to the oxygen atom and make the molecule relatively stable, even in highly acidic conditions.²² As exception to the high stability rule, however, P₂₂₂O has been reported to undergo fluorine-oxygen exchange in the presence of the dicationic imidazolium-phosphonium salt, [(SiMes)PFPh₂][B(C₆F₅)₄]₂.²³

Arguably, experimental ease contributed to popularity of this method, widely used in the modern literature. It must be considered, however, that P₂₂₂O is a hard donor. The effect of this can be seen when compared to the Child's method (Section 1.1.3.2), a soft crotonaldehyde donor. Between the two techniques, the series of boron acids: B(C₆F₅)₃, B(C₆F₅)₂(OC₆F₅), B(C₆F₅)(OC₆F₅)₂ and B(OC₆F₅)₃ has opposite order of Lewis acidity strength.²⁴ Consequently, AN methodology is suitable to assess interaction of Lewis acid with hard donors.

A variation on the Gutmann AN method was proposed by Beckett *et al.*, in which only one sample is analysed with a constant mass of P₂₂₂O dissolved in a constant volume of sample, removing the need to extrapolate to infinite dilution.²⁵ This is an effective variation for molecular acids with defined structures and has been widely used.²⁶⁻²⁸ However, where the probe may interfere with a dynamic equilibria, such as in chlorometallate ionic liquids, a change in the concentration of the probe can have a greater effect, therefore in these systems it is always recommended to extrapolate to infinite dilution.²¹

1.1.3.2 Child's Method

Childs method (1981) is based on the use of crotonaldehyde as a sensor molecule (Figure 2), where changes in ¹H and ¹³C NMR chemical shifts, originating from the probe molecule, inform about changes in Lewis acidity of the medium it is dissolved in.²⁹

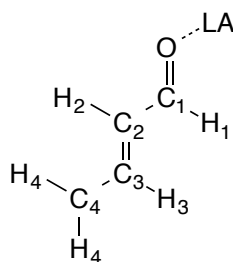


Figure 2. Crotonaldehyde sensor molecule developed by Childs et al.

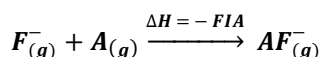
The strength of Lewis acidity can be measured by shifts of the H₃, H₄, C₃ and C₄ resonances (Figure 2). The complexation of a Lewis acid to crotonaldehyde is believed to maintain the conformation as *s-trans*, resulting in the Lewis acid being *syn* to the aldehyde proton but spatially removed from the other protons and carbons. Therefore, they are unaffected by changes to the anisotropy resulting from complexation and purely reflect changes in the electron distribution through the molecule. This technique is commonly used for analysis of boron containing complexes as it, along with the Gutmann AN technique (see Section 1.1.3.1), has been found to give a reliable comparison between species.²⁶

1.1.3.3 Adapted Solid State Methods

The Lewis acidity of both solids and liquids have been investigated by IR spectroscopy. Frequently a molecular probe, such as an N-donor, is used and the electron pair acceptor behaviour of the Lewis acid is measured spectroscopically. The use of a probe is similar to the techniques discussed previously with a stronger Lewis acid forming a stronger adduct. A stronger adduct will lower the vibrational frequency of the bond between the species, leading to an increased wavenumber. This allows for a direct comparison of species. Through this technique, Yang *et al.* produced a seminal study in which they order the relative Lewis acidity ionic liquids with [C₄mim]⁺ cations, finding increased acidity in the order CuCl < FeCl₃ < ZnCl₂ < AlCl₃.³⁰ In this study they applied two probes, pyridine and acetonitrile. Pyridine is effective as a probe molecule as the two distinct vibrations (Py- H) and (Py-Lewis acid) can be seen at *ca.* 1550 and 1450 cm⁻¹, respectively, allowing for the distinction between Brønsted and Lewis acidic sites, which cannot be achieved with Childs or Gutmann techniques.^{31,32} Acetonitrile has two characteristic IR active bands at 2292 and 2252 cm⁻¹ from CN stretching vibrations, which are shifted to a higher wavenumber in the presence of a Lewis acid, but remain unchanged by interactions with a Brønsted acid. To determine relative acidities, Yang *et al.* provided evidence of the species in equilibrium at different χ_{AlCl_3} , assigning the py-L.A. band at 1448 cm⁻¹ to [AlCl₄]⁻ whilst a band at 1454 cm⁻¹ to [Al₂Cl₇]⁻. For $\chi_{\text{AlCl}_3} \geq 0.55$, a band from the interaction between the acetonitrile and the Lewis acidic [Al₂Cl₇]⁻ can be observed.

1.1.3.4 Fluoride Ion Affinity

Another approach to quantifying Lewis acidity is through the thermodynamics of their reaction with a common species. The small size of the F⁻ anion means that it is capable of reacting with almost all Lewis acids, allowing for universal application. The most prevalent of these approaches is gas phase fluoride ion affinity (FIA). While several studies were aimed at ordering of Lewis acids by their ion affinity,^{33,34} it was the work of Bartlett *et al.* in 1984 which provided the first data which showed FIA to be a reliable method.³⁵ FIA, as defined by Equation 2, has subsequently become an effective technique for comparing Lewis acidity.³⁶



Equation 2

The main early issue was a lack of standardised technique, until the development of theoretical fluoride affinity calculations by Frisch *et al.* before the turn of the millennium.^{37,38} In 1996 and 2000 Dixon and colleagues demonstrated effective quantitative scale for fluoride ion affinities through computational approach, with the latter paper comparing a range of 106 Lewis acids, presenting them on a comparative pF⁻ scale (Equation 3).^{39,40}

$$pF^{-} = \frac{F^{-} \text{ affinity (kcal/mol)}}{10}$$

Equation 3

This method remains a commonly used measurement for acidity, however it requires computational calculations and so is not typically available to the experimental chemist, nor is it effective for describing systems such as ionic liquids with several species in equilibrium.

1.1.4 Superacidity

As with all aspects of Lewis acidity, the use of the term “superacid” varies based upon the acidity scale referred to. This contrasts with the Brønsted-Lowry superacidity, defined as a stronger Brønsted acidic than 100% H₂SO₄.⁴¹ For Lewis acids, since different scales of Lewis acidity place acidic species in different order, recommendations such as that by Olah that anything more acidic than anhydrous aluminium chloride should be classed as superacids, do not offer any directions for mode of comparison.⁴² Several perspectives for the definition of superacid have arisen since, from the effectivity of acid in catalysing a reaction, such as work by Hayashi *et al.* and Hasegawa *et al.* reporting “superacid catalysts” capable of promoting difficult Diels-Alder reactions,^{43,44} to the literal translation of describing metal triflates and triflimides as superacids, as derived from Brønsted superacids, HOTf and HNTf₂.⁴⁵ Krossing and co-workers postulated a FIA-based definition, stating that “molecular Lewis acids, which

are stronger than monomeric SbF_5 , in the gas phase, are Lewis superacids.³⁶ Using other scales a similar approach is taken, for example in the Gutmann AN scale, a superacid is described as having $\text{AN} > 100$, that is being more acidic than a 2 M solution of SbCl_5 in 1,2-dichloromethane.⁴⁶

1.2 The Boron Group and Borocations

1.2.1 Elements of the Boron Group

Group 13 consists of boron, aluminium, gallium, indium and thallium, collectively known as the boron group. The defining characteristic across this group is that they have 3 electrons in their valence shell, however the presence of filled d -orbitals means that aluminium, gallium, indium and thallium are post-transition metals, whereas boron is a non-metal or metalloid. This difference is clearly reflected in a range of properties of these elements. For example, as is typical of metals, the post-transition metals are conductors of both heat and electricity, whereas boron is only capable of conducting heat and electricity at high temperatures. Boron also differs in its appearance, as a black brown hard solid, compared to silver metallic appearance of the heavier members of Group 13. With three valence electrons, all boron group elements form the +3 oxidation state, however, with increasing atomic number down the group, the stability of the +1 oxidation state increases, to the degree that it is far more common in thallium compounds than the +3 state, owing to the inert pair effect.

All elements of the boron group form inherently electrophilic, stable complexes with halides, of a general formula MX_3 (ThX_3 compounds are less stable than their analogues based on lighter elements). The electrophilicity/Lewis acidity of these trihalides decreases down the group.⁴⁷ However, the bonding and molecular structure of trihalides are very different for boron and other Group 13 elements. Compounds of Group 13 metals with halides from chloride to iodide feature covalent bonds between the metal and the halide, and for aluminium, gallium and indium adopt a dimeric structure, M_2X_6 . Fluorides of post-transition metals fluorides are hexacoordinate and packed in a distorted octahedron, which gives them significantly higher melting points than other halides.⁴⁸ In contrast, boron halides all have a monomeric trigonal planar structure, D_{3h} , with the physical properties varying depending on the halide: BF_3 and BCl_3 are gases, BBr_3 is a liquid, and BI_3 is a solid at room temperature.⁴⁹

Lewis acidity of boron halides, quantified through the energy of interaction with an oxygen or nitrogen Lewis base, increases with the atomic radius of the halide.⁵⁰ This is perhaps unexpected, as the more electronegative halides would be expected to generate a more electron deficient boron centre. Initially, this counter-intuitive observation was believed to stem from back-bonding from the halide to the p -orbital of boron, highest for fluorine due to similar

orbital size to boron, and weakest for iodine. This interaction would increase electron density on the boron centre, Lowering its Lewis acidity and countering the electron withdrawing effect of halides.⁵¹ However, computational studies by Politzer and colleagues revealed that the $2p\pi$ orbital of boron was more populated in BCl_3 than BF_3 , and there was no systematic decrease in back-bonding as the halide size increased.⁵² Instead, Politzer and colleagues suggested that it was the interaction with the Lewis base which determined the Lewis acidity of the boron halides, which is to say that a greater charge capacity on the halide is responsible for greater interaction between Lewis acid and base in the order $\text{BF}_3 < \text{BCl}_3$.^{52,53} However, a more robust explanation is the changing energetic requirements for molecular distortion as the trigonal planar boron halide, on interaction with a Lewis base, becomes tetrahedral. With a strong Lewis base, such as an oxygen or nitrogen donor, its positivity repels the halide ligands, decreasing XBX bond angles, a distortion which is more efficient with the longer bond lengths, which increase with larger halides.¹⁶ In contrast, with a weak Lewis base, such as CO , this repulsion does not occur, the trigonal planar geometry is not affected, and the strongest Lewis acid in the series with respect to CO is – as expected – BF_3 .¹⁶ This again demonstrates the extremely subjective nature of Lewis acidity, which truly appears irrelevant without considering in the context of a particular base or a defined catalytic reaction.

1.2.2 Borocations

Borocations are inherently extremely electrophilic, because electrophilicity of the empty p orbital on boron is enhanced by the positive charge. Although syntheses of tetracoordinate borocations was published by Dilthey and colleagues in 1906,⁵⁴ this chemistry lay dormant until the mid-1980s, when Kölle and Nöth published a seminal review of boron cationic chemistry, laying the groundwork for the fundamentals of the field. They also formalised the nomenclature, coining the names borinium and borenium to describe dicoordinate and tricoordinate species, respectively, in addition to the previously described tetracoordinate boronium cation (Figure 3).^{55,56} Across this family of borocations, the geometry of the molecules is dictated by increasing sp -hybridization, with borinium cations having a near linear geometry from sp hybridized orbitals, borenium cations are trigonal planar with sp^2 boron, while boronium cations are tetrahedral with sp^3 hybridized orbitals.⁵⁷

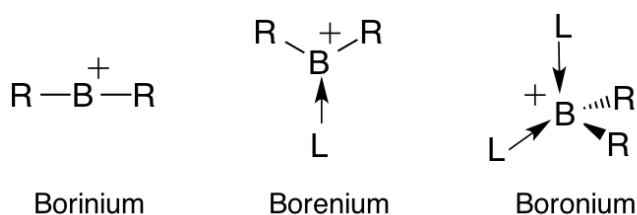


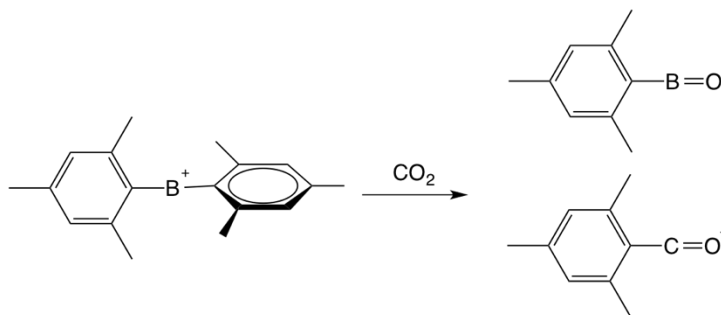
Figure 3. The three classically described borocations, divided by their coordination number. R represents a monoanionic group and L is a 2-electron donor ligand.

1.2.2.1 Borinium cations

It will not come as a surprise that the borinium species is incredibly reactive and consequently challenging to handle in solution, prone to interactions with either solvent molecules or any counterions. Therefore, most information on reactivity and structure of borinium ions originate from the gas phase studies.⁵⁷ Ligand selection is crucial in the development of stable borinium cations in the condensed phase. Early borinium cations, such as bis(diisopropylamido)boron, developed by Higashi *et al.*, were characterised using NMR and IR spectroscopies, but were reported to be unstable in a solvent.⁵⁸ Nevertheless, even these early compounds found their use in a recent work by Stephan and co-workers, employed for hydroboration of simple organic molecules, including a ketone, a nitrile and an alkyne.⁵⁹

Being isoelectronic to a hypothetical $\text{R}-\text{C}^{2+}-\text{R}$ cation, borinium cations' deviation from the octet rule gives them the potential for incredible reactivity through their electron deficiency, which continues to fascinate boron chemists. In 2014, Shoji and colleagues demonstrated a borinium cation stabilised by two mesityl groups (Scheme 2).⁶⁰ The exceptional Lewis acidity of this species is portended to by the chemical shift of its ^{11}B NMR spectroscopic signal at 93.9 ppm, significantly downfield with respect to previously reported borinium species (22 – 56 ppm).^{55,61,62} DFT and X-ray crystallographic studies indicate a degree of π -donation from the aromatic ligands, playing a crucial role in stabilisation, differing from previously reported structures with lone pair stabilisation from amino ligands.^{58,63} This molecule has been demonstrated to perform an unusual deoxygenation of CO_2 (Scheme 2) indicating its powerful Lewis acid-type reactivity,⁶⁰ and was used to generate a novel thioaroyl cation.⁶⁴

Scheme 2. The structure of the borinium cation $[B(\text{Mes})_2]^+$ and the products of arylation–deoxygenation of CO_2 .



1.2.2.2 Boronium cations

On the opposite side of reactivity to borinium species lie tetracoordinate boronium cations, the most stable form of borocations. With four ligands surrounding a small boron centre, steric crowding may become an issue, with bulky ligands typically disfavoured.⁵⁶ Their structure typically comprises two σ -donor ligands, often amines, and two covalently bonded groups.⁵⁷ Unlike highly reactive borinium and borenium species, they are typically air- and moisture-stable, owing to a filled coordination sphere, and therefore significantly easier to handle. However, this comes at a price of low reactivity in general. Electrophilic activity of boronium cations in reactions is realised by acting as “masked” borenium species, that is by losing an L-type ligand, or in $\text{S}_{\text{N}}2$ type reactions.⁶⁵

In the context of ionic liquids, boronium cations have been reported since 2005, the early years of mainstream ionic liquid research.⁶⁶ The synthesis of these cations was designed based upon the isolobal principle, whereby the structure of adjacent boron and nitrogen atoms have an overall character which can be approximated to that of carbon, being both adjacent to carbon and having one fewer and one more electron than carbon respectively. In their work on boronium ionic liquids, Fox *et al.* adapted well studied ionic liquids with N-N'-dialkylimidazolium cations to contain a $-\text{BH}_2\text{-NR}_3$ moiety replacing at $-\text{CH}_2\text{-CR}_3$ chain in the structures as an isolobal substitution. They subsequently patented the synthetic strategies for these cations in 2010.⁶⁷

1.2.2.3 Borenium cations

The study of borenium cations have been an area of significant growth over the last decade, and constitutes an important part of this thesis. Intermediate between borinium and boronium, borenium cations are typically used as strong Lewis acids in catalysis, as they have a formal positive charge on the boron, in combination with an empty 2p orbital, which generates high electrophilicity. Their structure typically features two covalently bound σ -donors (R) and one

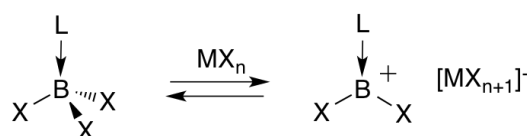
datively bound donor ligand (L) which serves to provide stability by reducing the electron deficiency of the boron centre. The stability afforded by the donor means that the synthetic chemist is offered more variation in the covalently bound R substituents, which are no longer relied upon for strong σ and π donation.⁶⁸ The most commonly encountered L ligands for these molecules are N- and O-donors.⁵⁷ When Piers *et al.* reviewed the state of play for borocation research in 2005, they reported that “well defined three-coordinate borenium cations have been almost as elusive as for their borinium counterparts” and predicted a “quantum leap” in their use.⁵⁷ In his 2015 review, Ingleson declared this to have been prescient as the field burgeons.⁶⁵

1.2.2.3.1 Synthetic strategies

There are four main synthetic strategies yielding borenium cations: halide abstraction by a metal halide, non-reversible bond heterolysis, reversible bond heterolysis and nucleophilic attack on a ligand appended onto a boron atom. These strategies are shortly described in this section.

The first observable borenium cation, synthesised by Wiggins and Ryschkewitsch in 1970,⁶⁹ was generated by halide abstraction from a tetracoordinate boron compound by inducing heterolysis of the B-X bond (Scheme 3). The result was a tricoordinate borenium cation accompanied by a halometallate anion, remaining in a dynamic equilibrium with the starting materials.

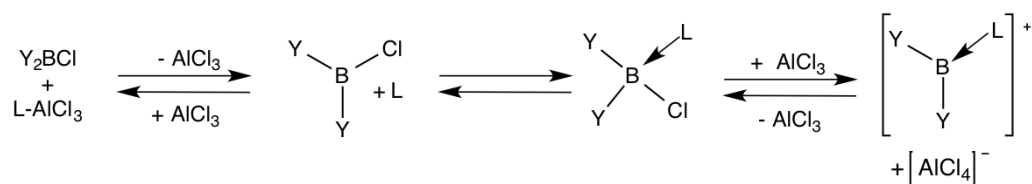
Scheme 3. Borenium synthesis *via* B-X bond heterolysis.



This equilibrium leads to simultaneous presence of multiple equilibrated species in solution. Ingleson and colleagues identified five different electrophilic species which can arise from such equilibrium, which makes it problematic to elucidate active species (or rather, results in several species with different levels of activity present).⁷⁰

A further issue is ligand scrambling, which induces further complication to the actual speciation, this is where ligands are exchanged between Lewis acidic centres.^{55,71} This was elegantly demonstrated by Solomon *et al.* to result from the strength of the charge on the boron atom.⁷² The transfer of a halide to the metal centre occurs *via* an $\text{S}_{\text{N}}2$ mechanism and a stronger attraction between the $[\text{AlCl}_4]^-$ and boron encourages the formation of a halide-bridged intermediate. Bagutski *et al.* demonstrated the equilibrium which forms during this synthesis in Scheme 4.⁷⁰

Scheme 4. The major equilibria present in borenium halometallate mixtures on the formation of [BY₂L][AlCl₄].



This is seen in the synthesis of borenium ionic liquids, with a general formula [BCl₂(mim)][Al₂Cl₇], which are in a dynamic equilibrium with BCl₃, [AlCl₄]⁻, [AlCl₃(mim)], [AlCl₂(mim)₂]⁺ and [AlCl₃(mim)₂] due to this redistribution effect.⁴ This equilibrium is identified by the emergence of a sharp peak at 47 ppm in ¹¹B NMR spectroscopy which corresponds to BCl₃. An extreme example of this mechanism was described in the synthesis of borenium ionic liquids reported by Coffie *et al.*⁴ In the presence of metal chlorides, the boron complex [BCl₃(P₈₈₈O)] dissociated with the phosphine oxide exclusively interacting with the metal centre with BCl₃ being the only boron containing species observed. The importance of the strength of the L donor interaction is reinforced as it needs to be strong enough to stabilise a tri-coordinate borenium centre following bond heterolysis, a good B-L overlap will also aid heterolysis by weakening the B-X interaction.⁶⁵ Therefore strongly electron withdrawing groups on the L donor species will reduce its ability to donate to the boron, making halide abstraction more challenging and in extreme cases lead to ligand scrambling.

Non-reversible bond heterolysis relies on the use of a halide abstracting agent in the form of a salt, which provides an anion for the borenium cation, and generates a removable side product (Scheme 5).

Scheme 5. Borenium synthesis *via* non-reversible bond heterolysis.

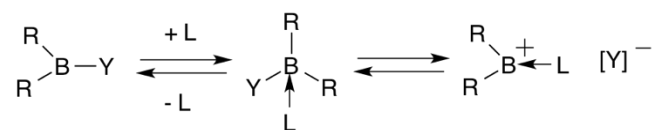


An example of halide abstracting agent used for this synthetic strategy, where the X in [BX₃L] is a hydride, is [Ph₃C][B(C₆F₅)₄], which gives an organic side product, Ph₃CH, easily removed by washing with an organic solvent.⁷³

Reversible bond heterolysis is based on using a charge-neutral tricoordinate boron species, [BR₂Y], as the precursor, and a ligand, L, which donates into the boron centre and weakens the B-Y interaction (Scheme 6). This differs from the route described in Scheme 5, as no

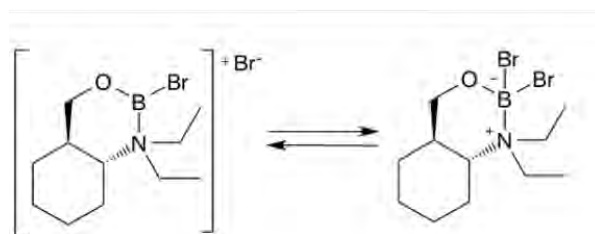
abstracting agent is required to initiate the B-Y bond cleavage, and makes the formation of a tricoordinate boron species entirely reversible, to yield $[\text{BR}_2\text{L}][\text{Y}]$.

Scheme 6. The formation of a tricoordinate boron cation *via* reversible bond heterolysis.



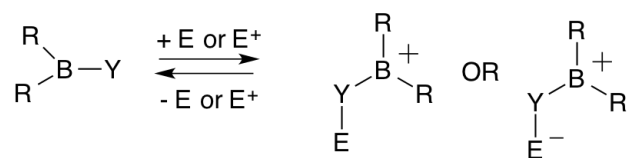
This pathway is commonly seen in borenium catalysts which have a “masked” tetracoordinate resting state (with extremely labile ligand) and the active catalytic species is formed on loss of a ligand, for example a halide, as exemplified by borenium salt developed by Hayashi *et al.* to catalyse enantioselective Diels-Alder reaction (Scheme 7).^{43,57}

Scheme 7. The enantiomerically pure borenium catalyst for the Diels-Alder reaction developed by Hayashi *et al.* and the “masked” borenium resting state.



Electrophile coordination to a ligand on boron can also result in the effective formation of a borocation (Scheme 8). In their review of borocations, De Vries *et al.* described the protonation of aminoboranes as the “oldest method for generating transient as well as stable borenium salts”.⁷⁴ This synthetic strategy has been expanded over the past decades with a wide range of electrophiles capable of attacking the nitrogen adjacent to the boron, such as BH_3 , and while these complexes may not contain a net charge (in the case of charge-neutral electrophiles), a borenium subunit can be identified. Furthermore, functionality of the overall species as a strong Lewis acid has been demonstrated, therefore Ingleson has found it appropriate to consider them as borocations.^{65,75}

Scheme 8. The formation of a borenium cation *via* the coordination of an electrophile.



1.2.2.3.2 Ligand development

The ligands on the boron centre play multiple roles. They are required to stabilise the charge on the boron by donating electron density. They are typically sterically bulky to prevent coordination by the anion, solvent or other species present. Finally they can also provide functionality to the borenium species, for example by modifying acidity or enantiomeric control. The development of ligands is described briefly in this section.

The first borenium cations synthesised by Wiggins and Ryschkewitsch contained simple N-donor ligands, such as 4-picoline which provided stabilization of the boron centre through electron donation and provided protection of the boron centre through steric bulk.^{55,69} This philosophy was continued by work by Narula *et al.* in the 1980s which expanded the family of borenium ions with chloroaluminate counter ions to include both the pyridine based donor but also a bidentate N,N,N',N'-tetramethylethylenediamine donor ligand to further protect the boron centre.⁷⁶ The function of borenium cations in broader catalysis during this period was not established, with studies on their function typically probing the species present in equilibria.⁷¹

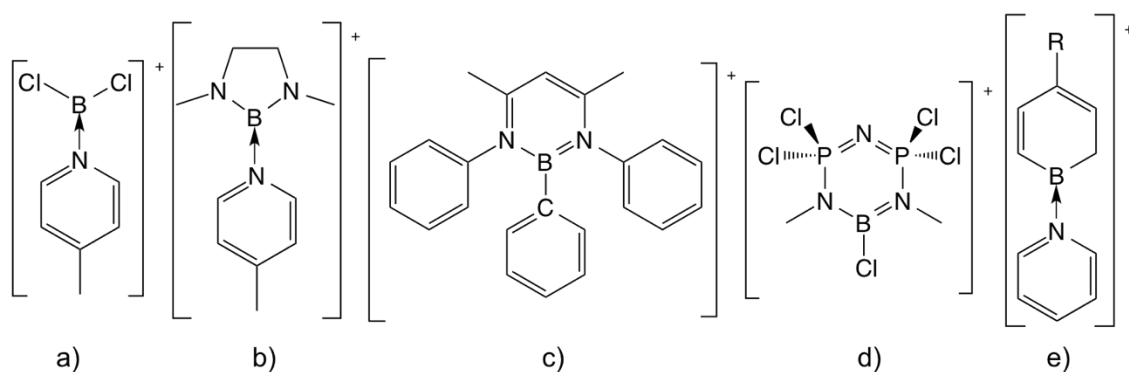


Figure 4. The development of borenium cations *via* boracycles from the first recorded borenium cation (a) in 1970,⁶⁹ the introduction of five-membered boracycle (b) in 1985,⁷⁶ an arylated analogue (c) by Cowley *et al.*,⁷⁷ Gates *et al.* formed a borazine-phosphazine hybrid borenium cation in 2003 (d)⁷⁸ and finally a nitrogen free boracycle (e) from Ghesner *et al.*⁷⁹

Boracycle synthesis continued as a key stabilisation focus of borenium cation synthesis over the following twenty years with several examples of isolatable rings reported, for example with bulky aryl substituents on the nitrogen groups which promoted crystallisation which

resulted in X-ray crystallographic identification of the borenium cation.⁷⁷ An interesting example of a borenium boracycle is that by Gates *et al.* (Figure 4d), which contains a ring constructed from PNP bonds in a borazine-phosphazine hybrid and has been found to be largely planar.^{78,80} This was followed by work from Ghesner *et al.* synthesising a borocyclic unit without nitrogen atoms and forming a borenium cation, stabilised by pyridine, in a manner familiar to the first borenium cations from the 1970s.⁷⁹

Bidentate ligands are commonly found in applications of borenium cations as they are less likely to undergo ligand scrambling. An example of this is the Diels-Alder catalyst developed by Hayashi in 1996, which features an enantiomerically pure borenium cation, shown in Scheme 7.⁴³ This catalyst was designed for its high Lewis acidity (which was alluded to in Section 1.1.4) which arises through the electron deficiency of the boron centre. However, through the ligand design, in creating a chiral bidentate ligand for the boron, the reaction becomes enantioselective giving enantiomeric excesses greater than 90% across a range of substrates.

1.2.2.3.3 Anion development

A variety of anions to accompany borenium cations have been used in the literature. When describing the development of their borinium cation in 2014, Shoji *et al.* supposed that the high Lewis acidity of the borinium cation would mean only the most inert and sterically hindered anions would avoid interaction, typified by the $[\text{HCB}_{11}\text{Cl}_{11}]^-$ carborane anion. To their surprise, also the more common $[\text{B}(\text{C}_6\text{F}_5)_4]^-$ anion was also appropriate, making the work far more synthetically accessible.⁶⁰ Borenium synthesis tends not to be quite so rigorous in its demands for anion steric hindrance owing to the extra coordination around the boron centre.

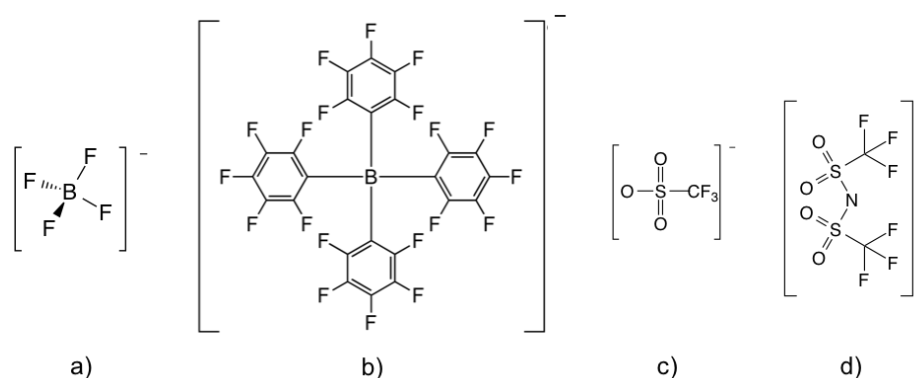


Figure 5. The structure of anions a) boron tetrafluoride, b) tetrakis(pentafluorophenyl)borate, c) triflate, $[\text{OTf}]^-$, and d) bistriflimide, $[\text{NTf}_2]^-$.

The high Lewis acidity of the cation necessitates a robust anion, with reports of fluoride abstraction with traditional $[\text{BF}_4]^-$ anions (Figure 5).⁸¹⁻⁸³ Although when sufficiently bulky

ligands are employed, the anion $[\text{PF}_6]^-$ has been shown not to interact with the borocation.⁸⁴ As discussed above, the $[\text{B}(\text{C}_6\text{F}_5)_4]^-$ anion is sterically crowded as to be effectively inert towards borocation centres and appeals to inorganic chemists for the π - π stacking capabilities of the phenyl rings which promote crystallisation. From an ionic liquids perspective, however, this is undesirable. Metal halides, such as $[\text{AlCl}_4]^-$, and even dimeric species such as $[\text{Ga}_2\text{Cl}_7]^-$, have been widely used to access borenium cations as they are effective halide abstracting agents. These anions are not necessarily innocent of any interaction with the boron centre, but Muthaiah *et al.* proposed that these interactions may be beneficial to the stabilisation of the cation, without reducing its Lewis acidity.⁸⁵ This work also explored the use of triflate and bistriflimide anions, shown in Figure 5, in borenium complexes. A neutral $[(\text{NHC})\text{BCl}_2(\text{OTf})]$ adduct formed on the introduction of triflate to these sterically encumbered boron centres. The boron chloride complex with the most bulky NHC, 1,3-di-*tert*-butylimidazolium, on combination with silver bistriflimide was determined by X-ray crystallography and ^{11}B NMR spectroscopy to form a borenium cation.⁸⁵

1.3 Lewis Acidic Ionic Liquids

Ionic liquids have come to be found in a huge variety of regions of the study of chemistry, as solvents, battery electrolytes and catalysts. Introducing Lewis acidity to ionic liquids is traditionally achieved through the anionic species, typically a halometallate and more specifically the chloroaluminate(III) anion. This contrasts with Lewis acidity across broader inorganic and synthetic chemistry where a huge variety of metal centres are utilised.

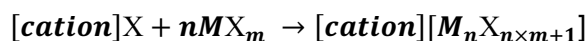
1.3.1 Historical Context

Traditionally it is accepted that the first ionic liquid observed was that reported by Paul Walden in 1914, the combination of ethylamine with concentrated acid giving $[\text{EtNH}_3][\text{NO}_3]$ with a melting point of 13-14 °C.⁸⁶ However it has been argued that work by Osteryoung, Wilkes and Hussey over the mid twentieth century meant use of the term “ionic liquid” typically referred to halometallate systems.⁸⁷ Indeed in his account of the history of ionic liquid Wilkes describes chloroaluminates as the bridge between traditional high melting molten salts (for example LiCl-KCl) and “present ionic liquids” (such as those with tetrafluoroborate or triflate anions).⁸⁸ Early work by Brown and Pearsall in 1952 demonstrated the use of chloroaluminates as catalysts for Friedel-Crafts alkylation, observing the $[\text{AlCl}_4]^-$ and $[\text{Al}_2\text{Cl}_7]^-$ anions in equilibrium with the intermediate toluenium cation.⁸⁹ This led to a natural curiosity for the development of an ionic liquid to catalyse the reaction and the use of $[\text{C}_2\text{mim}]\text{Cl} - \text{AlCl}_3$ in

Friedel-Crafts alkylation by Boon *et al.* demonstrated the first use of a Lewis acidic ionic liquid as a catalyst, its significance highlighted by the 686 citations it has today.⁹⁰

1.3.2 Chlorometallate Ionic Liquids

The synthesis of chlorometallate ionic liquids is typically a solventless combination of a metal halide and an organic halide salt in an exothermic (to varying degrees) process, to undergo the halide abstraction from the organic halide salt to form an anionic and cationic species Equation 4.



Equation 4

This synthetic method of combining components in different ratios was developed in the Air Force Academy by Hussey to generate low melting electrolytes for batteries.⁹¹ This method was discussed in the context of other commonly used techniques for ionic liquid synthesis by Welton,⁹² highlighting both the simplicity of the direct combination of components the need for caution due to the exothermic nature of the synthesis. The ionic liquids can be varied by their composition. This is expressed as the molar ratio of the metal halide, χ_{MCl_3} , as described in Equation 5.

$$\chi_{\text{MX}_m} = \frac{n(\text{MX}_m)}{\sum(n)}$$

Equation 5

By varying the value of χ_{MCl_3} it is possible to access a variety of homogeneous ILs, although the range of χ_{MCl_3} values which give this are dependent on the metal and organic cation.

1.3.2.1 Speciation

Across the range of χ_{MCl_3} values for homogenous chlorometallate ionic liquid an interplay between anions in equilibrium proceeds, with different anionic species present depending on the molar fraction of each component (Figure 6).

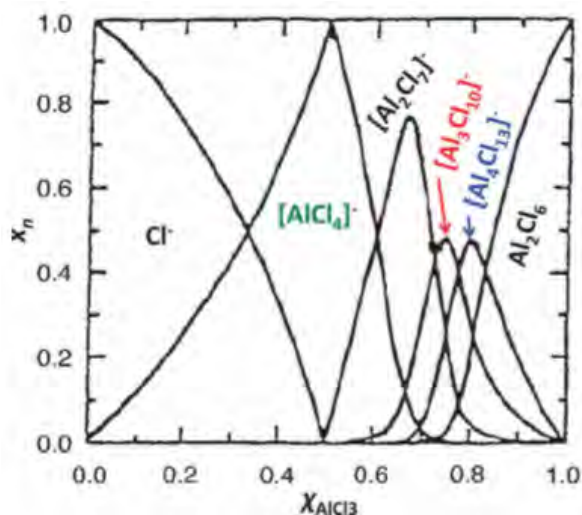


Figure 6. The concentration of anionic species in the system [C₂mim]Cl-AlCl₃ at 200 °C, calculated from a thermodynamic model. (adapted from)

The role of the cation in halometallate ionic liquids is traditionally considered to have no influence of the Lewis acidity of the system, although this has been challenged in recent work (see Section 1.3.4). Instead, these organic species are varied to control viscosity, density or melting point.⁹³ Conversely, anionic species are crucial to Lewis acidity, and influence both physical and chemical characteristics of the system. The generation of the phase diagram given in Figure 7 was achieved by Fannin *et al.*⁹⁴ and speciation of these systems using analytic techniques was carried out through Raman spectroscopy⁹⁵ and ²⁷Al NMR spectroscopy.⁹⁶

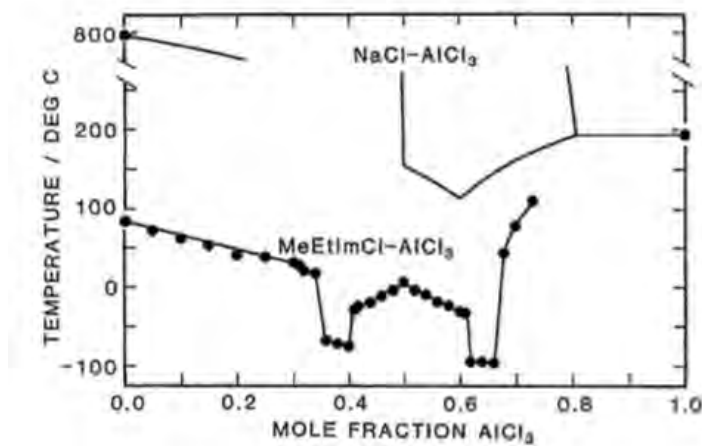
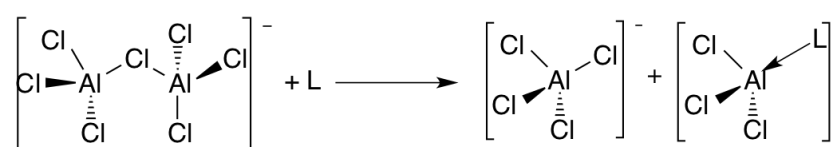


Figure 7. Phase diagrams of NaCl-AlCl₃ and 1-ethyl-3-methyl imidazolium chloride-AlCl₃.

In the phase diagrams given in Figure 7 for 1-ethyl-3-methyl imidazolium chloride-AlCl₃ (compared to NaCl-AlCl₃), at the equimolar composition (where $\chi_{\text{AlCl}_3} = 0.5$) a congruent melting point can be seen, associated with the exclusive presence of [C₂mim][AlCl₄]. At any other molar ratio, an equilibrium exists between different anionic species (see also Figure 6), which are crucial to the Lewis acidity/basicity. Halide anions, here Cl⁻, are Lewis basic.^{97,98}

The monomeric $[\text{AlCl}_4]^-$ is coordinationally saturated by the four chloride ligands, therefore not Lewis acidic (often considered ‘neutral’). Where the organic chloride salt is in excess (*i.e.* $\chi_{\text{AlCl}_3} < 0.5$) both chloride ions and $[\text{AlCl}_4]^-$ are in equilibrium, meaning that the composition will be Lewis basic. With an excess of AlCl_3 , $0.5 < \chi_{\text{AlCl}_3} \leq 0.67$, the equilibrated species are monomeric $[\text{AlCl}_4]^-$ and dimeric $[\text{Al}_2\text{Cl}_7]^-$. Although aluminium is tetracoordinate in both $[\text{AlCl}_4]^-$ and $[\text{Al}_2\text{Cl}_7]^-$, and with four chloride ligands aluminium is unable to achieve higher coordination owing to steric hindrance,^{19,21} the $[\text{Al}_2\text{Cl}_7]^-$ anion is strongly Lewis acidic in its behaviour. The structure of $[\text{Al}_2\text{Cl}_7]^-$ has been determined as shown in Scheme 9 below, with the chloride bridge is easily broken, allowing for what is termed ‘latent Lewis acidity’.⁶⁵

Scheme 9. Reaction between Lewis acidic $[\text{Al}_2\text{Cl}_7]^-$ with a Lewis base, L.



Above $\chi_{\text{AlCl}_3} > 0.67$, although larger chloroaluminate oligomers are postulated, they tend to be in equilibrium with solid AlCl_3 (the sample is not a homogeneous liquid but rather has a cloudy appearance or a solid deposit at the bottom of the vessel).

Although the archetypal chlorometallate ionic liquids contain aluminium, there is a wide range of metal centres capable of forming Lewis acidic ionic liquids.^{1,87} The speciation of these chlorometallates differs from that observed in aluminium. For compositions with low metal chloride loadings the anionic species detected are free chlorides and saturated chlorometallate anions. When the metal chloride concentrations increase from this saturated species then, as seen in the aluminium chloride example, there are three different possibilities which may occur. Firstly, the formation of oligomeric anions, such as those shown in Scheme 9, with bridging chlorides may occur, leading to latent Lewis acidity. Secondly monomeric but coordinatively unsaturated chlorometallate species form, which result in Lewis acidity of the composition. Finally, the excess metal chloride may precipitate out of the system.

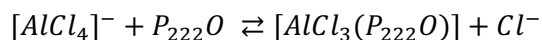
In the example of chlorogallate(III) ionic liquids the speciation of the anions is similar to that of aluminium, which is not surprising given their proximity in Group 13 of the periodic table. However, at higher concentrations of chlorogallate, ionic liquids remain homogeneous with no precipitation at $\chi_{\text{GaCl}_3} \leq 0.75$, and even higher GaCl_3 loadings. This corresponds to the existence of oligomeric anions such as $[\text{Ga}_3\text{Cl}_{10}]^-$, a strongly reactive species.⁹⁹⁻¹⁰¹

Following down the Group 13, indium(III) is larger and able to coordinate six chloride ligands, with the species $[\text{InCl}_6]^{3-}$ forming at $\chi_{\text{InCl}_3} = 0.25$, and $[\text{InCl}_5]^-$ believed to form at $\chi_{\text{InCl}_3} = 0.33$, although not explicitly proven.^{47,101,102} Chloroindate(III) anions do not form oligomeric

species, and where $\chi_{\text{InCl}_3} > 0.5$ the metal chloride precipitates from the liquid. However, $[\text{InCl}_4]^-$, which makes a congruently melting salt at $\chi_{\text{InCl}_3} = 0.5$, is not entirely Lewis-neutral, but instead mildly Lewis acidic as its coordination sphere is unsaturated.¹⁰³

1.3.2.2 Acidity

Gutmann AN approach has emerged as the method of choice for probing Lewis acidity of ionic liquids. This method was first applied to Lewis acidic ionic liquids in the late 1980s and early 1990s by Osteryoung and colleagues. In their first work the ionic liquids were aluminium chloride with either 1-ethyl, 3-methyl imidazolium chloride (ImCl) or N-(1-butyl)pyridinium chloride $[\text{C}_4\text{Py}]$ at different ratios.¹⁹ The acceptor number measurements recorded for these species demonstrated high Lewis acidity with a Gutmann AN of 103 recorded for the $[\text{C}_4\text{Py}]\text{Cl}-\text{AlCl}_3$ $\chi_{\text{AlCl}_3} = 0.67$. This demonstrated that the chlorometallate ionic liquids were slightly superacidic in AN terms. The effect of changing cation was demonstrated to be minimal, for example for both systems with $\chi_{\text{AlCl}_3} = 0.5$ ANs recorded the difference between the two values was just 0.4. However, in this work they also demonstrated that the basic composition $\text{AlCl}_3\text{-Bu-PyCl}$ $\chi_{\text{AlCl}_3} = 0.45$ gave an AN of 98.2. Speciation studies show that the anion which forms in this composition is $[\text{AlCl}_4]^-$, this interacts with the P_{222}O probe to undergo chloride displacement as described by Equation 6 below.¹



Equation 6

In subsequent work, the group studied systems where $\chi_{\text{AlCl}_3} \geq 0.5$ and using ^{31}P NMR spectroscopic data they were able to correlate the chemical shifts to the relative concentrations of $[\text{AlCl}_4]^-$ and $[\text{Al}_2\text{Cl}_7]^-$.¹⁰⁴ Gutmann acceptor number measurements of ionic liquids with chlorometallates with metals other than aluminium has also been demonstrated, Across several studies from Swadźba-Kwaśny and colleagues further work was taken to understand the effect of changing metal centre.^{21,105,106} This is summarised in Figure 8 where five metal chlorides with the structure MCl_x (where $\text{M} = \text{Al}^{\text{III}}, \text{Ga}^{\text{III}}, \text{In}^{\text{III}}, \text{Zn}^{\text{II}}$ and Sn^{II}) were combined with $[\text{C}_8\text{mim}]\text{Cl}$.

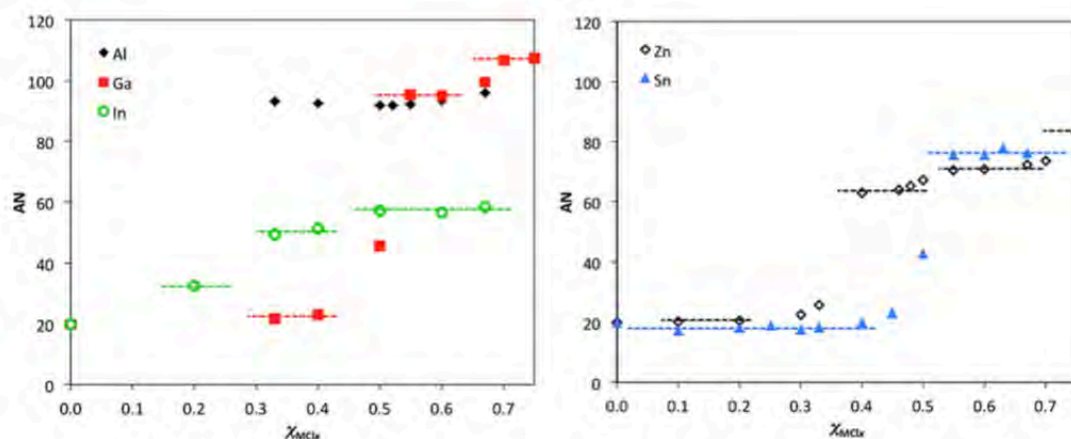


Figure 8. Gutmann acceptor number values recorded for ionic liquids $[\text{C}_8\text{mim}]\text{Cl-MCl}_x$ (where $\text{M} = \text{Al}^{\text{III}}, \text{Ga}^{\text{III}}, \text{In}^{\text{III}}, \text{Zn}^{\text{II}}$ and Sn^{II}) plotted against molar fraction. (adapted from ^{21,105,106})

Unlike for chloroaluminates, broad trends across compositional range are seen for other metal centres (Figure 8). For gallium systems three acidities are observed, at low concentrations of metal chloride, which are basic, the AN is around 22. At acidic concentrations $0.5 < \chi_{\text{GaCl}_3} < 0.67$ the acceptor number increases to around 95, finally at gallium chloride concentrations $\chi_{\text{GaCl}_3} > 0.67$ even higher AN values are recorded around 107. This is reflective of the formation of three gallium chloride anions: $[\text{GaCl}_4]^-$, $[\text{Ga}_2\text{Cl}_7]^-$ and $[\text{Ga}_3\text{Cl}_{10}]^-$ with the dominant species determining the measured acidity of the liquid. A far smaller range of AN values is reported for chloroindate(III) systems, from ~ 32 to 58. This is because unlike the oligomeric species which form in chloroaluminate or gallate systems, only the monomeric indium anions $[\text{InCl}_6]^{3-}$, $[\text{InCl}_5]^{2-}$ and $[\text{InCl}_4]^-$ form, and therefore even when $\chi_{\text{InCl}_3} > 0.5$ acceptor numbers do not increase above 58, indicating weak acidity.²¹ In chlorostannate(II) systems, a sharp jump in acidity is seen as the concentration of metal chloride overtakes that of the cation. This results from a change in the dominant anion, which is the non-acidic $[\text{SnCl}_3]^-$ for compositions where $\chi_{\text{SnCl}_2} < 0.5$, which gives an AN of *ca.* 18 but forms the dimeric $[\text{Sn}_2\text{Cl}_5]^-$ for compositions where $\chi_{\text{SnCl}_2} > 0.5$, which gives an AN of *ca.* 76.¹⁰⁶ Chlorozincate(II) systems also form dimeric structures, $[\text{Zn}_2\text{Cl}_6]^{2-}$, these are in equilibrium with the monomeric species, $[\text{ZnCl}_4]^{2-}$, and are present in compositions where $\chi_{\text{ZnCl}_2} > 0.33$, as evidenced by an increase in Gutmann acceptor number from about 20 to 75.

1.3.2.3 Applications

The use of chlorometallate ionic liquids has largely focused on aluminium systems, for their affordability and early development. Key examples in catalysis are applications as Lewis acids (*e.g.* in the Diels-Alder reaction), in carbocationic reactions (the generation of Brønsted superacidic species through reaction with water/protic additives), Friedel Crafts alkylations,

sulfonylations and arylations, and as co-catalysts in transition metal catalysis.^{87,92,107} As discussed previously, each halometallate system will vary in the anions which form, the concentrations at which they are found and the hydrolytic stability of the composition and therefore effective catalytic systems involving chlorometallate ionic liquids will vary for each metal.

Industrially, chlorometallates have been used in olefin oligomerisation in Difasol by IFP and in refinery alkylation in Ioniklyation by PetroChina using chloroaluminate systems.¹⁰⁸ In the Ioniklyation process isobutene is alkylated in a strongly Lewis acidic environment. In 2006 PetroChina revealed that, following testing in a pilot plant, a 65,000 tonne/year H₂SO₄ alkylation unit was retrofitted in China with a chlorometallate ionic liquid system, composed of an Al(III)/Cu(I) anionic species with a cation. The consequence of this retrofit was a yield increase compared to the sulfuric acid and a marked increase in capacity of the unit of 40 %.^{109,110} However the plant has since closed as a result of corrosion issues and chloride contamination of the product. In 2013 a similar system was introduced in a collaboration between PetroChina, Shell, Deyang and the National Science Foundation of China.¹¹¹

More recently the development of the ISOALKY technique has been developed by Chevron Phillips as a liquid alkylation catalyst, avoiding the use of hydrofluoric and sulfuric acids typically used in this process.¹¹² Developed over the course of 20 years, Chevron ran a small demonstration unit for 5 years in Salt Lake City, the success of which encouraged Honeywell UOP to licence the technology. In 2017 the company broke ground on the development of the retrofitting of the hydrofluoric acid unit to be compatible with the ISOALKY technology, and it is expected to be operational in 2020.¹¹³ The scheme of the plant is shown in Figure 9. The development of this process has led to Honeywell and Chevron receiving the 2017 Platts Breakthrough Solution of the Year award. A key advantage of using ionic liquid catalyst in this context is to avoid the need to transport significant quantities of hydrofluoric acid to the plant, the ISOALKY catalyst can be regenerated on site, reducing consumption. The process is also less sensitive, producing alkylate from a wider range of feedstocks than the previous catalysts.¹¹² The purity of the product is also higher, boasting minimal olefin and aromatic content.¹¹⁴

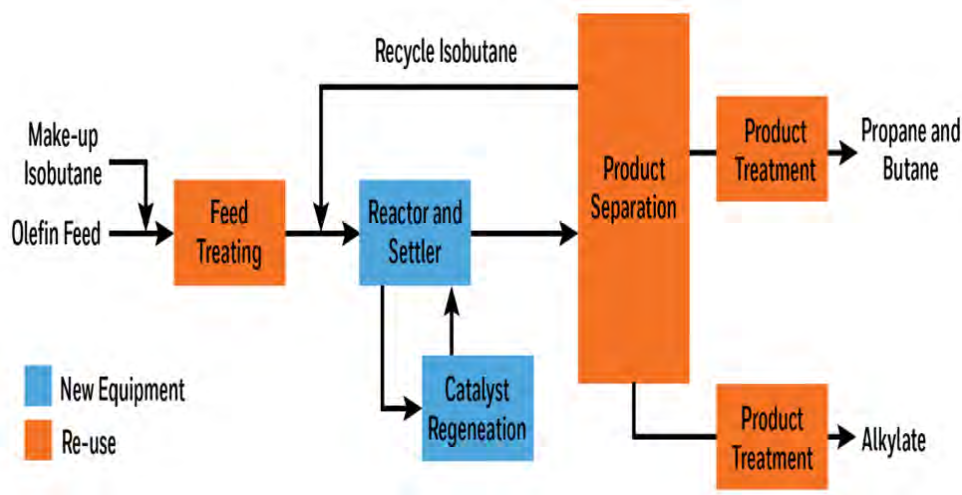


Figure 9. ISOALKY process plant scheme illustrating the retrofit which is currently underway.¹¹³

These plants demonstrate the industrial potential of Lewis acidic liquids in the production of high octane fuels from alkylates. In previous plants, either sulfuric or hydrofluoric acid had been used as the catalyst as it was believed that something more acidic, like aluminium(III) chloride, would be too acidic and promote side reactions.¹¹⁵ The work of Nobel laureate Yves Chauvin indicated that chloroaluminate ILs could catalyse isobutene-butene alkylations,¹¹⁶ this work was continued by Jess and colleagues across a series of papers.¹¹⁷⁻¹²¹ Crucially it is the acidity of the ionic liquid which determines its effectiveness as a catalyst in these reactions, in a study by Yoo *et al.* the effect of composition revealed that optimum catalytic activity for their system was achieved, not with the most or least acidic IL, but with a maxima in the middle of their range.¹²² This demonstrates the importance of Lewis acidic tunability and, with the dynamic equilibria which exist among the anionic species, the specific composition of the ionic liquid.

1.3.2.4 Limitations of chlorometallate ionic liquids

There are many advantages to using chlorometallate ionic liquids, as demonstrated in the previous section. However, a key handling challenge of working with chlorometallate species is their propensity to breakdown to release HCl in the presence of water.⁹² In synthesising ionic liquids with alkylimidazolium halide salts and similar, which are hygroscopic, care must be taken to ensure that they are dry prior to introduction to the metal halide.¹⁹ This produces additional species which are oxide- or proton- containing, interrupting the dynamic equilibrium so crucial to their Lewis acidity. Some of these species may be highly Brønsted acidic and this may be either disruptive or beneficial to the application.⁸⁷

Further to this, an intrinsic drawback of introducing these ionic liquids to large-scale industrial applications is their cost in comparison with widely available simple acids such as HF, H₂SO₄

and AlCl_3 . Therefore, not only in advocating their role as effective catalysts must their capabilities be demonstrably superior to current systems, but as far as possible their synthesis needs to be cost effective. When the ionic liquids discussed above are considered, however, they almost exclusively include expensive cations featuring an imidazolium moiety. The cation is typically a spectator ion in these systems, as the Lewis acidity comes from anionic species, and influences mainly the physical properties of the liquid. Consequently, the design of liquid Lewis acids with cheaper counter ions is an appealing prospect. In addition to this, whilst chloroaluminate ionic liquids are effective in Lewis acidic reactions, they do not offer further scope for tunability to act in a wider range of reactions. Formed exclusively of an aluminium centre surrounded by chlorides the acidity cannot be altered further and factors such as increased steric bulk cannot be introduced. Therefore, finding alternative Lewis acidic ions is essential for the development of Lewis acidic ILs into new classes of reactions.

1.3.3 *Liquid Coordination Complexes (LCCs)*

As a response to the drawback outlined in Section 1.3.2.4, whereby the organic cation in chlorometallate ionic liquids is typically both a spectator ion in terms of Lewis acidity and the most expensive component, a family of alternative liquid Lewis acids have been developed. These combinations of metal halides and simple organic molecules. These liquids show similar speciation to chlorometallates(III) ionic liquids and go by several names, including deep eutectic solvents, ionic liquid alternatives or liquid coordination complexes (LCCs), the last term used throughout this work.²

1.3.3.1 *Historical Context*

The use of metal halides in catalytic chemistry, particularly AlCl_3 , often involves the use a donor solvent molecule to modify the properties of the Lewis acid. These would be aprotic donor species, such as THF, MeCN or DMF.¹²³⁻¹²⁵ By varying the molar ratio of AlCl_3 in the solutions the Lewis acidity and reactivity can be controlled depending on requirements of the reaction.

The thrust of investigations by coordination chemists into the speciation of these interactions has been primarily through investigating solid adducts. In studies with a combination of AlCl_3 and THF, crystals which either demonstrate neutral species such as $[\text{AlCl}_3(\text{THF})]$ and $[\text{AlCl}_3(\text{THF})_2]$, or ionic species, such as $[\text{Al}_2\text{Cl}_2(\text{THF})_4][\text{AlCl}_4]$ have been revealed through crystallography and magic angle solid state NMR.^{77,126,127} In these works, the interest in liquid Lewis acids is focused not on what was observable through these techniques, but what was ‘unsuccessful’. Frequent allusion to oils which could not be crystallised from combinations of

organic molecules and metal chlorides captured the attention of ionic liquid chemists as potential liquid coordination complexes.

1.3.3.2 Speciation

Announcing the dawn of a new family of ionic liquids, in 2007 Abbott *et al.* presented eutectic mixtures of ZnCl_2 and a selection of amides and diols.¹²⁸ The depression in the melting point can be clearly seen in Figure 10, where urea is 78% molar composition or, in convention of ionic liquids, $\chi_{\text{ZnCl}_2} = 0.22$. Similar eutectic points were also detected for mixtures between ZnCl_2 and acetamide ($\chi_{\text{ZnCl}_2} = 0.20$), ethylene glycol ($\chi_{\text{ZnCl}_2} = 0.20$) and hexanediol ($\chi_{\text{ZnCl}_2} = 0.25$).

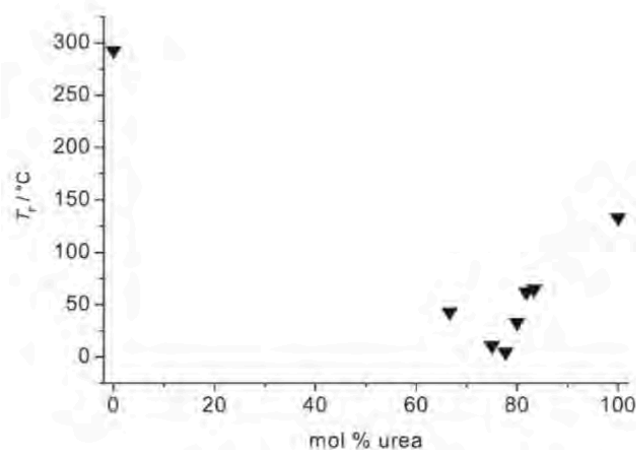
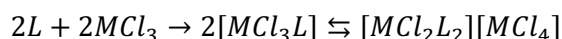


Figure 10. Phase diagram of the ZnCl_2 mixture showing melting point as a function of urea concentration.

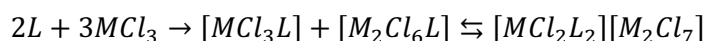
The focus of this work was on the physical properties, such as density, viscosity and conductivity, which were found to be largely similar to ionic liquids, but not on Lewis acidity (which, given large excess of organic donors, was unlikely to be high). Subsequent work of the Abbott group moved onto AlCl_3 , reporting that with the ligands urea, acetamide and N,N-dimethylurea, where $0.5 \leq \chi_{\text{AlCl}_3} \leq 0.60$, liquids formed.¹²⁹ The ambition to synthesise ionic liquids without expensive imidazolium cations was evident from the title of this work which asked “Do all ionic liquids need organic cations?” The primary focus of this paper was the physical characterisation of the liquids, however cyclic voltammetry suggested that no $[\text{Al}_2\text{Cl}_7]^-$ was present in equilibrium in acetamide and urea systems where $\chi_{\text{AlCl}_3} = 0.5$. Similar studies by Yoshii *et al.* focused on the mixture of 4-propylpyridine and AlCl_3 with compositions of $0.50 \leq \chi_{\text{AlCl}_3} \leq 0.60$ and dipropylsulphide at $\chi_{\text{AlCl}_3} = 0.51$.^{130,131} Mass spectrometry studies reported the absence of $[\text{Al}_2\text{Cl}_7]^-$, however, it must be noted that mass spectrometry may reveal erroneous results for anionic speciation.^{87,105}

Studies combining ^{27}Al NMR (Section 1.3.2.1) and Raman spectroscopies of systems containing acetamide (AcA), urea, thiourea, trioctylphosphine or trioctylphosphine oxide in combination with a metal halide (MCl_3) across the molar ratio ranges $0.50 \leq \chi_{\text{AlCl}_3} \leq 0.60$ and $0.50 \leq \chi_{\text{GaCl}_3} \leq 0.75$, revealed the existence of anionic, cationic and neutral coordination complexes, of both aluminium and gallium.² This contrasted with earlier report of Abbott and colleagues, and led the authors to coin the term liquid coordination complexes (LCCs), recognising a large proportion of charge-neutral components. Based on recorded spectra, equilibria were proposed to describe the interplay of species, with only monomeric species present for $\chi_{\text{MCl}_3} = 0.5$ (Section 1.3.2.1).



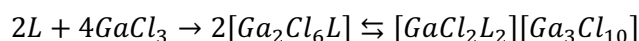
Equation 7

As with chlorometallate species, at higher metal chloride loadings, dimeric species are observed, the behaviour of the system at $\chi_{\text{MCl}_3} = 0.6$ (Section 1.3.2.1).



Equation 8

When the MCl_3 concentration is increased above $\chi_{\text{MCl}_3} = 0.6$ for aluminium systems it was reported that a solid/liquid equilibrium emerges with the deposition of solid AlCl_3 , due to inability of chloroaluminate complexes to form trimers – in analogy what is observed in chloroaluminate ionic liquids at $\chi_{\text{MCl}_3} > 0.67$. Work by Hu *et al.* formed compositions with AlCl_3 at molar ratios such that $\chi_{\text{AlCl}_3} > 0.67$ by dissolving the mixture in DCM to prevent solid deposition.¹³² These LCCs were formed with acetamide (AcA) N-methyl acetamide (NMA) and N,N-dimethylacetamide (DMA) and their speciation in solvent was observed using UV-vis, IR, Raman and ^{27}Al NMR spectroscopy. They found that with increasing aluminium chloride molar ratios the ionicity increased and molecular species more easily formed. This work demonstrated that whilst the AcA coordinated through oxygen, the NMA and DMA ligands were bidentate, coordinating through both O and N atoms. Again in analogy to chlorogallate ionic liquids, GaCl_3 LCCs have the ability to form oligomeric species, with homogenous liquids existing at ambient conditions up to $\chi_{\text{GaCl}_3} = 0.75$ forming.² This suggests the presence of stable oligomeric species of more than two metal centres (Figure 11).



Equation 9

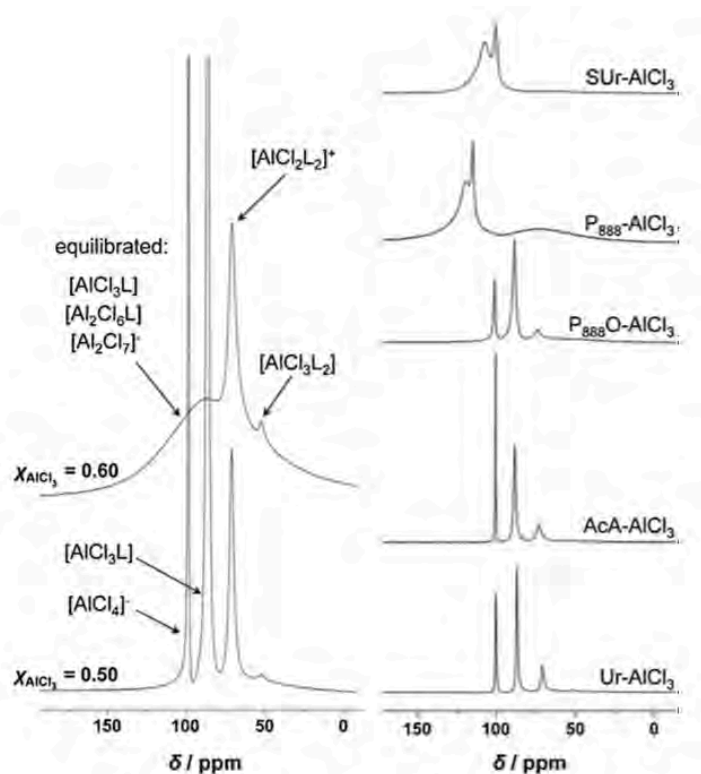


Figure 11. ^{27}Al NMR spectra showing speciation in (left) AcA- AlCl_3 $\chi_{\text{AlCl}_3} = 0.5$ and 0.6 , and (right) L- AlCl_3 $\chi_{\text{AlCl}_3} = 0.5$.

A series of aluminium bromide and chloride liquid coordination complexes with imidazolium cations were comprehensively characterised in work by Hog *et al.*, broadening the field to other halides.^{133,134} In this work they demonstrated the formation of liquids below 100 °C, where $\chi_{\text{AlBr}_3} \geq 0.5$, from the combination of aluminium bromide with aliphatic asymmetrical amines and phosphines. Subsequently they combined C₄im with aluminium bromide at molar ratios of $0.14 \leq \chi_{\text{AlBr}_3} \leq 0.75$ giving room temperature liquids at $\chi_{\text{AlBr}_3} = 0.44, 0.60$ and 0.67 . This produced a range of cleavage products, including the hexacoordinate $[\text{Al}(\text{C}_4\text{im})_6]^{3+}$ as Lewis basic cations were generated at lower molar ratios. Such 6-coordinate species with triple charge have not been reported for the chloride system, which contained single-charge $[\text{AlCl}_2(\text{C}_4\text{im})_4]^+$ and free chloride anions, in addition to free C₄im.¹³³ This is a consequence of the weaker bond energy of the Al-Br bond which can be overcome more easily to coordinate more L donor species.

1.3.3.3 Acidity measurements

The quantification of the Lewis acidity of LCCs can be achieved through the Gutmann acceptor number (Section 1.1.3.1). The work of Coleman *et al.* provides data for LCCs with the dimethylacetamide (DMA) ligand.² For DMA- GaCl_3 , $\chi_{\text{GaCl}_3} = 0.6$ the AN = 103, and for DMA- AlCl_3 , $\chi_{\text{GaCl}_3} = 0.6$ several P₂₂₂O peaks were recorded giving AN = 96-103. These can

be compared to chlorometallate ionic liquids $[\text{C}_8\text{mim}]\text{Cl}-\text{GaCl}_3$ $\chi_{\text{GaCl}_3} = 0.6$ which has an AN of 95 and $[\text{C}_8\text{mim}]\text{Cl}-\text{AlCl}_3$ $\chi_{\text{AlCl}_3} = 0.6$ which has an AN of 93.²¹ The Lewis acidity of amide- AlCl_3 LCC systems was determined by Hu *et al.*, their work used the P_{222}O probe to quantify acidity using NMR spectroscopy, although they did not calculate acceptor numbers, they did use it to identify the Lewis acidic species $[\text{AlCl}_2\text{L}_n]^+$ and $[\text{Al}_2\text{Cl}_7]^-$ were present in the system.¹³⁵ Further to this they used nitrobenzene as a molecular probe to measure the Lewis acidity *via in situ* IR titration and further integrated ^{27}Al NMR spectra to quantify the ratio of the cationic $[\text{AlCl}_2\text{L}_n]^+$ to the anionic $[\text{Al}_2\text{Cl}_7]^-$ and $[\text{AlCl}_4]^-$.

1.3.3.4 Applications

The strands of research based on applications of LCC systems have diverged based on their characteristics. Work focused on their ionic species through electrochemical research (from groups such as Abbott, Dai and Endres) or their Lewis acidity for catalytic applications (Swadźba-Kwaśny, Liu).

The classic Lewis acid catalysed reaction Friedel-Crafts alkylation of benzene with 1-decene was catalysed by gallium chloride LCCs.¹³⁶ Although AlCl_3 would have been the obvious choice in terms of catalyst cost, GaCl_3 was selected instead, as giving more scientific insight - that is, offering a greater range χ_{AlCl_3} values to be studied as homogeneous liquids. Whereas compositions around $\chi_{\text{AlCl}_3} = 0.50$ tend to crystallise easily and high concentrations of aluminium chloride $\chi_{\text{AlCl}_3} \geq 0.60$ precipitate an excess of AlCl_3 . Conversely gallium chloride LCCs generated for $\chi_{\text{GaCl}_3} \geq 0.60$ gave homogenous liquids. Unsurprisingly, greater concentrations of GaCl_3 gave higher rates than lower χ_{GaCl_3} values. In addition to this chlorogallate anions often form longer oligomeric structures, such as $[\text{Ga}_3\text{Cl}_{10}]^-$ and $[\text{Ga}_4\text{Cl}_{14}]^-$, which means that GaCl_3 does not precipitate out of solution.^{100,101} Furthermore, ligand selection had major influence on the entire process, demonstrating very high tuneability of the system: whereas LCCs with urea or DMA ligands gave higher reaction rates, the easier product separation was afforded by long chained organic ligands (P_{888} and P_{888}O).¹³⁶

In the alkylation of isobutane with 2-butene to produce high quality fuels, the LCC amide- AlCl_3 was successfully employed as a catalyst by Hu *et al.*¹³⁷ This work provided a comparison to chlorometallate ionic liquids and showed greater selectivity and fewer polyalkylates at the same molar ratio of AlCl_3 ($\chi_{\text{AlCl}_3} = 0.60$).

In the hydrogenation of toluene, a supported LCC (urea and AlCl_3 $\chi_{\text{AlCl}_3} = 0.6$) and chloroaluminate ionic liquid, $[\text{C}_4\text{mim}]\text{Cl}-\text{AlCl}_3$ $\chi_{\text{AlCl}_3} = 0.67$, were used to form solid catalysts with an ionic liquid layer (SCILLs) on a Pd/C surface.¹³⁸ The involvement of the liquid Lewis acids in both cases improved the rate of hydrogenation against the uncoated surface. Running

at lower temperatures of 40 °C, the IL-coated surface was more active than with the LCC, however, when the temperature was increased to 80 °C the LCC became significantly more active, yielding complete conversion in under 50 min. This improvement is believed to result not from changes to viscosity, but from changes to the speciation of the urea-AlCl₃ mixture.¹³⁸

Liquid coordination complexes formed from AlCl₃ with previously explored ligands, such as AcA, urea (Ur) and thiourea (SUR) were used in the Friedel-Crafts sulfination reaction between acetanilide and sulfur dioxide.¹³⁹ The product, 4-acetamidobenzenesulfonic acid, was generated at nearly 100% yield inside 60 min, using AcA-AlCl₃, $\chi_{\text{AlCl}_3} = 0.65$. The high solubility of SO₂ in this system offers an immediate advantage over conventional solvents. This work also explored AlBr₃-based systems, which gave much lower yields and this is likely to result from higher density and viscosity, limiting SO₂ dispersion.¹³⁹

In summary, whenever LCCs were compared to halometallate ionic liquids, it has been demonstrated that their performance differed significantly.

1.3.4 Ionic Liquids with Cationic Lewis Acids

As Lewis acids are defined as electron accepting species, there is something inherently contradictory in the design of Lewis acidic ionic liquids with Lewis acidic anions, which are by definition electron-rich. The first ionic liquids with strongly Lewis acidic anion was developed by Coffie *et al.*, featuring a tricoordinate borenium cation.⁴

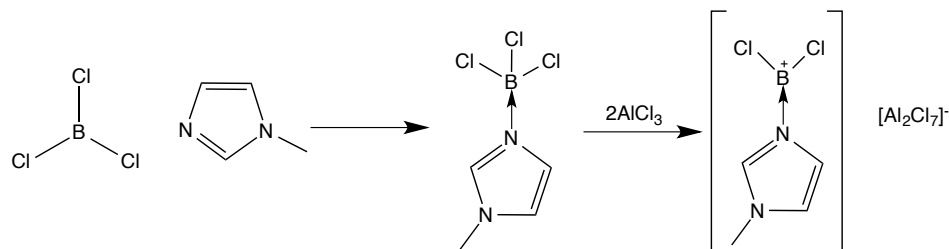
1.3.4.1 Historical Context

One of the most classic examples of Lewis acidity is the orbital overlap between boron trichloride and ammonia (Figure 1). Increasing electrophilicity further can be achieved through placing a positive charge on the boron centre; the cumulative Lewis acidity of the empty *p*-orbital and the net positive charge leads to greater acidity of tricoordinate borenium cations than tricoordinate boranes (Section 1.2.2.3). The use of borenium as a potent Lewis acid has been of great interest to inorganic chemists.

The borenium ionic liquids developed by Coffie *et al.*⁴ were synthesised *via* halide abstraction (Scheme 10), a synthetic strategy developed by Ryschkewitsch and Wiggins,⁶⁹ and adapted to the synthesis of ionic liquids by eliminating the use of a solvent in the second step. The first step of this synthesis is the formation of a tetracoordinate boron complex with an L-donor ligand, such as pyridine (py), 3-picoline (3-pic), 4-picoline (4-pic), 1-methylimidazole (mim), trioctylphosphine (P₈₈₈) and trioctylphosphine oxide (P₈₈₈O). The aromatic ligands are designed to stabilise the complex through donation to the electrophilic centre. Ligands with long alkyl chains were used by Coffie *et al.* to promote the formation of a liquid, rather than

crystallisation. These complexes are reacted with either one, two or three equivalents of MCl_3 , where M is either gallium or aluminium, in a solventless reaction, to give (nominally) a borenium cation with a chlorometallate anion.⁴

Scheme 10. Synthesis of a borenium ionic liquid.⁶⁹



Beyond borenium ionic liquids, solvate ionic liquids have been recently recognised as mildly Lewis acidic ionic liquids with acidity placed in the cation.^{140,141} Solvate ILs are formed through the dissolution of a metal salt with a poorly coordinating anion, such as lithium bistriflimide, $\text{M}[\text{A}]$, in a glyme (*Gn*) or glycol (*En*) (Figure 12).^{141,142} These liquids display high thermal stability (up to 200 °C),¹⁴³ high conductivity ($0.6\text{--}1.6\text{ mS cm}^{-1}$ at 30 °C) and low viscosity ($68.0\text{--}156.0\text{ mPa s}$).¹⁴⁰ This initial work with these systems by Watanabe and colleagues focused on forming electrolytes for metal-ion batteries, however in more recent studies their use as Lewis acidic media has been explored. In using coordination chemistry to access inexpensive and well-performing ionic liquid-like materials, they are very similar to LCCs.

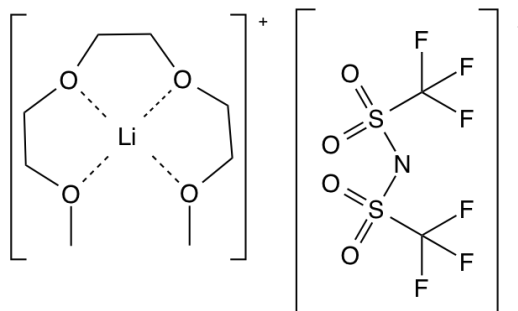


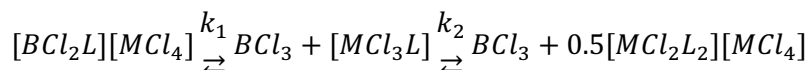
Figure 12. The structure of the solvate ionic liquid $[\text{Li}(\text{G3})][\text{NTf}_2]$.

Lewis acidity of lithium-bearing solvate ionic liquids, which are mixtures of $\text{Li}[\text{NTf}_2]$ and glymes or glycols, has also been measured using Gutmann acceptor number.¹⁴⁴ The effect of solvate IL formation on acidity was probed by taking the AN of the components, triglyme (G3) and tetraglyme (G4), with AN of *ca.* 0.2. The benchmark bistriflimide ionic liquid, $[\text{C}_4\text{mim}][\text{NTf}_2]$, was provided for a comparable value for the lithium bistriflimide salt in the environment of the solvate IL, and this gave two AN values of 11.9 and 3.10. The AN recorded for the systems $[\text{Li}(\text{G3})][\text{NTf}_2]$ and $[\text{Li}(\text{G4})][\text{NTf}_2]$ was 26.5, indicating mild Lewis acidity. It

is difficult however to make a direct comparison between this work and other AN measurements of ionic liquids, as they were recorded in benzene-d₆. In work which studied the ANs of a range of ionic liquids neat, Schmeisser *et al.* determined the ANs [C₂mim][NTf₂] and [C₈mim][NTf₂] to be 27.4 and 25.6 respectively,⁹⁷ indicating a depression of AN values from dissolution. Therefore, it may be expected that neat solvate ILs would give higher AN values. In terms of applications, solvate ionic liquids have been demonstrated to solvate and catalyse the Diels-Alder reaction and the synthesis of α -aminophosphinates.^{144,145} Nevertheless, they remain far weaker Lewis acids than borenium ionic liquids, which are the focus of this work.

1.3.4.2 Speciation of borenium ionic liquids

As with other Lewis acidic ionic liquids discussed in this chapter, species in borenium ionic liquids exist in a dynamic equilibrium, best viewed through the lens of NMR spectroscopy. The starting tetracoordinate boron complex gives a characteristic chemical shift of ~5-10 ppm in ¹¹B NMR spectroscopy. The halide abstraction produces a tricoordinate borenium cation which has an ¹¹B NMR signal of 30-50 ppm. When evaluating the NMR spectra of these ionic liquids another prominent peak is the sharp signal at 45±1 ppm which indicates the presence of BCl₃, clearly indicating ligand scrambling (Equation 10).



Equation 10

In the equation given above, the position of the equilibrium k_1 is most dependent on the strength of the interaction between the boron centre and the ligand, L, relative to the strength of its interaction with the metal centre, M. Across all samples, there was a relatively small degree of ligand transfer reported for N-donors, larger for trioctylphosphine and very large for P₈₈₈O, the only oxygen donor reported, where very little ligand remained on the boron centre and mostly transferred to the metal centre.⁴

1.3.4.3 Acidity measurements

In borenium ionic liquids reported by Coffee *et al.*, the measure of the Lewis acidity is really a measure of the degree of independence of the boron centre from the anion and therefore the availability of the empty *p*-orbital. Therefore, the ¹¹B NMR spectra for this family can give an indication of relative association between cation and anion with higher chemical shift indicating a less shielded boron centre. Indeed a comparison between systems with one and

two equivalents of metal chloride suggests that with the mononuclear anions, $[\text{MCl}_4]^-$, there is greater shielding of the boron centre than with dinuclear anions, $[\text{M}_2\text{Cl}_7]^-$ (Figure 13).⁴

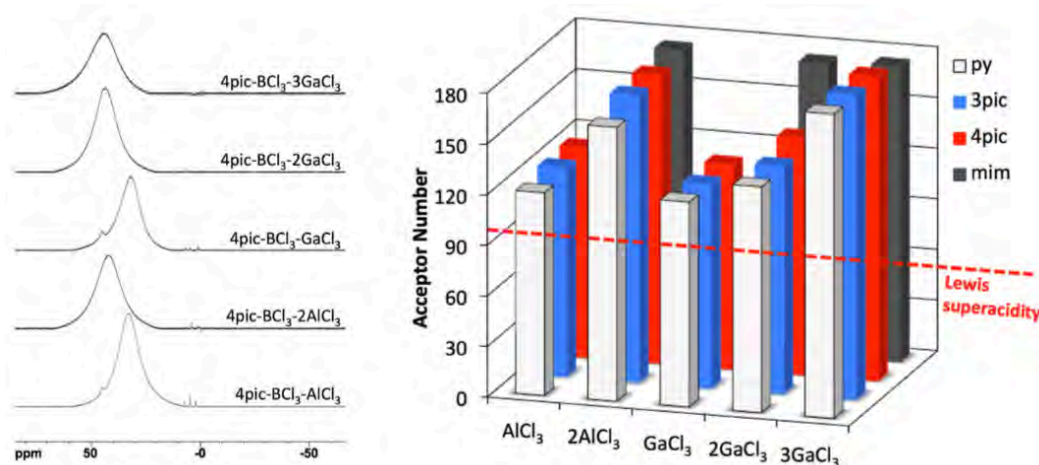


Figure 13. *Left* ^{11}B NMR spectra of neat borenium ILs with DMSO- d_6 lock (composition given on spectra); *right* Gutmann acceptor number values measured for borenium ILs of a general formula L- BCl_3 - $n\text{MCl}_3$, for four different ligands (L), two metals (M) and $n = 1-3$. (Adapted from ⁴)

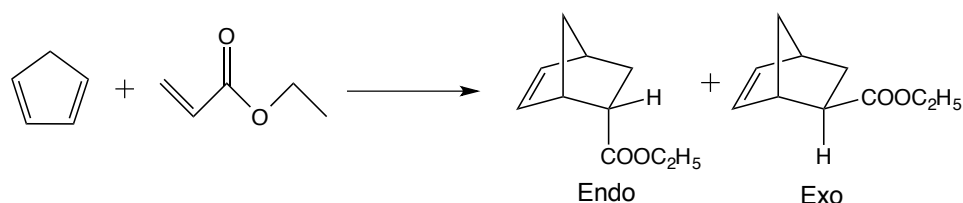
Quantitative measurements were achieved using the Gutmann acceptor number method on all systems of $\text{BCl}_3\text{L}-n\text{MCl}_3$. The measured acceptor numbers greater than 100 indicated Lewis superacidity of all tested systems (Figure 13, right). Further to this for some systems the acidity recorded was the highest reported in the literature with values greater than 180.⁴ These measurements confirmed what was apparent from the ^{11}B NMR spectroscopy: dinuclear metal chloride complexes interacted less with the free orbital on the boron allowing for a more naked borenium cation. The importance of this naked cation was also highlighted by the effect of solvation in DCM which reduced the acidity of the system. A characteristic of this system is that both anion and cation are strong Lewis acids, this was observable through ^{31}P NMR spectra with P_{222}O which gave two clear resonances for the system $[\text{BCl}_2(\text{mim})][\text{Al}_2\text{Cl}_7]$, one at 117.2 ppm and one at 84.2 ppm, relating to the cation and anion respectively coordinating to the probe molecule. These resonances gave ANs of 174 and 96 respectively. Whilst the borenium AN is significantly higher, the AN of the chlorometallate anion is almost superacidic and the fact that can compete with the naked borenium cation for the low concentration of P_{222}O demonstrates the significance of having two competing Lewis acidic centres.

1.3.4.4 Applications

The first reported application of borenium ionic liquids has been in the classic Lewis acid catalysed reaction the Diels-Alder cycloaddition (Scheme 11).¹⁴⁶ The substrate scope addressed in this work showed successful catalysis of a range of dienes and dienophiles with reactivity at 0 °C, giving full conversion within 15 minutes and high selectivity. The catalyst

concentration can be extremely low, with loadings at 0.10 mol%, and no haloborate side products detected. Crucially, independent of anion, the catalytic activity of each catalyst was found to correlate to the acceptor number recorded for borenium cation. This relationship was correlated through a sigmodal Boltzmann distribution, indicating that the cation is the most significant species in the catalytic process.

Scheme 11. Diels Alder reaction between cyclopentadiene to ethyl acrylate.



Very recently, the borenium ionic liquid $[\text{BCl}_2(\text{L})][\text{M}_n\text{Cl}_{3n+1}]$ (where L = pyridine or picoline, $\text{M} = \text{Al}$ or Ga and $n = 1$ or 2) was used in the Lewis acid catalysed oligomerisation of 1-decene, a reaction which produces lubricants for the automotive industry. The current industrial standard in this reaction is BF_3 , a highly toxic chemical which can produce HF , therefore finding alternative catalysts is a crucial goal for green chemistry. A range of chain lengths from C_{20} to C_{70} were generated, with the desired product being a blend of C_{30} and C_{40} . The choice of ligand affected the product, with pyridine producing a greater proportion of heavier products but with a greater proclivity to form branched chains compared with the methylated picoline. In addition, better performance was observed from chloroaluminate than chlorogallate anions, when accompanied by the same cation. In this case, there was no obvious correlation with acceptor number, which is easily justified through the carbocationic reaction mechanism. Lewis acids interact with adventitious moisture to generate superacidic protons, which protonate olefins and initiate carbocationic oligomerisation, which is then controlled by propagation/termination ratio. It stands to reason that Lewis acidity of the initiating species does not have direct translation to the reaction outcome.¹⁴⁷

In contrast with other reported Lewis superacids, borenium cations are not highly fluorinated and do not require elaborate ligands, meaning their syntheses are both relatively simple and inexpensive. This makes them potentially suitable for sustainable industrial applications. However, the ‘first generation’ of borenium ILs, reported by Coffie *et al.* suffered from ligand scrambling and multiple acidity sites, resulting in poor control of catalytic activity.

1.4 Motivation for This Work

This research project commenced as a continuation of earlier work in the Swadźba-Kwaśny group, developing liquid Lewis acids. Initially, it was a curiosity-driven structural exploration

of two groups of liquid Lewis acids: LCCs and borenium ionic liquids. In LCCs, it was interesting to expand beyond Group 13 metals and assess the scope for potential LCCs across the periodic table. In borenium ionic liquids, it was to synthesise more ‘elegant’ systems without chlorometallate anions, with one well-defined acidity centre, and explore their potential uses. Out of the two, the boron research strand developed into the main research theme of this thesis. Having developed halometallate-free borenium ionic liquids, and seeking for a relevant application, their use in the dynamically developing field of frustrated Lewis pairs (FLPs) was explored, ultimately leading to the synthesis of the first ionic liquid frustrated Lewis pair. In parallel, the behaviour of conventional FLPs in conventional ionic liquids was studied, using know-how of structural studies of the liquid phase through neutron scattering, which led to insights relevant to both ionic liquids and FLP communities.

2 LIQUID COORDINATION COMPLEXES

In this chapter a study on liquid coordination complexes is presented, using just two liquid-generating ligands, trioctylphosphine and trioctylphosphine oxide (soft and hard donor, respectively), combined with a range of metal chlorides: AlCl_3 , GaCl_3 , InCl_3 , SbCl_3 , SnCl_2 , SnCl_4 , TiCl_4 and ZnCl_2 . Both Lewis acidity and speciation were studied. A comparison between the Lewis acidity (Gutmann acceptor number) of the metal chlorides and their corresponding LCCs is presented. Through collaboration with the Chrobok group in Silesian University of Technology, AN measurements were correlated to catalytic activity of the LCCs in Diels-Alder cycloaddition. This work has been published in *Dalton Transactions*.³

2.1 Experimental

2.1.1 Materials and Methods

Aluminium(III) chloride (99.999%) and gallium(III) chloride (99.999%) were purchased in sealed ampules, under argon, from Alfa Aesar. Titanium tetrachloride (99%), tin tetrachloride (99.999%), tin dichloride (99.99%), indium trichloride (99%), zinc dichloride (98%) and antimony trichloride (99.95%) were all purchased from Sigma Aldrich and used as received. Trioctylphosphine oxide (99.5%) was provided by Cytec and dried under reduced pressure (80 °C, <1 mbar, 48 h) before use. Trioctylphosphine (99.5%) was provided by Cytec in a sealed canister under an inert atmosphere and used as received. Triethylphosphine oxide (99%) was purchased from Sigma Aldrich and used as received.

All experiments were performed in a glovebox (MBraun labmaster dp, <0.6 ppm of H_2O and O_2) or using Schlenk techniques under argon. All glassware was dried overnight in an oven (*ca.* 100 °C) prior to use.

^{31}P , ^{67}Zn , ^{115}In and ^{121}Sb NMR spectra were recorded on a Bruker Avance DPX 400 MHz spectrometer, at 162, 25, 88 and 96 MHz, respectively. ^{49}Ti and ^{119}Sn NMR spectra were recorded on a Bruker Avance DPX 600 MHz spectrometer, at 34 and 224 MHz, respectively. All samples were studied neat using a DMSO-filled, sealed capillary as an external deuterated lock.

2.1.2 Synthesis of LCCs

LCCs were synthesised on a 2 g scale, following the literature procedure.² All syntheses were carried out in an argon-filled glovebox (MBraun LabMaster dp, <0.6 ppm O_2 and H_2O). To a neutral donor ligand (0.25–1.00 mol eq.) a metal chloride was added in small aliquots into a sample *via* equipped with a PTFE coated magnetic stirrer bar. Heat was typically evolved. The

reaction mixture was stirred until the flask had cooled before additional aliquots were added. This was repeated until the desired molar ratio of metal chloride ($X_{\text{MCl}_x} = 0.50\text{--}0.75$) was reached. Afterwards, the reaction mixture was stirred (0.5–24 h, 30–80 °C) until a homogeneous liquid was obtained. All LCCs were stored in the glovebox until used.

2.1.3 Gutmann Acceptor Number Measurements

The Gutmann acceptor numbers of metal chlorides were measured as 1:1 adducts of MCl_x and triethylphosphine oxide (P_{222}O) as described by Gutmann.⁴⁶ Solutions of accurately weighed metal chlorides (*ca.* 0.58 mmol) in accurately known volumes of 1,2-dichloroethane (*ca.* 1.5 cm^3) were prepared to achieve concentrations of *ca.* 0.35 mol dm^{-3} . To each solution, 1 mol eq. of P_{222}O (*ca.* 0.58 mmol) was added, and the mixture was stirred for 30 min. All solids dissolved readily upon the addition of P_{222}O . The ^{31}P NMR spectra of the solutions were recorded, and then the solutions were diluted to *ca.* 0.25 mol dm^{-3} , and subsequently to *ca.* 0.20 mol dm^{-3} , with ^{31}P NMR spectra recorded for each concentration. The recorded ^{31}P NMR chemical shifts were plotted as a function of concentration and extrapolated to infinite dilution of P_{222}O in the studied sample. The acceptor number was calculated according to Equation 1.

For each LCC, three samples (*ca.* 1 g each) were weighed out accurately into sample vials. P_{222}O was weighed accurately into each sample (*ca.* 1, 2 and 3 wt%). ^{31}P NMR spectra were recorded for the three concentrations, and the chemical shift value was extrapolated to the value of infinite dilution. The acceptor number was calculated according to Equation 1.

For many Gutmann Acceptor number measurements multiple peaks were observed (Figure 14). Where multiple peaks were observed, the peak with the largest area was taken as this represents the Lewis acidic species with the greatest concentration, rather than an average of all the peaks with weighting on the basis of integral area as this method would be affected by ^{31}P NMR spectroscopic peaks for ^{31}P NMR signal of P_{888}O .

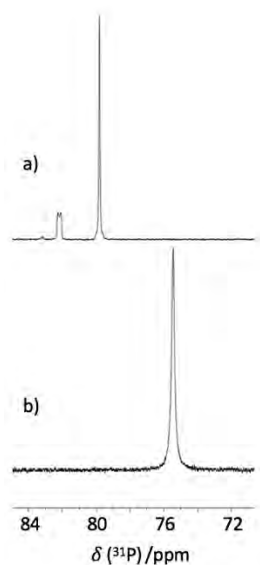


Figure 14. Gutmann acceptor number measurements, showing a) multiple $P_{222}O$ peaks for the sample $P_{222}O$ and $AlCl_3$ as $0.375 \text{ mol dm}^{-3}$ solution in 1,2- dichloroethane and b) a single $P_{222}O$ peak for the sample $P_{222}O$ and $GaCl_3$ as $0.375 \text{ mol dm}^{-3}$ solution in 1,2-dichloroethane.

2.1.4 General Procedure for the Diels-Alder Reaction

All reactions were carried out under dry argon. In a typical procedure, the LCC catalyst (0.1–1.0 mol% per 1.0 mol of dienophile) was placed in a two-necked round-bottom flask equipped with a stirring bar. Then, a mixture of ethyl acrylate (1.602 g, 16 mmol) and cyclopentadiene (1.586 g, 24 mmol) was added dropwise to the vigorously stirred (1500 rpm) reaction mixture in an ice bath. The reaction was carried out for 5–120 min, and its progress was monitored by gas chromatography. Afterwards, the reaction was quenched with a few drops of water, and 1 cm^3 of dichloromethane was added to homogenise the mixture prior to GC analysis.

GC analysis was performed using a PerkinElmer Clarus 500 gas chromatograph equipped with an SPBTM-5 column (30 m \times 0.2 mm \times 0.2 μm) with n-decane as the internal standard.

2.2 Synthetic Plan and Approach to Study Speciation

Previous studies, both by the Swadźba-Kwaśny group and by other groups, were focused mainly on LCCs based on aluminium halides (and, to a lesser extent, gallium chloride). The focus of this work was to scope out the properties of liquid coordination complexes based on a very broad range of metal centres, in particular Lewis acidic ones, and screen their performance as Lewis acid catalysts. The ligands selected, $P_{888}O$ and P_{888} , are similar in the length of carbon chain which surrounds the phosphorus centre, as well as having sterically a very similar bulk. However, the former one is a hard donor, and the latter one is a soft one. This work was designed to probe the effect of this on the speciation and Lewis acidity. The

selected length of the alkyl chains derives from insight gained from earlier studies on melting point in ionic liquids.¹⁴⁸ Alkyl chain lengths shorter than six carbons make a molecule more susceptible to crystallisation, while with longer alkyl chains the formation of waxy solids is a risk.

As discussed in the introduction (Section 1.3.3), the homogeneous liquid range for LCCs varies dependent on the oligomer formation at different molar compositions, for example for L-AlCl₃ (L = P₈₈₈O or P₈₈₈) the homogenous liquid range is $\chi_{\text{AlCl}_3} = 0.5\text{-}0.6$, whereas for gallium chloride systems this increases to $\chi_{\text{GaCl}_3} = 0.50\text{-}0.75$ (and possibly higher), as oligomeric chlorogallate anions form.² Throughout this chapter, the approach taken for the formation of novel LCCs was to synthesise an equimolar composition (*i.e.* $\chi_{\text{MCl}_x} = 0.5$) first; this was a liquid for all metal chlorides reported here. Further on, compositions with an excess of metal chloride ($\chi_{\text{MCl}_x} > 0.5$) were synthesised and their physical states are given in Table 1.

The most popular techniques to study speciation of metals in ionic liquids are: vibrational spectroscopies, such as IR and Raman spectroscopy, multinuclear NMR spectroscopy, electron paramagnetic resonance (EPR), X-ray photoelectron spectroscopy (XPS), X-ray absorption spectroscopies (XAS), in particular extended X-ray absorption fine structure (EXAFS) and UV-VIS spectroscopy. These techniques vary in their accessibility, with some, such as NMR spectroscopy widely available within university chemistry departments, and others, such as XAS, requiring a synchrotron X-ray source and involve specialised training for data processing and interpretation. Furthermore, each technique has its specific limitations: not all nuclei are NMR active, EPR is suitable for paramagnetic elements only, and the XAS family is limited by the X-ray absorption range available at various beamlines. Ideally, for an in-depth study, three techniques based on different principles should be combined.

This work encompassed a broad range of metal centres, intended as scoping study for their potential catalytic applications with LCCs, rather than an in-depth speciation study. At its core was discovering the composition that formed room-temperature homogenous liquids, study of their Lewis acidity (in terms of AN) and performance in a model reaction, in order to highlight interesting systems for the future in-depth work. At the same time, it was impossible to interpret these results without any insight into speciation of the newly formed LCCs. Multinuclear NMR spectrometry (nuclei studied are given in Table 2) was selected due to its accessibility and widespread use in the literature, in particular in the context of solution-state speciation studies of metal complexes. The assignment of peaks could be therefore validated by the literature insight, comparing the chemical shifts from similar structures in solutions. Furthermore, the selection of P₈₈₈ and P₈₈₈O ligands allowed for direct comparison between each LCC through a very convenient ³¹P NMR spectroscopy. ³¹P is a spin ½ nuclei, giving

sharp peaks and well resolved, informative spectra. To provide further confidence in proposed structures, where possible, structures have been rationalised through comparison with structures from the crystallographic database and, wider speaking, related to general knowledge of inorganic chemistry of each metal studied.

Table 1. Physical descriptions of LCCs synthesised in this work.

MCl_x	χ_{MCl_x}	$P_{888}O$	P_{888}
$AlCl_3$	0.50	Colourless liquid ^a	Yellow liquid ^a
	0.60	Yellow liquid ^a	Yellow liquid ^a
	0.67	Yellow liquid with white precipitate ^a	Yellow liquid with white precipitate ^a
$GaCl_3$	0.50	Colourless liquid ^a	Colourless liquid ^a
	0.60	Colourless liquid ^a	Colourless liquid ^a
	0.67	Colourless liquid ^a	Colourless liquid ^a
	0.75	Colourless liquid ^a	Colourless liquid ^a
$InCl_3$	0.50	Colourless liquid	Colourless liquid with white precipitate ^b
	0.60	Colourless liquid with white precipitate	Colourless liquid with white precipitate
$SbCl_3$	0.50	Colourless liquid	Liquid, redox reaction
	0.60	Colourless liquid	-
$SnCl_2$	0.50	Colourless liquid	Colourless liquid
	0.60	Colourless liquid with white precipitate	Colourless liquid with white precipitate
$SnCl_4$	0.50	Colourless liquid	Liquid, redox reaction
	0.60	Colourless liquid	-
$TiCl_4$	0.50	Yellow liquid	Red liquid
	0.60	Yellow solid with white powder	Red liquid
$ZnCl_2$	0.50	Colourless liquid	Colourless liquid
	0.60	Colourless liquid	Colourless liquid with white precipitate

^a Previously reported.² ^b A very small amount of precipitate.

Initially, Raman spectroscopy was intended to be used as a complementary speciation technique, being both easily available and reported to be useful in speciation of numerous chlorometallate ionic liquids, based on Ti(IV), Al(III), Ga(III), In(III) and Zn(II).⁸⁷ However, for unknown reason, Raman spectra of LCCs studied in this work were of poor quality due to strong fluorescence, originating from the ligands, and impossible to remove with previously-tried methods, such as stirring with activated carbon. Considering the scoping nature of this work, the decision was made to focus on multinuclear NMR spectroscopy, and pursue detailed speciation studies for individual systems of particular interest.

Table 2. The appearance of spectra from a range of heteronuclear NMR spectra.

Nucleus	Spin	Appearance of spectra
³¹ P	1/2	Sharp Peaks
²⁷ Al	5/2	Sharp Peaks
⁴⁹ Ti	7/2	Uninterpretable
⁶⁷ Zn	5/2	Uninterpretable
⁷¹ Ga	3/2	Uninterpretable
¹¹⁵ In	9/2	Uninterpretable
¹¹⁹ Sn	1/2	Broad Peaks
¹²¹ Sb	5/2	Uninterpretable

³¹P NMR spectrometry provided data allowing for comparisons between LCCs based on different metals, which was found to be extremely valuable. Furthermore, the metallic centres were investigated whenever possible. The crucial factor in the data obtained from these spectra is the nature of the nuclear spin. From previous work it has been shown that ²⁷Al NMR gives good spectra for these species, however ⁷¹Ga NMR gives peaks too broad to give any interpretable data about the system.² In this work NMR spectra of the nuclei ⁴⁹Ti, ⁶⁷Zn, ¹¹⁸In, ¹¹⁹Sn, and ¹²¹Sb were recorded, but only ¹¹⁹Sn gave interpretable signals. This is perhaps not surprising given the fact that all other metals have a quadrupolar nucleus (spin > 1/2), which results in very broad NMR signals as a result of rapid quadrupolar relaxation.

The ³¹P NMR spectroscopy results for all for all LCCs are given in Table 3 below, and compared to ³¹P NMR spectra of unbound ligands. To record data for the unbound ligands the liquid P₈₈₈ was studied neat (with a DMSO capillary) whilst the solid P₈₈₈O was recorded as a CDCl₃ solution. The $\Delta\delta$ ³¹P columns provide the change in chemical shift induced by coordination to a metal centre.

Table 3. ^{31}P NMR chemical shifts for all compositions which formed homogeneous liquids. Also given are the change in chemical shift of the ligand in the LCC.

		P ₈₈₈ O		P ₈₈₈	
		δ ³¹ P	Δδ ³¹ P	δ ³¹ P	Δδ ³¹ P
MCl _x	χ _{MClx}	/ppm			
AlCl ₃	0.00	49.91	-	-29.44	-
	0.50	75.20	25.29	-26.65	2.79
		77.38	27.47	-22.16	7.28
		76.57	26.66	-23.29	6.15
	0.60	77.37	27.46		
		78.07	28.16		
GaCl ₃	0.50	76.50	26.59	-9.87	19.57
		80.15	30.24		
	0.60	79.97	30.06	-5.99	23.45
		81.23	31.32		
	0.67	81.31	31.40	-2.61	26.83
		83.41	33.50		
	0.75	84.37	34.46	-0.86	28.58
		85.21	35.30		
	86.02	36.11			
InCl ₃	0.50	72.04	22.13	11.49	40.93
SbCl ₃	0.50	70.91	21.00	-2.77	26.67
	0.60	69.60	19.69		
SnCl ₂	0.50	70.96	21.05	-3.89	25.55
SnCl ₄	0.50	68.74	18.83	102.7	132.14
		71.40	21.49	(redox)	(redox)
	0.60	68.88	18.97		
		71.38	21.47		
TiCl ₄	0.50	87.27	37.36	27.68	57.12
	0.60			34.50	63.94
ZnCl ₂	0.50	65.56	15.65	-20.03	9.41
	0.60	68.23	18.32		

Interpretation of these results, supported by literature studies, knowledge of coordination chemistry of each metal, and analysis of extant crystallographic data, is given below, separately for each metal.

2.3 Aluminium-Based Liquid Coordination Complexes

Six different compositions were synthesised using aluminium chloride ($\text{P}_{888}\text{-AlCl}_3$, $\chi_{\text{AlCl}_3} = 0.50 - 0.67$ and $\text{P}_{888}\text{O-AlCl}_3$, $\chi_{\text{AlCl}_3} = 0.50 - 0.67$), as Table 1 indicates, a colourless liquid formed only for one composition ($\text{P}_{888}\text{O-AlCl}_3$, $\chi_{\text{AlCl}_3} = 0.50$) while the rest were yellow, a white precipitate formed for both ligands at the highest metal chloride concentration. These LCCs have been reported before and their speciation has been determined by ^{27}Al NMR and Raman spectroscopies. These systems will be used to demonstrate how ^{31}P NMR spectra, recorded for all LCCs in this study, provide evidence for the speciation in known LCCs. It is

demonstrated that, whenever spectra from both ^{27}Al and ^{31}P NMR spectroscopies are compared (Figure 15), the range of environments present is reflected in both sets.

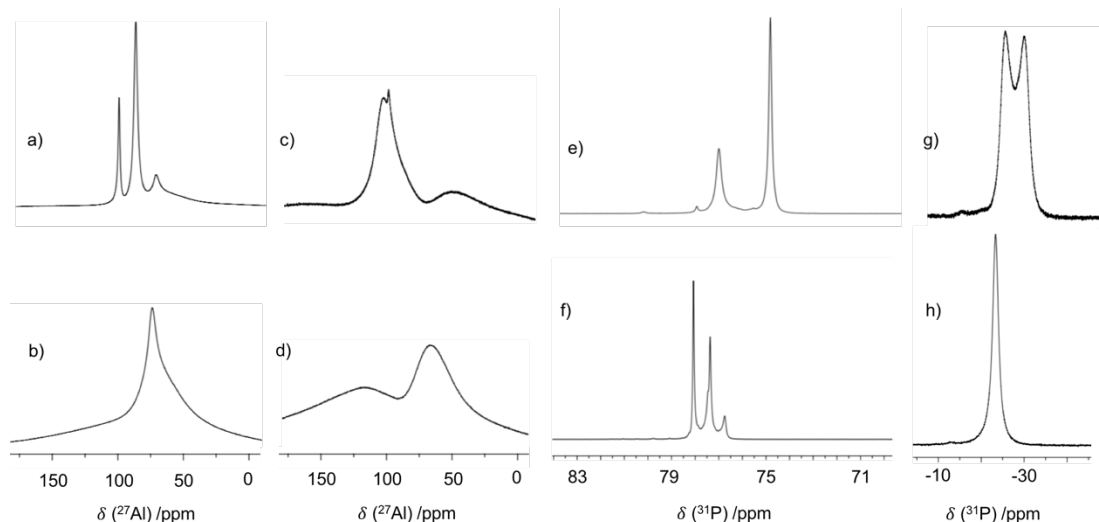
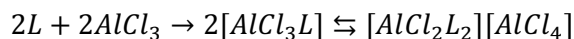


Figure 15. Comparison between ^{27}Al (a,b,c and d) and ^{31}P (e,f,g and h) NMR spectra of (a,e) $\text{P}_{888}\text{O}-\text{AlCl}_3$, $\chi_{\text{AlCl}_3} = 0.50$, (b,f) $\text{P}_{888}\text{O}-\text{AlCl}_3$, $\chi_{\text{AlCl}_3} = 0.60$, (c,g) $\text{P}_{888}-\text{AlCl}_3$, $\chi_{\text{AlCl}_3} = 0.50$, and (d,h) $\text{P}_{888}-\text{AlCl}_3$, $\chi_{\text{AlCl}_3} = 0.60$.

The speciation of these liquids has been elucidated in previous work. Where $\chi_{\text{AlCl}_3} = 0.50$, the speciation follows the equilibrium given below.



Equation 11

From Equation 11 it would be expected that there are three aluminium environments and two phosphorus environments. From $\text{P}_{888}\text{O}-\text{AlCl}_3$, $\chi_{\text{AlCl}_3} = 0.50$, the composition which gives the best spectra resolution, this can be clearly seen. Peaks in the ^{27}Al NMR spectrum indicate the presence of $[\text{AlCl}_4]^-$ at 102 ppm, $[\text{AlCl}_3(\text{P}_{888}\text{O})]$ at 89.59 ppm and $[\text{AlCl}_2(\text{P}_{888}\text{O})_2]^+$ at 73.25 ppm. These same species are reflected in the ^{31}P NMR spectra, with $[\text{AlCl}_3(\text{P}_{888}\text{O})]$ at 25.29 ppm and $[\text{AlCl}_2(\text{P}_{888}\text{O})_2]^+$ at 27.47 ppm, with the neutral adduct being more shielded. Increasing the metal halide concentration to $\chi_{\text{AlCl}_3} = 0.60$, a metal halide: ligand ratio of 1.5:1, allows the formation of the dinuclear $[\text{Al}_2\text{Cl}_7]^-$ complex, however longer oligomeric chains, such as $[\text{Al}_3\text{Cl}_{10}]^-$ are not stable and excess AlCl_3 precipitates so this is the highest metal halide ratio possible for this composition.^{91,92} The equilibrium at this composition can be expressed as in Equation 12.



Equation 12

The ^{27}Al NMR spectrum is not well resolved (Figure 15 a,b,c and d), giving one broad peak at 73.46 ppm, with a shoulder at about 50 ppm. The width of this peak results from the dynamic equilibrium between the monomeric and dimeric aluminium species, which is analogous to the equilibrium in chloroaluminate ionic liquids of $[\text{AlCl}_4]^-$ and $[\text{Al}_2\text{Cl}_7]^-$ anions. These anions also give a single broad ^{27}Al NMR peaks, as there is little change to the chemical shift on dimerization.⁹⁶ However, greater insight can be gained from the ^{31}P spectrum (Figure 15 e,f,g and h), which contains three signals, the first two of which were observed for the composition at $\chi_{\text{AlCl}_3} = 0.50$, $[\text{AlCl}_3\text{P}_{888}\text{O}]$ at 26.66 ppm and $[\text{AlCl}_2(\text{P}_{888}\text{O})_2]^+$, at 27.46 ppm. While the cation appears at the same chemical shift as in the LCC at $\chi_{\text{AlCl}_3} = 0.50$, the neutral adduct is more deshielded as a greater aluminium chloride concentration makes the composition more acidic. The third peak at 28.16 ppm is further deshielded, this corresponds to the species $[\text{Al}_2\text{Cl}_6\text{P}_{888}\text{O}]$ which does not form in the composition at $\chi_{\text{AlCl}_3} = 0.50$. These signals differentiate the species and support previous evidence for the behaviour of compositions between monodentate O-donors and aluminium chloride.^{2,132}

Comparing the behaviour of P-donors to the O-donors discussed above, it is expected that they will follow the same equilibria, however difference in the strength of interaction between aluminium and donor will result in different equilibrium constants. For the composition $\text{P}_{888}-\text{AlCl}_3$, $\chi_{\text{AlCl}_3} = 0.50$, the predicted two ^{31}P NMR peaks -26.65 and -22.16 ppm are visible (Figure 15g). The appearance of these singlets could be mistaken for a doublet, however if this were the case, the coupling constant for this doublet would have to be $^1J_{\text{P-Al}} = 467$ Hz, significantly higher than reported literature figures, which are always $^1J_{\text{P-Al}} < 300$ Hz.¹⁴⁹⁻¹⁵¹ Although significantly less well defined than the equivalent spectrum for P_{888}O , the ^{27}Al NMR spectrum (Figure 15c) for this composition the reported dominant peaks at 121, 117 and 74 ppm are visible, although care must be taken when assigning peaks at around 70 ppm in ^{27}Al spectra as a broad peak for the probe is present in this region.²

Finally the, fourth aluminium-based LCC sample was $\text{P}_{888}-\text{AlCl}_3$, $\chi_{\text{AlCl}_3} = 0.60$ (Figure 15d,h). Raman data for this composition were of very poor quality due to fluorescence,² however, a singlet was observed in the ^{31}P NMR spectrum at -23.9 ppm. The ^{27}Al spectrum features a broad peak with a maximum at *ca.* 113 ppm; this is consistent with AlCl_3 -phosphine adducts suggesting that the equilibrium of Equation 12 is strongly shifted to the left (the other feature in this spectrum being indistinguishable from the probe at *ca.* 70 ppm). However these AlCl_3 -phosphine adducts are known to be rare and the single peak in the ^{31}P NMR spectrum may indicate rapid exchange between species.¹⁵⁰⁻¹⁵² A definite conclusion for either interpretation is not possible to reach from this evidence and literature data for compositions with excess aluminium halide is limited.

2.4 Gallium-Based Liquid Coordination Complexes

Eight different compositions were synthesised using gallium chloride ($P_{888}\text{-GaCl}_3$, $\chi_{\text{GaCl}_3} = 0.50$ - 0.75 $P_{888}\text{O-GaCl}_3$ and $\chi_{\text{GaCl}_3} = 0.50$ - 0.75), as Table 1 indicates, these were all colourless liquid and unlike aluminium chloride the metal halide proportion could be increased to $\chi_{\text{GaCl}_3} = 0.75$ while still forming homogeneous liquids.² In contrast to aluminium-containing LCCs, the NMR active nuclei of the gallium centre, ^{69}Ga and ^{71}Ga , gave broad peaks which were uninterpretable, however previous work has established the speciation of these systems from Raman spectroscopic data.² The ^{31}P NMR spectroscopic data recorded for these systems is given in Figure 16.

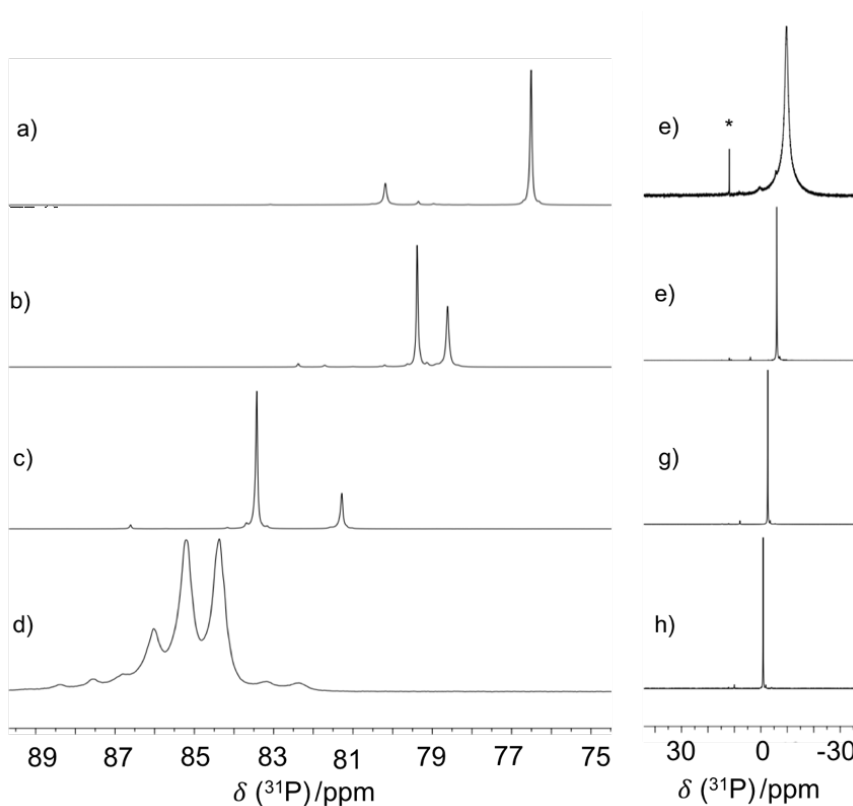
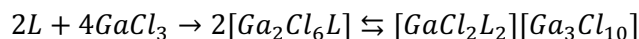


Figure 16. ^{31}P NMR spectra of L-GaCl_3 where $\text{L} = \text{P}_{888}\text{O}$ (left) or P_{888} (right) with compositions (a) $\chi_{\text{GaCl}_3} = 0.50$, (b) $\chi_{\text{GaCl}_3} = 0.60$, (c) $\chi_{\text{GaCl}_3} = 0.67$, and (d) $\chi_{\text{GaCl}_3} = 0.75$. (* denotes artefact)

For the O-donor compositions, it was expected that the equilibria are analogous to those found for AlCl_3 systems. From the ^{31}P NMR spectrum of $\text{P}_{888}\text{O-GaCl}_3$, $\chi_{\text{GaCl}_3} = 0.50$, following Equation 11, two different phosphorus environments are expected. Accordingly, a peak at 80.15 ppm, corresponding to $[\text{GaCl}_2(\text{P}_{888}\text{O})_2]^+$, and another at 76.50 ppm, corresponding to $[\text{GaCl}_3(\text{P}_{888}\text{O})]$, are observed. In contrast to $\text{P}_{888}\text{O-AlCl}_3$, $\chi_{\text{AlCl}_3} = 0.50$, where both of these peaks had a similar intensity (Figure 15e), for the gallium model the neutral adduct gives a far more prominent peak (Figure 16a). The composition $\text{P}_{888}\text{O-GaCl}_3$, $\chi_{\text{GaCl}_3} = 0.60$ is expected to

show three phosphorus environments as Equation 12 suggests, however the ^{31}P NMR spectrum shows two peaks at 81.23 ppm and 79.97 ppm (Figure 16b), again comparison with the aluminium analogue suggests that the systems are very similar and therefore the smallest peak may be obscured by a larger peak or merged with the baseline. Previous work has shown through Raman spectroscopy that the speciation of $\text{P}_{888}\text{O-GaCl}_3$, $\chi_{\text{GaCl}_3} = 0.60$ closely follows the aluminium analogue described by Equation 12.²

When the metal halide composition increases to $\chi_{\text{GaCl}_3} > 0.60$ it is no longer possible to draw direct comparison between gallium and aluminium systems, owing to the formation of oligomeric structures in the former, but not the latter. Consequently, a new equation is required to explain the dynamic equilibrium at $\chi_{\text{GaCl}_3} = 0.67$. In the ^{31}P NMR spectrum (Figure 16c), two signals at 83.41 and 81.31 ppm represent $[\text{Ga}_2\text{Cl}_6(\text{P}_{888}\text{O})]$ and $[\text{GaCl}_2(\text{P}_{888}\text{O})_2]^+$ respectively. Raman spectra align with the equilibrium proposed in Equation 13.²

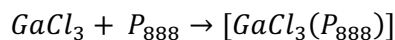


Equation 13

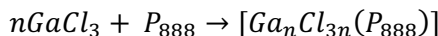
When the gallium chloride concentration is increased to the highest reported homogeneous value, $\chi_{\text{GaCl}_3} = 0.75$, ^{31}P NMR spectrum (Figure 16d) shows much broader signals than those at lower χ_{GaCl_3} values. Three relatively well-defined peaks and further low-intensity features suggest that the liquid contains many different equilibrated species.

For the P-donor compositions the ^{31}P NMR spectra are all similar, with a singlet peak which shifts from 0 ppm to -10 ppm from $\chi_{\text{GaCl}_3} = 0.5$ to 0.75. The peak at $\chi_{\text{GaCl}_3} = 0.5$ (Figure 16e) is broad and could represent multiple phosphorus environments in equilibrium, however the other peaks are all narrow and well-defined and as such are unlikely to conceal multiple structures. This is not in keeping with the speciation suggested by Coleman *et al.* which was derived from Raman spectroscopy.² However, when the original Raman data is re-evaluated, it is noticeable that there are fewer bands in the Ga-Cl stretching frequency for the P-donor, in comparison to GaCl_3 LCCs with non-phosphine adducts, suggesting that these systems may indeed contain a fewer complexes. In these Raman spectra the main band is at 349 cm^{-1} where $\chi_{\text{GaCl}_3} = 0.5$. This has been attributed to the neutral complex $[\text{GaCl}_3(\text{PPh}_3)]$, in work by Cheng *et al.*¹⁵³ Another paper from this group reported challenges in the synthesis of $[\text{GaCl}_2\text{L}_2]^+$ with a phosphine ligand, a species we would expect to see in Equations 11, 12 and 13 as molecular adducts, appear preferential to combinations of GaCl_3 with monodentate phosphines.¹⁵⁴ When the metal halide concentration increases to $\chi_{\text{GaCl}_3} = 0.60$ -0.75, the main band is found at 372 cm^{-1} , this has been observed in other LCCs and identified as the Ga-Cl stretch in neutral Ga^{III}

complexes $[Ga_nCl_{3n}(P_{888})]$. This molecular adduct formation can be summed up in the following equations which differ from those seen with $AlCl_3$ complexes and the harder $P_{888}O$ donor.



Equation 14



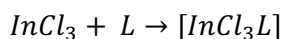
Equation 15

For gallium chloride LCCs there is a clear distinction in behaviour between hard and soft donor ligands, with both ionic and charge-neutral components forming with the former and molecular adducts strongly preferred with the latter. Work by El Hellani *et al.* investigating GaX_3 adducts with NHC donors showed that heterolytic splitting occurred with strong donors ($P_{888}O$), whereas homogeneous splitting occurred with weaker donors (P_{888}).¹⁵⁵

As with the aluminium chloride complexes, these are not new systems, and $P_{888}O-GaCl_3$ $\chi_{GaCl_3} = 0.6-0.75$ was found to be an effective catalyst for the Friedel-Crafts alkylation of benzene and 1-decene.¹³⁶ Therefore, in the context of Lewis acid catalysis, it is useful to emphasise that the lack of ionic species does not impair successful application.

2.5 Indium-Based Liquid Coordination Complexes

Following down the Group 13, the first indium-based LCCs have been synthesised. The two LCCs synthesised had the composition $P_{888}-InCl_3$ $\chi_{InCl_3} = 0.5$ and $P_{888}O-InCl_3$ $\chi_{InCl_3} = 0.5$. It has been observed in studies of chloroindate(III) ionic liquids have shown that at concentrations greater than $\chi_{InCl_3} = 0.5$ excess $InCl_3$ precipitates from the liquid.^{47,101,102} In this work, compositions with an excess of indium chloride contained white precipitate, and even at equimolar concentrations, $\chi_{InCl_3} = 0.5$, a small amount of white precipitate was observed. This was removed from the liquid by filtration before the NMR spectra were recorded. The ^{31}P NMR spectra recorded display just one broad singlet peak in each composition. For $P_{888}O-InCl_3$ $\chi_{InCl_3} = 0.5$ this is at 72.04 ppm and for $P_{888}-InCl_3$ $\chi_{InCl_3} = 0.5$ it is at 11.49 ppm. The ^{115}In NMR spectra provided no interpretable data, this in itself is informative as it is known from studying chloroindate(III) ionic liquids that the anion $[InCl_4]^-$ gives a broad but well-defined peak, as a consequence of its high symmetry as a tetrahedral molecule.⁴⁷ As this peak was not observed in either LCC, and only one peak is observed in the ^{31}P NMR spectra (Table 3), it appears that a simple molecular adduct forms in these liquids.



Equation 16

Considering this trend as we pass down the boron group, from both ligands giving ionic species (in addition to charge-neutral) with aluminium, to neither of the two ligands inducing such disproportionation in indium, it can be concluded that the increasing size of the metal atom plays a crucial role in the speciation. In contrast to aluminium and gallium chlorides, indium chloride is known to form tetra-, penta- and hexa- coordinated complexes with L-type donors, the coordination number dependent on the steric bulk of the ligands. This is a consequence of the larger atomic radius of indium. In publishing their work on crystal structures for indium halide complexes with phosphine oxide ligands, Robinson *et al.* demonstrated that a four-coordinate species is observed with P_{111}O , namely $[\text{InCl}_3(\text{P}_{111}\text{O})]$, but with the bulkier PPh_3O the six-coordinate cation $[\text{InCl}_2(\text{PPh}_3\text{O})_4]^+$ with the four-coordinate anion $[\text{InCl}_4]^-$ formed.¹⁵⁶ Altering a halide may also promote the ionic species to form: while $[\text{InCl}_3(\text{P}_{111}\text{O}_3)]$ is a molecular adduct, the analogous iodide was crystallised as $[\text{InI}_2(\text{Me}_2\text{SO})_4][\text{InI}_4]$.¹⁵⁷ In summary, although not observed in this work, heterolytic splitting of indium-based LCCs can be potentially achieved (if required for, for example, electrochemical applications) – particularly in a system with an excess of ligand, as a larger coordination number appears to be required for ionic species.

2.6 Antimony-Based Liquid Coordination Complexes

Among LCCs based on antimony, three were homogeneous liquids at room temperature: $\text{P}_{888}\text{--SbCl}_3$, $\chi_{\text{SbCl}_3} = 0.50$, $\text{P}_{888}\text{O--SbCl}_3$, $\chi_{\text{SbCl}_3} = 0.50$ and $\text{P}_{888}\text{O--SbCl}_3$, $\chi_{\text{SbCl}_3} = 0.6$. In the ^{31}P NMR spectrum of $\text{P}_{888}\text{--SbCl}_3$, $\chi_{\text{SbCl}_3} = 0.50$, the phosphine gave a singlet at -2.77 ppm. In the literature, similar systems are reported, for example a crystallographic study by Burford and colleagues that looked at three phosphine ligands: PPh_3 , PMe_3 and PCy_3 in conjunction with SbCl_3 .¹⁵⁸ In solution, the ^{31}P NMR shifts recorded in this work for neutral adducts with equimolar concentrations of phosphine to antimony chloride were seen over a range of 5.6 – 25.1 ppm and the complexes they formed with the antimony chloride varied. The key factor in this variation was steric bulk, with smaller ligands permitting polymeric chained complexes. For the complex $[\text{SbCl}_3(\text{PR}_3)]$ where R is a methyl group, which has a cone angle of 118 °, a polymeric chain is facilitated by bridging chlorides, shown in the crystal structures (Figure 17 left).^{158,159}

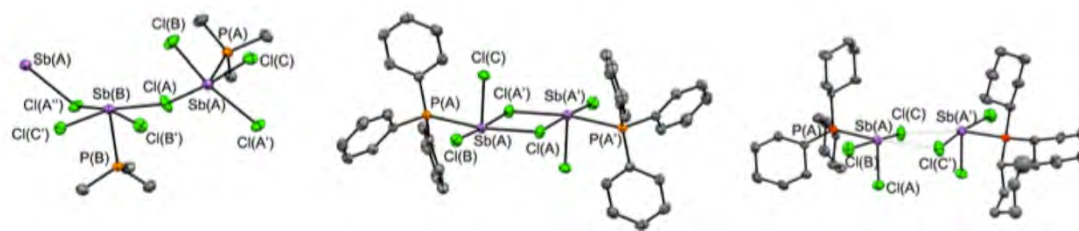
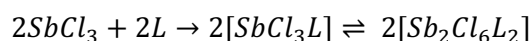


Figure 17. Crystal structures of (*left*) $\text{SbCl}_3(\text{PMe}_3)$ in a polymeric chain, (*centre*) in the dimeric $[\text{SbCl}_3(\text{PPh}_3)]$ and (*right*) in dimeric $[\text{SbCl}_3(\text{PCy}_3)]$.¹⁵⁸

For bulkier PCy_3 and PPh_3 ligands, which have cone angles of 170° and 145° respectively, a dimeric structure is observed in the solid state. Thus, the influence of the steric bulk can be seen reflected in the oligomer forming capabilities of the complexes, however the electronic effects also impact the structure of these crystals. A difference between the symmetry of the dimeric structures (Figure 17 centre and right) is apparent from longer Sb-Cl bond lengths on the bond which is trans to the phosphine in $[\text{SbCl}_3(\text{PCy}_3)]$. This is a consequence of the increased basicity of PCy_3 compared to PPh_3 with Tolman electronic parameters of 2056.4 cm^{-1} and 2068.9 cm^{-1} respectively and therefore a longer dimeric arrangement is observed with PCy_3 .¹⁵⁹ In this work the formation of this single neutral adduct is supported by ^{31}P NMR spectra, which indicate the formation of a single peak at -2.77 ppm . Following on from the work of Burford and colleagues, the long carbon chains would indicate that a dimeric structure could be expected, suggesting the equilibrium given in Equation 17.



Equation 17

The reactivity of this species led to its decomposition *via* oxidation during storage in the glovebox (under argon, in the absence of water or oxygen). This was reflected in ^{31}P NMR spectra (Figure 18). After two days of storage under inert conditions, a small peak at 103 ppm appeared, this corresponds to the phosphorus(V) peak of $[\text{P}_{888}\text{Cl}]^+$.¹⁶⁰ Following six months storage under inert conditions, the appearance of the sample had changed, with a solid black precipitate which was identified as antimony black, and the ^{31}P NMR spectrum of the residual liquid indicating a huge growth in the phosphorus(V) peak.

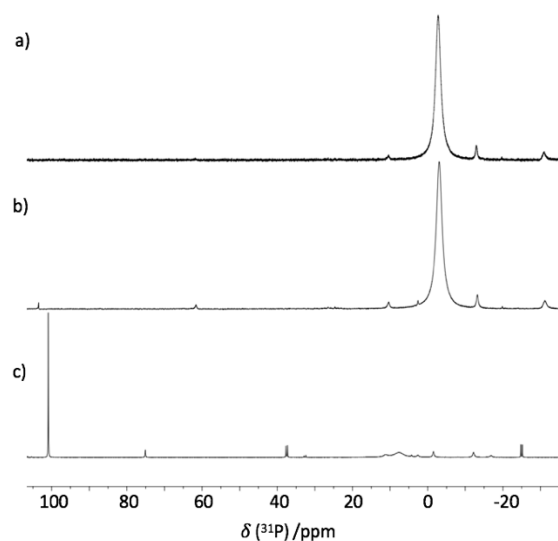
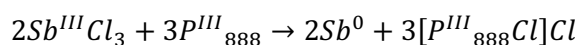


Figure 18. Changes to ^{31}P NMR spectra of $\text{P}_{888}\text{-SbCl}_3$, $\chi_{\text{SbCl}_3} = 0.50$ from a) immediately after synthesis, b) after two days under inert conditions and c) after six months under inert conditions.

These results suggest a complex redox reaction occurs as given in Equation 18.



Equation 18

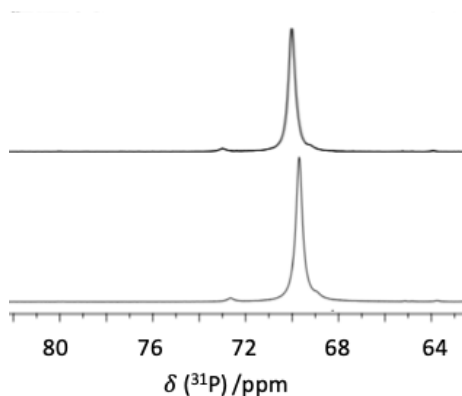


Figure 19. ^{31}P NMR spectra of $\text{P}_{888}\text{O-SbCl}_3$ $\chi_{\text{SbCl}_3} = 0.50$ (top) and $\chi_{\text{SbCl}_3} = 0.60$ (bottom).

Two LCCs based on the adducts of phosphine oxide with antimony chloride, $\text{P}_{888}\text{O-SbCl}_3$, $\chi_{\text{SbCl}_3} = 0.50$ and 0.60 , both gave singlets around 70 ppm in their ^{31}P NMR spectra (70.91 and 69.90 ppm, respectively, Figure 19). The work of the Burford and colleagues again shed some light on the chemistry of antimony complexes in the presence of phosphine oxides. The complex $[\text{SbCl}_3(\text{OPCy}_3)]$ was reported to give a singlet at 65.3 ppm in ^{31}P NMR spectra.¹⁶¹ This information is comparable to that with P_{888}O if the deviation from the non-coordinated

phosphine oxide is considered, for the work of Burford and colleagues this is $\Delta^{31}\text{P} = 15.6$ ppm, which is very similar to the deviations of $\Delta^{31}\text{P} = 21.0$ and 19.69 ppm for $\text{P}_{888}\text{O-SbCl}_3$, $\chi_{\text{SbCl}_3} = 0.50$ and 0.60 , respectively. Interestingly, the crystal structures reported by Burford and colleagues indicate the formation a bridged dimeric structure, analogous to that seen with the phosphine (Figure 17), with pentacoordinate square-based pyramidal geometry. Consequently, it is likely that for the composition $\text{P}_{888}\text{O-SbCl}_3$, $\chi_{\text{SbCl}_3} = 0.50$, a dimeric, neutral complex is the dominant product, forming according to Equation 17, where $\text{L} = \text{P}_{888}$. The similarity of the structure between the two ligands is believed to derive from the fact that the trans-labilising effect of P_{888} and P_{888}O does not significantly differ, as this is what Burford and colleagues postulate to be the driving factor in the structure determination of these complexes.^{158,161,162} It is difficult to argue that a different product should be forming for the same system at $\chi_{\text{SbCl}_3} = 0.60$, considering similarities in the ^{31}P NMR spectra (Figure 19). In conclusion, it seems likely that an oligomeric chain is forming in the liquid, with a similar structure as a lower concentrations of antimony chloride, but more studies would be required to confirm this.

2.7 Tin-Based Liquid Coordination Complexes

Tin chloride-based LCCs were synthesised from both SnCl_2 and SnCl_4 . Both ^{31}P and ^{119}Sn NMR spectra were possible to record at good quality, giving a greater breadth of available data for speciation.

2.7.1 Tin(II)-Based Liquid Coordination Complexes

Homogeneous liquids formed exclusively for $\chi_{\text{SnCl}_2} = 0.50$ for Sn(II) containing LCCs with both ligands, with higher concentrations of metal chloride containing solid, unreacted SnCl_2 . This indicates that oligomeric anions did not form. This is a contrast to ionic liquids with the $[\text{C}_2\text{mim}]^+$ cation which contain $[\text{Sn}_2\text{Cl}_5]^-$ anions where $\chi_{\text{SnCl}_2} > 0.50$ - its absence was the first indication that these LCCs contain only neutral species.¹⁰⁶ The combined ^{31}P and ^{119}Sn NMR spectroscopic data (Figure 20) paint a clear picture of speciation for the P_{888} complex, when compared to the previously reported $[\text{SnCl}_2(\text{P}_{222})]$ complex.¹⁶³

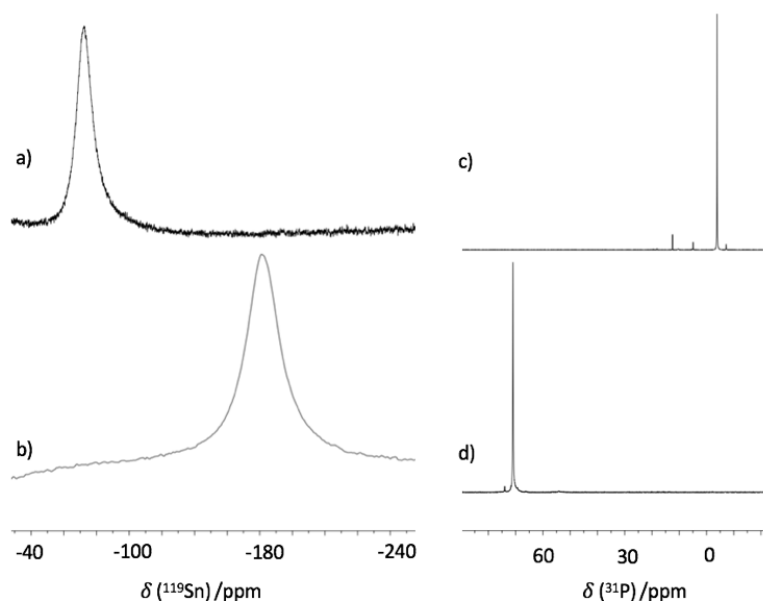
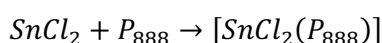


Figure 20. Sn(II) LCC NMR spectra of L-SnCl₂ LCCs at $\chi_{\text{SnCl}_2} = 0.50$ a) ^{119}Sn NMR spectrum of P₈₈₈-SnCl₂, b) ^{119}Sn NMR spectrum of P₈₈₈O-SnCl₂, c) ^{31}P NMR spectrum of P₈₈₈-SnCl₂, and d) ^{31}P NMR spectrum of P₈₈₈O-SnCl₂.

For the composition P₈₈₈- SnCl₂ $\chi_{\text{SnCl}_2} = 0.50$, a sharp singlet in the ^{31}P NMR spectrum is found at -3.98 ppm ($\Delta^{31}\text{P} = 25.55$ ppm), which is very similar to that of [SnCl₂(PET₃)], -3.7 ppm ($\Delta^{31}\text{P} = 16.3$ ppm). Similarly, for both systems, a broad singlet in the ^{119}Sn NMR is reported at -70.9 ppm for the LCC and at -82.5 ppm for [SnCl₂(P₂₂₂)]. Therefore, it can be assumed that the system reflects the formation of a simple charge-neutral complex [SnCl₂(P₈₈₈)], as described by Equation 19, which happens to have its melting point below ambient temperature.



Equation 19

In analogy to the complex formed for the phosphine, a complex containing [SnCl₂L], where L is an oxygen donor with alkyl or aryl groups, has not been reported in the Cambridge Structural Database (CSD). However, the tetracoordinate [SnCl₂L₂] is a far more common motif. Work from Gurnani *et al.* described the complexes [SnCl₂(PMe₃O)₂] and [SnCl₂(PMe₃O)₂], the NMR spectroscopic data for which is given in the table below.¹⁶⁴

Table 4. Comparison of NMR spectroscopic data for tin(II) complexes with oxide ligands.

Complex	χ_{SnCl_2}	^{119}Sn NMR peak/ ppm	^{31}P NMR peak/ ppm
[SnCl ₂ (PMe ₃ O) ₂] ¹⁶⁴	0.33	-204	51.2

$[\text{SnCl}_2(\text{PMe}_3\text{O})_2]^{164}$	0.33	Not reported	36.3
$\text{P}_{888}\text{O}-\text{SnCl}_2 \chi_{\text{SnCl}_2} = 0.50$	0.50	-179.5	70.96

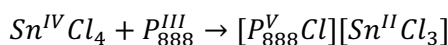
Table 4 suggests that the coordination around the tin centre is similar w the previously reported complexes and the system report herein, indicating a tetracoordinate tin. This is most specifically indicated by the chemical shift of the ^{119}Sn NMR spectrum, where a value around -100 ppm would indicate tricoordinate species, a chemical shift around 0 ppm would indicate neat SnCl_2 , but chemical shifts *ca.* 80 ppm correspond to tetracoordinate complexes.¹⁴⁹ However, the molar ratio of ligand to SnCl_2 is different in the LCC compared to the literature data (Table 4), although there is only one environment for both tin and phosphorus. To reconcile all this information, it was deduced that the $[\text{SnCl}_2\text{L}_2]$ structure is not representative. Instead a dimeric, neutral, structure with bridging chlorides is postulated $[\text{Sn}_2\text{Cl}_4(\text{P}_{888}\text{O})_4]$, formed as shown in Equation 20.



Equation 20

2.7.2 Tin(IV)-Based Liquid Coordination Complexes

For the system $\text{P}_{888}\text{-SnCl}_4 \chi_{\text{SnCl}_4} = 0.50$, a homogeneous liquid formed at room temperature. However, from ^{31}P NMR spectrum, a single peak was observed at 102 ppm, which corresponds to the phosphorus(V) peak of $[\text{P}_{888}\text{Cl}]^+$ (Figure 21),¹⁶⁰ indicating that a redox reaction had occurred. This was supported ^{119}Sn NMR spectra which gave a single peak at -38 ppm, which corresponds to a tricoordinate tin centre, as formed by Equation 21.¹⁴⁹ Further χ_{SnCl_4} values were not tested.



Equation 21

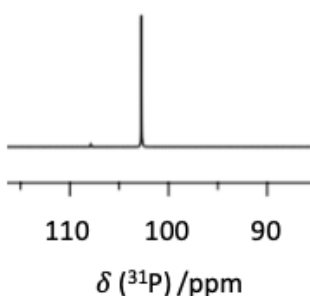


Figure 21. ^{31}P NMR spectra of $\text{P}_{888}\text{-SnCl}_4$ at $\chi_{\text{SnCl}_4} = 0.50$.

Working with the more reactive PMe_3 ligand, Burford and colleagues reported the successful synthesis and crystal structure determination of $[\text{SnCl}_4(\text{PMe}_3)_2]$ and reported no redox reactions.¹⁶⁵ However, the literature-described complex was synthesised under different conditions than these used in this work. Namely, Burford and colleagues used dichloromethane as a solvent, with the product crashing out of solution as a crystal. It is assumed that the solid state of the product impaired the rate of the redox reaction, and the authors have not reported solution-state ^{119}Sn NMR spectrum for this compound.

In contrast, two compositions of SnCl_4 combined with phosphine oxide ($\chi_{\text{SnCl}_4} = 0.50$ and 0.6) formed homogeneous, colourless liquids, stable according to NMR spectroscopic studies (^{119}Sn and ^{31}P NMR spectra are given Figure 22). In the ^{119}Sn NMR spectra, three peaks are visible at both concentrations, at the lower $\chi_{\text{SnCl}_4} = 0.50$ concentration, these are at -336.3 , -449.2 and -710 ppm, with the third peak splitting into fragments of a multiplet, tentatively resembling two doublets, at -709.5 ppm ($^2J_{^{119}\text{Sn}-^{31}\text{P}} = 149.4$ Hz) and at -711.7 ppm ($^2J_{^{119}\text{Sn}-^{31}\text{P}} = 109.2$ Hz). This splitting is not visible in the spectrum for $\chi_{\text{SnCl}_4} = 0.60$, however three peaks are observed at -211.1 , -449.2 and -710 ppm (Figure 22b). Appearing in both spectra, the peak at -710 ppm corresponds to the hexacoordinate tin species $[\text{SnCl}_4(\text{P}_{888}\text{O})_2]$.¹⁶⁶ Accordingly, the multiplets surrounding this peak correspond to the *cis* and *trans*-conformers around the octahedral centre, although the J-coupling varies from the reported $^2J_{^{119}\text{Sn}-^{31}\text{P}} = 144\text{--}216$ Hz value reported. The more downfield peak of -449.2 ppm can be attributed to the stoichiometric adduct of $[\text{SnCl}_4(\text{P}_{888}\text{O})]$. Finally, the chemical shift of the third peak differs between the two compositions (-336.3 ppm in $\chi_{\text{SnCl}_4} = 0.50$, -211.1 ppm in $\chi_{\text{SnCl}_4} = 0.60$) shifting further downfield with increasing concentration, it can be assigned to the neat SnCl_4 . The signal for neat tin(IV) chloride is found at -150 ppm, but here is likely affected by the dynamic equilibrium. Further evidence for the assignment of this peak comes from its visible increase in area with a greater tin(IV) chloride concentration.

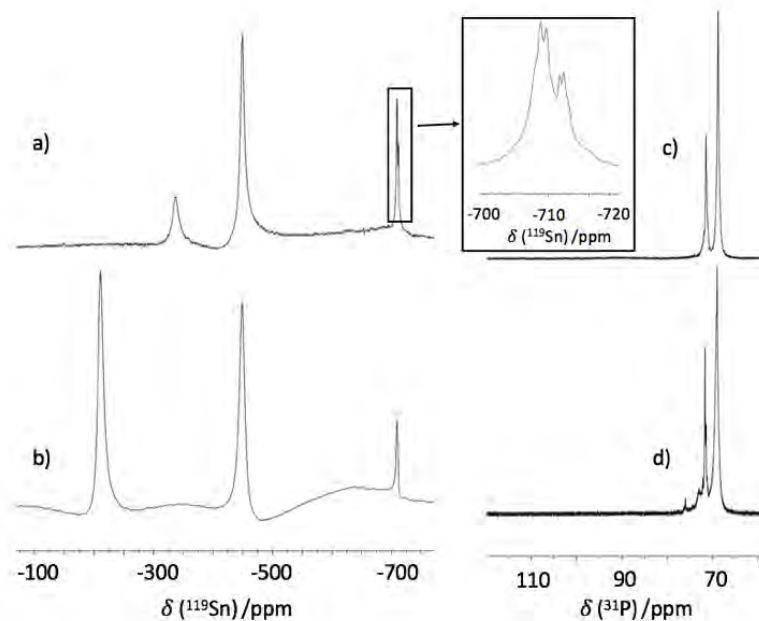


Figure 22. Tin(IV) LCC NMR spectra of $P_{888}O-SnCl_4$ LCCs a) ^{119}Sn NMR spectrum of $P_{888}O-SnCl_4$ at $\chi_{SnCl_4} = 0.50$, b) ^{119}Sn NMR spectrum of $P_{888}O-SnCl_4$ at $\chi_{SnCl_4} = 0.60$, c) ^{31}P NMR spectrum of $P_{888}O-SnCl_4$ at $\chi_{SnCl_4} = 0.50$, and d) ^{31}P NMR spectrum of $P_{888}O-SnCl_4$ at $\chi_{SnCl_4} = 0.60$.

In the ^{31}P NMR spectrum at $\chi_{SnCl_4} = 0.50$, there are two peaks at 68.74 and 71.40 ppm (Figure 22c), while in the spectrum recorded for $\chi_{SnCl_4} = 0.60$, signals are slightly less well defined and are grouped around 68.88 and 71.38 ppm (Figure 22d). This supports the evidence from the ^{119}Sn NMR spectrum, indicating that while there are three species containing tin, only two contain phosphorus. Therefore, the dynamic equilibrium (Equation 22) describes the most likely speciation of these phosphine oxide LCCs.



Equation 22

2.8 Titanium-Based Liquid Coordination Complexes

Titanium chloride formed red liquids at $\chi_{TiCl_4} = 0.5$ and 0.6 with P_{888} . With the $P_{888}O$ ligand a homogeneous yellow liquid formed for $\chi_{TiCl_4} = 0.5$ but a yellow solid containing some white precipitate formed at $\chi_{TiCl_4} = 0.6$.

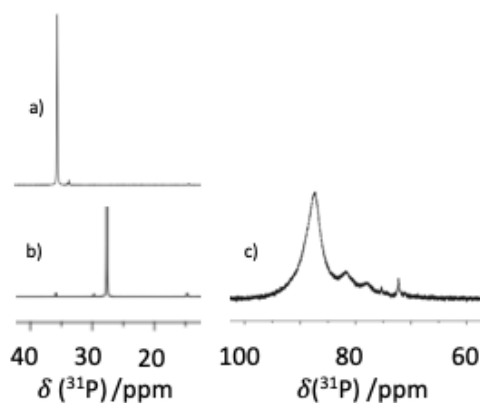
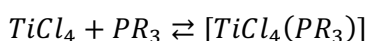


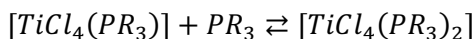
Figure 23. ^{31}P NMR spectra for L-TiCl₄ LCCs a) P₈₈₈-TiCl₄ at $\chi_{\text{TiCl}_4} = 0.50$, b) P₈₈₈-TiCl₄ at $\chi_{\text{TiCl}_4} = 0.60$ c) P₈₈₈O-TiCl₄ at $\chi_{\text{TiCl}_4} = 0.50$.

Comparing ^{31}P NMR signals in Table 3, the largest change in chemical shifts of phosphines, was recorded for titanium complexes, with $\Delta^{31}\text{P}$ values of 57.12 ppm for $\chi_{\text{TiCl}_4} = 0.5$ and 63.94 ppm for $\chi_{\text{TiCl}_4} = 0.6$, indicating a huge degree of deshielding (Figure 23a and b). Similarly high levels of ^{31}P deshielding were reported for TiCl₄ complexes with PPh₃ and PMe₃ ligands, with $\Delta^{31}\text{P}$ values of 26 and 71.2 ppm, respectively.¹⁶⁷ This strong interaction between phosphine and titanium is highlighted by a bright red colour, indicative of P – Ti^{IV} ligand metal charge transfer (LMCT) absorption, reported for the complexes: [TiCl₄(PPh₃)] and [TiCl₄(PPh₃)₂] with a $\lambda_{\text{max}} = \sim 480$ nm.¹⁶⁸

In dichloromethane solution, speciation of phosphine complexes of titanium chloride has been described as a series of complex, dynamic equilibria given in Equation 23-24, with Equation 25 expected to be more likely in lower temperatures.^{167,169,170}



Equation 23



Equation 24



Equation 25

The structure of the binuclear has been described as a dimeric complex with bridging chlorides (Figure 24).¹⁶⁷

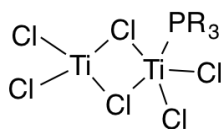
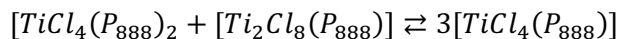


Figure 24. The proposed structure of $[\text{Ti}_2\text{Cl}_8\text{PR}_3]$.

In the equilibria presented in Equation 23-24, three different phosphorus environments are evident. While similar, it is possible to distinguish between them. Gordon *et al.* used variable temperature ^1H NMR spectroscopy experiments to study a complex of TiCl_4 with PMe_2Ph , at $\chi_{\text{TiCl}_4} = 0.4$. At room temperature just one peak corresponding to the methyl group was seen in the ^1H NMR spectrum recorded at 8 ppm but on cooling to -57°C , three unique environments were observed. By increasing the concentration of the titanium chloride to $\chi_{\text{TiCl}_4} > 0.67$ in C_6D_6 these three different signals were elucidated, for compositions with PEt_3 and PBU_3 , however at these high concentrations no free phosphine was observed.¹⁷⁰ At very low loadings of TiCl_4 ($\chi_{\text{TiCl}_4} = 0.09$), the dimeric structure was not detected, but instead free phosphine existed. In this work, one signal was recorded for each of the χ_{TiCl_4} values; however, the large downfield shift in the ^{31}P NMR spectrum in combination with the observed colour change demonstrating a P-Ti^{IV} interaction are in line with other studies, all of which point to the existence of a dynamic equilibrium (Equation 26), with exchange rate tuneable by the phosphine itself, solvent, temperature and other factors.



Equation 26

The complex of titanium chloride with P_{888}O , $\chi_{\text{TiCl}_4} = 0.5$, was a yellow homogeneous liquid. Its $\Delta^{31}\text{P}$ value of 37.36 ppm was the largest shift of any P_{888}O species measured (Table 3, Figure 23c), indicating that it is the most deshielded. Although there are no crystal structures of structures from equimolar phosphine oxide adducts, the crystal structure of $[\text{TiCl}_4(\text{Ph}_3\text{PO})_2]$ was reported in 2006.¹⁷¹ Trioctylphosphine oxide has found many uses in the context of Ti^{IV} chemistry, chiefly in extraction from strongly acidic solutions, where it is believed to form $[\text{TiCl}_4(\text{P}_{888}\text{O})_2]$,¹⁷² but also in the synthesis of titania (TiO_2) nanoparticles.¹⁷³ Surprisingly in this context, solution phase speciation studies on the complexes of TiCl_4 and phosphine oxides have not been carried out. In this work, the high degree of deshielding in the ^{31}P NMR spectrum suggests that there is a strong interaction between the oxygen and titanium, supporting the adduct formation. It can be a simple $[\text{TiCl}_4(\text{P}_{888}\text{O})]$ complex as the only product. The complex dynamic equilibria presented for the system with the soft phosphine donor of course also presented with just one ^{31}P NMR spectroscopic peak, and the idea that there is multiple oligomeric species in equilibrium cannot be fully discounted. However, the strength of the titanium-oxygen bond is expected to be much greater and as such it is less likely to be

a labile enough ligand for a range of species to be accessible. X-ray crystallographic study on a higher-melting analogue would be a useful extension of this work to gain greater understanding of the behaviour of this LCC system.

2.9 Zinc-Based Liquid Coordination Complexes

Zinc chloride formed colourless liquids at $\chi_{\text{ZnCl}_2} = 0.5$ and 0.6 with P_{888}O . With the P_{888} ligand a colourless liquid formed for $\chi_{\text{ZnCl}_2} = 0.5$ with some white precipitate forming at $\chi_{\text{ZnCl}_2} = 0.6$. Previous studies into the coordination species of zinc halides in the ionic liquid phase have suggested that a wide variety of oligomeric zinc structures can be observed, including $[\text{ZnCl}_4]^{2-}$, $[\text{Zn}_2\text{Cl}_6]^{2-}$ and $[\text{Zn}_4\text{Cl}_{10}]^{2-}$.^{105,174} Structures reported by crystallographers are highly dependent on relative concentrations of zinc halides and ligands, with low zinc loadings giving the structure $[\text{ZnX}_2\text{L}_2]$.¹⁵⁰ However, as with the oligomeric species seen in ionic liquids, at higher concentrations bridging chlorides are observed, exemplified by $[\text{ZnCl}(\text{P}^t\text{Bu}_3)(\mu\text{Cl})_2\text{ZnCl}(\text{P}^t\text{Bu}_3)]$ (Figure 25).¹⁷⁵

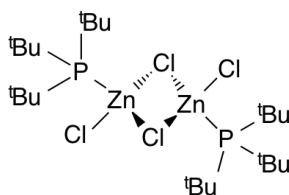


Figure 25. The structure of the equimolar combination of ZnCl_2 and P^tBu_3 as determined by crystallography.

In this work, only the ZnCl_2 - P_{888} $\chi_{\text{ZnCl}_2} = 0.5$ composition formed a homogeneous liquid, with greater zinc chloride loadings leaving an unreacted white precipitate of zinc chloride. The ^{31}P NMR spectroscopy showed a single peak and given the illustrated structure, the reaction is likely to proceed to form the adduct described by Equation 27 (Figure 26a).



Equation 27

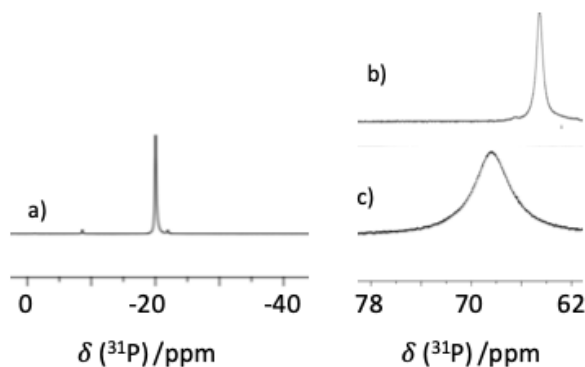


Figure 26. ^{31}P NMR spectra for L- ZnCl_2 LCCs a) $\text{P}_{888}\text{-ZnCl}_2$ at $\chi_{\text{ZnCl}_2} = 0.50$, b) $\text{P}_{888}\text{O-ZnCl}_2$ at $\chi_{\text{ZnCl}_2} = 0.50$ c) $\text{P}_{888}\text{O-ZnCl}_2$ at $\chi_{\text{ZnCl}_2} = 0.60$.

For $\text{ZnCl}_2\text{-P}_{888}\text{O}$ $\chi_{\text{ZnCl}_2} = 0.5$ and 0.6 both formed colourless, homogeneous liquids and were found to give a single peak in ^{31}P NMR spectra at 65.56 and 68.23 ppm, respectively (Figure 26b and c). As with titanium, phosphine oxides have been studied as zinc halide extracting agents. Although the adduct $[\text{ZnCl}_2(\text{P}_{888}\text{O})_2]$ is believed to be the product, which involves an excess of ligand, little actual research went into understanding the speciation of such complexes with phosphine oxide ligands.¹⁷⁶ With other oxygen donors, zinc halides typically form tetrahedral structures.¹⁷⁷ Therefore, from the evidence presented here, a similar reaction is expected to occur with the harder P_{888}O donor as was seen with the softer phosphine donor, with a bridged adduct forming (Equation 28). Like with titanium, an in-depth speciation study would be an interesting subject of further investigation.



Equation 28

2.10 Summary of Liquid Coordination Complex Speciation

The work presented in this section demonstrates a broadening of the scope of metal halides in the synthesis of Lewis acidic liquid coordination complexes. By using two different ligands, a phosphine and phosphine oxide, a comparison of the effects of hard and soft Lewis donors is achieved. The comparable structures of the ligands, both with three octyl chains prevented changes in their behaviour due to sterics, whilst the long chain length contributed to reducing the melting point of the LCCs formed, whilst avoiding wax formation.

Since LCCs containing the phosphine ligand underwent redox reactions with metals at higher oxidation stages, the P_{888}O ligand may be a more robust and versatile choice for generating LCCs for catalytic applications. Air-stable and known to act as capping agent, it is also

anticipated to be the best choice for using these systems as precursors for nanoparticle syntheses and – possibly - electrodepositions.

Using multinuclear NMR to observe the speciation of the metal centres was not possible for LCCs other than those containing aluminium or tin, however the use of ^{31}P NMR spectroscopy provided insight into the complexes formed. This aligned with metal NMR spectroscopy (where available) and speciation derived from comparisons with crystal structures. An interesting observation was the proclivity of molecular species to form for LCCs with metal halides other than Al or Ga, which had been the previous focus of studies. However, additional oligomeric and dimeric species have been proposed and the great variety of different species indicates the high levels of tunability in these systems, varying just metal halide, donor strength and relative concentrations. The results drawn from this work could be developed by the confirmation of speciation through techniques such as Raman and FT-IR spectroscopy, XPS, EXAFS or application-based techniques such as conductivity measurements which were beyond the scope of this work.

A summary of postulated speciation for all LCC described in this section is given in Table 5 and Table 6 below.

Table 5. The relative speciations of different LCCs with the formula $\text{MCl}_x\text{-P}_{888}\text{O}$.

MCl_x	χ_{MCl_x}	
AlCl_3	0.50	$2[\text{AlCl}_3(\text{P}_{888}\text{O})] \rightleftharpoons [\text{AlCl}_2(\text{P}_{888}\text{O})_2][\text{AlCl}_4]$
	0.60	$[\text{AlCl}_3\text{L}] + [\text{Al}_2\text{Cl}_6(\text{P}_{888}\text{O})] \rightleftharpoons [\text{AlCl}_2(\text{P}_{888}\text{O})_2][\text{Al}_2\text{Cl}_7]$
GaCl_3	0.50	$2[\text{GaCl}_3(\text{P}_{888}\text{O})] \rightleftharpoons [\text{GaCl}_2(\text{P}_{888}\text{O})_2][\text{GaCl}_4]$
	0.60	$[\text{GaCl}_3(\text{P}_{888}\text{O})] + [\text{Ga}_2\text{Cl}_6(\text{P}_{888}\text{O})] \rightleftharpoons [\text{GaCl}_2(\text{P}_{888}\text{O})_2][\text{Ga}_2\text{Cl}_7]$
	0.67	$[\text{GaCl}_6(\text{P}_{888}\text{O})] \rightleftharpoons [\text{GaCl}_2(\text{P}_{888}\text{O})_2][\text{Ga}_3\text{Cl}_{10}]$
	0.75	Complex Oligomers
InCl_3	0.50	$[\text{InCl}_3(\text{P}_{888}\text{O})]$
SbCl_3	0.50	$2[\text{SbCl}_3(\text{P}_{888}\text{O})] \rightleftharpoons [\text{Sb}_2\text{Cl}_6(\text{P}_{888}\text{O})_2]$
	0.60	Oligonuclear Cl-bridged complexes
SnCl_2	0.50	$[\text{Sn}_2\text{Cl}_4(\text{P}_{888}\text{O})_2]$
SnCl_4	0.50	$[\text{SnCl}_4(\text{P}_{888}\text{O})_2] + \text{SnCl}_4 \rightleftharpoons 2[\text{SnCl}_4(\text{P}_{888}\text{O})]$
	0.60	$[\text{SnCl}_4(\text{P}_{888}\text{O})_2] + \text{SnCl}_4 \rightleftharpoons 2[\text{SnCl}_4(\text{P}_{888}\text{O})]^a$
TiCl_4	0.50	$[\text{TiCl}_4(\text{P}_{888}\text{O})_2]$
ZnCl_2	0.50	$[\text{Zn}_2\text{Cl}_4(\text{P}_{888}\text{O})_2]$
	0.60	Oligonuclear Cl-bridged complexes

^aThis equilibrium does not represent the actual stoichiometry of this composition

Table 6. The relative speciations of different LCCs with the formula MCl_x-P_{888} .

MCl_x	χ_{MCl_x}	
$AlCl_3$	0.50	$2[AlCl_3(P_{888})] \rightleftharpoons [AlCl_2(P_{888})_2][AlCl_4]$
	0.60	$[AlCl_3L] + [Al_2Cl_6(P_{888})] \rightleftharpoons [AlCl_2(P_{888})_2][Al_2Cl_7]$
$GaCl_3$	0.50	$[GaCl_3(P_{888})]$
	0.60	$[Ga_2Cl_6(P_{888})]$
	0.67	$[Ga_3Cl_9(P_{888})]$
	0.75	Complex Oligomers
$InCl_3$	0.50	$[InCl_3(P_{888})]$
$SbCl_3$	0.50	$2[SbCl_3(P_{888})] \rightleftharpoons [Sb_2Cl_6(P_{888})_2] \rightarrow \text{redox}$
$SnCl_2$	0.50	$[SnCl_2(P_{888})]$
$SnCl_4$	0.50	Redox
$TiCl_4$	0.50	$[TiCl_4(P_{888})_2] + [Ti_2Cl_8(P_{888})] \rightleftharpoons 3[TiCl_4(P_{888})]$
	0.60	$[TiCl_4(P_{888})_2] + [Ti_2Cl_8(P_{888})] \rightleftharpoons 3[TiCl_4(P_{888})]^a$
$ZnCl_2$	0.50	$[Zn_2Cl_4(P_{888})_2]$

^aThis equilibrium does not represent the actual stoichiometry of this composition

2.11 Lewis Acidity Determination using a Spectroscopic Probe

Gutmann acceptor number was used to determine Lewis acidities of all room-temperature LCCs (introduction to AN measurements is described in Section 1.1.3.1). AN values collected for the studied LCCs are compared to the parent metal chlorides in

Table 7.

Table 7. Gutmann acceptor numbers recorded for metal halides, in 1,2 dichloroethane, and LCCs, recorded as neat liquids.

MCl _x	χ_{MCl_x}	Acceptor Number		
		MCl _x	P ₈₈₈ O	P ₈₈₈
AlCl ₃	0.50		85.4	83.3
	0.60		94.7	101.9
	1.00	85.6		
GaCl ₃	0.50		87.4	87.8
	0.60		96.3	95.6
	0.67		105.0	102.3
	0.75		107.3	104.9
	1.00	75.9		
InCl ₃	0.50		75.3	67.5
	1.00	74.3		
SbCl ₃	0.50		69.3	58.3
	0.60		76.2	
	1.00	61.4		
SnCl ₂	0.50		74.9	77.6
	1.00	75.2		
SnCl ₄	0.50		79.2	Redox
	0.60		77.0	
	1.00	79.6		
TiCl ₄	0.50		109.8	122.1
	0.60			135.9
	1.00	108.8		
ZnCl ₂	0.50		63.3	64.3
	0.60		65.8	
	1.00	66.0		

2.11.1 Lewis Acidity of Metal Halides

Surprisingly, AN values for Lewis acidic metal chlorides were very poorly reported in the literature, and even when some AN values were measured, diverse methodologies were used, preventing direct comparison between values from different authors. Therefore, it was found necessary to create a comprehensive and uniform acidity scale for the Gutmann acceptor numbers for metal halides. This was determined for a 1,2-dichloroethane solution at a concentration of 0.35 mol dm⁻³. This was the solvent used by Mayer *et al.* for the original

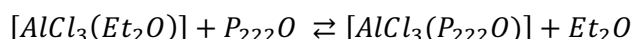
measurements and it was selected to give reliable comparison and, accordingly, AN values were measured by the procedure detailed in the original paper.⁴⁶ This entailed forming a 1:1 molar ratio between MCl_x and $P_{222}O$. The results (

Table 7) give the ordering of Lewis acidities in the order of $TiCl_4 > SbCl_5 > AlCl_3 > SnCl_4 > GaCl_3 \approx InCl_3 \approx SnCl_2 > ZnCl_2 > SbCl_3$. The challenge of using Gutmann acceptor numbers to give truly comparable Lewis acidity measurements is highlighted by the comparison between ANs given in this work (in 1,2-dichloroethane) and from previous work by Beckett *et al.* in diethyl ether, given Table 8.²⁵

Table 8. Comparison between metal halide Gutmann AN measurements in diethyl ether²⁵ and in 1,2-dichloroethane.

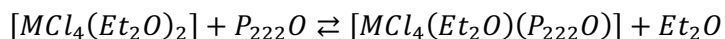
Metal Halide	AN _{DCE}	AN _{Et₂O} ²⁵
TiCl ₄	108.8	70
AlCl ₃	85.6	87
SnCl ₄	79.2	59

This data illustrates that the ordering of metal halides differs between solvents, with the ordering in diethyl ether being $AlCl_3 > TiCl_4 > SnCl_4$. In their work, Beckett and colleagues justify their measurements by finding strong correlation between the measurements taken using the Childs method (discussed in Section 1.1.3.2), however it is clear that the interaction between solvent and metal halide has a large influence on the AN values obtained for $TiCl_4$ and $SnCl_4$ and this changes the relative ordering of these metal halides. This can be explained by considering the different interactions that $TiCl_4$ and $SnCl_4$ have with diethyl ether compared to $AlCl_3$. With the former a hexacoordinate structure is formed, $[MCl_4(Et_2O)_2]$,^{166,178} however the interaction with the latter forms a tetrahedral complex, $[MCl_3(Et_2O)]$.¹⁷⁹ For both systems an equivalent ratio of probe molecule to metal complex is used, despite these differing coordination sphere. This explains why the AN values for $SnCl_4$ and $TiCl_4$ are suppressed: when $AlCl_3$ interacts with the $P_{222}O$ molecule, only chloride ligands surround the metal centre, as shown in the equation below.



Equation 29

In contrast, only one of the two molecules of solvent which surround the Ti^{IV} and Sn^{IV} centres is likely to be displaced by the probe molecule, due to the relative abundance of solvent molecules, and so the metal remains in interaction with the donating solvent molecule, as shown below.



Equation 30

In conclusion, the role of the solvent can cause deviation from the “true” Lewis acidity of a system by affecting different Lewis acidic centres differently, and to avoid it appears to be preferable to use a non-coordinating solvent. Furthermore, this discussion highlights that comparison between measurements in different solvents may not be truly reflective of Lewis acidity. Liquid Lewis acids, measured without solvent, may be giving a more accurate measurement of “naked” Lewis acidity (or at least, measurement burdened with one less variable).

Another technique employed to record relative Lewis acidities of metal halides was published by Kobayashi *et al.*,¹⁸⁰ based on the activity of a range of Lewis acids towards the catalysis of a silyl enol ether and the selectivity it gives towards aldehyde or aldimine products.

Lewis acids were subsequently classified into three classes, A – active, B – weak and C – inactive and further divided them within these categories as 1 – aldehyde-selective, 2 – aldimine-selective and 3 – neutral. A broad range of metal halides was ranked in this work, which gave a good opportunity for a more robust comparison. The Kobayashi scale fitted well against the metal halide acceptor numbers recorded here, with higher ANs corresponding to greater activity in the work by Kobayashi *et al.* (Figure 27). The only result not in discord was $SbCl_4$ which gave a relatively modest Gutmann acceptor number but is classed as an A-1 acid on the Kobayashi scale. This provides another reminder that Lewis acidity is a subjective measurement, largely probe-dependent and consequently different factors can influence quantification attempts.

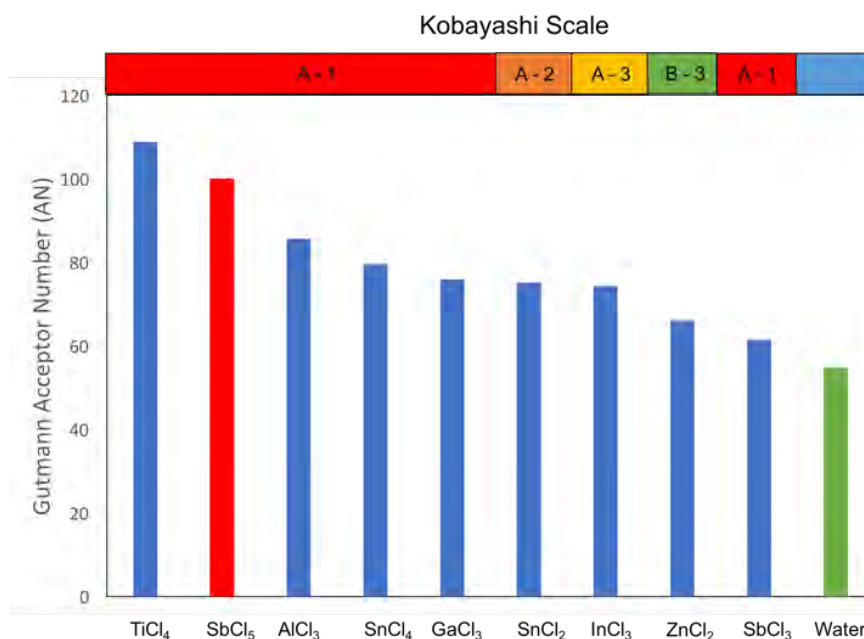


Figure 27. Comparison of relative Lewis acidities reported by Kobayashi *et al.*,¹⁸⁰ with the metal halide Gutmann acceptor numbers. Data for SbCl₅ and water taken from work by Gutmann *et al.*⁴⁶

2.11.2 Lewis Acidity of LCCs

As discussed earlier, a challenge in recording the Gutmann acceptor numbers for this work is the potential overlap between P₈₈₈O and P₂₂₂O peaks. This was addressed by synthesising an LCC based on the P₂₂₂O probe, AlCl₃-P₂₂₂O $\chi_{\text{AlCl}_3} = 0.5$, and recording its spectrum to be compared with AlCl₃-P₈₈₈O $\chi_{\text{AlCl}_3} = 0.5$. The AlCl₃-P₂₂₂O $\chi_{\text{AlCl}_3} = 0.5$ system was not a liquid at room temperature and required warming to 55 °C to record NMR spectra. Comparing the ³¹P NMR spectra recorded at the same temperature, there was a $\Delta\delta_{31\text{P}} = 5$ ppm difference in chemical shift between both signals, with two signals from P₂₂₂O at 80.37 and 82.28 ppm, compared to two signals from P₈₈₈O at 75.20 and 77.38 ppm. This was considered a large enough difference to allow for the accurate identification of peaks arising from the slightly more deshielded probe molecule.

The interaction that each LCC may have with the P₂₂₂O probe is dependent on a range of factors, including the species that are present in equilibrium, the strength of the interaction between the ligand and the metal halide itself. Consequently, it is not always simple to predict the species that will form with the probe and interpretation of Gutmann acceptor numbers is required to appreciate the observations. In particular, a crucial aspect is whether the metal complex is coordinatively saturated and therefore whether it can accept another ligand, or if either a chloride or phosphine/phosphine oxide must be substituted. To understand this, comparison with the data from metal halides in solution is essential (Figure 28).

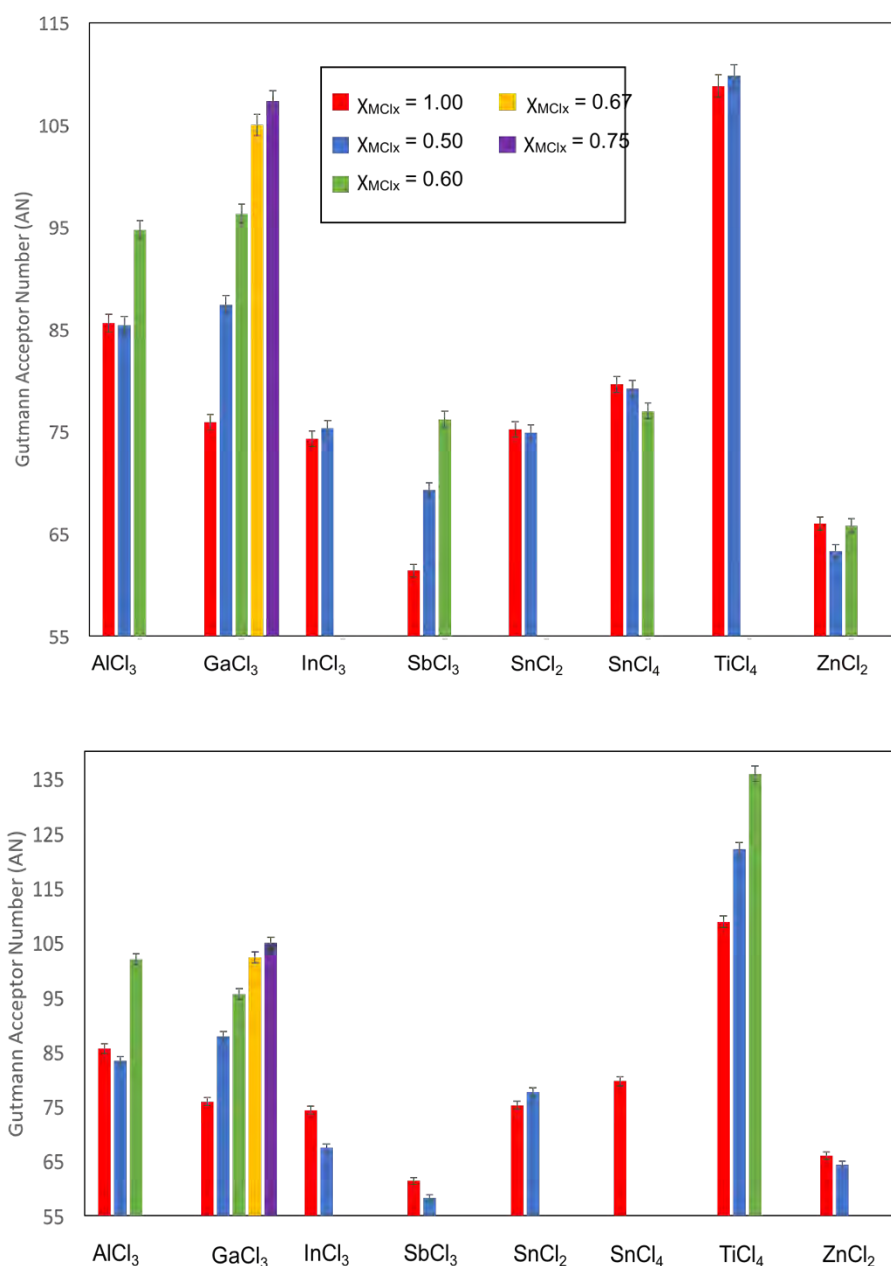
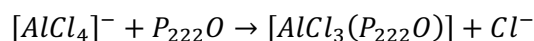


Figure 28. Comparison of ANs for metal halides (recorded in 1,2-dichloroethane), with ANs for all LCCs for MCl_x-L for all values of χ_{MClx} recorded. L = P₈₈₈O (top) and L = P₈₈₈ (bottom).

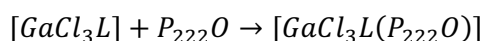
For ligands in a saturated complex, typically those around aluminium and gallium, it is expected that ligand substitution must be required for the probe molecule to bind. Although the ion [AlCl₄]⁻ is catalytically inactive as it has no acceptor capabilities, in Gutmann acceptor measurements it undergoes ligand substitution to form [AlCl₃(P₂₂₂O)], which gives an AN of 96.^{19,21} This is a consequence of the high electrophilicity of the aluminium(III) species may be interpreted as a failure of the Gutmann system, by altering the species being observed, as such it is regarded as a false reading. At the same time, this represents an actual interaction with an oxygen nucleophile, of basicity similar or higher to that of P₂₂₂O, therefore provides useful insight.

In this work, the LCC $\text{AlCl}_3\text{-L}$ $\chi_{\text{AlCl}_3} = 0.5$ has an acceptor number almost identical to that of AlCl_3 , as Equation 11 demonstrates this could arise from either tetracoordinate species of $[\text{AlCl}_4]^-$ or $[\text{AlCl}_3\text{L}]$, losing either a chloride or L species respectively would result in the formation of $[\text{AlCl}_3(\text{P}_{222}\text{O})]$ (Equation 31). It must be considered, however, that such a Gutmann AN is not necessarily reflective of catalytic activity, as a weaker nucleophile may not have the capability to displace a ligand and coordinate to the aluminium centre.

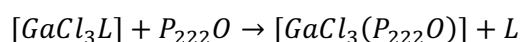


Equation 31

For chlorogallate ionic liquids, low acceptor numbers ($\text{AN} = 45$) were recorded for $[\text{GaCl}_4]^-$ (that is, for ionic liquid with monomeric anion, $\chi_{\text{GaCl}_3} = 0.5$). This suggests that the P_{222}O molecule neither displaces a chloride, nor does it coordinate to form a pentacoordinate complex.²¹ With $\text{AN} = 45$, the low acidity of $[\text{GaCl}_4]^-$ anion is more accurately reflected than its aluminium analogue. Conversely, ANs recorded in this work for $\text{GaCl}_3\text{-L}$ $\chi_{\text{GaCl}_3} = 0.5$ were significantly higher: $\text{AN} = 87.4$ for $\text{L} = \text{P}_{888}\text{O}$ and $\text{AN} = 87.8$ for $\text{L} = \text{P}_{888}$, exciding acceptor number for the neat metal halide, $\text{AN}_{\text{GaCl}_3} = 75.9$. The speciation of the complex with the probe molecule could either arise from Equation 32 or Equation 33. However, considering the steric bulk provided by the octyl chains of the ligands and knowing that the formation of the penta-coordinate species would be disfavoured, it seems likely that Equation 33 is a more accurate description of the speciation. This argument is strengthened by observations that LCCs with $\text{GaCl}_3\text{-L}$ $\chi_{\text{GaCl}_3} = 0.5$ are not active catalysts in carbocationic reactions. This suggests the active species is not present. This is reflected by $[\text{AlCl}_4]^-$ anions giving unrepresentatively higher ANs when the probe displaces a ligand.^{136,181}

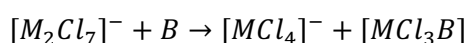


Equation 32



Equation 33

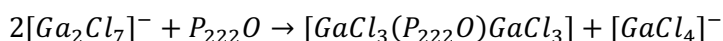
At higher concentrations of gallium and aluminium chloride, dimeric and oligomeric species are observed. Anions with the general formula $[\text{M}_x\text{Cl}_{(3x+1)}]^-$, or $[\text{Zn}_2\text{Cl}_6]^-$, are Lewis acidic as can react with a base (Equation 34).



Equation 34

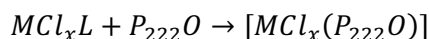
This ready reactivity towards Lewis bases is facilitated by their structure. Bridging chlorides between metal centres of oligonuclear complexes form the weakest bonds in the molecule. This allows for their cleavage with even a very weakly Lewis basic molecule. Several systems reported here contain oligomeric or dimeric species metal chloride species, these are $\text{GaCl}_3\text{-P}_{888}\text{O}$ $\chi_{\text{GaCl}_3} = 0.6$ and 0.67 , $\text{SbCl}_3\text{-P}_{888}\text{O}$ $\chi_{\text{SbCl}_3} = 0.6$ and $\text{ZnCl}_2\text{-P}_{888}\text{O}$ $\chi_{\text{ZnCl}_2} = 0.6$. Bridged oligomeric structures were also described for the LCCs $\text{SnCl}_2\text{-P}_{888}\text{O}$ $\chi_{\text{SnCl}_2} = 0.5$ and $\text{TiCl}_4\text{-P}_{888}\text{O}$ $\chi_{\text{TiCl}_4} = 0.5$ and 0.6 . These anions react with P_{222}O (as per Equation 34), because the weakly bound bridging chlorides in their structure make the Lewis acidic centre effectively accessible to any base. This is known as latent Lewis acidity, whereby seemingly saturated centre has an extremely labile ligand, allowing for this centre to act as a strong Lewis acid.⁶⁵ In consequence, AN for this adduct is identical to that of the neat metal halide, in analogy with the zinc and tin(II) LCCs.

Typically, ANs increase with greater metal chloride loadings (which is where oligomeric species form); this is highlighted with the example the LCCs $\text{TiCl}_4\text{-P}_{888}\text{O}$ $\chi_{\text{TiCl}_4} = 0.5$ and 0.6 , where the AN is greater than that of the metal halide for both cases, and oligomeric species are suggested to dominate these systems. In contrast, LCC $\text{TiCl}_4\text{-P}_{888}\text{O}$ $\chi_{\text{TiCl}_4} = 0.5$ forms a molecular adduct, $[\text{TiCl}_4\text{P}_{888}\text{O}]$, and the AN is identical to that of the metal chloride (indicating that the P_{222}O probe displaces the P_{888}O ligand). It is an observation also made in ionic liquid studies that increasing metal concentration leads to a stepwise increase in AN measurements, in line with increasing oligomer formation.^{21,105,106} For more Lewis acidic species the probe preferentially interact with the oligomeric species (Equation 35).



Equation 35

Some LCCs are form complexes which are coordinatively unsaturated. For these species, the interaction between the probe and metal will proceed as a classic Lewis acid-base adduct (Equation 36).



Equation 36

This type of interaction would be expected for monomeric compositions, which may be found for the species $\text{MCl}_x\text{-P}_{888}\text{O}$ where $\text{M} = \text{In(III)}$, Sn(IV) or Ti(IV) and for $\text{MCl}_x\text{-P}_{888}$ where $\text{M} = \text{In(III)}$ and Sn(II) . It is noticeable that for all of these (excluding $\text{InCl}_3\text{-P}_{888}$ $\chi_{\text{InCl}_3} = 0.5$) the same AN (within error bars) is recorded for the complex and the neat metal halide. The exception to this, $\text{InCl}_3\text{-P}_{888}$ $\chi_{\text{InCl}_3} = 0.5$, has a reduced AN compared to the metal halide (67.5 vs 74.3)

which is reflective of indium centre being less capable of accepting electron density, which in turn is a consequence of a strong orbital overlap between the indium centre and the phosphorus of the donor ligand. Therefore, the indium centre of $[\text{InCl}_3(\text{P}_{888})]$ binds less strongly to the P_{222}O molecule than neat indium chloride does, lowering the AN. Ionic liquids which contain the tetracoordinate $[\text{InCl}_4]^-$, have an even lower AN of 57.1,²¹ which has been ascribed to the negative charge on the molecule.

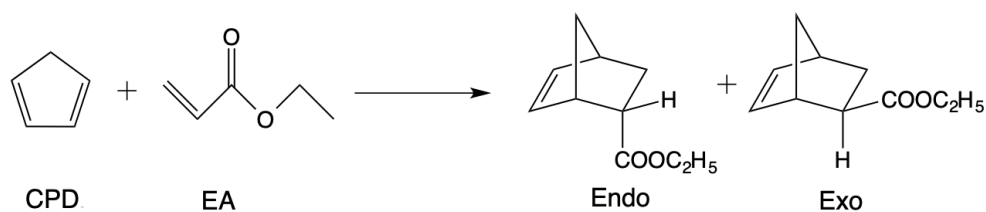
2.12 Lewis Acidity Determination Using a Model Reaction

Alternative to probe-based measures of Lewis acidity (AN, FIA – Section 1.1.3) is quantifying Lewis acidity through the ability of Lewis acid to promote a model reaction. This has already been used by Hayashi *et al.*, who proposed the measure of Lewis superacidity based on the performance of a Lewis acid in Diels-Alder chemistry (Section 1.1.4).⁴³

In this work, the ability of LCCs to act as catalysts in a Diels-Alder reaction was explored, in collaboration with the group of Prof. A. Chrobok from the Department of Chemical Organic Technology and Petrochemistry at Silesian University of Technology; Diels-Alder reactions were carried out by Dr K. Matuszek.

The model Diels-Alder reaction was the cycloaddition of cyclopentadiene (CPD) to ethyl acrylate (EA), shown in Scheme 12. The reaction is popular for demonstrating Lewis acid strength as both the conversion and the selectivity towards *endo:exo* relate to it.¹⁸² It has been used previously as a benchmark reaction in studying Lewis acidic borenium ionic liquids.¹⁴⁶ In this work, the reaction was solventless, carried out in an ice-bath, with the diene in excess. The LCC (10 mol% per EA) was introduced neat and dissolved in the reagents. LCCs of a general formula $\text{MCl}_x\text{-P}_{888}\text{O}$ $\chi_{\text{MCl}_x} = 0.5$ were tested, as this included all metal halides and had relatively simple to understand speciation.

Scheme 12. Model Diels-Alder reaction between cyclopentadiene (CPD) and ethyl acrylate (EA) used in this study.



For the LCCs studied there was large variation in catalytic performance (Figure 29), ranging from low reactivity and selectivity: $\text{AlCl}_3\text{-P}_{888}\text{O}$ $\chi_{\text{AlCl}_3} = 0.5$, $\text{GaCl}_3\text{-P}_{888}\text{O}$ $\chi_{\text{GaCl}_3} = 0.5$, $\text{ZnCl}_2\text{-P}_{888}\text{O}$ $\chi_{\text{ZnCl}_2} = 0.5$ and $\text{SbCl}_3\text{-P}_{888}\text{O}$ $\chi_{\text{SbCl}_3} = 0.5$, through moderate activity and reasonable selectivity recorded for $\text{SnCl}_2\text{-P}_{888}\text{O}$ $\chi_{\text{SnCl}_2} = 0.5$ and $\text{InCl}_3\text{-P}_{888}\text{O}$ $\chi_{\text{InCl}_3} = 0.5$, to extremely high

performance found for $\text{TiCl}_4\text{-P}_{888}\text{O}$ $\chi_{\text{TiCl}_4} = 0.5$ and $\text{SnCl}_4\text{-P}_{888}\text{O}$ $\chi_{\text{TiCl}_4} = 0.5$. This indicated that this Diels-Alder reaction was appropriate to distinguish between the Lewis acidic strengths of these LCCs.

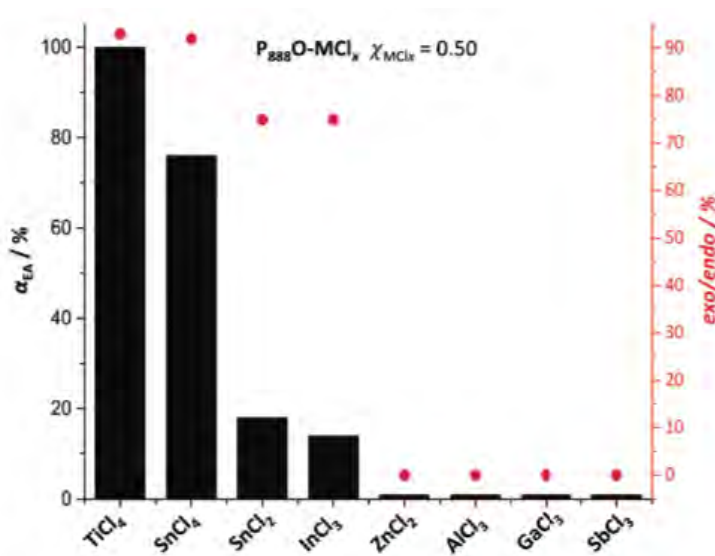


Figure 29. Catalytic performance in terms of conversion and stereoselectivity for LCCs with a general formula $\text{MCl}_x\text{-P}_{888}\text{O}$ $\chi_{\text{MCl}_x} = 0.5$ (results provided by Dr Matuszek).

A comparison between conversion of the dienophile to the product catalysed by each LCCs with Gutmann acceptor number recorded for each LCCs was plotted (Figure 30). A Boltzmann sigmoidal curve fits these data points well, with two outliers. In general, the trend demonstrates the strong relationship between Lewis acidity, as determined by Gutmann acceptor number, and reactivity towards dienophile conversion, aligned with previous work with on borenium ionic liquids.¹⁴⁶ This is remarkable, because in the borenium ionic liquids study, all Lewis acids had a borenium centre, whereas in this comparison - each LCC features a different metal. Despite differences in hardness/softness, only two outliers have been reported. The two outliers to this correlation, $\text{AlCl}_3\text{-P}_{888}\text{O}$ $\chi_{\text{AlCl}_3} = 0.5$ and $\text{GaCl}_3\text{-P}_{888}\text{O}$ $\chi_{\text{GaCl}_3} = 0.5$, demonstrate no reactivity towards dienophile conversion, despite high Gutmann acceptor number values. This is in agreement with previous studies which showed that LCCs composed of $\text{AlCl}_3\text{-L}$ $\chi_{\text{AlCl}_3} = 0.5$ and $\text{GaCl}_3\text{-L}$ $\chi_{\text{GaCl}_3} = 0.5$ were catalytically inactive, in contrast to compositions with greater concentrations of metal halide, featuring bi- or oligomeric complexes.^{136,138,181}

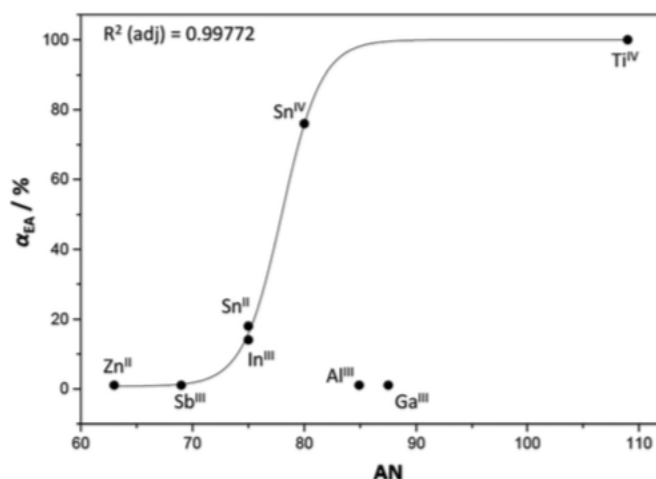


Figure 30. Dienophile conversion rates in the model Diels-Alder reaction catalysed by LCCs with the general formula $MCl_x-P_{888}O$ $\chi_{MCl_x} = 0.5$, plotted against the Gutmann acceptor numbers of each LCC.

This catalytic study illustrates that whereas AN is generally a good measure of Lewis acid catalytic activity, it is not always the case, and fundamental understanding of the reacting species is absolutely crucial. When the $P_{222}O$ probe reacted through a simple addition to a coordinatively unsaturated Lewis acid (Equation 36), or through the breaking of a bridging halide bond (Equation 34 and Equation 35), the AN corresponded well to the catalytic activity of the LCC, following the Boltzmann sigmoidal curve. In contrast, for $AlCl_3-L$ $\chi_{AlCl_3} = 0.5$ and $GaCl_3-L$ $\chi_{GaCl_3} = 0.5$, where the $P_{222}O$ probe was most likely substituted for the chloride (Equation 31), it gave artificially high AN values and these are not reflective of catalytic activity. This is supported by the fact that, in studies with borenium ionic liquids, where each composition contains coordinatively unsaturated Lewis acidic centres, there was strong correlation between AN values and catalytic activity, with no outliers.¹⁴⁶

2.13 Conclusions

The Lewis acidity of metal halides was quantified in this work, using a non-coordinating solvent and finding good agreement with the reactivity determined Kobayashi scale.¹⁸⁰ The Lewis acidity of metal halides was found to decrease in the order $TiCl_4 > SbCl_5 > AlCl_3 > SnCl_4 > GaCl_3 \approx InCl_3 \approx SnCl_2 > ZnCl_2 > SbCl_3$. This contribution is hoped to be useful for a wider scientific community, making impact beyond the field of Lewis acidic ionic liquids and related catalytic processes.

Lewis acidities of LCCs were also measured; LCCs were found to have equal or greater ANs compared to their corresponding metal halides. The results were related to speciation studies and contextualised by the interactions between the probe and the most acidic species in the liquid. The modes of interaction between probe and LCC were classified as either 1)

substituting a ligand around a coordinatively saturated metal centre, 2) breaking a weak chloride bridge in a dimeric or oligomeric complex, which was interpreted as “latent Lewis acidity” or 3) adduct formation with a coordinatively unsaturated molecule. The former being more common with Ga/Al systems and the third being more common with the other metal centres. The application of LCCs as catalysts in Diels-Alder reactions has shown a good agreement between increasing Lewis acidity and reactivity for species whose AN was believed to derive from the interactions described by 2) or 3) above.³ In contrast, interaction with P₂₂₂O defined as mode 1) was not reflected in catalytic performance, truly reflective of the challenge in measuring Lewis acidity. It was understood that the probe was basic enough to replace a ligand, and form [AlCl₃(P₂₂₂O)] adducts (indistinguishable from AlCl₃ when interacting with P₂₂₂O), but the nucleophile in Diels-Alder was too weak a base.

There are a number of preliminary speciation studies results arising from this work that could be of interest for a more in-depth study. For example, the system of InCl₃-P₈₈₈O $\chi_{\text{InCl}_3} = 0.5$ has an AN of 75.3, significantly more acidic than ionic liquids of similar composition, which gave ANs around 57.²¹ Indium-containing ionic liquids are known to be relatively easy to handle, moisture tolerant catalysts and these results suggest that these LCCs may be used in replacement of the ILs as more powerful catalysts. Furthermore, the acidity of titanium chloride LCCs was significantly higher than that of other systems, with TiCl₄-P₈₈₈O $\chi_{\text{TiCl}_4} = 0.5$ having an acceptor number 109.8, very similar to the neat metal halide at 108.9. However, in contrast to neat TiCl₄, which rapidly reacts with atmospheric moisture to release HCl fumes, the stability of the complex was greatly enhanced, making it an easier and catalyst to work with (despite its still high moisture sensitivity).

3 BORENIUM IONIC LIQUIDS

This work builds on the first report on borenium ionic liquids in 2015 by Coffie *et al.*,⁴ to deliver development beyond cation or anion families published in this original paper. Several strategies were adopted to improve upon the first generation of borenium ionic liquids which, albeit being very powerful Lewis acidic catalysts, had three major shortcomings: unwanted equilibria with neutral species, Lewis acidic anion that limited control over reactivity, and high chloride content. Firstly in the archetypal borenium ionic liquid, $[\text{BCl}_2(\text{mim})][\text{Al}_2\text{Cl}_7]$, the nominal species are involved in a series of complex equilibria, involving BCl_3 , $[\text{AlCl}_4]^-$, $[\text{AlCl}_3(\text{mim})]$, $[\text{AlCl}_2(\text{mim})_2]^+$ and $[\text{AlCl}_3(\text{mim})_2]$.⁴ This poses two challenges: various Lewis acidic species of poorly controlled reactivity, so utilising the borenium ions in specific catalytic applications becomes more challenging, and the presence of volatile BCl_3 , limiting thermal stability and posing potential danger of leaching. Another challenge was the use of chlorometallate anions; even without the dynamic equilibrium generating various Lewis acidic species, the anion was still a strong Lewis acid, active in catalytic processes. Again, this caused challenges in designing certain catalytic applications, which are task specific for the borenium ion, for example use in frustrated Lewis pair (FLP) chemistry, where the Lewis acidic and basic centres are sterically bulky to prevent adduct formation, or in asymmetric catalysis with chiral ligand on boron. Finally, whilst Lewis acidic ionic liquids which high halide content, especially chloroaluminates, are used in industrial applications (Section 1.3.2.3), they are highly corrosive due to the presence of chloride anions. This is possibly the single largest drawback in industrial applications of Lewis acidic ionic liquids, and the core reason of failure in some piloted technologies.^{109,110} In this chapter, several attempts to address all three of these shortcomings is described.

3.1 Experimental

3.1.1 Materials and Methods

All experiments were performed in a glovebox (MBraun labmaster dp, <0.6 ppm of H_2O and O_2) or using Schlenk techniques under argon. All glassware was dried overnight in an oven (*ca.* 80 °C) prior to use. Materials and synthesised products were stored in the glovebox. Solvents were dried over molecular sieves, 3 Å, and stored under Ar. Boron trichloride (1.0 M in heptane) was purchased from Sigma Aldrich in a sealed bottle and used as received. Catechol (99%) was purchased from Fluorochem, recrystallised from toluene and sublimed before use. Methylimidazole (99%) was purchased from Sigma Aldrich in a sealed bottle and used as received. Triethylamine (>99%) was purchased from Sigma Aldrich and distilled over molecular sieves, 3 Å and stored under argon. Tri-*tert*-butyl phosphine (98%) was purchased

from Sigma Aldrich and used as received. Trioctylphosphine (99.5%) was provided by Cytec in a sealed canister under an inert atmosphere and used as received. Trioctylphosphine oxide (99.5%) was provided by Cytec and dried under reduced pressure (80 °C, <1 mbar, 48 h) before use. Triethylphosphine oxide (99%) was purchased from Sigma Aldrich and used as received. Trimethylsilyl trifluoromethanesulfonate (99%) and N-methyl bis((trifluoromethyl)sulfonyl)imide (>90%) were purchased from Sigma Aldrich and used as received.

^1H , ^{11}B , ^{13}C , ^{19}F and ^{31}P NMR spectra were recorded on a Bruker Avance DPX 400 MHz spectrometer at 400, 128, 100, 376 and 162 MHz, respectively. Boron complex ionic liquid precursors were studied either in DCM using a DMSO-filled, sealed capillary as an external deuterated lock or in C_6D_6 depending on solvent solubility. All borenium ionic liquid samples were studied neat using a DMSO-filled, sealed capillary as an external deuterated lock.

3.1.2 Purification of Catechol

Catechol (8 g, 72.6 mmol) was dissolved in toluene (50 cm^3 , 70 °C, 1 hour), cooled in a fridge (7 °C, 12 h) and a white precipitate formed. The precipitate was collected by Büchner filtration. The precipitate was sublimed (80 °C, 10^{-2} mbar, 12 hours) to give a white crystalline product. Yield 6.45 g, 80.6 %. ^1H NMR (400 MHz, DMSO) δ 6.72, 6.59 $^{13}\text{C}\{^1\text{H}\}$ NMR (101 MHz, DMSO) δ 145.17, 119.20, 115.61.

3.1.3 Synthesis of B-chlorocatechol Borane, BcatCl

Catechol (3.99 g, 36.3 mmol, 0.9 eq) was weighed out into a flask equipped with a magnetic stirrer bar in an argon filled glovebox. The flask sealed, removed and attached to an argon Schlenk line. It was placed in a dry ice/acetone bath standing on a heater-stirrer, and cooled to -78 °C under argon (30 mins). BCl_3 in heptane (1M, 40.34 cm^3 , 40.3 mmol, 1 eq.) was added dropwise over an hour. Subsequently, the dry ice/acetone ice bath was removed, the mixture was brought to room temperature and stirred overnight. The product was then dried (0 °C, 10^{-2} mbar) and purified by sublimation and stored in the glovebox. Yield 3.85 g, 69%, ^1H NMR (400 MHz, C_6D_6) δ 7.23, 7.11 $^{13}\text{C}\{^1\text{H}\}$ NMR (101 MHz, C_6D_6) δ 146.85, 122.88, 112.53 ^{11}B NMR (128 MHz, C_6D_6) δ 28.87.

3.1.4 Synthesis of B-catechol Triflate, BcatOTf

In an argon filled glovebox, BcatCl (0.288 g, 1.87 mmol) was weighed into a flask equipped with a stirrer bar. To this trimethylsilyl triflate (0.414 g, 1.87 mmol) was added dropwise, with stirring. The flask sealed, removed and attached to an argon Schlenk line. The reaction was allowed to proceed (55 °C, 1 h, vigorous stirring) and the evolved methyl chloride removed *in*

vacuo at room temperature (25 °C, 10^{-2} mbar, 2 hours). The product, stored in the glovebox, was a viscous golden-coloured liquid. NMR recorded as a neat liquid with DMSO filled external lock. Yield 0.42 g, 84% ^1H NMR (400 MHz, DMSO) δ 6.61 (bs), ^{11}B NMR (128 MHz, DMSO) δ 21.48, ^{19}F NMR (376 MHz, DMSO) δ -78.66

3.1.5 General Procedure for the Synthesis of Boron Complexes

In an argon-filled glovebox, BcatCl (1 eq.) was added into a flask equipped with magnetic stirrer bar and dissolved in dry DCM. The flask was sealed, removed from the glovebox and attached to an argon Schlenk line, then placed on a heater-stirrer with an ice bath. To this solution, a ligand (1 eq., dissolved in dry DCM) was added dropwise *via* a syringe, at a slow rate to minimise any heating of the sample (0 °C, 1 h, vigorous stirring). The resulting complex was then dried (25 °C, 10^{-2} mbar, 2 h, stirring) and stored in the glovebox. NMR spectra interpreted in Section 3.2.

3.1.6 General Procedure for the Synthesis of Borenium Ionic Liquids with Chlorometallate Anions

In a typical example, in an argon filled glovebox, to a flask equipped with a magnetic stirrer bar and [Bcat(P^tBu₃)Cl] (0.388 g, 1.08 mmol), GaCl₃ (0.570 g, 3.26 mmol, 3 eq.) was added slowly and a golden liquid formed. This was stirred overnight, and the product was received as a mobile liquid. Yield 0.96 g, 100%. An identical procedure was followed for 2 eq. of MCl₃ (M = Al or Ga), which were liquid during the exothermic reaction, but formed brown solids upon cooling to ambient temperature. NMR spectra interpreted in Section 3.3.1.

3.1.7 General Procedure for the Synthesis of Borenium Ionic Liquids with Chloride Free Anions

In an argon filled glovebox, the boron complexes synthesised as described in Section 3.1.5 (1 eq.) were placed in a pear shaped flask (25 cm³), dissolved in dry DCM, and to this solution a halide abstracting agent, TMSOTf or MeNTf₂ (1.1 eq) was added dropwise *via* a syringe. This reaction mixture was sealed with a gas tap and was allowed to react at ambient conditions (ambient temperature, stirring, 1 h), and subsequently at slightly elevated temperature (50 °C, stirring, 2 h). The flask was closed with a gas tap, removed from the glovebox and attached to an argon Schlenk line. Solvent was then carefully removed (0 °C, 10^{-2} mbar, 1 h) and the resulting liquid was transferred to the glovebox. NMR spectra interpreted in Section 3.3.2.

3.1.8 Synthesis of Bistriflimidic Acid

Lithium bistriflimide (1.00 mol eq.) and sulfuric acid, (3.00 mol eq.) were combined in a cylindrical Kugelrohr flask and fixed to a Kugelrohr distillation/sublimation apparatus, connected to a Schlenk line, with a collecting flask cooled with dry ice. The sample was sublimed in the Kugelrohr (50 °C, 10^{-2} mbar, 1 h). White crystals formed in the collection flask. The hygroscopic, fuming sublimate was melted using a heat-gun directly into a Schott DURAN bottle with a sealable, corrosion-resistant cap. The product was obtained as a white, low-melting crystalline solid. $^{13}\text{C}\{^1\text{H}\}$ NMR (101 MHz, DMSO) δ 53.25 (q), ^{19}F NMR (376 MHz, DMSO) δ -76.03

3.1.9 Synthesis of $[\text{BCl}_2(\text{mim})][\text{NTf}_2]$ from HNTf_2

In an argon-filled glovebox, bistriflimidic acid (0.663 g, 2.34 mmol) was placed in a flask (10 cm^3) and dissolved in DCM (4 cm^3). This was added to then and added slowly to $[\text{BCl}_3(\text{mim})]$ (0.440 g, 2.21 mmol) dissolved in DCM (20 cm^3). The flask was then sealed with a gas tap and removed to an argon filled Schlenk line and stirred (40 °C, 12 h). A white liquid formed upon the addition, and after the reaction was completed it was dried (55 °C, 10^{-2} mbar, 2 h). Sample subsequently was heated slightly more to encourage the removal of HCl (60 °C 15 h). The product had a dark brown, highly viscous appearance. NMR spectra interpreted in (Section 3.3.2.2.1).

3.1.10 Synthesis of Silver Bistriflimide

Lithium bistriflimide (1.8 g, 6.4 mmol, 1.00 equiv.), was dissolved in deionised water. Concentrated HCl (12M) was added to afford a polyhydrate of the protonated species, bistriflimidic acid. This was extracted into with diethyl ether (10 cm^3) and the organic phase was separated. The diethyl ether was removed under reduced pressure, using rotary evaporator (25 °C, 6.6 mbar, 10 mins). The aqueous phase was then washed again with diethyl ether and this process was repeated three times. The residue was subsequently dissolved in acetonitrile (35 cm^3) and silver carbonate (0.9 g, 3.52 mmol, 0.55 equiv.) was added. The reaction mixture was stirred (25 °C, 2 h) and a white precipitate formed. The reaction mixture was filtered and product dried (25 °C, 10^{-2} mbar, 1 h). The resulting colourless liquid was dissolved in diethylether (10 cm^3) and stirred (25 °C, 1 h). The product was dried using a rotary evaporator (25 °C, 6.6 mbar, 30 mins) and dissolved in H_2O (25 cm^3) and the mixture was stirred (1 h). The product was dried (25 °C, 10^{-2} mbar, 1 h) and gave a white solid. Recrystallisation from CH_2Cl_2 afforded the product as a white solid (1.68 g, 68%). $^{13}\text{C}\{^1\text{H}\}$ NMR (101 MHz, CD_3CN) δ 117.93 ppm, ^{19}F NMR (376 MHz, CD_3CN) δ -80.15 ppm

3.1.11 Synthesis of $[BCl_2(mim)][NTf_2]$ from $AgNTf_2$

In an argon filled glovebox, silver bistriflimide (0.87 g, 2.24 mmol) was added to a solution of $[BCl_3(mim)]$ (0.44 g, 2.21 mmol) in dry DCM (20 cm³) in a round-bottomed flask (50 cm³) equipped with a stirring bar. The flask was sealed with a gas tap, removed from the glovebox and attached to an argon Schlenk line. This mixture was vigorously stirred (40 °C, 12 h) and subsequently the post-reaction mixture was filtered *via* cannula filter into a dry argon-filled round-bottomed flask (50 cm³) to remove the white solid precipitate. The filtrate was dried (25 °C, 10⁻² mbar, 1 h). The product was subsequently heated (45 °C, 4 days) in the glovebox to encourage AgCl formation and samples removed in sealed NMR tubes for observation by NMR spectroscopy (Section 3.3.2.2.1)

3.1.12 Gutmann Acceptor Number Measurements

For each borenium ionic liquid, three samples (*ca.* 0.5 g each) were weighed out accurately into sample vials. P₂₂₂O was weighed accurately into each sample (*ca.* 1, 2 and 3 wt%) and mixed thoroughly. ³¹P NMR spectra were recorded for the three concentrations, and the chemical shift value was extrapolated to the value of infinite dilution. The acceptor number was calculated according to Equation 1.

3.1.13 Differential Scanning Calorimetry Measurements

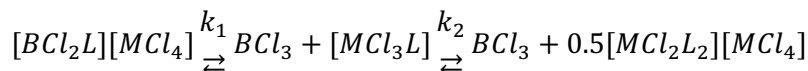
DSC scans were recorded using TA DSC Q2000 with a TA 90 refrigerated cooling system and an autosampler under dry nitrogen furnace purge (50 ml min⁻¹). Sample temperature was ramped between -50 °C and 120 °C at 5 °C min⁻¹ and for each three cycles were recorded.

The samples were accurately weighed (0.0005 g) into medium pressure Tzero alodined hermetic pans, ensuring that the samples were evenly distributed and had good contact with the base of the pan and the DSC pan was then sealed using the press with DSC dies. The weighed samples were then removed from the glovebox and placed in the autosampler carousel of the DSC instrument. An empty sealed pan of the same type was used as a reference sample.

3.2 Boron Complexes

As discussed in Section 1.3.4, borenium ionic liquids with chlorometallate anions are extremely potent Lewis acids. However, chlorometallate anions remain in equilibrium with the cation through ligand scrambling (Equation 37), meaning that several different species with Lewis acidic properties are constantly present. This hinders the development of a borenium catalyst for applications where a careful control of the catalytic centre is crucial,

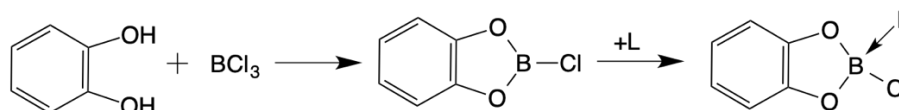
especially in asymmetric catalysis (with bidentate chiral ligands on the boron centre) and in frustrated Lewis pairs chemistry.



Equation 37

The first stage of this work focused on limiting the possibility of ligand scrambling by developing a borenium centre with a bidentate ligand. Catechol was selected as a ligand which has already been used in the syntheses of borenium cations, and the synthesis of B-chlorocatecholborane could be readily achieved similar synthetic methods similar to those used in the synthesis of $[BX_3L]$ complexes.^{183,184} A general scheme of the synthesis of a B-catecholboron complex is given (Scheme 13).

Scheme 13. The formation of the B-catecholboron complex.



The challenge in this synthesis lied in avoiding the removal of BCl_3 during sublimation of the product. Excessively harsh conditions led to the formation of $[B_2Cat_3]$, which may be identified by ^{11}B NMR signal at ~ 22 ppm (Figure 31).¹⁸⁵ The loss of BCl_3 could be avoided by removing solvent under reduced pressure, while the flask with the reaction mixture was immersed in an ice bath, and prompt return to ambient pressure once the solvent is removed (avoiding prolonged exposure to vacuum).

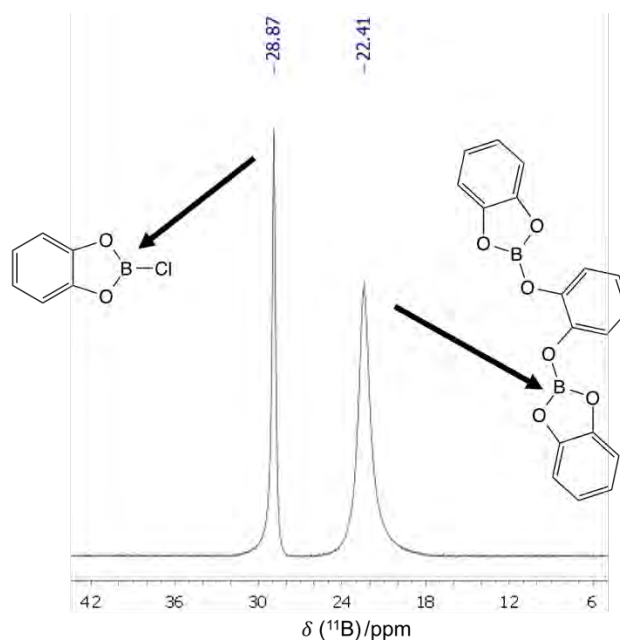


Figure 31. ^{11}B NMR spectrum showing the presence of both B-chlorocatecholborane and $[\text{B}_2\text{Cat}_3]$ forming in similar proportions.

The catechol interacts with the boron centre through both the oxygens acting as X-type donors, forming a tricoordinate, charge-neutral boron compound. To this, L-donor ligands were added (forming charge-neutral, tetracoordinate precursor to a borenium cation) to provide electron density to the boron centre and increase the stability of the tricoordinate borenium cation. In this work, five ligands were explored as L-donors – methylimidazole, triethylamine, tri-*tert*-butyl phosphine, trioctylphosphine and trioctylphosphine oxide (Figure 32).

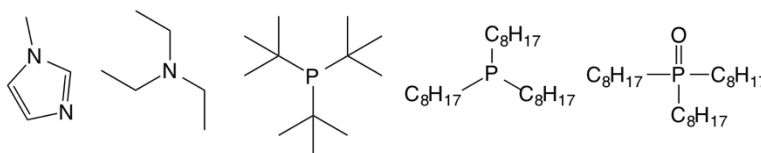


Figure 32. Donor ligands included in this work: 1-*r* methylimidazole, triethylamine, tri(*tert*-butyl phosphine), trioctylphosphine and trioctylphosphine oxide

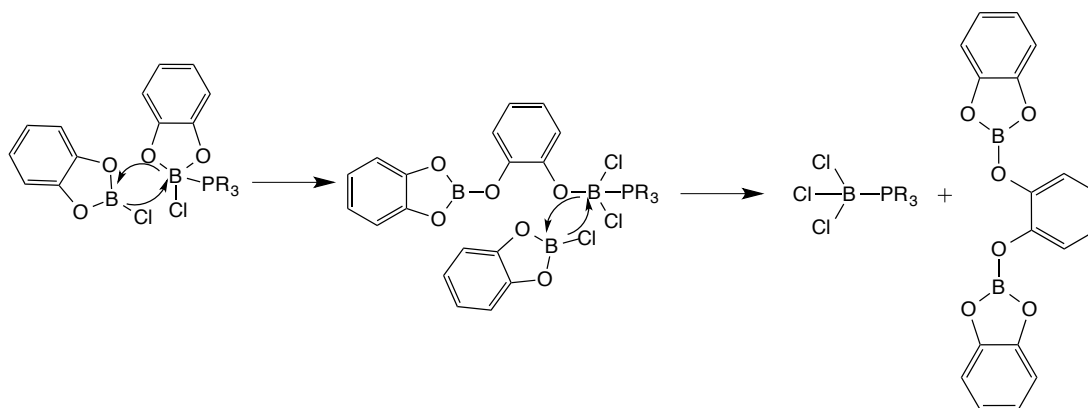
The selection of ligand for controlling the properties speciation of borenium ionic liquids important, as demonstrated in previous work.⁴ The ligands used in this work were selected as they include both N-, P- and O-donors. It is known that N-donors can interact strongly with boron, being from the same period, in comparison to third row donors such as phosphorus, as better overlap between orbitals is achieved for the former.¹⁸⁶ The use of methylimidazole, further to this provides π -back donation from its aromatic system, which increases the donation to the boron centre and helps keep the ligand bound to the boron centre. The risk for an O-donor on a boron centre was observed in earlier work on borenium ionic liquids which showed

was a greater tendency towards adduct dissociation with an O-donor compared to N-donor.^{1,68} This effect is crucial in the presence of metal halides with which the ligand will form adducts.⁴

The inclusion of P^tBu₃ in this work was motivated by the ^tBu group, which is known to be highly electron donating, from Tolman parameters, increasing the basicity of the tri-substituted phosphine.¹⁵⁹ Finally, the inclusion of trioctylphosphine and trioctylphosphine oxide was inspired by the previous work on LCCs in (Chapter 2), rather than literature on boron complexes: the inclusion of long alkyl chains drive the formation of a liquid, and both a soft and a hard donor are explored comparatively. Trioctylphosphine and trioctylphosphine oxide present themselves as an ideal ligands to promote the formation of a liquid, following halide abstraction, following the same rationale as that discussed for LCCs in Chapter 2. Further to this, the use of phosphine ligands allows for the use of ³¹P NMR spectroscopy, a highly sensitive technique.

Care must be taken when preparing these complexes, as some phosphines have been shown to promote the redistribution of the [PR₃BcatCl] to [B₂Cat₃] and [PR₃BCl₃]. A 1993 paper by Westcott *et al.*, using the [BcatH], rather than the chloride, reported that this redistribution was promoted by phosphines with large cone angles.¹⁸³ This redistribution is also enhanced by an excess of [BcatH]. However, they described this process as slow and consequently only an issue in particularly slow catalytic applications, *i.e.* the hydroboration of hindered alkenes. Just under a decade later, in 2001, further work from the same group was concerned with a similar effect in B-chlorocatechol borane, which is the subject of this work.¹⁸⁵ In this study it was demonstrated the key factor was the basicity of the phosphine with a less basic phosphine promoting redistribution. This ties to conclusions from their previous work that the presence of free borane promotes the redistribution, as a less coordinating phosphine will lead to a greater concentration of [BcatCl]. The mechanism for this redistribution may be understood by the changing availability of bonding orbitals around the boron centre with the coordination of a phosphorus reducing the availability of the π -bonding orbitals for the O-donors. This increased electron density on the oxygen encourages it to attack electrophilic boron centres on free [BcatCl] molecules. This leads to the opening of the five membered BO₂ ring and the transfer of a chloride between them (Scheme 14).

Scheme 14. Mechanism for the redistribution of $[\text{PR}_3\text{BcatCl}]$ in the presence of BcatCl .¹⁸⁵



In this work this information was important to ligand selection as a strong interaction between the boron and the ligand is crucial to reduce the presence of free $[\text{BcatCl}]$. The highly basic P^tBu_3 ligand, which was not found to undergo this effect in the original paper by Coapes *et al.* was employed.¹⁸⁵ They also reported no decomposition in the case of N-donors, likely as a result of good boron-nitrogen orbital overlap, including with triethylamine which is used in this work. The ‘ionic liquid-inspired’ ligands, P_{888} and P_{888}O , were expected to provide a degree of steric hindrance to boron-boron interaction through the long alkyl chains, whilst the inductive effects of these chains made the phosphorus centre more basic than shorter chained analogues. Accordingly, no $[\text{B}_2\text{Cat}_3]$ formation was detected in this work with ligands attached to the boron centre.

Adducts formed between the ligands (Figure 32) and the synthesised B-chlorocatecholborane were synthesised as a variation on the method introduced by Marder and colleagues *via* air sensitive methods.¹⁸⁵ In their work, the synthesis was performed in toluene and at scale of around 0.1 g. Few details were given regarding vacuum strength and temperature. In this work, toluene was substituted with DCM, as it is easier to remove *in vacuo* due to a lower boiling point. This was important because the minimum possible exposure to vacuum was desired to minimise the risk of evacuating BCl_3 . The reactions were exothermic as a result of bond formation and additions were performed in an ice bath, similarly to the formation of the boron complexes synthesised for previously reported borenium ionic liquids, with BCl_3 added to the ligand at $-78\text{ }^\circ\text{C}$.⁴ The appearance of these precursors varied for the different ligands: $[\text{BcatCl}(\text{mim})]$ presenting as a clumpy white solid, both $[\text{BcatCl}(\text{P}^t\text{Bu}_3)]$ and $[\text{BcatCl}(\text{N}_{222})]$ forming white solids and both $[\text{BcatClP}_{888}]$ and $[\text{BcatCl}(\text{P}_{888}\text{O})]$ forming slightly yellow liquids, with a slight yellow colouration (Figure 33).

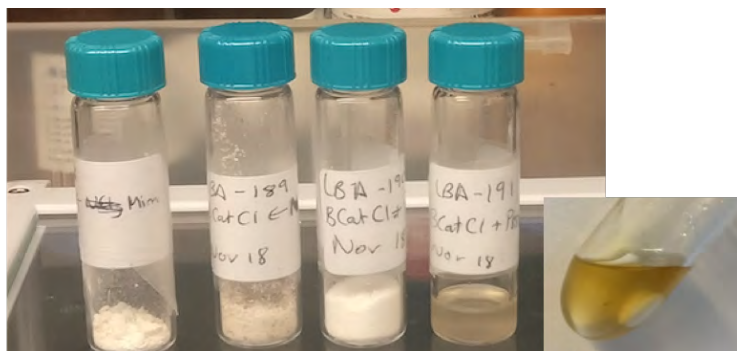


Figure 33. The adducts formed from the combination of [BcatCl] with a ligand (L) where L is (l-r) methylimidazole, triethylamine, tri-*tert*-butyl phosphine, trioctylphosphine and trioctylphosphine oxide

The adducts were characterised by ^{11}B NMR spectroscopy (Figure 34). From these spectra it can be seen that a tetracoordinate boron centre forms with peaks significantly more shielded than tricoordinate [BcatCl].

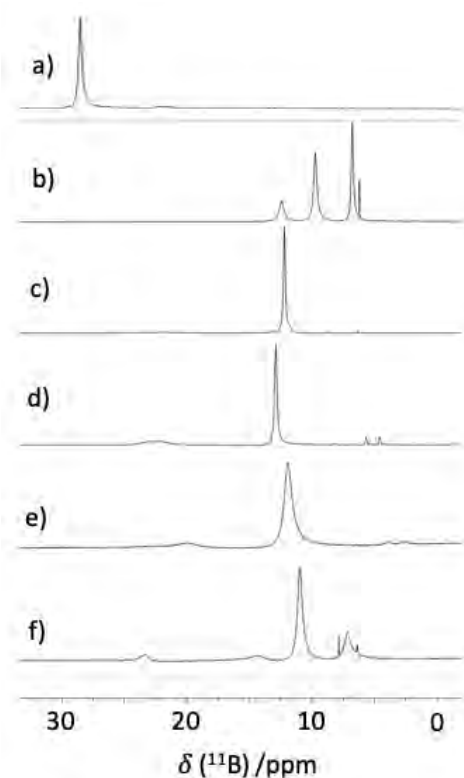


Figure 34. The ^{11}B NMR spectrum of a) BcatCl, compared to spectra of [BcatClL] adducts, where L is: b) methylimidazole, c) triethylamine, d) tri-*tert*-butyl phosphine, e) trioctylphosphine and f) trioctylphosphine oxide (samples dissolved in DCM)

Multiple ^{11}B NMR shifts were recorded in some cases. For the adduct of methylimidazole and BcatCl, these were at 6.20, 6.79, 9.74 and 12.44 ppm; these multiple species were reflected in the aromatic region of the ^1H NMR spectrum (Figure 35), where there are a large number of additional peaks. The expected integrations for the methyl imidazole region would be three

for the methyl groups and one each for the protons on the ring. In this spectrum the methyl protons are all in the same environment. This corresponds well to approximately four protons in the catechol group at 7.01, 6.93, 6.89 and 6.81 ppm. For the protons on the methyl imidazolium ring there are clearly two environments which represent approximately 35% in one environment (with signals at 8.56, 7.43 and 7.32 ppm) and approximately 70% in another environment (with signals at 8.89, 7.41 and 7.36 ppm). This could indicate that there are two interactions between the boron and methyl imidazole and this idea is further reinforced by the appearance of multiple peaks in the ^{11}B NMR spectrum.

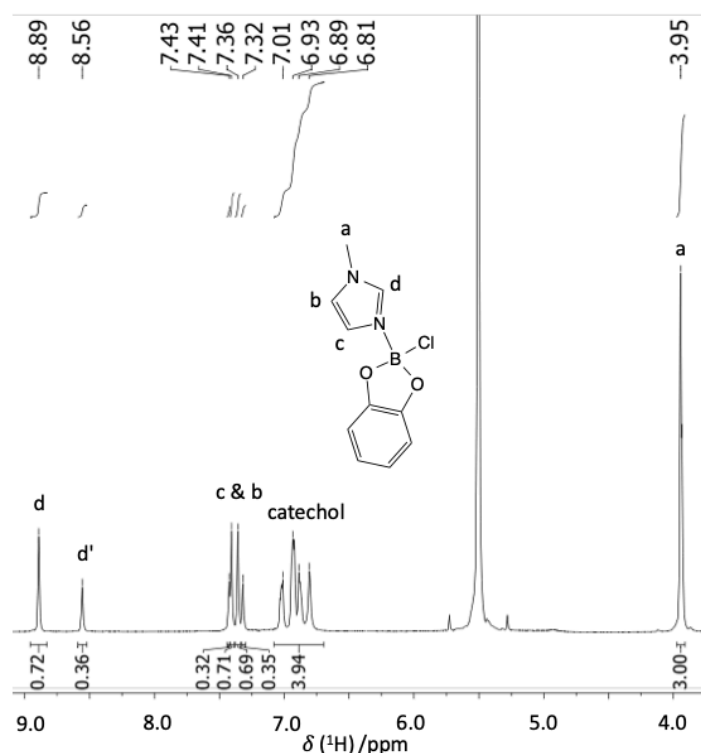


Figure 35. The ^1H NMR spectra of adduct $[\text{BeatCl}(\text{mim})]$ in DCM with a DMSO-d_6 capillary.

Combined ^{11}B and ^1H NMR data suggest that the structure formed is not the expected $[\text{BeatCl}(\text{mim})]$, although the methyl imidazole peaks are clearly distinguished. For all other adducts (Figure 34) the main coordination peak is at ~ 12 ppm, which the third largest peak in this spectrum. This suggests that the structure of this adduct is not as anticipated; seeing that the structure of each ligand has not been altered, ligand scrambling between chloride and methylimidazole is anticipated. This leads to three tetra-coordinate environments for boron and two environments for the methyl imidazole protons, as suggested by ^1H and ^{11}B NMR spectroscopy (Equation 38).



Equation 38

Owing to this complicated speciation, it was determined that the formation of a borenium ionic liquid on combination of $[\text{BCatCl}(\text{mim})]$ with a halide abstracting agent would be unlikely to give the desired product. Further to this, the inclusion of the aromatic imidazolium ring encourages π - π stacking interactions, expected to increase the melting point. Nevertheless, it has been decided to pursue a trial experiment with the syntheses of a borenium ionic liquid *via* halide abstraction with MeNTf_2 . This produced a non-homogenic solid which appeared to decompose into a purple solid on heating, rather than melting (Figure 36). The use of the methyl imidazole ligand was thus discontinued as it did not appear to offer the desired results.

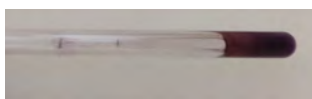


Figure 36. The appearance of the product of reaction of $[\text{BCatCl}(\text{mim})]$ with MeNTf

Other adducts pursued in this work gave much more promising results. In their 2001 paper, Marder and colleagues report the synthesis of the adducts $[\text{BCatCl}(\text{N}_{222})]$ and $[\text{BCatCl}(\text{P}^t\text{Bu}_3)]$.¹⁸⁵ The ^{11}B NMR spectra reported here Figure 34 correspond well to the peaks reported by Coapes *et al.* For the triethylamine complex here the peak is at 12.41 ppm compared to 13.3 ppm in the literature, and for the tri-*tert*-butyl phosphine complex, the peak in this work is at 12.88 ppm and in the literature at 15.2 ppm. The difference in chemical shifts can be explained through different solvents, in this work the spectra were taken in DCM with a sealed DMSO-d_6 capillary compared to CDCl_3 for the triethylamine complex and C_6D_6 with 10% Ph-Me. No splitting from the interaction between boron and phosphorus was reported at room temperature by Coapes *et al.* and similarly, there is no splitting in the spectra recorded for this work. However, the ^{11}B NMR signal has a broad appearance with a flat peak, suggesting that splitting is present, albeit not fully resolved. The ^{31}P NMR spectra reported for the tri-*tert*-butyl phosphine complex showed a signal at 25.5 ppm (with no splitting),¹⁸⁵ in good agreement with the 24.82 ppm observed in this work.

Complexes of trioctylphosphine and trioctylphosphine oxide with B-chlorocatechol borane have not been reported in the literature. In this work, both of these complexes were measured in benzene- d_6 . For trioctylphosphine, one prominent peak in the ^{11}B NMR spectrum is observed at 11.96 ppm, which is more shielded with respect to $[\text{BCatCl}]$ by $\Delta^{11}\text{B} = 16.91$ ppm and broadly in line with the reported chemical shift of $[\text{BCatCl}(\text{PEt}_3)]$, which gave signal at 11.3 ppm, and indicate the shift to tetracoordinate region of ^{11}B NMR spectroscopy (Figure 37).¹⁸⁵ The ^{31}P NMR spectrum also featured just one peak at -13.46 ppm, deshielded with

respect to free trioctylphosphine by $\Delta^{31}\text{P} = 15.98$ ppm. This suggests rather conclusively that one complex, $[\text{BcatCl}(\text{P}_{888})]$, has formed.

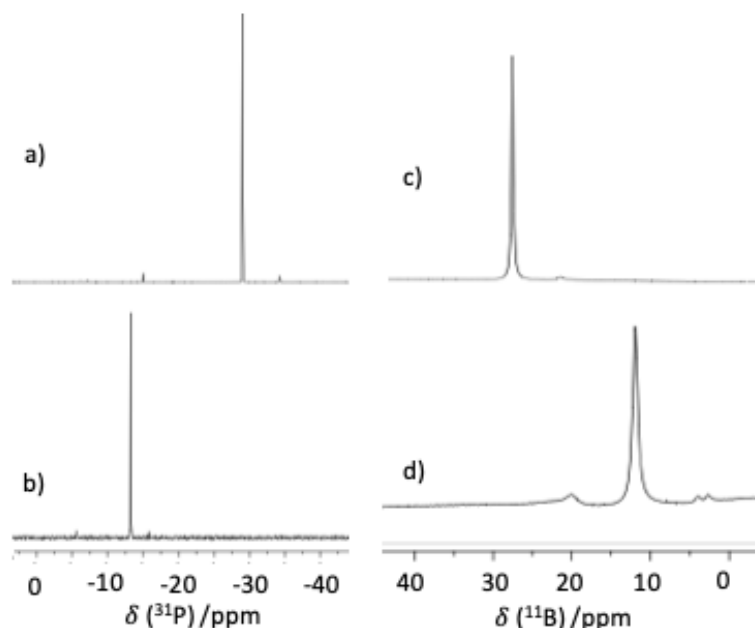
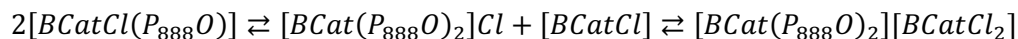


Figure 37. NMR spectra of $[\text{BcatCl}(\text{P}_{888})]$ and starting materials: ^{31}P NMR spectra of a) P_{888} (neat with a DMSO-d_6 capillary) and b) $[\text{BcatCl}(\text{P}_{888})]$ in C_6D_6 ; ^{11}B NMR spectra of c) $[\text{BcatCl}]$ (in DCM with a DMSO-d_6 capillary) and d) $[\text{BcatCl}(\text{P}_{888})]$ in C_6D_6 .

Conversely, for the trioctylphosphine oxide complex, two signals are observed in the ^{11}B NMR spectrum, these are found at 10.97 ppm and 7.16 ppm and have relative integrations of 2 : 1 (Figure 38). Additional small peaks are observed at 24.80 and 14.34 ppm, the identities of these are unknown as they do not match exactly to either $[\text{BcatCl}]$ or $[\text{B}_2\text{Cat}_3]$ species and instead this suggests that a range of boron containing species are in equilibrium.

In the ^{31}P NMR spectrum, two peaks are observed at 79.07 and 76.25 ppm, these have a relative integration of 0.5 : 1 suggesting that they each correspond to one of the two ^{11}B spectrum peaks. The change of chemical shift in the ^{31}P NMR spectrum, with respect to free trioctylphosphine oxide, was $\Delta^{31}\text{P} = 29.16$ and 26.34 ppm. This suggests that multiple coordinations between the phosphine oxide and the boron centre exist. This is likely to indicate the formation of a disubstituted boron complex as the similarity of the two ^{31}P chemical shifts suggest that they are almost equivalent environments. The additional ^{11}B NMR peak at 7.16 ppm suggests that the species remains tetracoordinate as this is the region expected for a tetracoordinate complex. Work by Shaffer *et al.* synthesised the tetracoordinate boron species $[\text{Li}(\text{THF})][\text{B}(\text{O}_2\text{PPh}_2)_2(\text{C}_2\text{O}_4)]$ which contains a central boron atom surrounded by four oxygen atoms and in ^{11}B NMR spectroscopy its chemical shift was found at 7.99 ppm.¹⁸⁷ This chemical shift is similar to the 7.16 ppm observed in this work. This all suggests that a complex

dynamic equilibrium is set up which contains a range of boron species and two phosphorus environments, plausible equilibria represented by Equation 39. In addition to this a small peak in the ^{11}B NMR spectrum at 23.5 ppm and another in the ^{31}P NMR spectrum at 62 ppm may represent small quantities of starting materials.



Equation 39

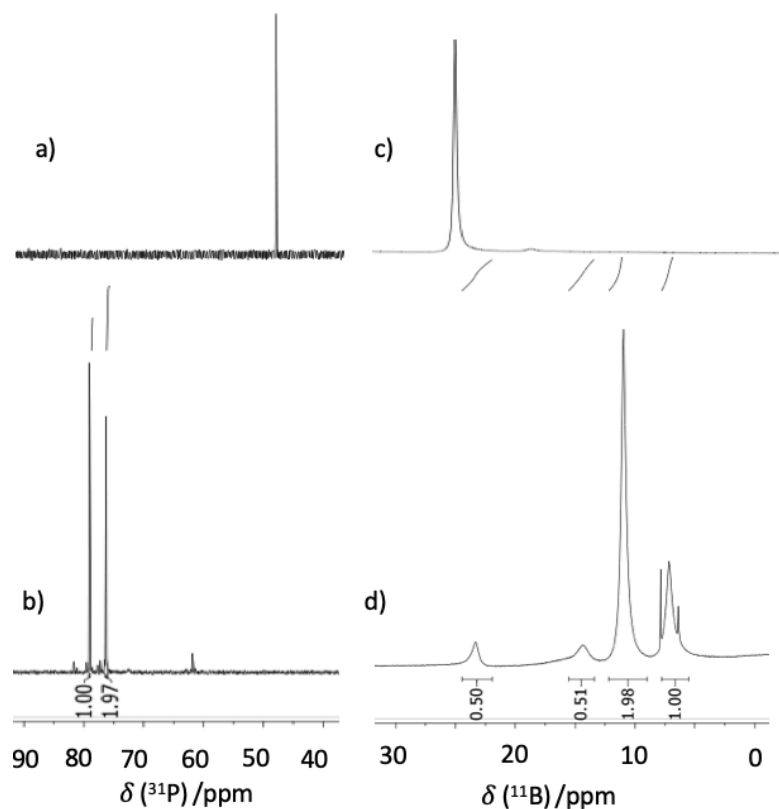


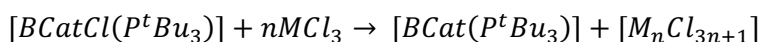
Figure 38. NMR spectra of $[\text{BcatCl}(\text{P}_{888}\text{O})]$ and starting materials: ^{31}P NMR spectra of a) P_{888}O (recorded in CDCl_3) and b) $[\text{BcatCl}(\text{P}_{888}\text{O})]$ in C_6D_6 ; ^{11}B NMR spectra of c) $[\text{BcatCl}]$ in DCM with a $\text{DMSO}-d_6$ capillary and d) $[\text{BcatCl}(\text{P}_{888}\text{O})]$ in C_6D_6 .

Despite this complicated equilibrium, reaction of the adduct with TMSOTf or MeNTf_2 halide abstracting agents (discussed further in this chapter) resulted in homogenous liquids with uncomplicated speciation. Therefore, in contrast to non-homogenic solid which formed on combination of $[\text{BcatCl}(\text{mim})]$ with the same halide abstracting agents, the $[\text{BcatCl}(\text{P}_{888}\text{O})]$ adduct was used in subsequent research. Furthermore, the BcatCl adducts with triethylamine, tri-*tert*-butyl phosphine and trioctylphosphine were used for further synthesis of ionic liquids.

3.3 Ionic Liquid Synthesis

3.3.1 Chlorometallate Anions

The generation of ionic liquids in an equivalent manner to that with previously reported borenium liquids,⁴ *i.e.* with chlorometallate anions, but with the catecholate cations, was investigated in a quick test experiment (Equation 40), before attempting to combine these new cations with new anions. The boron complex studied in this work was [BcatCl(P^tBu₃)], as the precursor to the cation, [Bcat(P^tBu₃)]⁺, which has been reported as a solution species by Stephan *et al.* and Ingleson *et al.*¹⁸⁸⁻¹⁹⁰



Equation 40

In the reaction of [BcatCl(P^tBu₃)] with two equivalents of either aluminium chloride or gallium chloride, solid products were formed. However, the ¹¹B NMR spectrum of [Bcat(P^tBu₃)] [Al₂Cl₇] in C₆D₆, gave a peak at 28.68 ppm, similar to the 29.9 ppm ¹¹B NMR signal reported by Dureen *et al.* for [Bcat(P^tBu₃)] [B(C₆F₅)₄] in CD₂Cl₂.¹⁸⁸ This suggested that borenium salt has been synthesised, albeit not in the form of ionic liquid. In a subsequent attempt, the reaction of [BcatCl(P^tBu₃)] with three equivalents of gallium chloride, gave a golden brown liquid (Figure 39).

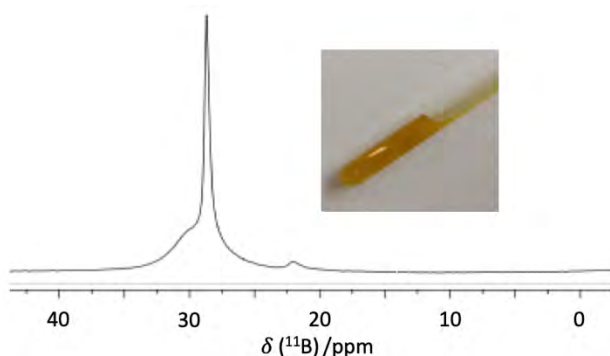


Figure 39. ¹¹B NMR spectrum for the salt [Bcat(P^tBu₃)] [Ga₃Cl₁₀] in deuterated benzene and (inset) the ionic liquid [Bcat(P^tBu₃)] [Ga₃Cl₁₀].

Compared to room-temperature borenium ionic liquids reported by Coffie *et al.*,⁴ the aromatic catecholate ligand increased the melting point of the salts, which is attributed to π - π stacking effects. It was found promising, however, that a borenium cation could be generated *via* halide abstraction, rather than through proton abstraction reported by Dureen *et al.*, and that a room-temperature product could be accessed. This gave hope for easily accessible borenium ionic

liquids with good speciation control, as the generation of B-chlorocatechol borane complexes, as detailed in Section 3.2, was a relatively simple synthesis.

3.3.2 Chloride-Free Anions

Abandoning chlorometallate anions has been explored for dual benefit: removing additional Lewis acidic centres, interfering with the reactivity of the main boron centre, and removing chlorides, which are of a major concern in industrial applications, incurring corrosion issues. The anions used in this work were bistriflimide and triflate (Figure 40).

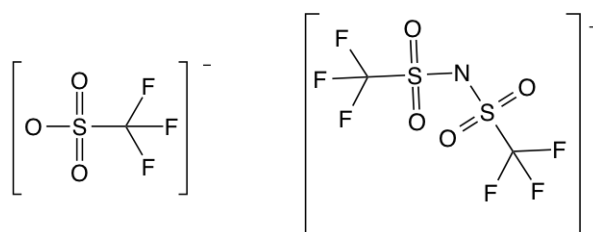


Figure 40. The structures of the triflate, [OTf]⁻ (left) and bistriflimide, [NTf₂]⁻ (right) anions.

It is a classic trope of the history of ionic liquid chemistry that classically trained organic chemists will complain of forming a room temperature oil on salt formation, depriving them of the powerful characterising of single crystal X-ray crystallography, and this will indicate the discovery of a new ionic liquid. Such a frustration was reported by Umemoto *et al.* in their synthesis of N-(2,2,2-trifluoroethyl)pyridinium trifluoromethanesulfonate.¹⁹¹ This inspired Cooper *et al.* to investigate the use of triflate anions to generate ionic liquids with high stability for electrochemical and battery development.¹⁹² In their work, they extolled the advantages of triflates over chlorometallate in being unreactive to towards electrodepositions and having a lower symmetry than tetrahaloaluminate anions, with a structure more reminiscent of [Al₂Cl₇]⁻, helping to suppress melting point.

The bistriflimide anion was introduced to the world of ionic liquids almost simultaneously by Koch *et al.* and Bonhote *et al.*, searching for increased stability and hydrophobicity in ionic liquids.^{193,194} The work by Bonhote *et al.* presents a convincing account of a wide range of ionic liquids with hydrophobic properties. This was an important development as, until this, ionic liquids had either featured halometallate anions, which decompose in the presence of water, or so-called “air and water stable” ionic liquids with anions such as nitrates, ethanoate or sulfate, which conversely can absorb tremendous amounts of atmospheric water.¹⁰⁸

In this work, these anions were selected because they are typically regarded as relatively non-coordinating, or at least forming weak adducts which could give rise to “masked” type borenium centres.⁶⁵ Furthermore, they do not contain aromatic groups which could increase

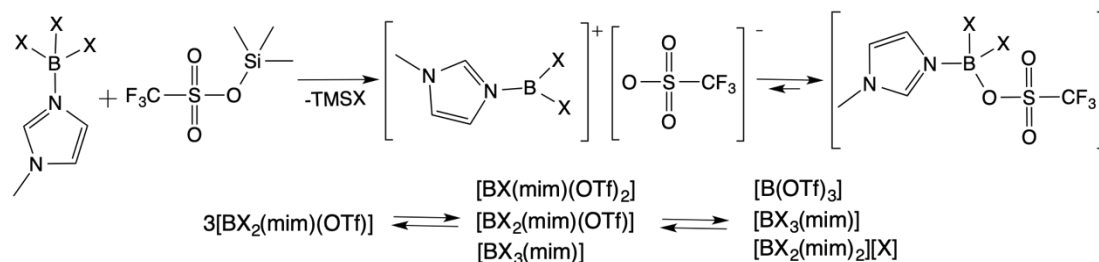
melting point through π - π stacking. They do not contain labile halides, which have been shown to be a huge challenge in commercialising Lewis acidic ionic liquids as corrosion and impurities from chloride anions limits plant life span and reduces the profitability of manufacturing processes. Commercially, their precursors are available as acids, salt of lithium, sodium or silver, and as esters, N-methyl bistriflimide (MeNTf₂) and trimethylsilyl triflate (TMSOTf), respectively – all of which can be used in halide abstraction. In particular, the reactions with esters produce methyl chloride and trimethylsilyl chloride as side products, both of which are highly volatile, meaning both easy removal from the product, preventing an equilibrium reversing the ion formation, and opening the opportunity to drive the equilibrium under a gentle vacuum.

Of course, these anions have their own shortcomings, being more expensive than many chlorometallates and highly fluorinated. However, their weak basicity, the multitude of synthetic strategies that their precursors offer, and demonstrated propensity to form ionic liquids were all good motivations to explore this research angle.

3.3.2.1 *Borenium Triflate Systems*

In the unpublished work from another PhD student in this group,¹⁹⁵ the combination of TMSOTf with boron complexes of the general formula BX₃L (where X = chloride or fluoride L = methylimidazolium, 4-picoline, dimethylacetamide, trioctylphosphine or trioctylphosphine oxide), with the intention of generating ionic liquids of a general formula [BX₂L][OTf], gave liquid compounds with tetracoordinate boron species. ¹¹B NMR spectra of the products featured exclusively signals in the tetracoordinate region (0-10 ppm), indicating the generation of the charge-neutral adduct [BX₂L(OTf)], and the absence of free borenium cations. As discussed previously for halometallate borenium ionic liquids, the inherent issue of a ligand scrambling still existed in these complex. It has been observed that when these compositions were left for a period of several months inside an argon filled glovebox, the complex continues to rearrange, with white crystals identified as B(OTf)₃ found on the walls of the storage vials. The initial reaction leading to the formation of [BX₂L(OTf)], followed by subsequent scrambling reactions is postulated below.

Scheme 15. The products of the combination of $[BX_3(\text{mim})]$ with TMSOTf, forming a tetracoordinate boron adduct *via* halide abstraction (top) and the formation of boron triflate *via* a postulated ligand scrambling pathway (bottom).



The apparent lack of free p orbital has not been perceived as drawback in itself, and the reports on latent, high Lewis acidity of triflate adducts to borocations from Corey and colleagues gave hope that these compounds could be used as liquid Lewis acids.^{75,196} Indeed, Gutmann acceptor number measurements for these adducts remained rather high, all with values a bit greater than 100, indicating a degree of superacidity. However, there was a caveat to this optimistic outcome.



As seen in the Chapter 2, ANs are describing the strength of the Lewis acid-probe bond, but they do not distinguish between a Lewis acid with a vacant orbital (readily accepting any base) and a latent Lewis acid, that needs to overcome the energy of breaking a weak bond (such as bridging chloride or substituting a weakly coordinating ligand). For example, in Chapter 2, the anions $[\text{AlCl}_4]^-$ was shown to react with P_{222}O to form $[\text{AlCl}_3(\text{P}_{222}\text{O})]$, giving the same AN as AlCl_3 . However, when applied as catalyst in, for example the Diels Alder reaction demonstrated in Chapter 2, $[\text{AlCl}_4]^-$ has not been acting as an active Lewis acid; all nucleophiles in these reactions have proven to be less capable of breaking the Al-Cl bond than the P_{222}O probe molecule, and the reactivity was controlled by this inability to break this bond. Conversely, if a weaker interaction existed between the Lewis acid and the adduct, it was entirely plausible that it would be an active Lewis acid. This concept of “masked” borenium cations is well established and accounts for a significant proportion of boronium reactivity reported in the literature.⁶⁵ For example in 1998, Atwood and colleagues demonstrated the use of a tetracoordinate boron complex coordinating either a THF solvent molecule or triflate anion, which was capable of forming a tri-coordinate species in the initiation of the polymerisation of propylene oxide.¹⁹⁷ In this case, the triflate anion, acting as a weakly-bound X-donor ligand, is being displaced by the P_{222}O probe molecule. Unfortunately, preliminary work involving Diels-Alder reaction showed these triflate systems as inactive.¹⁹⁵ Nevertheless, despite this initial failure, considering weak coordination from triflate and reported literature reactivity,⁷⁵ it was anticipated that a more nucleophilic dienophile, or another reaction system, could be catalysed by $[BX_2\text{L}(\text{OTf})]$ complexes – which motivated this work.


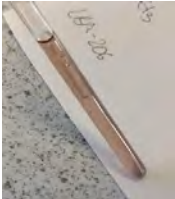
A key target of this work, focused on BF_3 as the starting material, was to discourage the ligand scrambling effect. As discussed in the previous section, the use of the catecholate ligand was directed at this, through bidentate interactions discouraging dissociation. Furthermore, forming catechol borenium cations with a general formula $[\text{BcatL}]^+$ gives a chloride-free ionic liquid, preventing the re-formation of BCl_3 molecules which are corrosive, Lewis acidic and volatile.

The synthesis of borenium triflate ionic liquids were performed in the glovebox. For borenium ionic liquids with halometallate anions, a solventless synthesis was the simplest and most efficient approach. However, when using trimethylsilyl triflate (TMSOTf) it was found that dissolution in dry DCM allowed for better mixing between substrates and a more even heating across the sample to push halide abstraction to completion. Therefore, the synthesis proceeded through the solvation of boron complex of the general formula $[\text{BcatCIL}]$, followed by the slow, dropwise addition of TMSOTf. The mixture was stirred and, when the addition was finished, it was allowed to react at 50°C under argon on a Schlenk line. Finally, solvent was removed *in vacuo*, at room temperature.

The products of these reactions had a range of appearances at room temperature (Table 9), with the long alkyl chains of trioctylphosphine and trioctylphosphine oxide reducing the melting points of the complexes, as seen for the boron complexes formed with these ligands (Table 9). Differential scanning calorimetry (DSC) plots are given in Appendix B.

Table 9. Physical appearances of systems formed from the combination of boron complexes with the general formula $[\text{BcatCIL}]$ and TMSOTf, along with ^{19}F NMR signals for each sample, recorded neat at 350 K.

Compound	Appearance at room temperature	^{19}F NMR signal (ppm)	Photo
$[\text{Bcat}(\text{N}_{222})(\text{OTf})]$	Very light brown crystalline structure	-78.92	
$[\text{Bcat}(\text{P}^t\text{Bu}_3)(\text{OTf})]$	Fine white powder	-77.96	

[Bcat(P ₈₈₈)(OTf)]	Colourless liquid	-78.05	
[Bcat(P ₈₈₈ O)(OTf)]	Light brown liquid	-78.14	

All products were analysed by multinuclear NMR spectroscopy: ¹¹B and ¹⁹F NMR spectra were recorded for all samples, in addition to ³¹P NMR spectra acquired where appropriate. The samples were measured neat, to avoid solvent coordination to the boron centre and other solvation effects. Solid samples were measured at elevated temperatures, above their melting point.

The ¹⁹F NMR spectra, recorded at 350 K, provided little information, all featuring one singlet at *ca.* -78 ppm (Figure 41). This is only a small shift from the ¹⁹F peak of TMSOTf which is observed at -79 ppm, however this matches previous work for [BCl₃(OTf)L] systems where the change to the CF₃ peak was similarly *ca.* -78 ppm.¹⁹⁵ For ionic liquid systems similar triflate peaks are also seen from -78 to -79 ppm indicating that this is a typical value.¹⁹⁸ The ¹⁹F NMR chemical shifts recorded for each system are in Table 9.

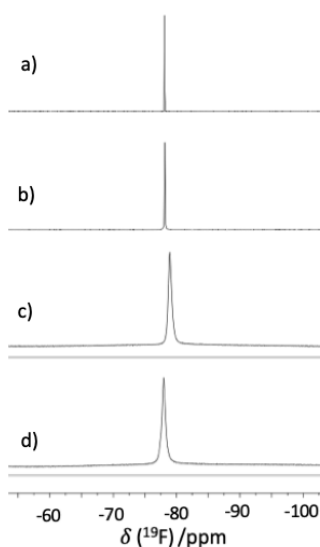


Figure 41. The ¹⁹F NMR spectrum of [BcatL(OTf)] adducts, where L is: a) trioctylphosphine, b) trioctylphosphine oxide c) triethylamine, d) tri-*tert*-butyl phosphine (samples recorded neat at 350 K with a DMSO-*d*₆ capillary).

3.3.2.1.1 Speciation of $[\text{Bcat}(\text{OTf})(\text{P}_{888})]$ and $[\text{Bcat}(\text{OTf})(\text{P}_{888}\text{O})]$

For the systems $[\text{Bcat}(\text{OTf})(\text{P}_{888})]$ and $[\text{Bcat}(\text{OTf})(\text{P}_{888}\text{O})]$ it was possible to record neat NMR spectra at room temperature. The two ^{11}B NMR spectra (Figure 42) are broadly similar; it is evident that tetracoordinate boron adducts were formed between the boron and the triflate group as the peak is in the 0-10 ppm region: at 8.26 ppm for $[\text{Bcat}(\text{OTf})(\text{P}_{888})]$ and 6.29 ppm for $[\text{Bcat}(\text{OTf})(\text{P}_{888}\text{O})]$. Whilst they remain in the tetracoordinate region, both spectra differ from the ^{11}B NMR spectra of their corresponding starting materials. Signal for $[\text{Bcat}(\text{P}_{888})(\text{OTf})]$ is shielded by $\Delta^{11}\text{B} = 3.7$ ppm with respect to $[\text{BcatCl}(\text{P}_{888})]$ (Figure 37). The spectrum for $[\text{Bcat}(\text{OTf})(\text{P}_{888}\text{O})]$ is significantly simpler than that for its starting material, $[\text{Bcat}(\text{OTf})(\text{P}_{888}\text{O})]$ (Figure 38), and the signal for the product is not obviously aligned with any of the starting material signals. Notably, the signal for the phosphine complex is a doublet ($J_{\text{B-P}} = 160.6$ Hz, where a study on ^{31}P - ^{11}B coupling constants reported values 165 -174 Hz for phosphines bonded to boron trihalides),¹⁹⁹ while for the phosphine oxide it is a singlet. In the ^{31}P NMR spectrum (Figure 43) a corresponding quartet is observed with the same coupling constant.

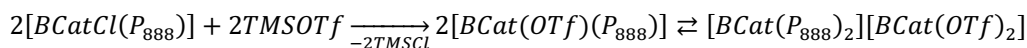


Figure 42. ^{11}B NMR spectrum for (top) $[\text{Bcat}(\text{OTf})(\text{P}_{888})]$ and (bottom) $[\text{Bcat}(\text{OTf})(\text{P}_{888}\text{O})]$, at room temperature.

Sharp signals at tetracoordinate region postulate that tri-coordinate species are absent from this liquid at room temperature; these compounds could be possibly termed as a liquid coordination complex (if such nomenclature is appropriate for a non-metallic, main group element), but not ionic liquid, due to apparent absence of ionic species.

The ^{31}P NMR spectra (Figure 43) showed more than one environment, casting some doubt on the simple speciation suggested by ^{11}B NMR spectroscopy. Importantly, they did not show the presence of any free ligand (phosphine or phosphine oxide): if free phosphine were present, it would be observed at *ca.* -30 ppm, whereas free phosphine oxide would be at 50 ppm. This suggests that the ligands remain coordinated, with several species across the equilibrium.

For the P_{888} system, two peaks are observed in the ambient ^{31}P NMR spectrum (Figure 43): at 12.82 and -11.28 ppm, with 1 : 4 ratio. The more shielded one, at -11.28 ppm ($J_{\text{B-P}}^1 = 160.6$ Hz, similar to the literature), has coupling constant matching that of the boron spectrum, suggesting that it corresponds to the adduct, $[\text{BcatP}_{888}(\text{OTf})]$. The deshielded signal, accounting for 20 % of the ligand by integration, may account for the usual issue of ligand scrambling (Equation 41), with higher symmetry of the $[\text{Bcat}(\text{P}_{888})_2]^+$ cation accounting for a sharper signal.



Equation 41

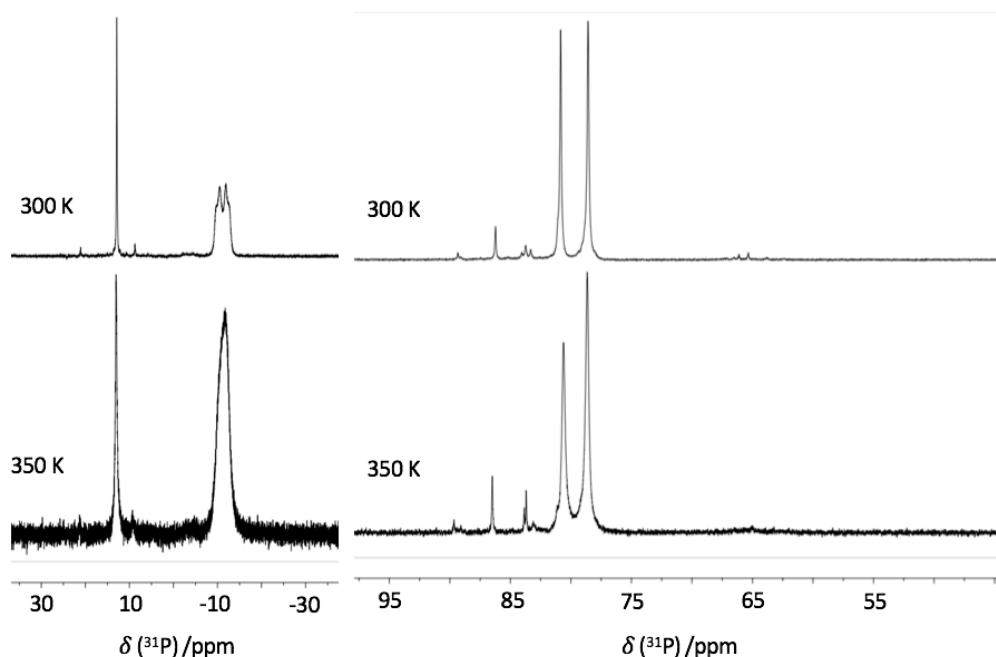
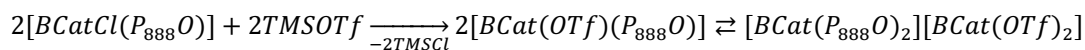


Figure 43. Comparison of ^{31}P NMR spectra of liquids with the general formula $[\text{Bcat}(\text{OTf})\text{L}]$, where $\text{L} =$ (left) P_{888} and (right) P_{888}O , at 300 and 350 K.

The ^{31}P NMR spectrum of $[\text{Bcat}(\text{OTf})(\text{P}_{888}\text{O})]$ features two main signals at 80.84 and 78.58 ppm, and several low-intensity ones, of which that at 86.22 ppm was most prominent. In comparison, the ^{31}P NMR spectrum of $[\text{BcatCl}(\text{P}_{888}\text{O})]$ (Figure 38) featured two main signals at 79.07 and 76.25 ppm, in addition to very minor peaks. The two main signals in this spectrum

(Figure 43) may correspond to the neutral and ionic form, following Equation 42, slight deshielding resulting from the substitution of the chloride ligand with a triflate one.



Equation 42

The more deshielded signals were not present prior to the introduction of TMSOTf. In their work on catechol boron cations, Del Grosso *et al.* report that the species $[\text{TMS}(\text{OP}_{222})(\text{OTf})]$, as giving a peak in the ^{31}P NMR spectrum at 92.8 ppm.¹⁸⁴ Taking into consideration that the corresponding P_{888}O signals would be a bit more shielded (Chapter 2), this could possibly indicate the formation of a small quantity of $[\text{TMS}(\text{P}_{888}\text{O})(\text{OTf})]$, this is reinforced by the presence of a peak in the ^{13}C NMR spectrum, as seen in Figure 44.

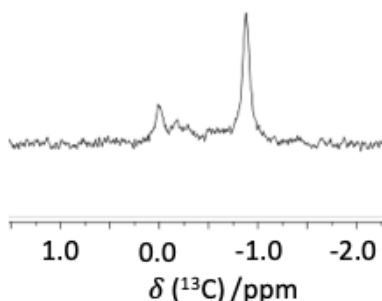


Figure 44. ^{13}C NMR spectrum for $[\text{Bcat}(\text{OTf})(\text{P}_{888}\text{O})]$ indicating the generation of $[\text{TMS}(\text{P}_{888}\text{O})(\text{OTf})]$.

As shown in Figure 43, variable temperature ^{31}P NMR did not reveal significant changes in signals for either $[\text{Bcat}(\text{OTf})(\text{P}_{888})]$ or $[\text{Bcat}(\text{OTf})(\text{P}_{888}\text{O})]$. This was in contrast to VT ^{11}B NMR spectroscopy, which brought a major insight into the nature of both systems (Figure 45).

Upon heating a sample of $[\text{Bcat}(\text{OTf})(\text{P}_{888})]$, an additional peak was revealed, indicating additional environments. Although at 300 K only one ^{11}B NMR signal was found, corresponding to $[\text{Bcat}(\text{OTf})(\text{P}_{888})]$, a second peak (*ca.* 21 ppm) emerged at 320 K, which can be assigned to the formation of the tricoordinate $[\text{Bcat}(\text{P}_{888})]^+$. This is quite shielded for a tricoordinate cation, which can be justified by a relatively strong interaction with $[\text{OTf}]^-$.

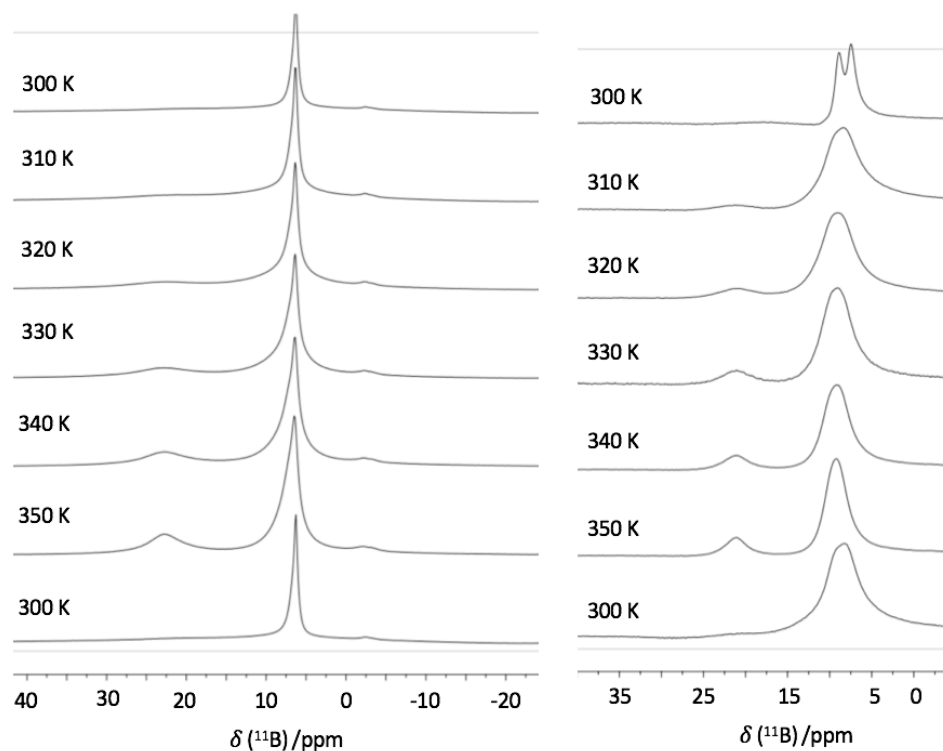


Figure 45. The ^{11}B NMR spectra for (left) $[\text{Bcat}(\text{P}_{888})][\text{OTf}]$ and (right) $[\text{Bcat}(\text{P}_{888}\text{O})][\text{OTf}]$, at a range of temperatures.

In analogy, for $[\text{Bcat}(\text{OTf})(\text{P}_{888}\text{O})]$ the major tetracoordinate species is represented by a dominant broad peak in the ^{11}B NMR spectra in the tetracoordinate region. However, upon heating an additional peak emerges at ~ 23 ppm, which suggests the tricoordinate cation $[\text{Bcat}(\text{P}_{888}\text{O})]^+$, accompanied by $[\text{OTf}]^-$ anion.

Importantly, for both samples, upon cooling back to ambient temperature, spectra returned to the same form as before heating (Figure 45, bottom spectra), except for the poorly-resolved doublet in $[\text{Bcat}(\text{OTf})(\text{P}_{888})]$, which can be accounted for by certain lag in sample cooling.

3.3.2.1.2 Speciation of $[\text{Bcat}(\text{N}_{222})(\text{OTf})]$ and $[\text{Bcat}(\text{P}^t\text{Bu}_3)(\text{OTf})]$

To understand the speciation of the systems $[\text{Bcat}(\text{N}_{222})(\text{OTf})]$ and $[\text{Bcat}(\text{P}^t\text{Bu}_3)(\text{OTf})]$, which are solid at room temperature, it was necessary to heat them in the NMR spectrometer, in order for comprehensible spectra to be obtained (see VT ^{11}B NMR spectra in Figure 46). In contrast to examples discussed in Section 3.2, there was little change in the number and shape of signals, beyond the increasing resolution of the peaks.

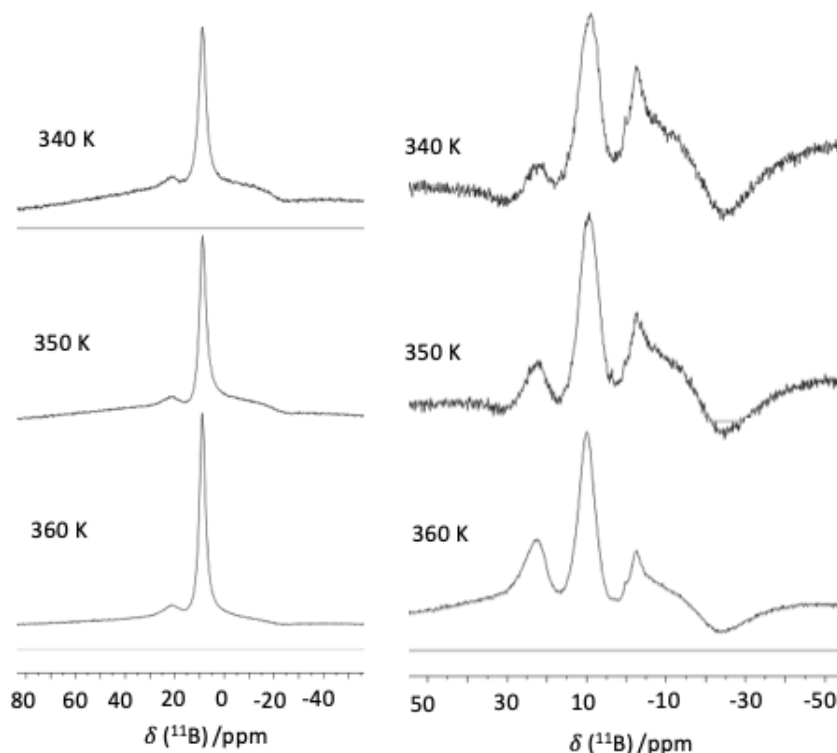


Figure 46. The ^{11}B NMR spectra for (left) $[\text{Bcat}(\text{N}_{222})(\text{OTf})]$ and (right) $[\text{Bcat}(\text{P}^t\text{Bu}_3)(\text{OTf})]$ at temperatures from 340 to 360 K.

For $[\text{Bcat}(\text{N}_{222})(\text{OTf})]$, there was one major peak at 8.44 ppm (350 K) in the ^{11}B NMR spectrum, likely to be an adduct of the formula $[\text{Bcat}(\text{N}_{222})(\text{OTf})]$ – it was considerably upfield shifted from the 12.41 ppm peak reported for the chloride complex. A much smaller peak was observed at 21.59 ppm (increasing to 21.71 ppm with increasing temperature), accounting for about 5% of the major peak area across the temperature range. This signal was in a typical region for a tricoordinate complex, and therefore could represent a small quantity of tricoordinate $[\text{Bcat}(\text{OTf})]$ previously reported at 21.6 ppm by Del Grosso *et al.*¹⁸⁴ In other work, Del Grosso *et al.* have reported a ^{11}B NMR peak for the $[\text{Bcat}(\text{N}_{222})]^+$ cation at 27.9 ppm, with an $[\text{AlCl}_4]^-$ counterion.¹⁸⁹ As the chemical shifts of species in dynamic equilibrium can be shifted from reported positions, this signal could be also attributed to $[\text{Bcat}(\text{N}_{222})]^+$. Both ^1H and ^{13}C NMR spectra (Appendix A) were of too poor quality to provide any clarification, and nitrogen NMR rarely produces useful information. Therefore, two alternative sets of dynamic equilibria were proposed for this system: Equation 43 and Equation 44.



Equation 43



Equation 44

The ^{11}B NMR spectra of $[Bcat(OTf)(P^tBu_3)]$ (Figure 46) featured three signals at -2.83, 9.27 and 21.91 ppm, which were less well resolved than spectra of the $[Bcat(OTf)(N_{222})]$ complex. The highest intensity signal at 9.27 ppm can be assigned to $[Bcat(OTf)(P^tBu_3)]$, slightly shielded compared to the signal for $[BcatCl(P^tBu_3)]$ at 12.88 ppm (Figure 34). The signal at 21.91 ppm, in the tricoordinate region, could be assigned to either a charge-neutral $[Bcat(OTf)]$,¹⁸⁴ or a cationic $[Bcat(P^tBu_3)]^+$. The most surprising is the signal at -2.8 ppm, suggesting a very electron-rich tetracoordinate boron, on this basis potentially deriving from an anion, $[Bcat(OTf)_2]^-$. The presence of this anion requires a counter ion which would be $[Bcat(P^tBu_3)]^+$ which is represented by the peak at 21.91 ppm. Free borenium cations with the structure $[Bcat(P^tBu_3)]^+$ would be expected at 29.89 ppm in the ^{11}B NMR spectra, according to work by Stephan *et al.* and previously described chlorometallate structures in this work.¹⁸⁸ However, this peak may be more shielded as a consequence of the equilibrium and the strong attraction between the boron centre and triflate anion (Equation 45).

Further light on this speciation can be shed by the ^{31}P NMR spectrum (Figure 47), with two phosphorus environments.

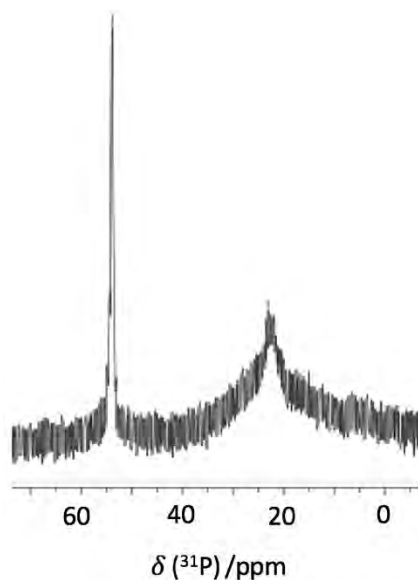
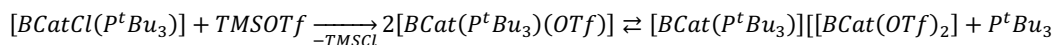


Figure 47. ^{31}P NMR spectrum for $[Bcat(OTf)(P^tBu_3)]$ at 360 K.

The broad peak at 22.94 ppm indicates a bound phosphine, in analogy to the tetracoordinate $[BcatCl(P^tBu_3)]$ complex which gave the ^{31}P NMR at 24.82 ppm. The second, sharper peak represents free P^tBu_3 . This suggests that the very sterically hindered P^tBu_3 has been partially dissociated from the boron complex, accounting for the additional peak at -2.8 ppm,

representing the complex $[\text{Bcat}(\text{OTf})_2]$. The most plausible equilibria in this system are proposed in Equation 45.



Equation 45

In summary, it was demonstrated that the speciation of $[\text{Bcat}(\text{OTf})\text{L}]$ adducts depends on both the ligand, L, and the temperature. Whereas they did feature in some cases borenium cations and other ionic species, there is always a significant proportion of charge-neutral species. This does not impair their possible use as liquid/low melting Lewis acidic catalysts. As a preliminary screening of their potential activity, Gutmann AN values were measured.

3.3.2.1.3 Gutmann Acceptor Number Measurements

Lewis acidity of $[\text{Bcat}(\text{OTf})\text{L}]$ adducts was measured *via* the Gutmann acceptor number, discussed in Sections 1.1.3.1 and 2.11. The ^{31}P NMR spectra, recorded neat in the liquid phase (300 K), are reported in Table 10. In all tested samples the P_{222}O probe gave one signal, except for $[\text{Bcat}(\text{P}_{888})(\text{OTf})]$, where two signals were recorded for each probe concentration. AN values listed in Table 10 suggest that the $[\text{Bcat}(\text{OTf})\text{L}]$ adducts are potently strong Lewis acids, on par or exceeding Lewis acidity of chloroaluminate ionic liquids (AN = 96).¹⁹ It is notable, however, that all of these values are lower than for the catechol-free borenium ionic liquids/systems previously measured, with a $[\text{BCl}_2\text{L}]^+$ or a $[\text{BCl}_2(\text{OTf})\text{L}]$ structural motif. This reflects the greater donation from the catechol onto the boron centre, which reduces its electrophilicity.

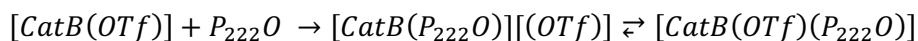
Table 10. AN values for all $[\text{Bcat}(\text{OTf})\text{L}]$ liquids (measured at 300 K) shown with the $\delta^{31}\text{P}$ resonances recorded (in ppm) measured for solutions of these liquids containing 1, 2 and 3 mol% P_{222}O (referenced to $\delta^{31}\text{P}$, H_3PO_4 85% = 0 ppm).

Compound	$\delta^{31}\text{P}$			AN
	1%	2%	3%	
$[\text{Bcat}(\text{OTf})(\text{N}_{222})]$	88.24	88.15	88.07	106.4
$[\text{Bcat}(\text{OTf})(\text{P}^t\text{Bu}_3)]$	85.7	85.86	86.85	98.7
$[\text{Bcat}(\text{OTf})(\text{P}_{888})]^a$	88.2	88.07	87.91	106.5
$[\text{Bcat}(\text{OTf})(\text{P}_{888})]^a$	83.28	83.31	83.32	94.6
$[\text{Bcat}(\text{OTf})(\text{P}_{888}\text{O})]$	85.18	85.22	85.36	98.9

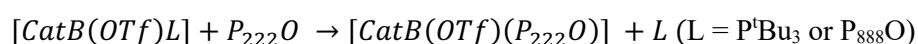
^aTwo signals from the probe recorded for each composition

Assigning the AN values to particular Lewis acidic species that the P_{222}O probe might be interacting with is a difficult undertaking; however, certain assumptions may be made based

on speciation studies in this work and on the literature. Assuming error bars on AN values to be ± 0.5 ppm,²¹ there are three AN values recorded: AN = 106, 99 and 95. Del Grosso *et al.* reported the chemical shift of the complex $[\text{CatB}(\text{P}_{222}\text{O})][\text{OTf}]$ at 85.4 ppm,¹⁸⁴ which corresponds well to the AN = 99 reported for tri-*tert*-butyl phosphine and trioctylphosphine oxide. The formation of $[\text{CatB}(\text{P}_{222}\text{O})][\text{OTf}]$ could proceed either through Equation 46 (addition to free acid) or Equation 47 (ligand substitution in a latent acid). It should also be noted, that there is high likelihood that in reality, tetracoordinate boron species are formed.

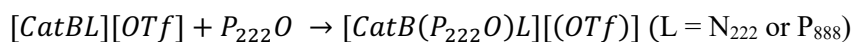


Equation 46

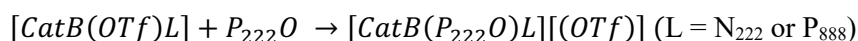


Equation 47

The higher acceptor number, AN = 106, could be related to the $[\text{CatB}(\text{P}_{222}\text{O})\text{L}]^+$ (L = N₂₂₂ or P₈₈₈) complex, formed either with free borenium cation (Equation 48), or by substitution of $[\text{OTf}]^-$, which becomes a counterion (Equation 49). The higher electrophilicity derives from N- or P-donor being less donating than the triflate.



Equation 48



Equation 49

As shown through this discussion, it is not possible to tell whether the measurement was performed for “masked” species, that required ligand substitution, or for a Lewis acid with a free p orbital on boron. It is also unclear what is the origin of the second signal found for the $[\text{Bcat}(\text{P}_{888})(\text{OTf})]$ sample. Nevertheless, combined with speciation studies, AN measurements offer certain indirect information about the speciation of the active Lewis acid in the system, and they provide a rather direct insight into the expected strength of interaction of these acids with a nucleophile (especially a hard one).

3.3.2.2 Borenium Bistriflimide Systems

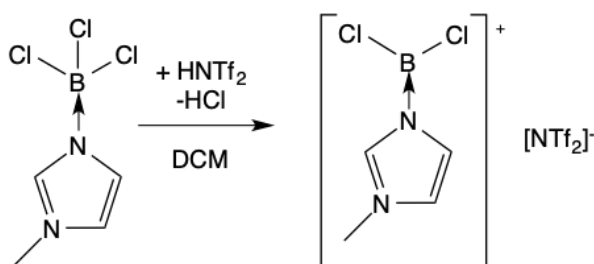
3.3.2.2.1 Development of the Synthetic Procedure

Moving onto less coordinating anions, in this work borenium ionic liquids with bistriflimide counterions, $[\text{NTf}_2]^-$, were explored for the first time. The first attempt to generate a $[\text{BCl}_3\text{L}][\text{NTf}_2]$ ionic liquid was made using the $[\text{BCl}_3(\text{mim})]$ complex as the starting material; it has been successfully used by Coffie *et al.* to generate the cation $[\text{BCl}_2(\text{mim})]^+$ on combination with either GaCl_3 or AlCl_3 .⁴

In contrast to the triflate study, where TMSOTf was used as the sole halide abstracting agent and the potential anion precursor, in this work three synthetic approaches were tested, using bistriflimidic acid (HNTf_2), methyl bistriflimide (MeNTf_2), silver bistriflimide, $\text{Ag}[\text{HNTf}_2]$.

Bistriflimidic acid was synthesised from lithium bistriflimide and sulfuric acid (Section 3.1.8). Subsequently, it was reacted with $[\text{BCl}_3(\text{mim})]$ to yield a salt and HCl as a side product (Scheme 16).

Scheme 16. The formation of $[\text{BCl}_2(\text{mim})][\text{NTf}_2]$ using bistriflimidic acid as the halide abstracting agent.



The reaction between $[\text{BCl}_3(\text{mim})]$ and Lewis acidic metal halides (MCl_3 , where $\text{M} = \text{Al}$ or Ga), as described by Coffie *et al.*, was carried out under solventless conditions, and proceeded rather fast.⁴ In contrast, the Brønsted acidic bistriflimidic acid was found to react extremely slowly, and chloroform was found to be the best solvent to enhance this reaction mixing. However, once the mixing occurred, the reaction still proceeded extremely slowly, and the most effective driving force was to use a high vacuum to force the evolution of HCl .

The formation of the product was followed by ^1H NMR spectroscopy, monitoring a growing set of imidazole peaks slightly downshifted from the $[\text{BCl}_3(\text{mim})]$ peaks (Figure 48). After three days at 60°C *in vacuo*, the product was an extremely viscous, slightly brown liquid. However, it was clear from the spectra that even under these harsh conditions, a complete conversion to the product has not been achieved, with integrations of the peaks suggesting a 1:1.1 ratio of product to starting material.

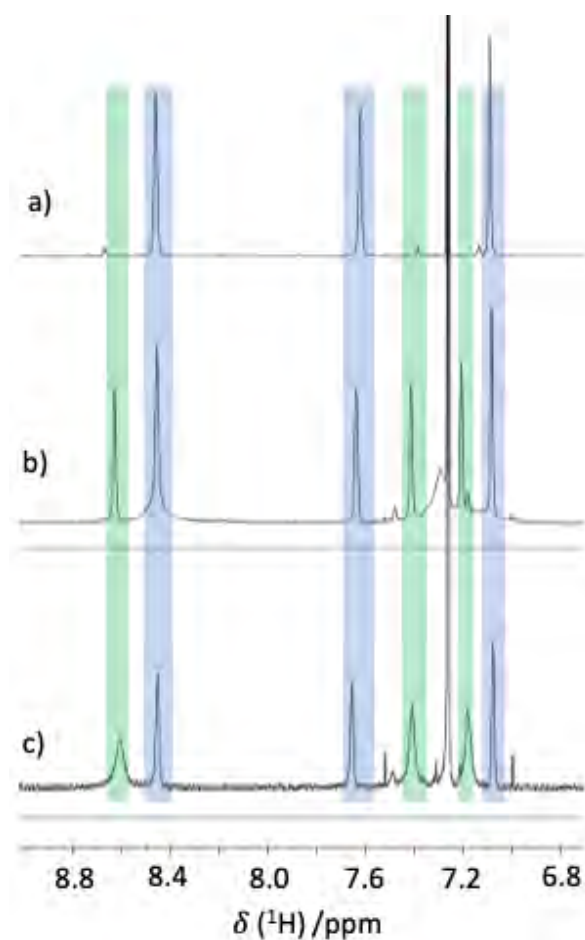
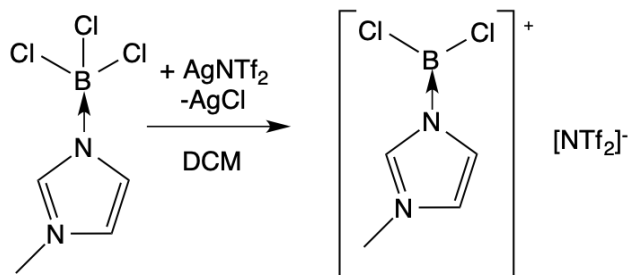


Figure 48. Comparison of ^1H NMR spectra of a) $[\text{BCl}_3(\text{mim})]$ b) the reaction mixture of $[\text{BCl}_3(\text{mim})]$ and HNTf_2 , after stirring for 15 h at $60\text{ }^\circ\text{C}$ *in vacuo*, and c) the product following stirring for three days at $60\text{ }^\circ\text{C}$ *in vacuo*. The starting material peaks are highlighted in blue, while the product peaks are highlighted in green.

If even harsher conditions were used, there was a risk that BCl_3 could be removed from the product, destroying the borenium complex (in these experiments the spectra in Figure 48 disprove this is happening, as the peaks from the acidic proton at 8.45 and 8.60 ppm, would be otherwise upfield). Nevertheless, this method was found inefficient and has not been pursued further.

Silver bistriflimide was synthesised from silver carbonate (Section 3.1.10). When combined with $[\text{BCl}_3(\text{mim})]$, the driving force of the reaction was expected to be the formation of a highly insoluble AgCl side product (Scheme 17). This reaction was performed in dichloromethane, the solvent in which $[\text{BCl}_3(\text{mim})]$ is most soluble, at “NMR scale” of 0.03 g.

Scheme 17. The formation of $[\text{BCl}_2(\text{mim})][\text{NTf}_2]$ using silver bistriflimide as the halide abstracting agent.



On mixing of the reactants, an off-white solid appeared, indicative of silver chloride formation, and the sample was filtered to remove this. The sample was shaken on the Varimix over the course of four days, at 45 °C, and followed by ^1H NMR spectroscopy (Figure 49).

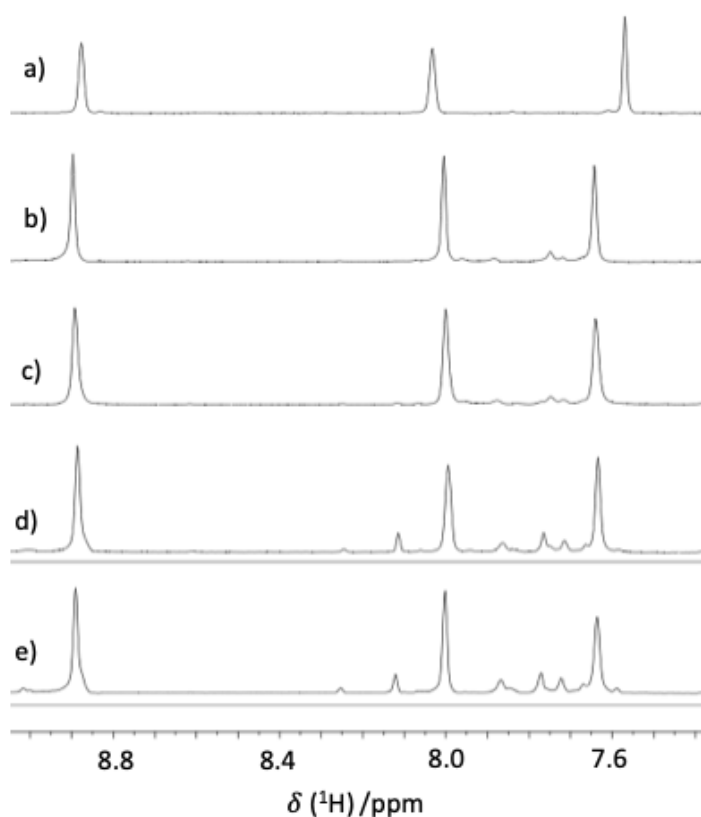


Figure 49. ^1H NMR spectra showing a) the starting material $[\text{BCl}_3(\text{mim})]$ in DCM and the products of the reaction mixture of silver bistriflimide and $[\text{BCl}_3(\text{mim})]$ in DCM with a DMSO-d_6 capillary, over four days (b-e).

On the first day, only starting material was present (Figure 49a and b). The following days a additional peaks in the methylimidazole region were observed. This came with heating the reaction mixture at 45 °C to drive the formation of AgCl . When taken in combination with the ^{11}B NMR spectrum (Figure 50), which shows that there are no peaks in the tri-coordinate region (20-40 ppm) it appears that the product forming upon heating was not ionic,

[BCl₂(mim)][NTf₂], but most likely that the adduct [BCl₂(NTf₂)(mim)], with a signal at 3.68 ppm. *N.B.*, the main peak in the ¹¹B NMR spectrum is that of the starting material [BCl₃(mim)] at 5.5 ppm.

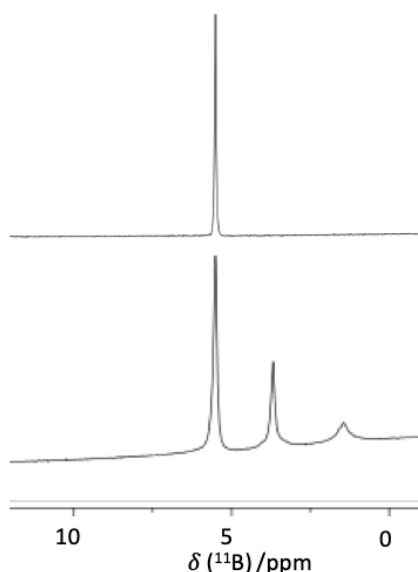
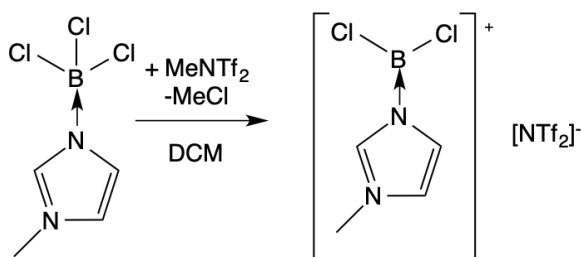


Figure 50. The ¹¹B NMR spectrum of (top) the starting material [BCl₃(mim)] (in CDCl₃) and (bottom) [BCl₃(NTf₂)(mim)] from silver bistriflimide (in DCM with a DMSO-*d*₆ capillary).

The third synthetic strategy relied on a commercial methyl bistriflimide as the bistriflimide source, abstracting chloride to give the highly volatile MeCl as a side product (Scheme 18).

Scheme 18. The formation of [BCl₂(mim)][NTf₂] using methyl bistriflimide as the halide abstracting agent.



The reaction was firstly trialled at “NMR scale” to test the efficiency of the halide abstraction. The reagents were combined in DCM and stirred overnight at 55 °C, before evacuating solvent and MeCl, which produced a dark yellow, viscous liquid. The ¹H NMR spectra of the starting material, [BCl₃(mim)], and the product were recorded in different solvents: the former in chloroform (Figure 51, top) and the latter neat (Figure 51, bottom). This could account for the difference observed in the NMR shifts; nevertheless, the NMR signals clearly have a different distribution in the product spectrum than in the top spectrum (Figure 51). This suggests that the equilibrium sits further towards the product than was observed when using AgNTf₂ and

HNTf₂. Multiple environments around imidazole are likely to account for multiple orientations around the boron centre, as well as ligand scrambling.

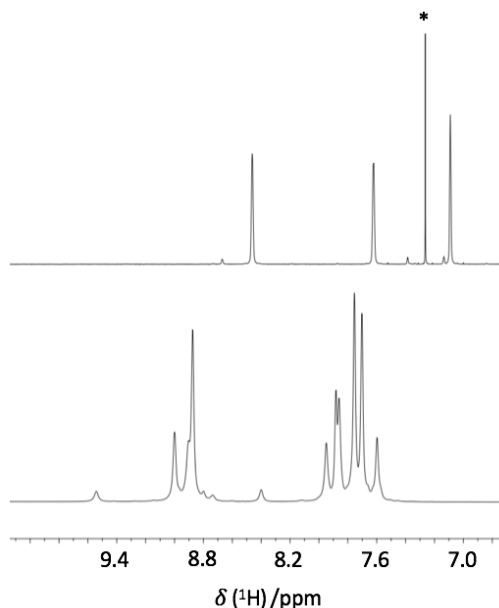


Figure 51. ¹H NMR spectra of starting material, [BCl₃(mim)] (top, in chloroform) and the product of reaction with methyl bistriflimide (bottom, neat with a DMSO capillary). * marks solvent peak

The ¹¹B NMR spectrum (Figure 52) showed the development of several tetracoordinate boron species: a broad peak at 2 ppm, a mostly obscured signal at 2.83 ppm and a sharp signal at 0.51 ppm, in addition to the sharp peak of the starting material at 5.51 ppm.

Although clearly not a free tetracoordinate borenium species, the interaction between the boron and the coordinated bistriflimide group was probed by measuring the Gutmann acceptor number of the system. The AN recorded for this system is 109.2, suggesting that it is a superacid; it is the most likely that the probe displaced the [NTf₂][−] anion, forming [BCl₂(mim)(P₂₂₂O)][NTf₂].

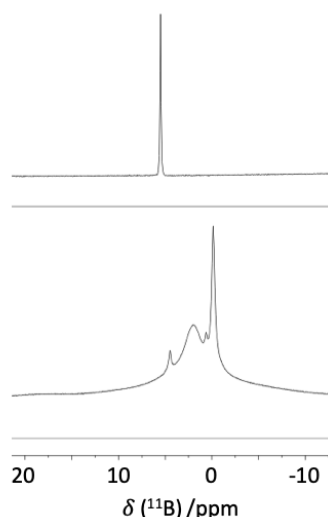


Figure 52. ^{11}B NMR spectrum of (top) $[\text{BCl}_3(\text{mim})]$ in CDCl_3 and (bottom) the product of the reaction of $[\text{BCl}_3(\text{mim})]$ with MeNTf_2 (solventless, with DMSO capillary).

Seeing prevalent ligand scrambling, the synthesis of $[\text{BCl}_3(\text{NTf}_2)(\text{mim})]$ was not scaled up past the “NMR scale”. Instead, it was concluded that using the methyl ester was the cleanest route to access a bistriflimide system, and the subsequent synthetic effort was focused on the BcatCl starting material.

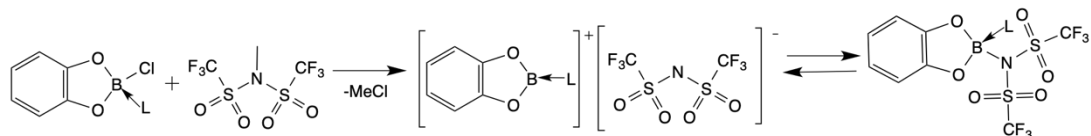
3.3.2.2.2 Synthesis of the $[\text{BcatL}][\text{NTf}_2]$ systems

In analogy to the work discussed in Section 3.3.2.1, the strategy to synthesise liquids of the general formula $[\text{BcatL}][\text{NTf}_2]$ paralleled the synthetic route towards $[\text{BcatL}][\text{OTf}]$, and the same ligands were employed: L = triethylamine, tri-*tert*-butyl phosphine, trioctylphosphine and trioctylphosphine oxide (Figure 32). This work had a very similar focus to the previous section, with the key difference being the more sterically bulky bistriflimide anion, with more dispersed charge, intended to discourage coordination to the boron centre. The contrast between the triflate and bistriflimide anion for catalytic applications is highlighted by Corey *et al.*, showing that greater activity in the Diels-Alder reaction is seen for oxazaborolidine based borenium catalysts with bistriflimide anions than with triflate anions.²⁰⁰ What is important, the existence of both tri- and tetracoordinate boron species in equilibrium were reported, with a ratio between the species at 1:1.2, suggesting that the tetracoordinate form is more favoured.^{74,200} Despite being partially masked, the borocation was found to be an efficient catalyst, which motivated also this work.

Synthetic procedure using MeNTf_2 paralleled that with trimethylsilyl triflate: reactants were combined in the glovebox in dry DCM, stirring and heating at 50 °C before removal of solvent and chloromethane (ice bath, *in vacuo*). Again, the product was expected to be an equilibrated





mixture of the charge-neutral adduct and the salt, the equilibrium constant dependent upon steric and electronic influences (Scheme 19).

Scheme 19. The main products of the reaction between catechol boron complex and methyl bistriflimide.



The products formed in these reactions were in general more liquid at room temperature than their triflate counterparts, although also here a range of physical appearances were observed (Table 11). Based on qualitative observation, the long-chained ligands gave the least viscous liquids. Differential scanning calorimetry (DSC) plots are given in Appendix B.

Table 11 Physical appearances of systems formed from the combination of boron complexes with the general formula [BcatCIL] and MeNTf₂.

Compound Name	Appearance at room temperature	Photo
[Bcat(NTf ₂)(N ₂₂₂)]	Golden brown liquid	
[Bcat(NTf ₂)(P ^t Bu ₃)]	Light brown liquid	
[Bcat(NTf ₂)(P ₈₈₈)]	Colourless liquid	
[Bcat(NTf ₂)(P ₈₈₈ O)]	Golden liquid	

The speciation for these systems, studied by the multi-nuclear NMR spectroscopy, is temperature-dependant and appears more complex than that of the triflate analogues. The relative integration of signals in ^{19}F , ^{31}P and ^{11}B NMR spectra are presented in a tabulated form (Table 12, Table 14 and Table 13), and will be used to underpin general discussion pertaining to all spectra. This will be followed by in-depth analysis of each example, illustrated by the actual spectra recorded for the relevant sample.

For all bistriflimide compounds, two sharp, well-resolved peaks were observed in the ^{19}F NMR spectrum: at *ca.* -74 and *ca.* -80 ppm (Table 12). Although the more shielded one was close to the chemical shift of MeNTf_2 (at -73.9 ppm), the assignment to the starting material was excluded, as the removal of methyl group was confirmed by ^1H and ^{13}C NMR spectroscopy (Section 3.1.7). The ^{19}F NMR signal for a “free” bistriflimide in ionic liquids is known to appear at *ca.* -80 ppm.²⁰¹ In a contrasting example, bistriflamide group bound *via* a strong covalent bond can give a ^{19}F NMR peak as far downfield as -70 ppm.²⁰² In the speciation of $[\text{UO}_2(\text{NTf}_2)(\text{DPPMO}_2)_2][\text{NTf}_2]$, a broad ^{19}F NMR peak at -78 ppm was recorded at 298 K, which resolved into two sharp signals (-77 and -79 ppm) at 208 K.²⁰³ These two were assigned to coordinated and free bistriflimide, respectively. Signals in this work were assigned to boron-coordinated (-74 ppm) and free (-80 ppm) bistriflimide. In contrast to the triflate analogues, free $[\text{NTf}_2]^-$ anion was found in every sample, integrating between 39% and 76% of the total bistriflamide content.

Table 12. Chemical shifts and relative integrations of ^{19}F NMR spectra for compositions $[\text{Bcat}(\text{NTf}_2)\text{L}]$.

Compound Name	T (K)	$\delta^{19}\text{F}$ / ppm (% integration)	
		{B-NTf ₂ }	[NTf ₂] ⁻
[Bcat(NTf ₂)(N ₂₂₂)]	300	-74.3 (61%)	-80.2 (39%)
	350	-74.3 (53%)	-79.9 (47%)
[Bcat(NTf ₂)(P ^t Bu ₃)]	300	-74.5 (29%)	-79.6 (71%)
	350	-74.2 (24%)	-79.5 (76%)
[Bcat(NTf ₂)(P ₈₈₈)]	300	-74.0 (29%)	-79.9 (71%)
	350	-74.9 (24%)	-79.5 (76%)
[Bcat(NTf ₂)(P ₈₈₈ O)]	300	-74.5 (42%)	-79.8 (58%)
	350	-74.1 (41%)	-79.34 (59%)

^{11}B NMR spectra are sensitive to the coordination number and ligands; across the four samples, there were five groups of ^{11}B NMR signals recorded, at *ca.* 2, 6, 12, 21 and 27 ppm (Table 13). The three former ones are typically sharp and correspond to the tetracoordinate region, and the two latter are very broad and are assigned to the tricoordinate region. The chemical shift around 12 ppm displays much stronger temperature dependence than the other four signals. Because of the extreme breadth of tricoordinate signals, relative peak areas are orientational only, possibly informing about the relative increase/decrease of a signal in the function of temperature.

Signals for the two tricoordinate species are quite shielded, owing to the electron-donating catechol ligand.¹⁸⁹ Although $[\text{Bcat}(\text{NTf}_2)]$ is not a known compound, it's chemical shift can be expected to be similar to $[\text{Bcat}(\text{OTf})]$, reported at 21.6 ppm.¹⁸⁴ The $[\text{BcatL}]^+$ cations are expected around 27 ppm.¹⁸⁸ Assuming negligible tendency of catecholate to undergo ligand scrambling, tetracoordinate ^{11}B NMR signals can be assigned to three plausible combinations of ligands: $[\text{Bcat}(\text{NTf}_2)\text{L}]$, $[\text{Bcat}(\text{NTf}_2)_2]^-$ and $[\text{BcatL}_2]^+$.

Table 13. Chemical shifts and relative integrations of ^{11}B NMR spectra for compositions $[\text{Bcat}(\text{NTf}_2)\text{L}]$.

Compound Name	T (K)	$\delta^{11}\text{B}$ / ppm (% integration)			
[Bcat(NTf ₂)(N ₂₂₂)]	300	11.92 (100%)			
	350	20.11 (22%)		13.05 (88%)	
[Bcat(NTf ₂)(P ^{<i>i</i>} Bu ₃)]	300	27.53 (32%)		6.34 (78%)	
	350	26.91 (37%)		22.0 (31%) 6.61 (32%)	
[Bcat(NTf ₂)(P ₈₈₈)]	300	21.83 (41%)		10.55 (12.9%) 1.84 (46%)	
	350	21.82 (64%)		14.00 (13%) 1.84 (31%)	
[Bcat(NTf ₂)(P ₈₈₈ O)]	300	6.42 & 5.12 (76%)			2.20 (23%)
	350	28.20 (9.3%) 22.64 (22%)		6.53 & 5.39 (57%) 2.46 (11%)	

^{31}P NMR spectra (Table 14), recorded for three phosphorus-bearing samples, feature two or three signals at various proportions. Very interestingly, signals for P_{888} and P_{888}O were deshielded with respect to a neat ligand in hexane, but the signal for the sterically-hindered P^iBu_3 was shielded with respect to the neat phosphine in benzene. This has been previously been reported by groups studying the coordination of phosphines to catechol boranes, with Coapes *et al.* reporting the shift to higher frequencies compared to free phosphine for triethyl

and trimethyl phosphines, but towards lower frequencies for sterically hindered tri-*tert*-butyl and tricyclohexyl phosphine.¹⁸⁵ In general, ³¹P NMR chemical shifts of phosphines vary hugely, for example trimethyl phosphine has a chemical shift of -61.4 ppm compared to 60 ppm for tri-*tert*-butyl phosphine, despite their both being trialkyl phosphines.²⁰⁴ This is because multiple factors contribute to electronic environment of the phosphorus. Considering the series methyl, ethyl, *iso*-propyl and *tert*-butyl, according to inductive effects, it would be expected that the *tert*-butyl group would provide the most shielding to the phosphorus, resulting in it having the lowest chemical shift, however the reverse is true.¹⁸⁵ These huge gulfs in chemical shift arise from steric effects around the phosphorus centre.²⁰⁵ The larger the alkyl group is, the greater the s-character of the phosphorus carbon bonds and the greater the p-character of the lone pair. The lone pair provides greater shielding of the nucleus than bonding pairs and greater s-character makes this more effective. As the lone pair is involved in bonding when an adduct forms, this interplay between steric and electronic effects is no longer crucial to the shielding around the phosphorus centre, leading to considerable shifts from the frequency of the free phosphine to the bound ligand.

In assigning ³¹P NMR signals in this work (Table 14), there are three plausible species bearing the L-donor ligands to be considered: [Bcat(NTf₂)L], [BcatL₂]⁺ and [BcatL]⁺. Since these signals are generally sharp, the integrations bear more meaning than those for ¹¹B NMR spectra. However, caution must be exercised when integrating ³¹P NMR signals as the standard technique results in an uneven nuclear Overhauser effect, whereby cross-relaxation between spin-active nuclei affects measurements. In addition, the nucleus exhibits long longitudinal relaxation times (*T*₁) causing variance between phosphorus environments.

Table 14. Chemical shifts and relative integrations of ³¹P NMR spectra for phosphorus containing compositions [Bcat(NTf₂)L].

Compound Name	T (K)	Free L / ppm	$\delta^{31}\text{P}$ / ppm (% integration)		
[Bcat(NTf ₂)(P ^{<i>t</i>} Bu ₃)]	300	60 ^a	55.0 (15%)	49.2 (78%)	19.7 (7%)
	350		55.0 (17%)	49.2 (77%)	19.7 (7%)
[Bcat(NTf ₂)(P ₈₈₈)]	300	-29 ^b	30.5 (47%)	12.2 (37%)	-11.8 (15%)
	350		30.9 (46%)	12.5 (38%)	-11.8 (16%)
[Bcat(NTf ₂)(P ₈₈₈ O)]	300	50 ^b	82.8 (14%)	78.5 (85%)	
	350		82.6 (11%)	81.1 (2.8%)	78.6 (86%)

^a Recorded in benzene,¹⁸⁵ ^b recorded in hexane.³

Based on the above analysis, it appears that these systems have similar speciation and the assignment of spectra is a simple task. Nevertheless, when looking at the actual spectra for each system individually, it can be noted that there are stark differences between the deceptively similar samples.

3.3.2.2.3 Speciation of $[\text{Bcat}(\text{NTf}_2)(\text{N}_{222})]$

The room-temperature ^{11}B NMR spectrum of $[\text{Bcat}(\text{NTf}_2)(\text{N}_{222})]$ features a sharp signal at 11.92 ppm, which remains the main feature across the studied thermal range of 300 – 350 K (Figure 53).

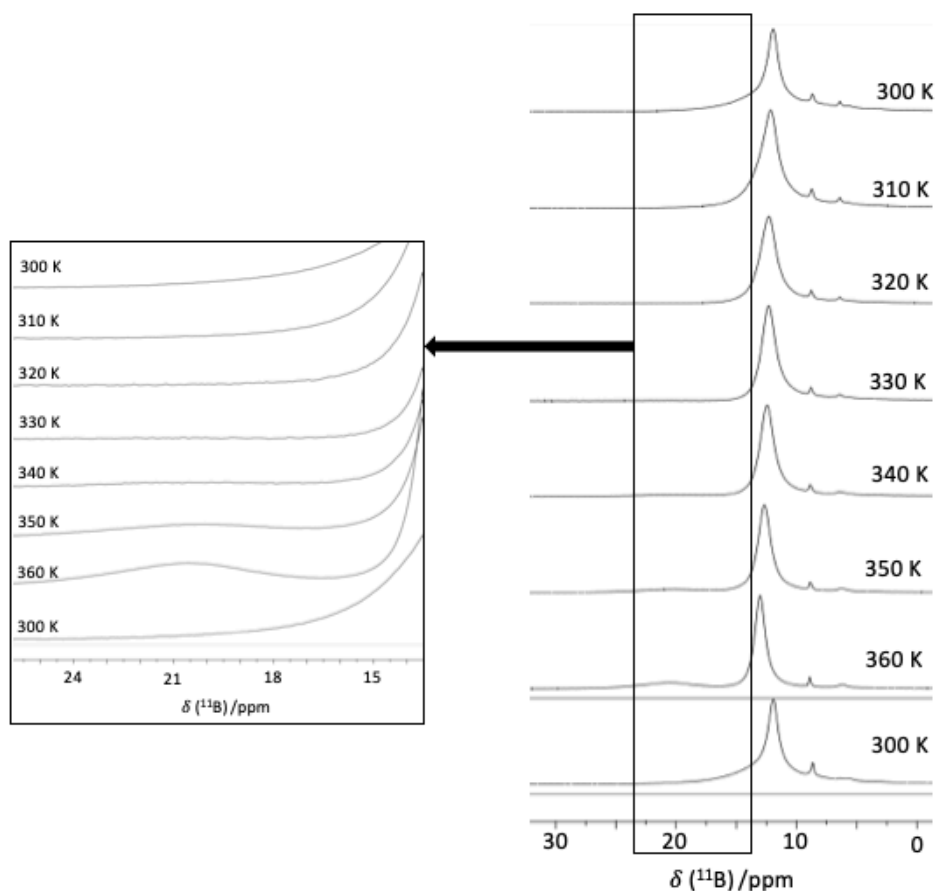
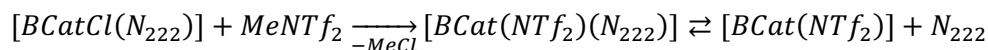


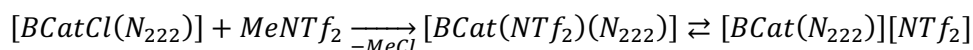
Figure 53. The ^{11}B NMR spectra for $[\text{Bcat}(\text{NTf}_2)(\text{N}_{222})]$ and at increasing temperatures from 300 to 360 K (26.85 to 86.85 °C), and again at 300 K following cooling. Insert shows the emergence of peak at 21 ppm over this temperature range.

This shows that the main species is a tetracoordinate adduct. In addition to two or three very minor signals in the tetracoordinate region, a broad peak appears in the tricoordinate region at around 20.11 ppm on heating to 360 K. This is comparable to the peak which emerged at 19.99 ppm for the composition $[\text{Bcat}(\text{OTf})(\text{N}_{222})]$ which was assigned to $[\text{Bcat}(\text{OTf})]$ or $[\text{Bcat}(\text{N}_{222})]^+$. This peak disappears on cooling; therefore, it is associated with a rather shielded

tricoordinate species, which is generated by an equilibrium reaction from a tetracoordinate one. The ^{11}B NMR signal of the borenium cation in $[\text{Bcat}(\text{N}_{222})][\text{AlCl}_4]$ is reported at 27.9 ppm,¹⁸⁹ however this peak may be shifted as a result of interaction with a slightly more coordinating anion. Therefore, two possible dynamic equilibria are proposed in Equation 50 and Equation 51.



Equation 50



Equation 51

The room-temperature ^{19}F NMR spectrum (Figure 54) features two peaks at -74.3 and -80.2 ppm; on heating, the proportion of free $[\text{NTf}_2]^-$ increases further (Table 12). In keeping with the principle of Ockham's razor, the presence of one main tetracoordinate boron species and significant quantity of free bistriflimide is best explained through Equation 51, while assuming that the signal for the $[\text{Bcat}(\text{N}_{222})]^+$ is largely merged with the baseline.

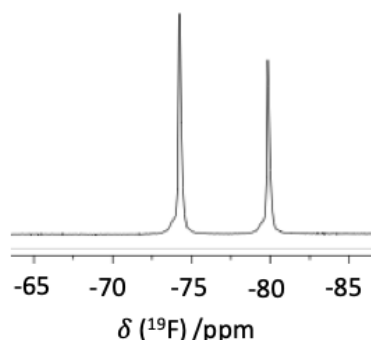


Figure 54. The ^{19}F NMR spectrum for $[\text{Bcat}(\text{NTf}_2)(\text{N}_{222})]$.

3.3.2.2.4 Speciation of $[\text{Bcat}(\text{NTf}_2)(\text{P}^t\text{Bu}_3)]$

The room-temperature ^{11}B NMR spectrum of $[\text{Bcat}(\text{NTf}_2)(\text{P}^t\text{Bu}_3)]$ features a sharp signal at 6.34 ppm in the tetracoordinate region, which remains the main feature across the studied thermal range of 300 to 350 K (Figure 55). As temperature rises, two minor signals, upfield from the main peak appear, at 5.20 and 4.74 ppm, in addition to a broad feature at 26.8 ppm. The ^{11}B NMR signal reported by Dureen *et al.* for $[\text{Bcat}(\text{P}^t\text{Bu}_3)][\text{B}(\text{C}_6\text{F}_5)_4]$ was at 29.9 ppm,¹⁸⁸ whereas the salt $[\text{Bcat}(\text{P}^t\text{Bu}_3)][\text{Al}_2\text{Cl}_7]$ dissolved in deuterated benzene gave an ^{11}B NMR peak at 28.7 ppm (Section 3.3.1). This suggests that $[\text{Bcat}(\text{P}^t\text{Bu}_3)]^+$ has formed here, with ^{11}B NMR signal slightly more shielded due to the presence of $[\text{NTf}_2]^-$, which is stronger coordinating than either $[\text{B}(\text{C}_6\text{F}_5)_4]^-$ or $[\text{Al}_2\text{Cl}_7]^-$. Furthermore, as the temperature reaches 350 K, a further

feature was visible with maximum around 22.0 ppm, and strongly overlapping with the stronger signal at 28.7 ppm, possibly signifying the presence of [Bcat(NTf₂)].

Since P^tBu₃ is extremely bulky, it does not lend itself to easy formation of the [Bcat(NTf₂)(P^tBu₃)] adduct in large quantities, and absolutely excludes the formation of [Bcat(P^tBu₃)₂]⁺. This suggests [Bcat(NTf₂)₂]⁻ as the most probable tetracoordinate, accounting for the signal at *ca.* 6.5 ppm.

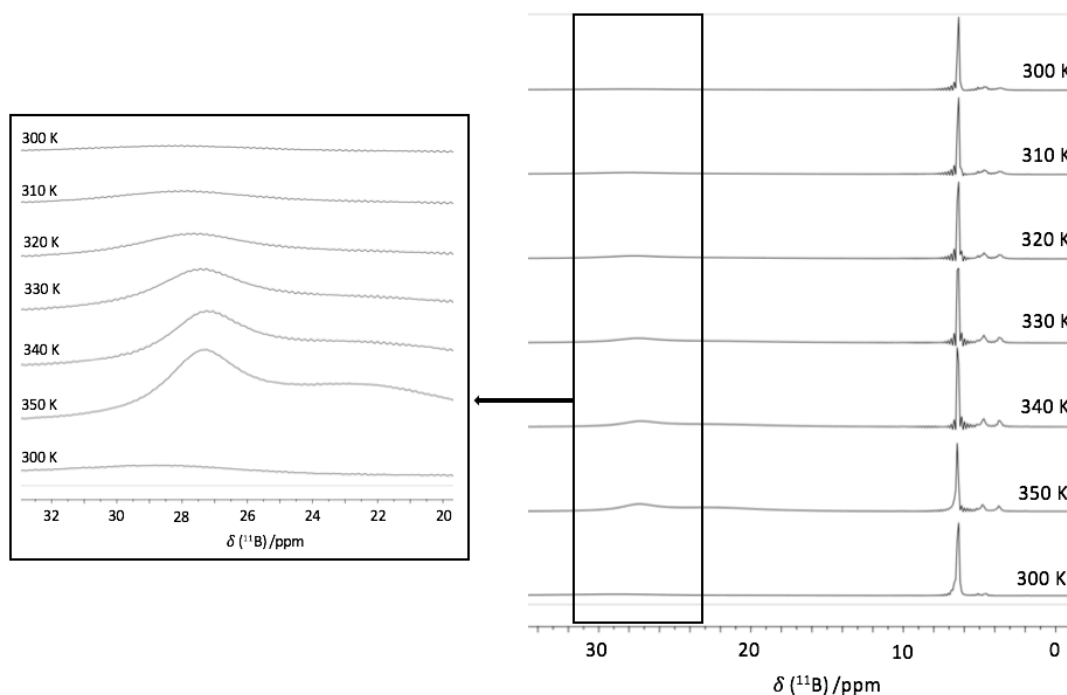


Figure 55. The ¹¹B NMR spectra for [Bcat(NTf₂)(P^tBu₃)] and at increasing temperatures from 300 to 350 K (26.85 to 76.85 °C) and again at 300 K following cooling. Insert shows the emergence of peak at 26.79 ppm over this temperature range.

The main peak in the ³¹P NMR spectra (Figure 56) is at 49 ppm, and accounts for *ca.* 75% of phosphine present in the sample (Table 14). This matches with the -79.8 ppm peak in the ¹⁹F NMR spectrum (Figure 57), which accounts for about 75% of total [NTf₂]⁻, as per Table 12. Disregarding integrations derived from the ¹¹B NMR spectroscopy, it is plausible that these two signals correspond to the ionic liquid, [Bcat(P^tBu₃)]⁺[NTf₂]⁻, that makes up most of the sample. Although the main ³¹P NMR signal does not split even at higher temperatures, it does have a flat top (Figure 56, bottom inset) which potentially hints at P-B coupling.

The sharp ³¹P NMR peak at 55.0 ppm (Figure 56) is only by Δδ_{31P} = 5 ppm more shielded than the free phosphine in benzene and shows no signs of coupling; accounting for dynamic equilibria and solvent effects, it could be assigned to the free phosphine.

Finally, a minor ^{31}P NMR peak (integrating to 7%) was found at 19.7 ppm, with splitting pattern of a quartet (1:1:1:1) which is characteristic of a phosphorus coupling to ^{11}B ($I = 3/2$) giving a coupling constant of 149 Hz. Coapes *et al.* have reported on a similar tetracoordinate adduct, $[\text{BcatCl}(\text{P}^t\text{Bu}_3)]$, which they studied in benzene at $-40\text{ }^\circ\text{C}$.¹⁸⁵ This compound gave a ^{31}P NMR signal at 25.5 ppm, with coupling constant of 158 Hz, suggesting that the signal recorded here does indeed correspond to $[\text{Bcat}(\text{NTf}_2)(\text{P}^t\text{Bu}_3)]$.

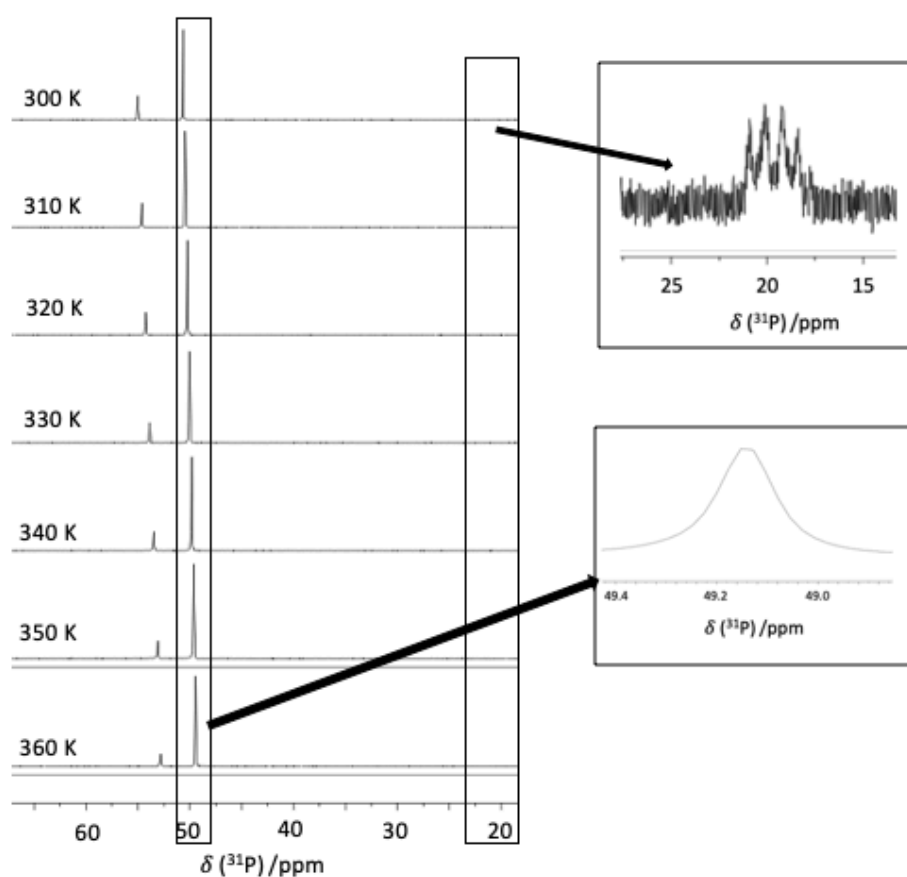


Figure 56. The ^{31}P NMR spectra and for $[\text{Bcat}(\text{NTf}_2)(\text{P}^t\text{Bu}_3)]$ and at increasing temperatures from 300 to 350 K (26.85 to 76.85 $^\circ\text{C}$).

Based on all other assignments, the ^{19}F NMR signal at -74 ppm (Figure 57), accounting for about 25% of $[\text{NTf}_2]^-$ in the sample, corresponds to all coordinated bistriflamide units, mostly $[\text{Bcat}(\text{NTf}_2)_2]^-$, but also $[\text{Bcat}(\text{NTf}_2)(\text{P}^t\text{Bu}_3)]$.

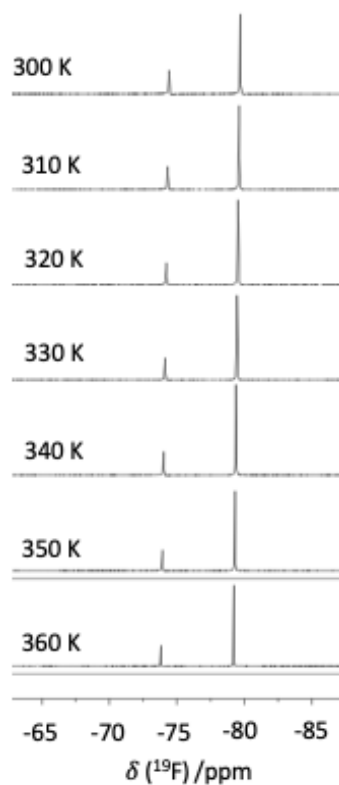
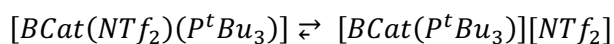


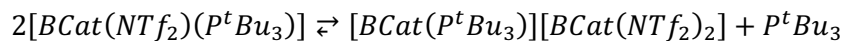
Figure 57. ^{19}F NMR spectra for $[\text{BCat}(\text{NTf}_2)(\text{P}^t\text{Bu}_3)]$ at increasing temperatures from 300 to 350 K (26.85 to 76.85 °C)

In conclusion, the compound noted in the beginning of this discussion as $[\text{BCat}(\text{NTf}_2)(\text{P}^t\text{Bu}_3)]$ is mainly present in its ionic liquid form (Equation 52), accounting for about 75% of the sample.



Equation 52

To a lesser degree, this transient adduct undergoes disproportionation with free phosphine release (Equation 54). In addition, at higher temperatures, it appears that the $[\text{BCat}(\text{NTf}_2)_2]^-$ dissociates further, releasing the tricoordinate $[\text{BCat}(\text{NTf}_2)]$ and free $[\text{NTf}_2]^-$.



Equation 53

3.3.2.2.5 Speciation of $[\text{Bcat}(\text{NTf}_2)(\text{P}_{888})]$

The room-temperature ^{11}B NMR spectrum of $[\text{Bcat}(\text{NTf}_2)(\text{P}_{888})]$ is distinctly different from that of its P^tBu_3 analogue, with three distinct peaks observed across the range of temperatures at 21.8, 10.5 and 1.8 ppm (Figure 58). The relative integrations of these peaks (Table 13) and their chemical shifts alter over the temperature ramp to 360 K, and the return of the complex to its original coordination pattern did not occur as quickly as for other complexes. In contrast to other samples, signals in tri- and tetracoordinate regions are of comparable breadth. Upon heating, the peak at 10.55 ppm shifts downfield, and in the peak at 1.8 ppm a doublet emerges on heating. Its coupling constant ($^1J_{\text{B-P}} = 159.7 \text{ Hz}$) corresponds well to boron-phosphine coupling.¹⁸⁵ In keeping with assignments for the previous two systems, the signal at 21.8 ppm is consistent with the tricoordinate $[\text{Bcat}(\text{NTf}_2)]$, although it may also correspond to a slightly shielded $[\text{Bcat}(\text{P}_{888})_2]^+$ cation. The middle peak at *ca.* 12 ppm is the tetracoordinate adduct, $[\text{Bcat}(\text{NTf}_2)(\text{P}_{888})]$, whereas the most shielded signal must arise from the $[\text{Bcat}(\text{P}_{888})_2]^+$ cation.

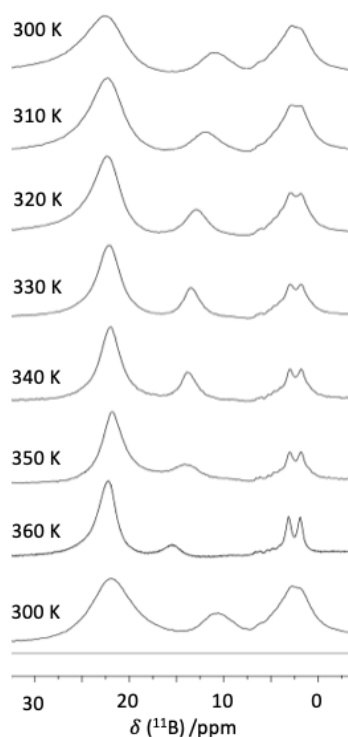


Figure 58. The ^{11}B NMR spectra for $[\text{Bcat}(\text{NTf}_2)(\text{P}_{888})]$ and at increasing temperatures from 300 to 360 K (26.85 to 86.85 °C) and again at 300 K following cooling.

The corresponding ^{31}P NMR spectra showed negligible variation as a function of temperature (Table 14). In the spectrum recorded at 300 K (Figure 59, left), the most deshielded signal at 30.5 ppm represents $[\text{Bcat}(\text{P}_{888})]^+$, accounting for 47% of the ligand, which roughly corresponds to 41% of boron accounted for by the corresponding signal at 21.83 ppm in ^{11}B

NMR spectrum. This suggests that this ^{11}B NMR signal may largely represent the cation, rather than the neutral $[\text{Bcat}(\text{NTf}_2)]$. The peak at 12.2 ppm represents the tetracoordinate cation $[\text{Bcat}(\text{P}_{888})_2]^+$, and the smallest and most shielded signal at -11.8 ppm originates from $[\text{Bcat}(\text{NTf}_2)(\text{P}_{888})]$, which gave rise to the lowest intensity signal in the ^{11}B NMR spectrum as well. In the presence of two cations, it is unsurprising that between 71 to 76% of bistriflamide anions are in their free form, as indicated by the -79.9 ppm signal in the corresponding ^{19}F NMR spectrum (Figure 59, right). The coordinated bistriflamide (-74.0 ppm) is present in both $[\text{Bcat}(\text{NTf}_2)(\text{P}_{888})]$ and $[\text{Bcat}(\text{NTf}_2)]$.

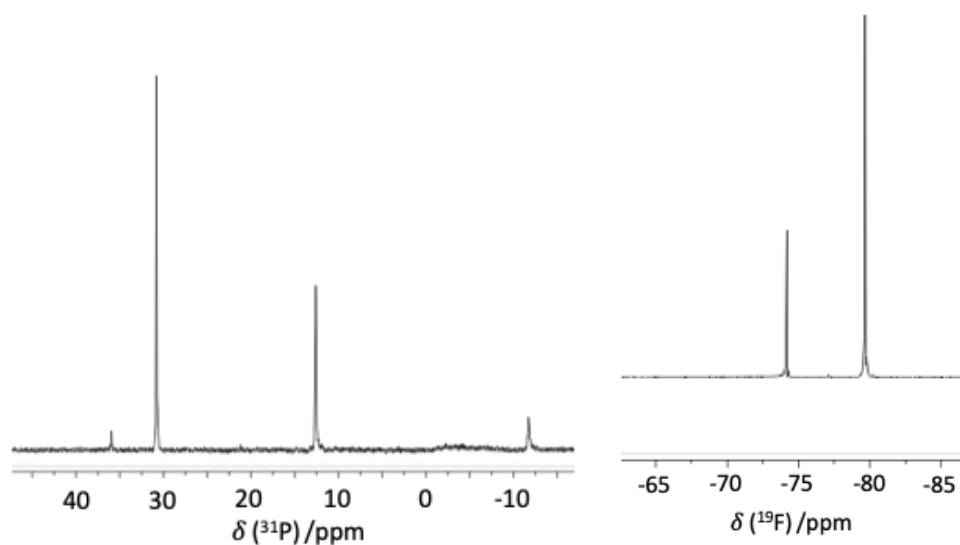
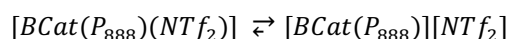


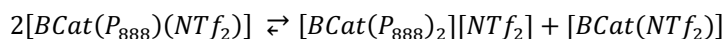
Figure 59. NMR spectra of $[\text{Bcat}(\text{NTf}_2)(\text{P}_{888})]$ at 300 K: ^{31}P (left) and ^{19}F (right)

In conclusion, whereas an appreciable quantity of the $[\text{Bcat}(\text{NTf}_2)(\text{P}_{888})]$ adduct is found in the sample, about half of boron is present in the form of borenium ionic liquid, $[\text{Bcat}(\text{P}_{888})][\text{NTf}_2]$ (Equation 54).



Equation 54

At the same time, in order to account for the significant proportion of $[\text{Bcat}(\text{P}_{888})_2]^+$, disproportionation reaction as per Equation 55 is likely to occur.



Equation 55

3.3.2.2.6 Speciation of $[\text{Bcat}(\text{NTf}_2)(\text{P}_{888}\text{O})]$

Spectra recorded for $[\text{Bcat}(\text{NTf}_2)(\text{P}_{888}\text{O})]$ make an interesting comparison with the formerly-discussed $[\text{Bcat}(\text{NTf}_2)(\text{P}_{888})]$, where the two ligands are of very similar geometry, but oxygen is a harder donor than phosphorus. In the ^{11}B NMR spectrum of $[\text{Bcat}(\text{NTf}_2)(\text{P}_{888}\text{O})]$, recorded at 300 K (Figure 60), there are two well-resolved sharp signals: at 2.20 and 6.42 ppm, in addition to a peak around 5.12 ppm, largely obscured by the signal at 6.42 ppm, but similar in intensity to that at 2.20 ppm. The most logical assignment of these three tricoordinate signals is to attribute the largest peak at 6.42 ppm to the charge-neutral adduct, $[\text{Bcat}(\text{NTf}_2)(\text{P}_{888}\text{O})]$, and the two smaller peaks to the product of ligand scrambling: $[\text{Bcat}(\text{P}_{888}\text{O})_2]^+$ and $[\text{Bcat}(\text{NTf}_2)_2]^-$. On heating, two broad peaks emerge in the tricoordinate region: at 22.64 and 28.20 ppm, which can be attributed to $[\text{Bcat}(\text{NTf}_2)]$ and $[\text{Bcat}(\text{P}_{888}\text{O})]^+$. It is evident that this system has lower propensity to form tricoordinate species than the P_{888} -based one, with only *ca.* 30% of signals in the tricoordinate region, at the highest studied temperature of 350 K (Table 13).

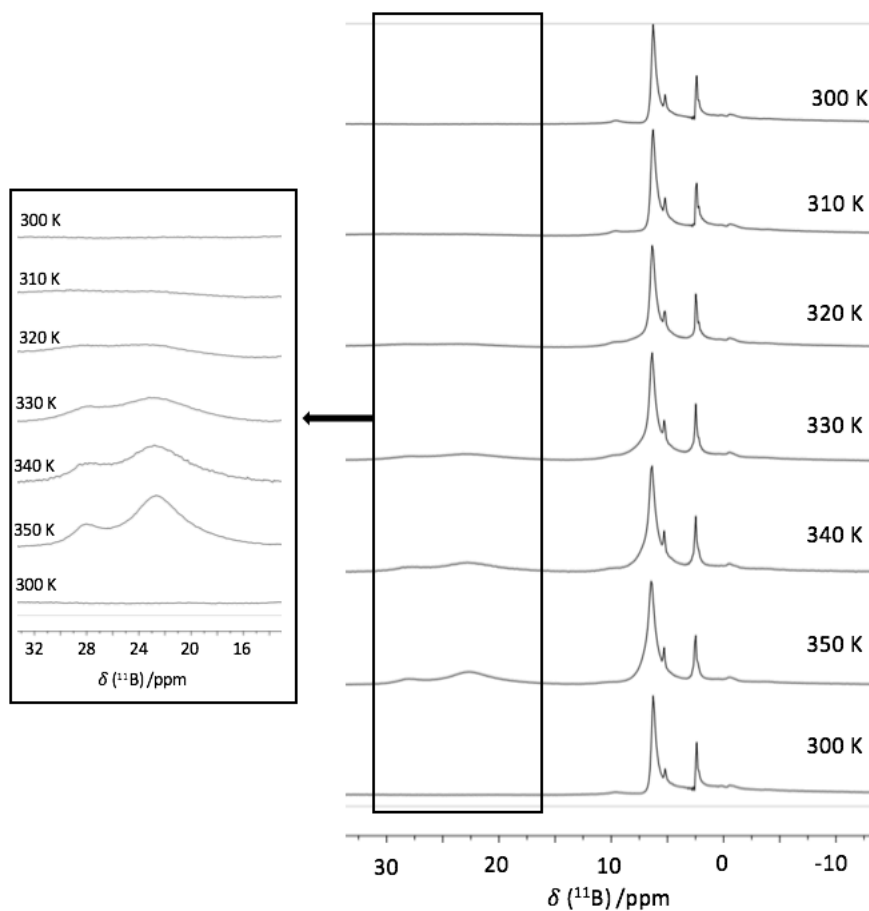


Figure 60. The ^{11}B NMR spectra for $[\text{Bcat}(\text{NTf}_2)(\text{P}_{888}\text{O})]$ at increasing temperatures from 300 to 350 K (26.85 to 76.85 °C) and again at 300 K following cooling, inset showing formation of peaks at 28.20 and 22.64 ppm over this temperature range.

Three prominent peaks in the ^{31}P NMR spectrum (Figure 61, left) are at 82.8, 81.1 and 78.5 ppm, compared to the triflate analogue which featured two peaks at 80.8 and 78.6 ppm. Surprisingly, with increasing temperature they do not change in proportion or chemical shift (Table 14), demonstrably insensitive to changes in geometry on boron. Being further from the boron centre, the ^{31}P nuclei in phosphine oxide will be less sensitive to steric crowding around boron, while retaining sensitivity to electron withdrawing effect of cationic/neutral charge on this centre. Following this reasoning, the lower-intensity signals at 82.8 and 81.1 ppm are therefore assigned to cationic boron species, $[\text{Bcat}(\text{P}_{888}\text{O})_2]^+$ and $[\text{Bcat}(\text{P}_{888}\text{O})]^+$, whereas the main signal at 78.5 ppm corresponds to charge-neutral species, chiefly to the charge-neutral $[\text{Bcat}(\text{NTf}_2)(\text{P}_{888}\text{O})]$.

The ^{19}F NMR spectra (Figure 61) have similar proportion of free $[\text{NTf}_2]^-$ (-79.5 ppm) and the coordinated bistriflamide (-74.9 ppm). This is very surprising considering low proportion of tricoordinate species found in the corresponding ^{11}B NMR spectra, however the presence of some bound bistriflimide represented by this -79.5 ppm peak cannot be excluded as demonstrated by Cornet *et al.* whereby this peak differentiated into two environments on cooling to -65°C .²⁰³

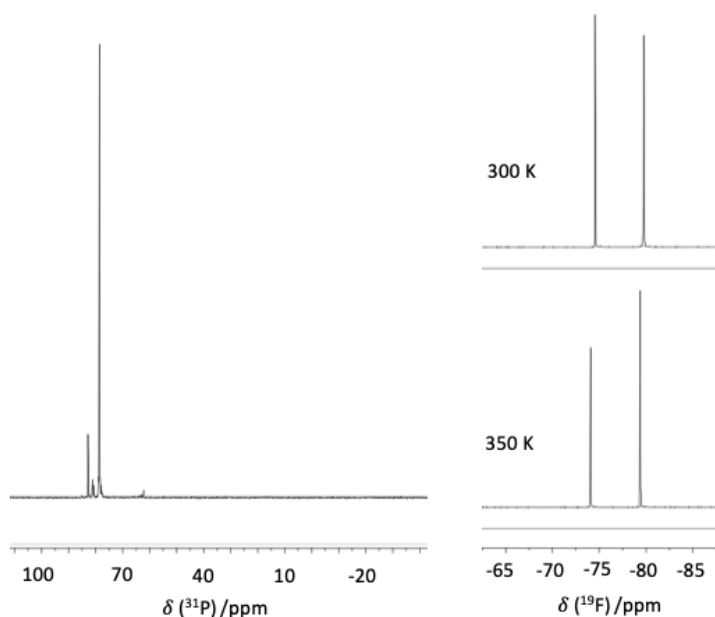
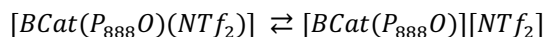


Figure 61. NMR spectra of $[\text{Bcat}(\text{NTf}_2)(\text{P}_{888}\text{O})]$: ^{31}P at 300 K (left); ^{19}F at 300 K (top right) and ^{19}F at 350 K (bottom right).

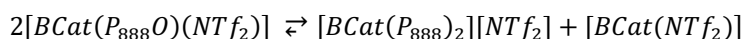
The conclusion to this speciation is similar to that for the trioctylphosphine analogue although, as a consequence of a harder donor the equilibria in this system lies in a different place. The major product remains the tetracoordinate $[\text{Bcat}(\text{NTf}_2)(\text{P}_{888}\text{O})]$ adduct is found in the sample,

and just 10% of the boron is present in the form of the borenium ionic liquid, [Bcat(P₈₈₈)] [NTf₂] on heating (Equation 56).



Equation 56

The other products in equilibrium, which form even at room temperature, account for the small proportion of [Bcat(P₈₈₈O)₂]⁺, which is generated *via* a disproportionation reaction (Equation 57).



Equation 57

As a general summary of these speciation studies, it can be stated that bistriflimide systems are more prone to the formation of tricoordinate boron compounds than their triflate analogues. Their speciation is far more complex, and even a comprehensive, multinuclear NMR study supported by prior studies found in the literature could not deliver definitive answers. Most likely, the vibrational spectroscopic techniques of IR and Raman spectroscopy could provide more insight to the speciation of these systems in the liquid state. The anion [NTf₂]⁻ has been well studied, in particular by Raman spectroscopy, to observe its *cis*- and *trans*- conformers and this technique would be well placed to distinguish between bound and unbound species.²⁰⁶ Whilst single crystal X-ray has been used to study boron-phosphorus interaction and probe bond lengths/angles,^{185,188} it does not provide information about species in the dynamic equilibrium of the liquid state (crystallisation tends to bring out one of the equilibrated liquid-state structures, much like in the Schrödinger's cat paradox). Finally, the use of mass spectrometry is not suitable for speciation studies when liquid equilibria are considered, as it alters sample's environment to the gas phase one, sometimes giving results which do not correspond to the speciation within the liquid state.^{87,207} Amongst less popular techniques, angle-resolved X-ray photoelectron spectroscopy (ARXPS) has been used to probe the surface structure of bistriflimide containing ionic liquids.²⁰⁸ Most XPS techniques could be used, provided that these samples are stable under ultra-high vacuum, which may not be the case. This obstacle is removed for liquid jet photoelectron spectroscopy, which could provide a good insight into the electronic environment of boron, provided that sufficiently weakly coordinating solvent will be used. All this research was outside the time-frame for this work, but will be continued within the Swadźba-Kwaśny research group.

3.3.2.2.7 Gutmann Acceptor Number Measurements

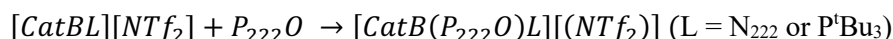
Gutmann acceptor number measurements were recorded as an indication of the potential strength of bistriflamide systems as Lewis acids for catalytic applications. For all samples, at all probe concentrations, only one signal was found in their ^{31}P NMR spectra. Results, summarised in Table 15, demonstrate very high Lewis acidities, oscillating around the arbitrary Lewis superacidity threshold of 100.

Table 15. AN values for all [Bcat(NTf₂)L] liquids at 300 K shown with the $\delta^{31}\text{P}$ resonances recorded (in ppm) measured for solutions of these liquids containing 1, 2 and 3 mol% P₂₂₂O (referenced to $\delta^{31}\text{P}$, H₃PO₄ 85% = 0 ppm).

Compound	$\delta^{31}\text{P}$			AN
	1%	2%	3%	
[Bcat(NTf ₂)(N ₂₂₂)]	87.73	87.90	87.82	105.1
[Bcat(NTf ₂)(P ^t Bu ₃)]	91.20	91.13	91.22	113.1
[Bcat(NTf ₂)(P ₈₈₈)]	83.30	83.30	83.35	94.6
[Bcat(NTf ₂)(P ₈₈₈ O)]	85.18	85.18	85.18	99.1

The AN value for [Bcat(NTf₂)(N₂₂₂)], 105.1, was similar to that of the triflate analogue (106.4, Table 10). Likewise, AN for [Bcat(NTf₂)(P₈₈₈O)], recorded at 99.1, was similar to the triflate analogue (98.9), and AN value for [Bcat(NTf₂)(P₈₈₈)], 94.6, was identical with one of the two signals recorded for [Bcat(OTf)(P₈₈₈)].

Aligned with reasoning presented in Section 3.3.2.1.3, [Bcat(NTf₂)(N₂₂₂)] is likely to react to form a cationic species, following Equation 58 and/or Equation 59. Both the triflate and the bistriflamide system featured ^{11}B NMR signals at 20-21 ppm, indicating similar electrophilicity of the tricoordinate species and the similarity of the AN, indicating probable the presence of [Bcat(N₂₂₂)]⁺ as the main Lewis acidic species in both systems.

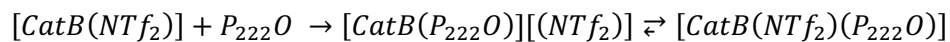


Equation 58



Equation 59

At the same time, the slightly less acidic systems, [Bcat(NTf₂)(P₈₈₈O)] and [Bcat(NTf₂)(P₈₈₈)], are possibly reacting with the probe to form charge-neutral species (Equation 60 and/or Equation 61).



Equation 60



Equation 61

Finally, AN for [Bcat(NTf₂)(P^tBu₃)] was 113.1, much higher compared to 98.7 recorded for the triflate analogue. This is notable, because only in [Bcat(NTf₂)(P^tBu₃)] there was a free [Bcat(P^tBu₃)]⁺ detected, suggesting that interaction of this system with the probe follows Equation 58.

Having described the effect of heating on the speciation of these samples, especially with a view to probe the relative acidities of tetra- and tricoordinate and complexes, the AN of [Bcat(NTf₂)(P₈₈₈)] was measured at a range of temperatures (300 to 360 K). The value obtained from this experiment did not change with temperature, remaining at 94.6 through all temperatures, suggesting that despite the dynamic equilibrium of this system, the final product of the reaction of a Lewis acidic borenium species with the probe remains the same.

3.4 Conclusions

The synthesis of new liquid Lewis acids based on boron were described. Boron complexes were designed with a bidentate ligand and a range of L-donors, selected to stabilise a positive charge on the boron centre. The development of boron complexes featuring a bidentate catechol ligand builds on work reported in the literature from the groups of Ingleson and Stephan. Two ligands previously used by these groups, triethylamine and tri-*tert*-butyl phosphine were incorporated into this work and two new ligands, trioctylphosphine and trioctylphosphine oxide, which are used in ionic liquid and LCC research to suppress melting points, were introduced. Tetracoordinate boron complexes were synthesised and characterised, and the final products were derived through the reaction with halide abstracting agents, trimethylsilyl triflate and methyl bistriflimide. Clean products were obtained through the removal of volatile by-products, TMSCl and MeCl, respectively.

NMR spectroscopy was used to investigate the speciation of the liquids and low melting solids which resulted from these reactions. The major products for all compositions were tetracoordinate adducts, [Bcat(OTf)L] or [Bcat(NTf₂)L], represented by a peak in the ¹¹B NMR spectrum around 10 ppm. Each sample was heated to 350 K, which revealed the emergence of tricoordinate species: [BcatL]⁺ and/or [BcatOTf]/[BcatNTf₂]. Bistriflimide systems had higher propensity to feature tricoordinate systems; based on ³¹P and ¹⁹F NMR

spectra it was concluded that ^{11}B NMR spectroscopy possibly underestimates the quantity of tricoordinate species due to very broad signals that prevent precise integration.

Gutmann acceptor numbers were recorded to quantify acidity, which was high (around 100, which is the border for ‘Lewis superacidity’), but not as high as that of ‘first generation’ borenium ionic liquids, of a general formula $[\text{BCl}_2\text{L}][\text{M}_2\text{Cl}_7]$.⁴ This lower acidity resulted from replacing two chloride ligands with a bidentate O-donor (catecholate), and possibly from stronger nucleophilicity of the $[\text{OTf}]^-/[\text{NTf}_2]^-$ anions compared to the less coordinating chlorometallate ones (that is, competition of these anions with the probe). Interestingly, except for the sample based on P^tBu_3 , there was no difference between acidities of triflate and bistriflamide systems as measured by Gutmann AN. It is however speculated, that in reactions when less basic nucleophiles are used, the propensity of both anions to make a good living group will make a difference.

Future work with these system can focus either on their speciation (as outlined in Section 3.3.2.2.6) on their application in catalysis as strong liquid Lewis acids. In particular, the focus of this work should be on using these ionic liquids for frustrated Lewis pair applications as they have similar structures to FLP Lewis acids used by Dureen *et al.* and Clark *et al.*^{188,190} Chloride free Lewis acidic ionic liquids are appealing catalysts for industrial applications, although for large-scale uses, bistriflimide and triflate anions would require replacing with less expensive ones. Compared to ‘first generation’ of borenium ionic liquids, equilibria are limited and BCl_3 does not evolve, which means that there is greater control over catalytic reactivity.

4 FRUSTRATED LEWIS PAIRS IN IONIC LIQUIDS

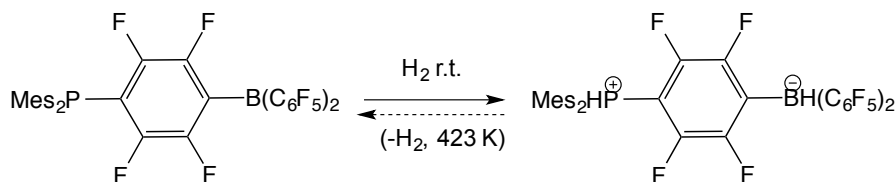
This Chapter deviates from the research strand devoted to the development of Lewis acidic ionic liquids described in the previous two Chapters. Instead, it is dedicated to studying Lewis acidic and basic molecules (frustrated Lewis pairs) in solution. Background, rationale for this work, experimental challenges and results will be outlined. This work leads on to Chapter 5, which combines research strands on FLPs and ionic liquids.

4.1 Introduction to Frustrated Lewis Pairs

4.1.1 Concept of Frustrated Lewis Pairs and Metal-Free H_2 Activation

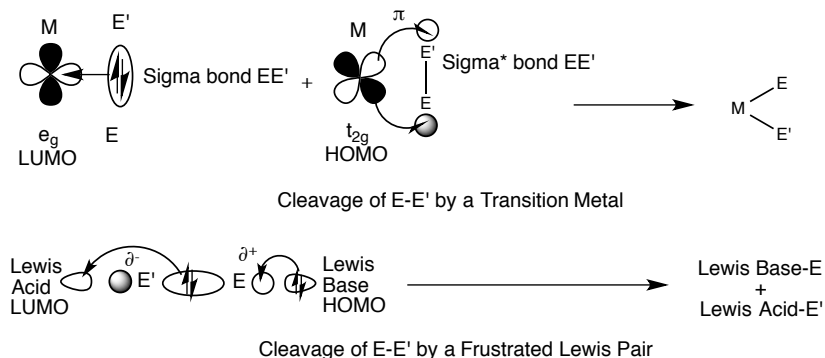
In 2019, Douglas Stephan credited the renaissance of main-group chemistry to the discovery of frustrated Lewis pairs (FLPs).²⁰⁹ This is a reasonable assertion, with 1293 papers on the topic published since their initial discovery in 2006, until September 2019 when this thesis was submitted. In a 2006 *Science* paper,²¹⁰ Stephan and co-workers announced an exciting, metal-free reaction of splitting dihydrogen molecule using phosphorus and boron centres on a pair of sterically hindered borane and phosphine (Scheme 20) In this example, an inflexible linker and bulky groups prevent the molecule from self-quenching but a small dihydrogen molecule is able to enter into this gap and undergo heterolytic cleavage.

Scheme 20. The first FLP reaction reported by Stephan *et al.* in 2006.²¹⁰



Soon named frustrated Lewis pairs (FLPs), these systems represent an elegant approach to metal-free homogenous catalysis, achieved by exploiting steric repulsions to prevent reactive Lewis acidic and basic centres from forming adducts. Unquenched Lewis acidic and basic centres act in a manner analogous to that of transition metals, when presented with a substrate small enough to fit between them. Where a transition metal is capable of simultaneously donating and accepting electron density to and from a substrate, such as hydrogen, in FLP the Lewis acid and base work in tandem to donate electrons (from the HOMO of the Lewis base) and accept electrons (from the LUMO of the Lewis acid), as shown in Scheme 21.

Scheme 21. Representation of the orbital interactions in substrate cleavage (E-E') by i) a transition metal and ii) an FLP.



The name and defined concept of frustrated Lewis pairs may be relatively new, but work by chemists such as Brown and Wittig in the 1940s and 1950s discovered that adduct formation could be prevented between centres, which would be expected to react, if they were sufficiently sterically hindered.²¹¹ Over the following 50 years, this observation was regarded as remarkable yet scarcely utilised, except in niche examples, such as amphiphilic chelation molecules.^{212,213} Following the 2006 publication, the area flourished rapidly. In 2007, this concept was expanded intermolecular FLPs, where the Lewis acid and base moieties are on different molecules.²¹⁴ The classic FLP system of tris(pentafluorophenyl)borane (BCF) with PR_3 (where R = *tert*-butyl or mesityl groups made FLP chemistry more accessible through the use of simple off-the-shelf chemicals.²⁰⁹ Using intermolecular species allowed Stephan and colleagues to demonstrate a lack of interaction between Lewis acid and base in the absence of a substrate, even on cooling to $-50\text{ }^\circ\text{C}$.²¹⁴ On combination with hydrogen, however, the formation of a salt was observed by ^1H NMR spectroscopy (although in this particular case the reaction was not reversible and H_2 could not be extracted from the product upon heating).^{210,214}

4.1.2 Encounter Complexes

The mechanism by which FLPs split hydrogen is a fascinating subject of ongoing study. In the seminal 2006 paper, it is speculated that the interaction was initiated by H_2 reacting with the Lewis acidic functionality.²¹⁰ A subsequent 2007 paper sought to clarify the mechanism of FLP hydrogen cleavage.²¹⁴ As baseline for their study, Stephan and colleagues took solutions of R_3P (R = *t*-Bu, $\text{C}_6\text{H}_2\text{Me}_3$) with $\text{B}(\text{C}_6\text{F}_5)_3$ in toluene (0.99 mmol) and monitored them by $^{31}\text{P}\{^1\text{H}\}$, ^1H , ^{11}B , and ^{19}F NMR spectroscopy. At this low concentration, no evidence for the formation of a Lewis acid-base adduct was detected. Furthermore, no interaction was found, either between the Lewis acid and H_2 in the absence of a base, or *vice versa*. From this, a simultaneous mechanism of tri-molecular reaction was suggested, whereby the base donates

into the σ^* orbital as the acid receives electrons from the σ orbital of the H_2 molecule, which led to the transition metals analogy (Scheme 21).

A range of computational studies into the encounter problem followed. The first DFT study by Papai and colleagues proposed that the reaction proceeded *via* a loosely bound but energetically strained Lewis acid-base complex with an association energy $\Delta E = 4.18 \text{ kJ mol}^{-1}$ (about half of a classical Lewis adduct), stabilised by non-bonding interactions.²¹⁵ This work supported the hypothesis that electron transfer proceeds *via* simultaneous $\text{'Bu}_3\text{P} \rightarrow \sigma^*(H_2)$ and $\sigma(H_2) \rightarrow \text{B}(\text{C}_6\text{F}_5)_3$ donation, with a linear P-H-H-B axis calculated in the transition state. This became known as the electron transfer model and required three molecules to come together for each reaction, two of which are unable to react with each other, which is obviously very entropically unfavourable. However, considering better than anticipated reaction kinetics, a concept of a pre-organised state, the “encounter complex” between Lewis acid and Lewis base, which would receive the H_2 in a two-molecular fashion, was conceived. This sparked the discussion about the nature of weak bonds holding the encounter complex together. In modelling the interaction between PMes_3 and BCF, Kim *et al.* found that the stabilisation from dispersive non-covalent interactions, such as lone pair to π donation, was greater than that of π - π stabilisation.²¹⁶ A modelling study by Bako *et al.* presented evidence that these encounter complexes could be present in a relevant concentration in solution.⁶ A two-step pathway was suggested (Figure 62), which illustrates the formation of the encounter complex as a small initial energy barrier before the transition state will form on combination with H_2 .²¹⁷ This energy barrier was found to be minimal in MD simulation; however, the formation of a stable associated step was likely to be discouraged by both entropic and solvent effects.⁶

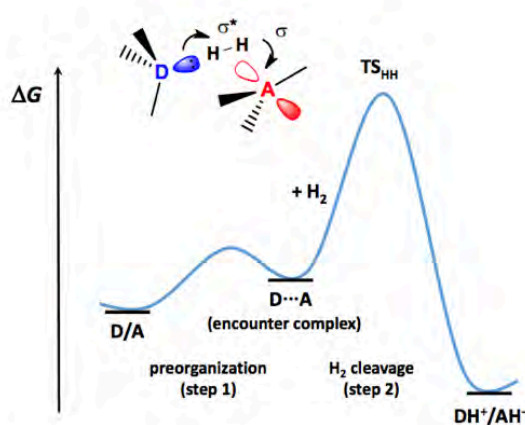


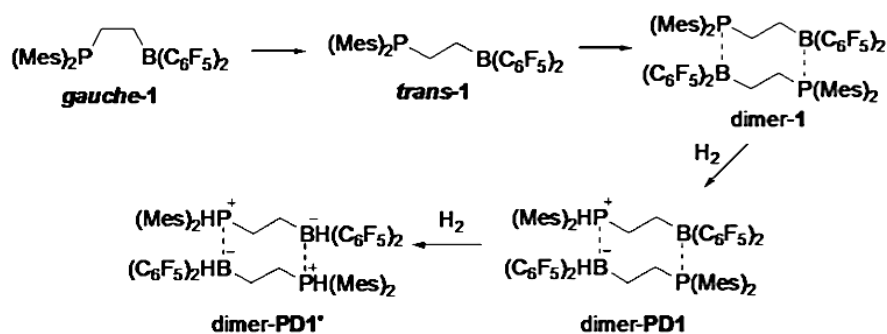
Figure 62. Free energy profile for the activation of dihydrogen by an FLP (adapted from ²¹⁷)

At the start of 2010, a counter mechanistic theory was postulated by Erker and colleagues, who suggested that H_2 activation resulted from the polarisation by an electric field between

the δ^+ Lewis acidic and δ^- Lewis basic groups.²¹⁸ The thrust of this argument drew from the fact that the electric field strength required for H₂ splitting (0.05 – 0.06 a.u.) is almost identical to that between P-B in the FLP P^tBu₃ with B(C₆F₅)₃. Furthermore, they argued, it accounted for the similar reactivity of chemically different FLP systems. In 2013, however, Rokob *et al.* published a DFT study comparing both mechanisms across a range of six FLPs comprising both intra- and intermolecular species.²¹⁹ In this work, none of the FLPs had a high enough electric field, 0.09 a.u., to facilitate hydrogen splitting. Further to this, transition states showed a bent {Lewis acid \cdots H \cdots Lewis base} geometry, justified through the electron transfer model, as frontier orbitals arranged themselves for optimal overlap. This paper was widely accepted as providing evidence to confirm the electron transfer model, and it is telling that the electric field model is not referred to in the Erker and Stephan review of 2015.²²⁰

Further evidence for preorganised intermolecular encounter complexes came, perhaps surprisingly, from work on intramolecular FLPs. Zeonjuk *et al.* determined that the energy profile of intramolecular FLPs, such as that given in Scheme 22, produced transition states with too high a barrier if they acted as intramolecular catalysts, compared to more favourable activation as a dimeric species.²²¹

Scheme 22. The reaction of the FLP (Mes)₂PCH₂CH₂B(C₆F₅)₂ with a dihydrogen molecule *via* a dimeric intermolecular pathway, which has been shown to be preferred to the intramolecular pathway. (adapted from ²²¹)



Finally, analysing a Sn/N FLP, Das *et al.* modelled the interaction between the Lewis acidic SnⁱPr₃OTf and the Lewis basic DABCO, and found that the formation of an encounter complex involved also a triflate anion.²²² This encounter complex was held together through hydrogen bonding (from C-H bonds to both O and F) and dispersive interactions, fitting with previous descriptions. Interestingly, two alternative encounter complexes appeared to have the capacity for H₂ activation (Figure 63), in each triflate playing a different role. What is crucial, both encounter complexes were reported to be endergonic in formation, as these non-covalent interactions are not observed experimentally.²²²

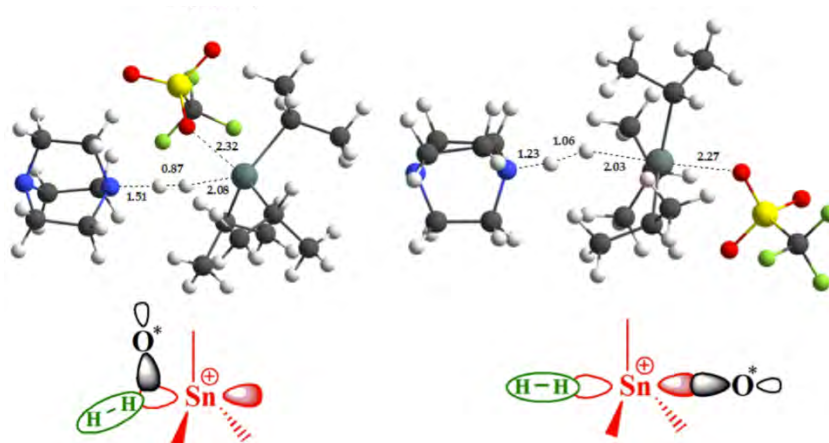


Figure 63. Geometry-optimised structures of transition states for $i\text{Pr}_3\text{SnOTf/DABCO}$ FLPs with different triflate positions. Orbital overlap structures show the non-bonding orbitals $\sigma(\text{H}_2)$, empty p-orbital on Sn, and a O^* orbital from OTf are given below (adapted from ²²²)

In contrast to the broad range of theoretical studies, since Welch *et al.* reported in 2007 that 0.99 mmol of BCF and P^tBu_3 in toluene showed no evidence of adduct formation in multinuclear NMR spectroscopy, direct evidence of the encounter complex formation has been limited.²¹⁴ Indirect evidence was provided in a 2013 paper, which used low temperature ^1H , ^{19}F HOESY for the system BCF/ PMes_3 .²²³ With the phosphine in great excess, line broadening of the *para* fluorine of BCF in a mixture with PMes_3 was observed (Figure 64).²²³ This re-enforced the statement about the endergonic nature of encounter complex formation (*viz.* free energy plot in Figure 62).²¹⁷ Further to this, in 2017 Houghton *et al.* carried out a calorimetric study to probe the mechanism of H_2 activation by BCF/ PMes_3 , and found that the reaction occurred through a single termolecular step, thus confirming that H_2 did not interact with either the Lewis acid or base individually.²²⁴ The model of a “solvent separated” FLP encounter complex, proposed by Rokob *et al.*,²¹⁵ was well matched to the kinetic model from this calorimetric study. In the same work, the kinetic isotope effect (KIE) was used to determine how the rate of reaction was altered by activating D_2 vs. H_2 . No change in the reaction rate was observed, supporting earlier suggestions that assembly of the BCF/ PMes_3 encounter complex into the solvent cage is the rate determining step.²²⁴

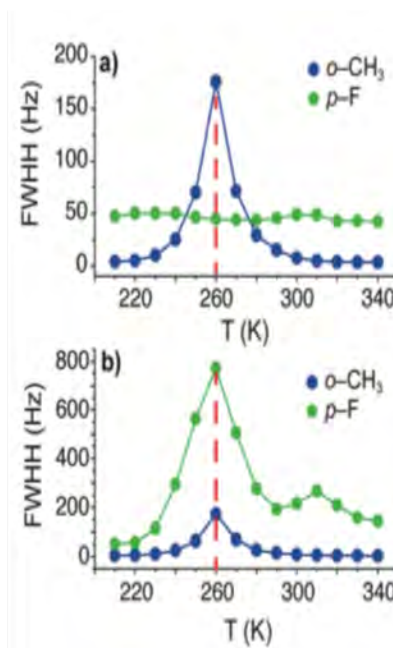


Figure 64. Comparison of peaks at full width half-height as a function of temperature (T) of the signals due to the *ortho*-Me of PMes₃ (240 mM) and *para*-F of BCF (15 mM) in (a) isolated species and (b) as a mixture.²²³

The interest in incorporating frustrated Lewis pairs in this work arose from the general interest of the Swadźba-Kwaśny group in Lewis acid catalysis and Lewis acids in the liquid phase. FLPs have been a major development in the general area of Lewis acidity, and very intensively studied, but it was embraced mainly by the Main Group community. It was realised that experimental evidence for the encounter complex could be provided using skills developed to study the structure of ionic liquids, namely neutron scattering.

In this work, the first challenge was to synthesise deuterated versions of sterically hindered phosphines used in FLPs, as contrast in neutron scattering experiments. The second part required conducting neutron scattering experiments at the ISIS Neutron and Muon Source, followed by data analysis (kindly carried out by Prof. Holbrey)

4.2 Experimental

4.2.1 General

Tert-butyl chloride was synthesised at the ISIS deuteration facility. Mesitylene-d₁₂ (98 atom% D), hydrobromic acid (48 wt% in H₂O ≥99.99%), hydrogen peroxide (30 wt % in H₂O), phosphorus trichloride (99%), magnesium ribbon (>99.5%), copper(I) iodide (>99.5%), lithium bromide (>99%) were purchased from Sigma Aldrich and used as received. Mg ribbon was stored in the glovebox prior to use. The glovebox used in this work was MBraun Labmaster dp, operating typically under argon, at or below 0.6 ppm of H₂O and O₂. ¹³C and

^{31}P NMR spectra were recorded using a Bruker Avance DPX 400MHz spectrometer. Electrospray mass spectrometry was performed using a Waters LCT Premier mass spectrometer.

4.2.2 Preparation of Bromomesitylene- d_{11}

A flask containing mesitylene- d_{12} (12.02g, 100 mmol) with water (50 cm^3) was covered in foil, HBr (48%, 11.4 cm^3) and H_2O_2 (30%, 20.4 cm^3) were added slowly, and the reaction was allowed to proceed (stirring, darkness, 24 h). An excess of sodium sulfate was then added and the product was extracted into hexane. The product was dried with magnesium sulfate to give bromomesitylene (16.3 g, 82% yield). $^{13}\text{C}\{^1\text{H}\}$ (101 MHz, C_6D_6) δ 137.95, 136.32, 129.12, 124.30, 23.70, 20.74.

4.2.3 Preparation of Trimesitylphosphine- d_{33}

A two necked, oven-dried flask (100 cm^3) was equipped with a septum. Magnesium turnings (1.22 g, 50.21 mmol) were placed in the flask, which was then sealed with a gas tap and removed from the glovebox to an argon Schlenk line. To this bromomesitylene- d_{11} (8.78g, 41.84 mmol) in dry THF (20 cm^3) was added dropwise. The reaction started after gently heating with a water bath. After the addition was completed, the mixture was heated to reflux (40 $^\circ\text{C}$, 1 hr). After it was cooled to room temperature, the solution of the Grignard reagent was transferred into the dropping funnel of an identical apparatus using a cannula. The solution was then added dropwise to a solution of phosphorus trichloride (1.14, 8.36 mmol) in dry THF (15 cm^3) at -78°C and under argon. Afterward, the resulting suspension was stirred (-78°C , 1 hr). Then, saturated NaCl solution (25 cm^3) was added. The organic layer was separated. The aqueous layer was extracted two times with portions of THF (10 cm^3). The combined organic phases were dried using sodium sulfate. The solvent was evaporated under reduced pressure to yield a slightly yellow solid. The raw product was recrystallized from hot chloroform to give the desired product as a colourless, crystalline solid. (0.882 g, 25% yield). ^{31}P NMR (162 MHz, DMSO) δ -37.23 (s) $^{13}\text{C}\{^1\text{H}\}$ (101 MHz, DMSO) δ 141.51, 136.72, 128.84, 21.36, 19.38.

4.2.4 Preparation of Tri(*tert*-butyl)phosphine- d_{27}

Magnesium ribbon (1.80 g, 74.1 mmol) was activated inside an argon filled glovebox by scratching with sandpaper, then cut into flakes and transferred into an oven-dried two-necked round-bottomed flask (100 cm^3) equipped with a septum, a tap and a stirring bar. The flask was removed from the glovebox, attached to an argon Schlenk line, and placed on a heater stirrer equipped with an aluminium heating mantle. The magnesium was stirred overnight at

ambient temperature to further activate the magnesium. Then, dry tetrahydrofuran (20.0 cm³) was added, followed by a crystal of iodine, and the flask was heated to 40 °C. Subsequently, a small portion of *tert*-butyl chloride-*d*₉ (6.27 g, 61.7 mmol) was added to initiate the reaction, with the solution turning green, before the remainder was added dropwise. Subsequently, a small amount of dibromoethane (0.10 g, 0.57 mmol) was added dropwise to encourage the reaction, which was then allowed to proceed (40 °C, overnight), before being cooled back to room temperature. In another oven-dried two-necked round-bottomed flask (100 cm³), equipped with a stirring bar and connected to an argon Schlenk line, a solution of phosphorus trichloride (1.70 g, 12.35 mmol), with lithium bromide (0.107 g, 1.24 mmol) and copper(I) iodide (0.235 g, 1.24 mmol) in dry THF (15 cm³). The flask was placed on a heater stirrer equipped with an acetone-dry ice bath (-78 °C), and the mixture was allowed to cool with vigorous stirring. The solution of the Grignard reagent was transferred *via* cannula filter into the PCl₃ solution, stirred at -78 °C. The dry ice-acetone bath was then removed and the reaction mixture was brought to ambient temperature and left to react for a further 2 hours on reaching this temperature (2 h, vigorous stirring). The solvent was removed under reduced pressure (25 °C, 10⁻² bar) and the product was dissolved in pentane (25.0 cm³). Degassed water (25.0 cm³) was subsequently added and the flask was vigorously shaken by hand, the organic layer was removed *via* cannula transfer into an oven dried flask (100 cm³) and again washed with degassed water (25.0 cm³). This was transferred *via* cannula into an oven dried flask (100 cm³). Finally, the organic phase was dried using sodium sulfate and the liquid phase was transferred *via* cannula filtration into an oven dried flask (100 cm³). The solvent was removed under reduced pressure in an ice bath (0 °C, 10⁻² bar), to give a colourless crystalline solid (0.469 g, 18.8% yield). ³¹P NMR (162 MHz, benzene-*d*₆) δ 58.0 (s) ¹³C {¹H} (101 MHz, benzene-*d*₆) δ 37.0 (d) J_{C-P} = 51.3 Hz, δ 31.4 (m); m/z (-ve ion electrospray) [M-H]⁻ C₁₂D₂₇P required 230.3631, found 230.3623

4.3 Deuterated Phosphine Synthesis

4.3.1 Justification – Contrast for Neutron Scattering Studies

Neutron diffraction is a highly effective technique for observing structures in the liquid state, applicable to study the structure of neat liquids and solutes alike.²²⁵⁻²²⁹ This includes the studies of structures of ionic liquids and deep eutectic solvents.²³⁰⁻²³⁵

Hydrogen/deuterium substitution is a crucial and very powerful tool in neutron diffraction experiments. While X-ray scattering of each atom is dependent on the atomic number (Z), in neutron scattering the incident beam interacts with the nucleus of the atoms. This means protons have a very large scattering cross section, around x10.7 larger than that of deuterium

and x24.8 larger than that of ^{31}P .²³⁶ Owing to the differences in the sign of the coherent scattering between ^1H and ^2H (-3.74 fm and 6.67 fm), the comparison of the data recorded from the isotopically substituted systems is a very useful tool in computer simulations.²³⁶ Furthermore, although ^1H scatters best, it provides a lot of inelastic scattering which detracts from overall data quality. Therefore, for neutron scattering measurements, it is most beneficial to study both protiated and deuterated analogues of the species of interest, in addition to equimolar mixtures for best data quality.

4.3.2 Synthesis of Deuterated Phosphines

Tertiary phosphines are important molecules across a wide range of chemical processes, used industrially as ligands to transition metal catalysts and as reducing agents.^{237,238} Whereas protiated phosphines are often inexpensive and readily available, this is not the case for their deuteriated analogues.

The challenge in the synthesis of deuteriated molecules arises from the differing kinetics of the reaction, which are in fact utilised when measuring the kinetic isotope effect.^{239,240} In addition to this, the starting materials availability can vary greatly in comparison to the literature method for the synthesis of protiated compounds, owing to the limited availability of deuteriated compounds, unless D_2O can be used.²⁴¹ Finally, the cost of deuteriated analogues is much higher than that of their protiated counterparts, meaning that reactions tend to be optimised using protiated materials, before moving onto the deuteriated synthesis, which does not provide direct comparison due to said kinetic isotope effect.²⁴² This often results in decreased yields and increases the probability of side-product formation.

4.3.2.1 Trimesityl phosphine- d_{33}

In his compendium of steric effects of a vast range of phosphines, Tolman reported the cone angle of trimesityl phosphine as being 212° (Figure 65).¹⁵⁹ This is the largest angle reported and demonstrates the sheer steric volume of three bulky mesityl rings.

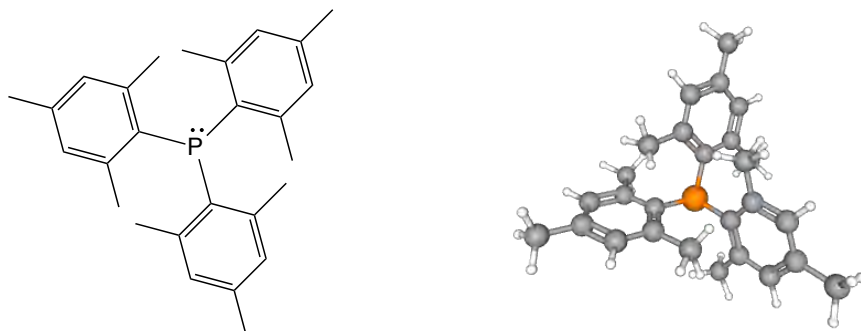
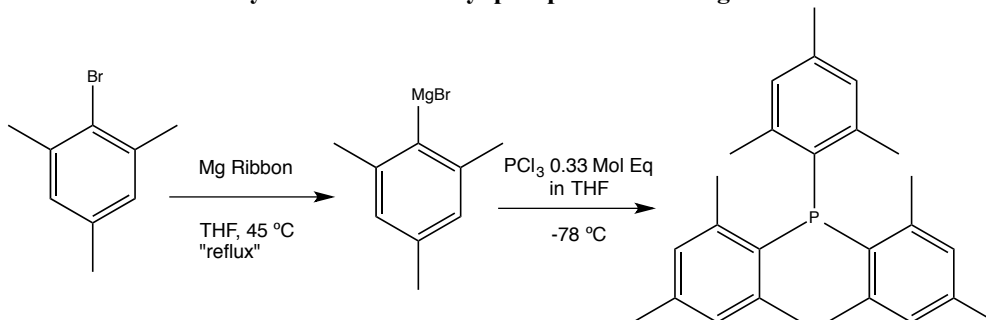


Figure 65. The structure of trimesityl phosphine (left 2D, right 3D).

As an incredibly sterically hindered main group base, it has been widely used in FLP applications and as such it seemed an ideal target for studying FLP interactions using neutron scattering.^{214,243} The synthesis proceeds *via* a Grignard intermediate (Scheme 23). This synthetic method was adapted from work by Reissman *et al.*²⁴⁴

Scheme 23. The synthesis of trimesityl phosphine *via* a Grignard intermediate.



The key challenge encountered in this synthesis was the avoidance of a secondary phosphine species. Where the desired PMes_3 gives a peak at -37 ppm in ^{31}P NMR spectroscopy, a secondary peak at -31 ppm was also apparent, in varying but significant intensities (Figure 66). Since the corresponding oxide appears at 25 ppm, oxidation product was excluded as the source of additional signal. ^1H NMR spectra suggested the presence of incredibly similar species, with an identical integration of protons relative to each other in both species. This suggested that the mesityl ring retained the same interactions with the phosphorus centre. It was initially speculated that this secondary peak could come from a different orientation of peaks around the ring, restricted by their bulk, suggesting two isomeric forms of Pmes_3 . However, this had never been previously reported, so no convincing argument could be made to support this supposition.

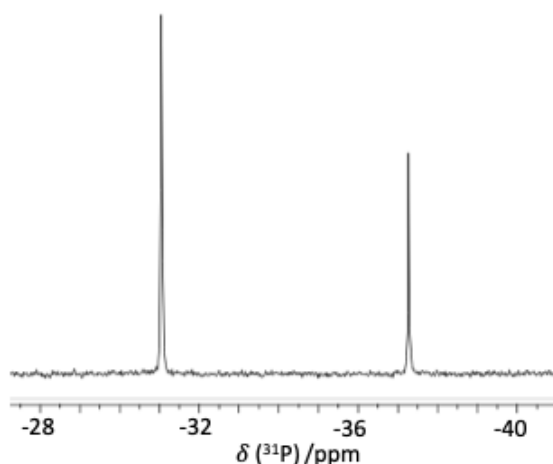


Figure 66. ^{31}P NMR spectrum showing the formation of the side product $\text{Mes}_2\text{P-PMes}_2$ (at -31 ppm) and PMes_3 (at -37 ppm) with a ratio of 66:33 of side-product: desired product.

Concluding that two different phosphines were present, attempts to separate them were made using column chromatography. A solvent system was designed using toluene, in which the crude product was highly soluble, and hexane, in a range of ratios (Table 16).

Table 16. The results of thin layer chromatography of the crude product containing both PMes_3 and $\text{Mes}_2\text{P-PMes}_2$.

Hexane:Toluene	Spot 1 (R_f)	Spot 2 (R_f)
100:0	No separation one long streak	
87.5:12.5	0.25	0.60
75:25	0.24	0.59
62.5:37.5	0.06	0.28
50:50	0.06	0.35

From these plates, the best definition was found for the ratio 50:50 between toluene and hexane and a column was run with this solvent system. Unfortunately, when analysed, no fractions contained a purified product. However, fortuitously, a crystal grew on the base of the column which revealed the structure of the side product. It was found to be 1,1,2,2-tetrakis(2,4,6-trimethylphenyl)diphosphine (Figure 67), a species which had never been reported as a side product of this reaction.

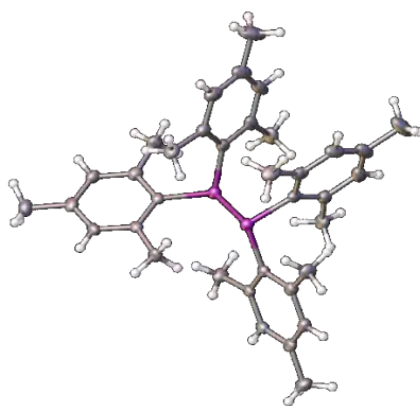
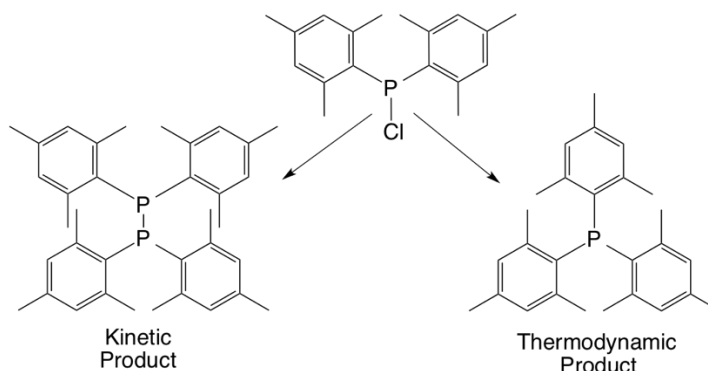


Figure 67. Structure of 1,1,2,2-tetrakis(2,4,6-trimethylphenyl)diphosphine as obtained from single crystal X-ray diffraction.

Following the identification of both species synthesised, it was attempted to inhibit the reaction pathway towards the undesired diphosphine. A review of the literature which suggested that a xenon lamp could facilitate the conversion of PMes_3 to $\text{Mes}_2\text{P-PMes}_2$, it was speculated that $\text{Mes}_2\text{P-PMes}_2$ forms *via* a radical process, therefore the reaction was carried

out in the absence of light.^{245,246} This had no effect on the ratio of the two products. Subsequently, it was discovered that scaling up from 20 to 40 mmol resulted in increase in the proportion of the desired product. This led to the supposition that there are two competing reaction pathways, a kinetic one leading to Mes₂P-Pmes₂ and a thermodynamic one leading to Pmes₃ (Scheme 24). Whereas Pmes₃ was the energetically-favoured, thermodynamic product, the kinetic product was the diphosphine, its formation encouraged due to steric congestion around the phosphorus centre following disubstitution.

Scheme 24. Proposed pathways for the synthesis of Pmes₃ and Mes₂P-Pmes₂ via kinetic and thermodynamic pathways.



Following this realisation, an effort was made to enhance the formation of the thermodynamic product. The initial synthetic procedure had involved cooling the product to -78 °C for several hours following combination of the Grignard intermediate with phosphorus trichloride, as suggested by literature sources, to prevent excessive heating.²⁴⁴ This depression of the temperature encouraged the formation of the kinetic product, which has a lower activation barrier. By returning the reaction to room temperature immediately following the combination of reagents, the system has more energy and thermodynamic product, which is the lower energy product is favoured. the reaction was modified to minimise the amount of time the reaction was cooled following the addition of the Grignard reagent to PCl₃. This was effective in eliminating the formation of side-product (Figure 68), however this was not reproducible for the deuterated analogue. However, this technique clearly enhanced the selectivity from that in Figure 66.

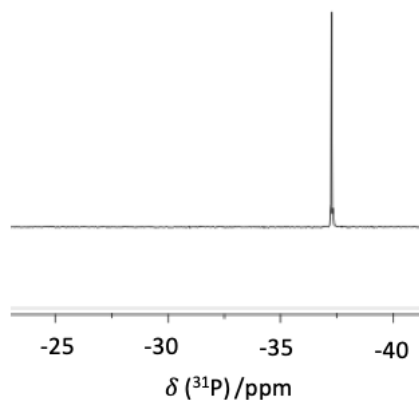
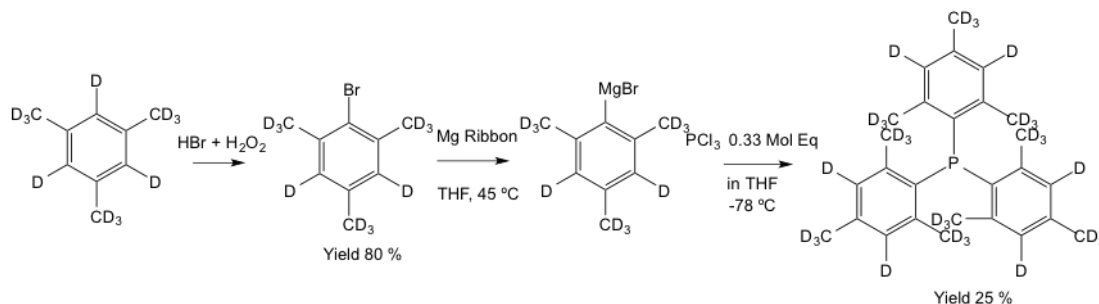


Figure 68. ^{31}P NMR spectrum showing PMes_3 .

Following optimisation of the synthetic pathway for protiated PMes_3 , synthesis of its deuteriated analogue was attempted. This was initially hindered by the lack of availability of deuterated bromomesitylene. Fortunately, mesitylene- d_{11} is a commercially available NMR standard and could be brominated with hydrobromic acid in the presence of hydrogen peroxide, in the absence of light (Scheme 25), giving 80% yield. To avoid reducing this yield, unreacted mesitylene was not removed from the post-reaction mixture, being inert in subsequent reaction steps.

Scheme 25. Synthesis of deuterated trimesityl phosphine.



The remainder of the reaction proceeded under the same conditions as with the non-deuterated starting materials, and gave a 25% yield with a 87:13 ratio of desired product to diphosphine (Figure 69). The yield was lower compared to literature values of 85% for the protiated analogue,²⁴⁴ however it is expected that yields are lower for deuterated analogues as the methodology is optimised using protiated equivalents.

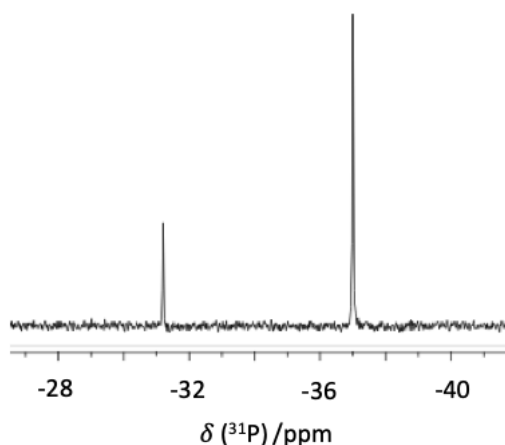


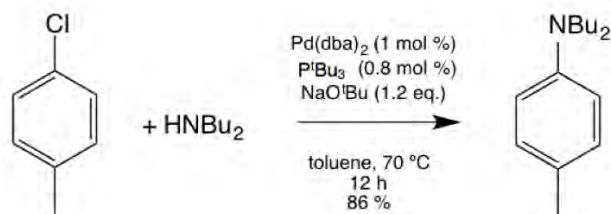
Figure 69. ^{31}P NMR spectrum showing the formation of $\text{PMes}_3\text{-d}_{33}$ (at -37 ppm) and the side product $\text{Mes}_2\text{P-PMes}_2$ (at -31 ppm).

4.3.2.2 *Tri-tert-butyl phosphine-d₂₇*

Tri-*tert*-butyl phosphine is most commonly used in palladium-catalysed cross coupling reactions and as a reducing agent. It is one of the most electron donating phosphines known, as calculated from its Tolman electronic parameter.^{159,247} This allows for the promotion of reactions with less reactive substrates and under milder conditions. In addition, it has a very large cone angle (182 °) compared to other common phosphines such as triphenyl phosphine (145 °) and trimethyl phosphine (118 °), even if it is smaller than that of trimesityl phosphine (212 °).¹⁵⁹ A large cone angle increases steric hindrance around the phosphorus centre and reduces the likelihood of the formation of by-products during catalytic reactions, promoting the lifetime of unsaturated intermediates.²⁴⁸

In combination with palladium, P^tBu_3 has been used in a wide variety of cross coupling reactions.²⁴⁸ With $\text{Pd}(\text{dba})_2$ it may be used in the amination of aryl halides, enolates and similar carbon nucleophiles (Scheme 26). In the Heck reaction the catalyst $\text{P}^t\text{Bu}_3/\text{Pd}_2(\text{dba})_3$ is more active than other phosphines (such as PCy_3 and $\text{P}(o\text{-Tol})_3$ which did not give active catalysts).²⁴⁹ More recently they have been regularly incorporated into frustrated Lewis pair (FLP) systems.²¹⁴

Scheme 26. P^tBu_3 as a catalyst in cross coupling reactions.



Reported in 1967, initial synthetic attempts to yield P^tBu_3 *via* PCl_3 and a Grignard intermediate produced only P^tBu_2Cl , regardless of the degree of excess of the Grignard reagent.²⁵⁰ Demonstrating that it was the incredible bulk around the phosphorus centre, the reaction of P^tBu_2Cl with isopropyl magnesium bromide gave very low yields of the tertiary phosphine (22%). Organolithium compounds were found to be more reactive towards P^tBu_2Cl and tri-*tert*-butylphosphine was synthesised from P^tBu_2Cl with one equivalent of $tBuLi$. This technique afforded modest overall yields of around 17%.

Improvement was needed if P^tBu_3 could be considered for catalysing reactions on a great scale. The first direct synthesis of P^tBu_3 from PCl_3 was described by Srivastava *et al.* in 1985.²⁵¹ This work avoided the use of Grignard reagents entirely, reacting 3.2 equivalents of $tBuLi$ with PCl_3 under a dry nitrogen atmosphere at room temperature. The fact that this addition does not require cooling and reacts under reflux for 50-60 hours reflects the challenge of forcing three large *tert*-butyl groups around the phosphine centre given the high reactivity of $tBuLi$ in other reactions.

In a study developing catalysts for the Heck reaction, Hartwig and colleagues showed that the use of copper(I) iodide in the presence of lithium bromide made the addition to *tert*-butylchlorophosphine of organomagnesium compounds possible.²³⁸ This method is applied to P^tBu_3 in two patents from 2003 using PCl_3 and P^tBu_2Cl starting materials from the companies Bayer and Hokko respectively.^{252,253} These techniques are currently used on an industrial scale, the former requiring cooling to $-20\text{ }^\circ\text{C}$ and 10 mol% CuI and 20 mol% $LiBr$ but presenting the obvious advantage of using PCl_3 as a starting material. In contrast the route used by Hokko calls for gentle warming at $20 - 40\text{ }^\circ\text{C}$ and just 1 mol% of a $CuCl$ catalyst. The challenge in transferring these techniques into the research lab and onto a small scale is highlighted by Fleckenstein *et al.* in their review stating that “this reaction appears to require very carefully controlled conditions to produce significant amounts of product”.²⁵⁴

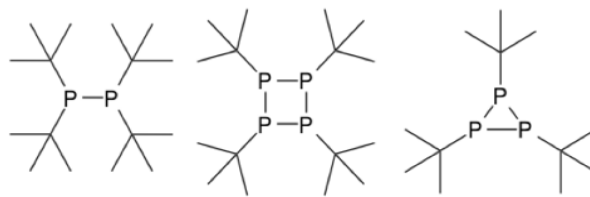


Figure 70. Side products generated in the synthesis of P^tBu₃.

The diphosphine, tetracyclic phosphine and triphosphine may be recognised by ³¹P NMR peaks at 45 ppm, -60 ppm and -70 ppm and -110 ppm respectively. It is interesting that the tetra and tri – cyclophosphines form with relative ease in this reaction as under the same conditions a Grignard reaction between PCl₃ and (2,4,6-Me₃C₆H₂)MgBr (to synthesise trimesityl phosphine) produces only the diphosphine side product. This is surprising as the cone angle of the mesityl group is 212 ° which is significantly larger than that of P^tBu₃ at 182 ° sterically therefore it would be expected that a phosphorus-phosphorus bond would form more readily and the equivalent structures to those in Figure 70 would form.

The difference between the two ligands however extends beyond their size and the mesityl ligand is significantly more donating than the *tert*-butyl ligand. This is illustrated by the difference in chemical shift between PMes₃ and P^tBu₃, which are -27 ppm and 60 ppm, respectively. This corresponds to a stronger P-C bond with a mesityl ligand, favouring the thermodynamic pathway, which generates the PR₃ product. In contrast, the kinetic products involve phosphorus-phosphorus bonds. Therefore, in theory, the desired product can be promoted by running the reaction at a higher temperature, as was seen with trimesitylphosphine. However, in the practical experiments reported herein there was no difference in the formation of side products whether the reaction was cooled by dry ice/acetone bath, an ice bath or ran at room temperature.

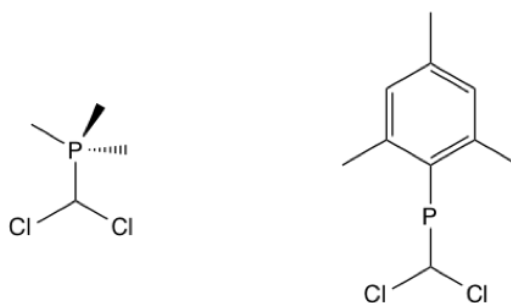


Figure 71. Comparison of mono-substituted intermediate species.

The first step of the reaction was the formation of a Grignard reagent. This was encouraged by activating magnesium ribbon by brushing it with sandpaper to create a rough surface and cutting it into small flakes. Furthermore, the magnesium flakes were stirred overnight under

an inert atmosphere, to increase the available exposed magnesium sites. The Grignard formation was very exothermic, which made the slightly higher boiling THF preferable to the more volatile diethyl ether. On the other hand, gentle heating over a heating mantle was essential to overcome activation energy and initiate the reaction. Once initiated, however, the reaction required cooling in an ice bath to prevent the loss of reactants with boiling solvent. Achieving the balance between heating and cooling was the key to achieving high concentrations of the Grignard reagent in the solution. The generation of the Grignard intermediate is also promoted by the addition of a crystal of iodine and by adding a few drops of dibromoethane, both of these techniques were found to promote Grignard intermediate generation in this reaction.²⁵⁵

The synthesis of tri-*tert*-butylcyclotriphosphane was described in 1989 as proceeding from a reaction at reflux temperatures in THF between $t\text{-BuPCl}_2$ and magnesium with a byproduct of MgCl_2 .²⁵⁶ This highlights the challenge of this synthesis with both the cyclic product and trialkylphosphine forming in almost identical experimental conditions. To limit the formation of species with multiple phosphines it is essential to ensure a high concentration of $t\text{-BuMgCl}$ to encourage multiple *tert*-butyl groups to coordinate to the phosphorus centre and give the desired product.

Side reactions are promoted by the aid of reducing agents which promote the formation of the phosphorus-phosphorus bond. The synthesis of the cyclo-tetraphosphine (Figure 70) was reported to be highly selective from the reaction of $(t\text{-Bu})\text{PCl}_2$ with bis-imidazoline, therefore, it is very important to remove any potential reducing agents before the addition of the Grignard reagent, $t\text{-BuMgCl}$, to the solution of phosphorus trichloride. This obviously precludes the running of the reaction over any remaining magnesium ribbon. The Grignard solution should be transferred *via* a cannula filter to minimise transfer of any magnesium which could facilitate the formation of phosphorus-phosphorus bonds.

In the second step of the reaction, the main challenge lay in minimising the radical side reactions, which lead to the formation the diphosphane and cyclic products (Figure 70).

Since the bulky *tert*-butyl group in $t\text{-BuPCl}_2$ introduces steric hindrance to the phosphorus centre, the formation of P-P bonds is favoured over the second $t\text{-Bu}$ substituent, even more so in adding the third $t\text{-Bu}$ to $t\text{-Bu}_2\text{PCl}$. In consequence, it is far easier to achieve selectivity towards the undesired side-products (Figure 70), than it is for P^tBu_3 . For example, the literature synthesis of tri-*tert*-butylcyclotriphosphane was described as a straightforward reaction of $t\text{-BuPCl}_2$ and magnesium, at THF reflux, with a by-product of MgCl_2 ,²⁵⁶ highly selective synthesis of cyclotetraphosphine (Figure 70b) from P^tBuCl_2 with bis-imidazoline has also been reported.²⁵⁷

In order to enhance selectivity to P^tBu_3 , it was important to remove any potential reducing agents, inhibit radical reaction pathways, and to use large excess of the Grignard reagent ($tBuMgCl$), while keeping rather high dilution of PCl_3 . In order to avoid any remaining traces of magnesium ribbon (the main source of a potential reducing agent), the addition of the Grignard reagent to the solution of PCl_3 was performed *via* a cannula filter. To inhibit radical pathways, following the work reported in patents to Bayer and Hokko,²⁵²⁻²⁵⁴ lithium bromide and copper(I) iodide were added to the PCl_3 solution before the Grignard reagent was added, at 10 mol% loading of both salts. Increasing the quantity of lithium bromide to 20 mol%, as reported in the patent, did not have a significant impact on yield.²⁵²

To confirm the effect of these salts on selectivity, a simple experiment was carried out, reacting an excess of PCl_3 with $tBuMgCl$, in the presence and absence of 10 mol% of CuI and $LiBr$ (Figure 72, spectra a and b, respectively). When both salts were present (Figure 72a), dichloro(*tert*-butyl) phosphine (PCl_2tBu) was generated as a single product ($\delta_{31P} = 190.0$ ppm).²⁵⁸ In contrast, in the absence of these salts, the radical reactions have not been inhibited, resulting in a wide range of products (Figure 72b), which provides convincing evidence that the desired reaction pathway is controlled by the introduction of small quantities of CuI and $LiBr$.

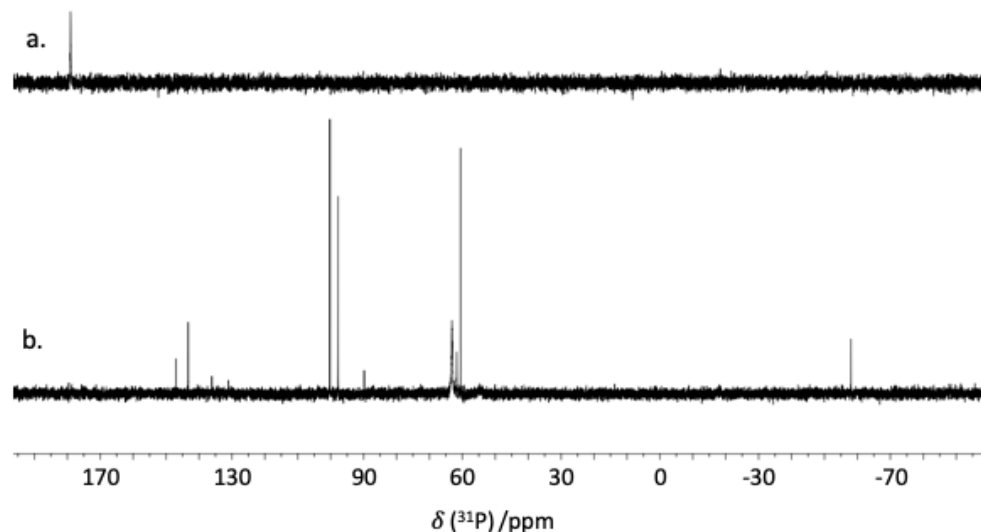
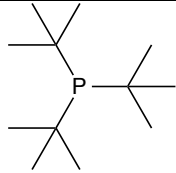
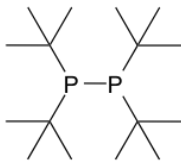
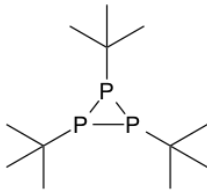
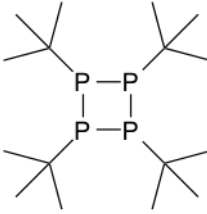
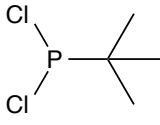
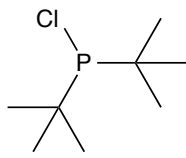
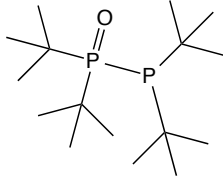
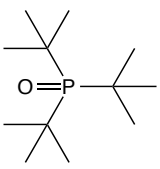


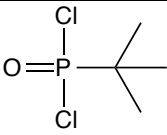
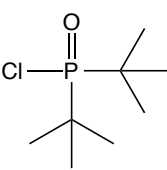
Figure 72. A comparison of ^{31}P spectra a) with and b) without copper(I) iodide and lithium bromide at a 5% mol ratio.

All the side-products in Figure 72 gave ^{31}P NMR signals more shielded than PCl_2tBu . Although they have not been individually assigned, the literature reports on a broad range of side products and by-products (

Table 17).

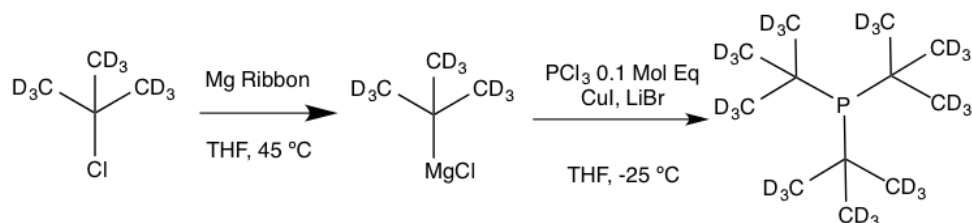
Table 17. The detected side and by- products from the synthesis of tri-*tert*-butyl phosphine (in benzene).

Species	Structure	³¹ P NMR chemical shift (ppm)
Tri- <i>tert</i> -butyl phosphine		60
Tetra- <i>tert</i> -butyldiphosphine		41
Tri- <i>tert</i> -butylcyclotriphosphine		-70
Tetra- <i>tert</i> -butylcyclotetraphosphine		-60
Dichloro(<i>tert</i> -butyl) phosphine		190
Bis(<i>tert</i> -butyl) chlorophosphine		147
Tetra- <i>tert</i> -butyldiphosphine -1 oxide		45 & 90
Tri- <i>tert</i> -butyl phosphine oxide		68

Dichloro(<i>tert</i> -butyl) phosphine oxide		70
Bis(<i>tert</i> -butyl) chlorophosphine oxide		95

Procedure for the synthesis of tri-*tert*-butyl phosphine-*d*₂₇ (Scheme 27) was developed by combining aspects of the methodology developed for its protiated analogue.

Scheme 27. The synthesis of deuterated tri-*tert*-butyl phosphine.



Following synthesis, P^tBu₃-*d*₂₇ was purified by removing the reaction solvents, dissolving the products in dry pentane and the washing with degassed water. The organic phase was then dried and, upon removal of solvent, P^tBu₃ was obtained as a colourless, crystalline solid. The structure of the product was confirmed by ¹³C and ³¹P NMR spectroscopy (Figure 73), combined with mass spectrometry, and was consistent with P^tBu₃-*d*₂₇. This product demonstrated 100% selectivity which was important for collecting reliable neutron scattering data, however the yield was moderate at 18.8% for the final step. Considering the pyrophoric nature of this phosphine, it was crucial to maintain full air exclusion and ensure that all solvents were well degassed; failure to do so resulted in rapid formation of oxidation products.

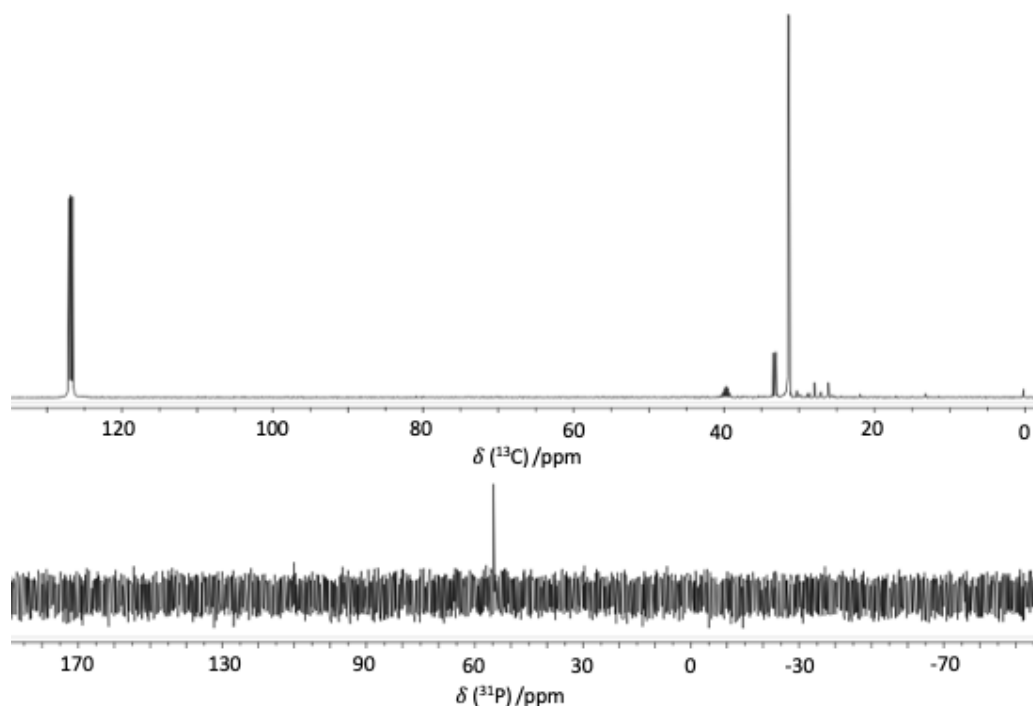


Figure 73. ^{13}C and ^{31}P NMR spectra of tri-*tert*-butyl phosphine- d_{27} in C_6D_6 (solvent peak in ^{13}C at 128 ppm).

4.4 Neutron Scattering

Neutron scattering data were recorded at the Small Angle Neutron Diffractometer for Amorphous and Liquid Samples (SANDALS) beamline at ISIS, which is designed for the study of liquid samples. All data were processed by Prof. Holbrey.

In the first set of experiments, equimolar concentrations of BCF/ PMes_3 in benzene were studied. However, following initial data processing it was found that the model was unable to distinguish between the solvent molecule, benzene, and the mesityl rings surrounding the phosphine, meaning the data was uninterpretable. In the second attempt, the BCF/ P^tBu_3 pair was used, because P^tBu_3 does not contain any aromatic rings, so is structurally distinctive from benzene, but has been shown to form FLP complexes.²¹⁴

Due to the relative insensitivity of neutron scattering, in comparison with NMR spectroscopy, the concentration of phosphine and borane was at the maximum possible borane concentration (limiting factor), and the concentration of phosphine was matched. A high concentration gave the additional advantage of increasing the likelihood of encounter complex formation. Data was recorded for samples of P^tBu_3 and BCF at a concentration of 160 mmol in benzene- h_6 , benzene- d_6 and in a 1:1 H/D mixture. This concentration is equivalent to a ratio of 1:1:70 of solvate molecules to solvent molecules. The neutron scattering data was processed using the Gudrun software,^{259,260} being reduced to correct for instrumental parameters. This reduced data

was modelled using EPSR,²⁶¹ with a cubic simulation box of sides 47.8 Å in length, containing 10 P^tBu₃, 10 BCF and 700 benzene molecules, to mirror the relative concentrations of each molecule in the experimental phase.

The data-driven model is typically used to derive partial radial distribution functions, which describe statistical mechanics of liquids by determining the probability of finding a particle in an infinitesimal shell, at a certain distance from another particle. In this work it is the distance between boron and phosphorus which is being observed to determine whether they are found closer to each other than the statistical probability would be if they had no interaction. An increased probability of their being found closer to each other would suggest an interaction between P^tBu₃ and BCF molecules and provide evidence of the formation of an encounter complex.

The partial radial distribution function for the system BCF/P^tBu₃ in benzene shows that the interactions between benzene and phosphine and between benzene and borane are more likely than interactions between the phosphine and borane. This is not surprising, as the majority of molecules would be expected to be solvated by benzene. The peak for the benzene-borane correlation (Figure 74 black line) comes at around 4 Å, this likely represents the interaction between the empty p-orbital on the boron centre and the aromatic system of the benzene which is capable of π -donation. For phosphine-benzene interactions (Figure 74 red line) the peak does not emerge until ~ 7 Å, this is likely to be because the bulky tert-butyl ligands surrounding the phosphorus centre make a closer approach by the benzene molecules impossible. The benzene-benzene correlation (Figure 74 blue line) demonstrates first shell packing with a maximum at ~ 5.8 - 6.0 Å, this is consistent with previously reported data on the packing of bulk neat benzene.²⁶²

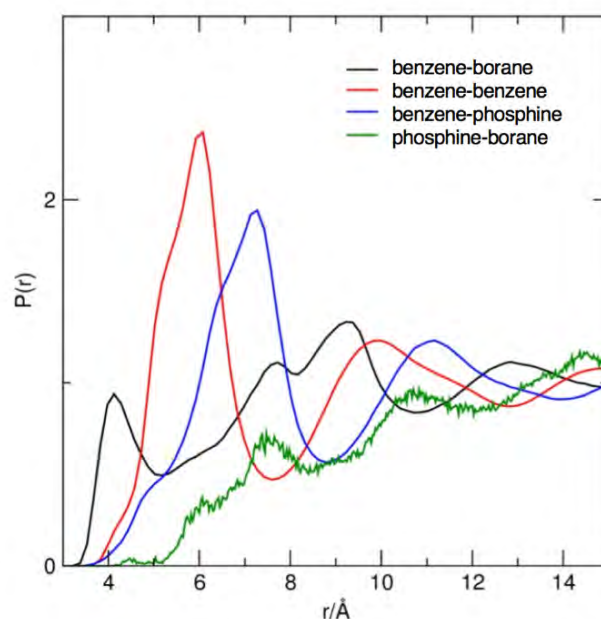


Figure 74. Comparison of the small $\text{P}^t\text{Bu}_3 \cdots \text{BCF}$ correlation in the EPSR model of the experimental data with the larger radial distribution functions (RDFs) between BCF and benzene (black), P^tBu_3 and benzene (blue) and the benzene-benzene self-correlation (red).

Encounter complexes are expected to be represented as peaks in the partial radial distribution function for the interaction between phosphine and borane, which accumulate over time as the simulation runs, representing their forming and disassociating in solution. From two independently run data-driven simulations (Figure 75) two peaks are observed which are believed to illustrate the association of the P^tBu_3 and BCF molecules in solution. From both models these two signals appear as a small peak is observed at $\sim 8 \text{ \AA}$, followed by a second peak at $\sim 10.5 \text{ \AA}$. Beyond 14 \AA , the molecules form a homogeneous distribution as this is where the correlation indicates a probability of 1. As previously discussed, neutron scattering is not an overly sensitive technique and as such, although the concentration of 160 mmol is higher than catalytic concentrations of FLP, this is still low for neutron scattering detection. This accounts for the difference between the two refinement models as site-site specific interactions gave poor resolution. Despite this, both refinements clearly feature peaks *ca.* 8 and 10.5 \AA .

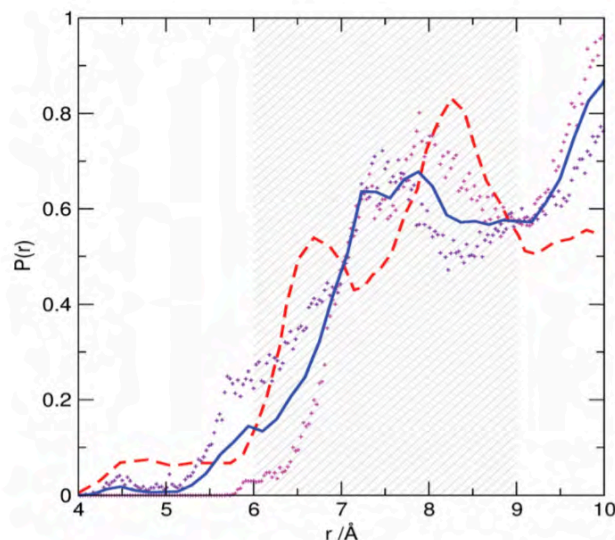


Figure 75. The plot of the P-B pair partial radial correlation function (blue) between P^tBu₃ and BCF in benzene (1:1:70), averaged from two independent data-driven simulation models (purple and magenta data points), and compared to the equivalent correlation from DFT simulation of P^tBu₃ and BCF in toluene (red line).⁶ Correlation distances corresponding to the range of ‘solvent-separated’ pairs (6–9 Å) are indicated by the shaded region.

If there were no chemical interactions at play in this system, the expected behaviour of the probability curve would be a straight line from 0 probability at 0 Å, to a probability of 1 at 14 Å, as this is where complete homogeneity occurs. Therefore, to understand the meaning of the peaks and their relationship with the interaction between the phosphorus and boron centres of the FLP molecules, the deviation from this line is symptomatic. Considering the proportion of molecules at each separation distance, the deviation of P-B separation distances at 5.7 Å is < 1%, suggesting that there is no interaction between these molecules at this short distance. However, this value increases over separation distances of 6–8 Å to 4.9% at 8 Å. The separation distance of 8 Å is relevant to previous studies of FLP encounter complexes, it is of the same order reported by Bako *et al.* as the distance of “solvent separated” FLPs in their DFT model of the same system.⁶ Furthermore it appears to be consistent with the 2D NMR studies reported by Rocchigiani *et al.* for the H/F contact distances between FLPs in solution.²²³ The increase of 4.9% of molecules at P-B distances of 8 Å, which suggests that around 5% of molecules form encounter complexes at any one time, is also in correlation with the DFT results of Bako *et al.*⁶ This data also ties in with the expectation that the encounter complex is a short-lived phenomenon, demonstrating its low concentration and transient nature. Therefore, this peak at 8 Å ties in with previously reported data from computational modelling and NMR spectroscopic studies, suggesting that neutron scattering techniques offer the opportunity to observe FLP encounter complexes directly for the system of BCF/P^tBu₃ in benzene.

4.5 Conclusions

The synthesis of deuterated analogues of two sterically hindered phosphines: trimesitylphosphine and tri-*tert*-butyl phosphine, has been accomplished *via* Grignard techniques. This work relied on synthetic procedures previously published for protiated analogues,^{244,252} however the methods were modified to feature less cooling and minimise the formation of side products. The synthesis of tri-*tert*-butyl phosphine has been submitted as a paper to the Journal of Labelled Compounds and Radiopharmaceuticals as its synthesis had not been previously reported. Both were used in neutron scattering experiments, albeit only the P^tBu₃ data could be interpreted.

This work has demonstrated the potential of neutron scattering as a viable technique for observing the formation and concentration of transient encounter complexes. The results corroborate well with previously reported DFT model and are in agreement with 2D NMR spectroscopy.^{6,223} A “solvent separated” association between BCF/P^tBu₃ in benzene was demonstrated, through the detection of modelled interatomic distance between boron and phosphorus around 8 Å. The low concentration of encounter complexes which has been experimentally observed was suggested to be *ca.* 5% of FLP molecules. Future neutron scattering work arising from this could include comparing the BCF/P^tBu₃ FLP in different solvents, or different FLP systems to observe changes in encounter complex concentrations arising from different conditions. This would provide information about the effect of encounter complex concentration on the catalytic activity of the FLP. In a second trip to ISIS in this work neutron scattering data was recorded of BCF/P^tBu₃ in benzene with H₂ added to provide a comparison with the system in the absence of hydrogen, however the data from this experiment has not been modelled at the time of writing.

These results were published in Chemical Communications discussing the use of neutron scattering to observe encounter complex formation.⁵ Additionally, the synthesis of deuterated tri-*tert*-butyl phosphine is described in a paper submitted to the Journal of Labelled Compounds and Radiopharmaceuticals.

5 FRUSTRATED LEWIS PAIRS IN/AS IONIC LIQUIDS

The work described in Chapter 4 was primarily with the behaviour of frustrated Lewis pairs in molecular solvents. This Chapter describes the first reported study on ionic liquids as solvents for FLPs, and subsequently – the study of first ionic liquids that were designed to act as ionic liquid FLPs, including the capacity for hydrogen splitting.

5.1 Experimental

5.1.1 Materials and Methods

All experiments were performed in a glovebox (MBraun labmaster dp, <0.6 ppm of H₂O and O₂) or using Schlenk techniques under argon. All glassware was dried overnight in an oven (*ca.* 80 °C) prior to use. Materials and synthesised products were stored in the glovebox. Solvents were dried over molecular sieves, 3 Å, and stored under Ar. Tri-*tert*-butyl phosphine (98%) and BCl₃ (1.0 M in pentane) was purchased from Sigma Aldrich in a sealed bottle and used as received. Triphenyl phosphine (99%) and 1,8-Bis(dimethylamino)naphthalene (99%) were purchased from Sigma Aldrich and dried (60 °C, 10⁻² mbar, overnight) prior to use. 1-methyl imidazole (99%), N,N diisopropyl ethyl amine (>99%), 2,2,4,6 tetramethyl piperidine (99%) were purchased from Sigma Aldrich and purified by distillation prior to use. Tris(pentafluorophenyl)borane (>98%) was purchased from Tokyo Chemical Industry and purified by sublimation before use.

¹H, ¹¹B, ¹³C, ¹⁹F, ²⁷Al and ³¹P NMR spectra were recorded on a Bruker Avance DPX 400 MHz spectrometer at 400, 128, 100, 376, 104 and 162 MHz, respectively.

5.1.2 Preparations of Solutions in Benzene-d₆

In an argon filled Mbraun glovebox, solutes were dissolved in benzene-d₆ at a concentration of 160 mmol and were transferred into a flame dried Norell IPV valved NMR sample tube for intermediate pressure. These samples were observed *via* NMR spectroscopy and these are interpreted in Section 5.2.

5.1.3 Preparations of Solutions in [C₁₀mim][NTf₂]

In an argon filled Mbraun glovebox, solutes were dissolved in [C₁₀mim][NTf₂] at a concentration of 160 mmol was transferred into a flame dried Norell IPV valved NMR sample tube for intermediate pressure with a DMSO-d₆ filled, sealed capillary as an external

deuterated lock. These samples were observed *via* NMR spectroscopy and these are interpreted in Section 5.2.

5.1.4 Hydrogenation of $B(C_6F_5)_3$ and P^tBu_3 Dissolved in Benzene- d_6

In an argon filled Mbraun glovebox $B(C_6F_5)_3$ and P^tBu_3 were dissolved in benzene- d_6 at a concentration of 160 mmol to a total volume of 2 cm³. This was removed to an argon filled gas line and set to stir vigorously. The gas was then switched to pure hydrogen with no exposure to air and the sample was stirred overnight. The following morning the sample was purged with argon and removed to the glovebox. The sample was transferred into a flame dried Norell IPV valved NMR sample tube for intermediate pressure. This sample was observed *via* NMR spectroscopy and these are interpreted in Section 5.3.

5.1.5 Hydrogenation of $B(C_6F_5)_3$ and P^tBu_3 Dissolved in $[C_{10}mim][NTf_2]$

In an argon filled Mbraun glovebox $B(C_6F_5)_3$ and P^tBu_3 were dissolved in $[C_{10}mim][NTf_2]$ at a concentration of 160 mmol to a total volume of 2 cm³. This was removed to an argon filled gas line and set to stir vigorously. The gas was then switched to pure hydrogen with no exposure to air and the sample was stirred overnight. The following morning the sample was purged with argon and removed to the glovebox. The sample was transferred into a flame dried Norell IPV valved NMR sample tube for intermediate pressure. This sample was observed *via* NMR spectroscopy and these are interpreted in Section 5.3.

5.1.6 Synthesis of $[BCl_2mim][M_2Cl_7]$

An adduct of Boron trichloride with methyl imidazole was prepared using an argon Schlenk line, by dropwise addition of a base (0.9 equiv) To a vigorously stirred mixture of boron trichloride (1m solution in heptane, 1.0 equiv) and DCM (20 cm³) at -78 °C, attached to an argon Schlenk line, methyl imidazole was added dropwise (0.9 equiv). This was allowed to stir (1 hr, RT) After the reaction excess reactants and solvents were removed under reduced pressure and the adduct was dried under high vacuum (60 °C, 10⁻² bar, overnight). This was removed to an argon-filled glovebox. A metal(III) chloride (2 equiv) was added slowly to the boron trichloride adduct (1equiv) and left to react until a homogenous mixture was obtained (30–50 °C, 2 hr). The resulting product was stored in the glovebox. ¹H NMR (400 MHz, CDCl₃) δ 8.46 (s, 1H), 7.62 (s, 1H), 7.09 (s, 1H), 3.92 (s, 3H), ¹³C NMR (100 MHz, CDCl₃) δ 136.44, 124.78, 122.26, 35.95, ¹¹B (128 MHz, CDCl₃) 44.7, 39.9, ²⁷Al (104 MHz, CDCl₃) 107.4, 76.2 (sh).

5.1.7 Combination of bases with $[B\text{Cl}_2\text{mim}][M_2\text{Cl}_7]$

Reactions were performed in an argon-filled glovebox. Amine or phosphine bases, 0.1 or 0.5 mol eq. were added to the borenium ionic liquid (1 mol eq.) and left to react under stirring (3hr, RT). The products were observed *via* NMR spectroscopy and these are interpreted in Section 5.4.1.

5.1.8 Synthesis of $[Bcat(P_{888})][NTf_2]$ with 1 eq. of P^tBu_3

To a sample of $[Bcat(NTf_2)(P_{888})][NTf_2]_2$, prepared as described in 3.1.7, in an argon filled glovebox, 1 eq. of P^tBu_3 was added and this was allowed to react under stirring until a homogeneous liquid formed (3 hrs, RT). The products were observed *via* NMR spectroscopy and these are interpreted in Section 5.4.2.

5.2 Frustrated Lewis pairs in inert ionic liquids

Following the successful modelling of encounter complexes by neutron scattering, reported in Section 4.4, the low concentration of encounter complexes was noted. This is known to be a crucial limiting factor in the kinetics of FLP mediated reactions.²¹⁴ Stabilisation of encounter complexes could increase their concentration and lifespan, enhancing the kinetics of FLP-catalysed reactions, and make FLPs a more appealing and more realistic alternative to the main-stream catalytic systems. In this study, the use of ionic liquid media to reduce the diffusivity of FLP components was explored.

The FLP system P^tBu_3/BCF , also studied in benzene as described in Chapter 4, was dissolved in 1-decyl-3-methylimidazolium bistriflamide, $[C_{10}\text{mim}][NTf_2]$, at a concentration of 160 mmol (matching that used in benzene studies). To ensure that no interaction was observed between ionic liquid and the FLP components, the individual components were individually dissolved in ionic liquid at a concentration of 160 mmol. The dissolution of either or both components in the ionic liquid did not lead to any colour change. This contrasts to in benzene where a light yellow colour has been observed on combination of the FLP components. This has been ascribed to the formation of trace quantities of $[^tBu_3P(C_6F_4)B(C_6F_5)_2]$.²⁶³ These solutions were studied using ^{31}P and ^{19}F NMR spectroscopy, of which results illustrate that there was no oxidation or hydrolysis. From NMR spectroscopy of individual components in the ionic liquid, there was no strong interaction arising between ionic liquid and the components, beyond small changes owing to greater solvent polarity (Table 18). However, most importantly, the solution of both FLP components in the ionic liquid featured additional peaks, both in the ^{31}P and ^{19}F NMR spectra.

Table 18. ^{19}F and ^{31}P NMR signals of solutions of the BCF/ P^tBu_3 FLP and its individual components in benzene- d_6 and in an ionic liquid, $[\text{C}_{10}\text{mim}][\text{NTf}_2]$ at a concentration of 160 mmol.

	^{19}F signals/ppm	^{31}P signals/ppm
P^tBu_3 in benzene- d_6	-	58
P^tBu_3 in $[\text{C}_{10}\text{mim}][\text{NTf}_2]$	-	60
BCF in benzene- d_6	-134, -149, -161	-
BCF in $[\text{C}_{10}\text{mim}][\text{NTf}_2]$	-133, -157, -166	-
FLP in benzene- d_6	-139, -152, -162	61
FLP in $[\text{C}_{10}\text{mim}][\text{NTf}_2]$	-134, -138, -140 -151, -156, -160, -164, -165, -166	53, 61

These additional peaks do not appear for the FLP mixture in benzene (Figure 76). In the ^{19}F NMR spectrum, three environments are observed which correspond to the *ortho*, *meta* and *para* environments. These demonstrate little deviation on combination with the phosphine, with the largest shift of 3 ppm appearing for the *meta* fluorines. The key difference between the two ^{19}F NMR spectra, however, is the appearance of six additional peaks upfield of the three major peaks. These additional signals may be explained as the BCF entering a weak, but relatively long-lasting interaction with P^tBu_3 , as would be expected for an encounter complex. The consequence of this interaction is that the three perfluorophenyl ligands are no longer in identical electronic environments. The peak area ratio of the signals from free BCF in the ionic liquid against the new minor signals is 1 : 0.312. This suggests that *ca.* 24% of the BCF underwent a change of electronic environment upon contact with P^tBu_3 .

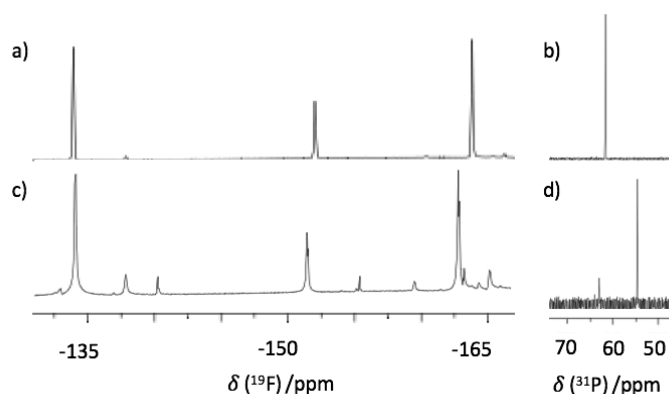


Figure 76. Spectra of the FLP, BCF/ P^tBu_3 , and its components, in $[\text{C}_{10}\text{mim}][\text{NTf}_2]$ (a) ^{19}F NMR spectrum of BCF, (b) ^{31}P NMR spectrum of P^tBu_3 , (c) ^{19}F NMR spectrum of BCF/ P^tBu_3 and (d) ^{31}P NMR spectrum of BCF/ P^tBu_3 .

For the ^{31}P NMR spectrum, a change on introduction of both FLP species is also observed. In the ^{31}P NMR spectrum in the absence of BCF, a single peak is observed at ~ 60 ppm, which is very similar to that observed for this species in benzene- d_6 . On addition of BCF, in the spectrum of the FLP solution, this signal is slightly shifted due to solvent effect ($\Delta^{31}\text{P} = +1$ ppm). The major peak, however, is a new upfield peak at 53 ppm ($\Delta^{31}\text{P} = 8$ ppm). The measured peak area ratio between the free P^tBu_3 signal and the new signal is about 0.29 : 1, which indicates that *ca.* 78% of phosphine molecules experience a change in electronic environment. On average, when phosphines form adducts with strong Lewis acids, their ^{31}P NMR signal shifted downfield by about $\Delta_{31\text{P}} = +20$ ppm, for example, triphenyl phosphine adduct with BH_3 has $\Delta_{31\text{P}} = +26$ ppm compared to free triphenylphosphine.^{3,264} Therefore, this change where the ^{31}P nuclei is slightly shielded, rather than deshielded, does not suggest adduct formation, but a different interaction mode.

These additional resonances observed for the FLP mixture dissolved in $[\text{C}_{10}\text{mim}][\text{NTf}_2]$, but not when the individual components are dissolved helps to give clear evidence for interaction between the phosphine and borane. Furthermore, the observation of these encounter complexes, which are incredibly transient in molecular solvents, though NMR spectroscopy suggests that they are longer lived in ionic liquids. This points to the stabilisation of these species in the ionic liquid medium. This is likely to arise as a result of the multi-domain nature of ionic liquids discussed previously. Interestingly, the stoichiometric ratio of species that seem to partake in this interaction is not equimolar, but around 3 : 1 for BCF : P^tBu_3 . From these data, it is impossible to make definitive assignments to the nature of the association. However, it is clear that about 24% of BCF and 78% of P^tBu_3 are in different environments in the FLP solution which, in the absence of other factors, should be attributed to the interaction between the FLP components.

The nature of the interaction observed here is unlikely to be a direct acid-base interaction, with the Lewis base lone pair pointing in the direction of the Lewis acid empty orbital (and possibly partial orbital overlap), because the ^{31}P NMR signal was shielded, rather than deshielded. This is in agreement with earlier results for the orientation of FLP encounter complexes in organic solvents by Bako *et al.* (DFT) and Rocchigiani *et al.* (2D NMR spectroscopy), who suggested that FLPs form “solvent-separated pairs”, with many equally probable association orientations through H/F interactions.^{6,223} The results describe in this work, although not conclusive, align with this interpretation. However, in this work FLP components are solvated not by molecules, but by the ions of the ionic liquid, which appears to stabilise the encounter complex. This stabilisation can be attributed to high cohesive energy densities and internal pressure, combined with slow diffusivity in ionic liquids, which leads to matrix isolation.²⁶⁵⁻²⁶⁹ The specific effect of ionic liquids on the lifetime of encounter complexes is not fully conclusive, however other work on the behaviour of solutes in ionic liquids suggests that whilst they may not promote the FLP formation, they are likely to reduce its tendency for disassociation when formed.

Unlike molecular solvents, ionic liquids contain multiple charged domains on a molecular level which differently interact with solutes. This comparison between molecular and ionic solvents is best described by the plots (Figure 77).²⁶⁶ Here, from computationally derived square functions ($S(q)$), which describe coherent X-ray scattering intensity, the interactions between molecules at short and longer ranges can be observed. For molecular solvents, there is one single feature over the region of intermolecular interactions, perhaps excluding a small peak in the methanol curve for hydrogen bonding. As the x-axis is in the units \AA^{-1} , these interactions are at the shorter range of intermolecular interactions, indicating interactions between neighbouring atoms. Conversely, for ionic liquids, typically three peaks are observed over increasing intermolecular distances. The peak at the largest values of q is similar to that observed in molecular solvent and represents a range of interactions between neighbouring molecules, both inter- and intra-molecular in nature, but predominantly from cation-anion interactions.²⁷⁰ The intermediate value of q , typically around 0.85 \AA^{-1} represents interactions between cation-cation and anion-anion species, resulting in charge alternation.^{271,272} The feature at the lowest value of q represents an arrangement at a length greater than charge alternation, with polar-polar and apolar-apolar densities in sync and polar-apolar densities out of sync, illustrating longer range coupling and typically only observed in ionic liquids with long carbon chains.^{270,271,273}

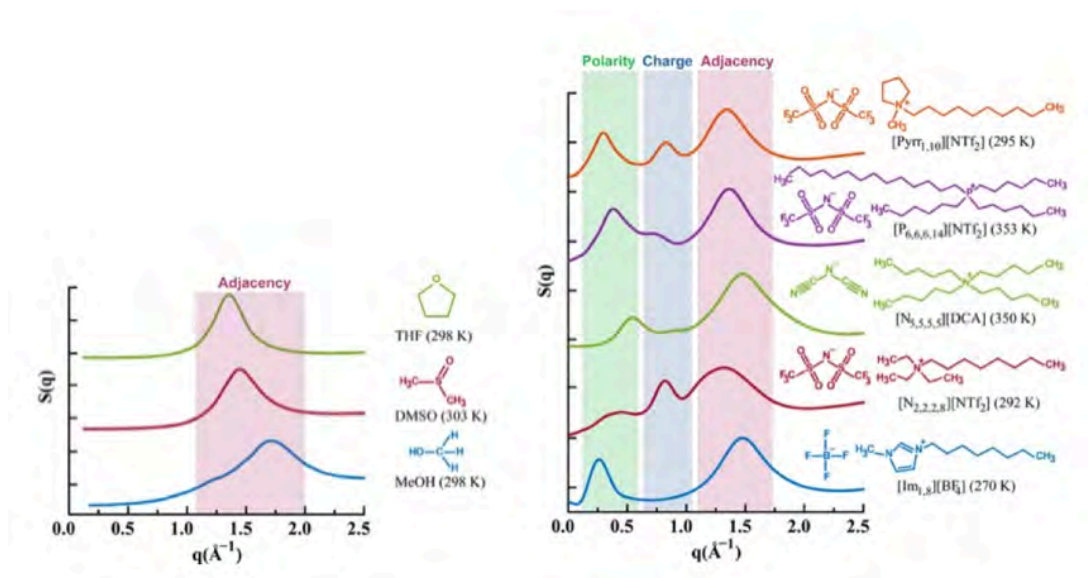


Figure 77. Computationally derived square functions ($S(q)$) (which is a function of X-ray scattering intensity against concentration and atom type) for (left) molecular solvents and (right) ionic liquids graphs developed by Araque *et al.* based on computational derivations from Kashyap *et al.*^{266,270-273}

For an ionic liquid such as $[\text{C}_{10}\text{mim}][\text{NTf}_2]$ (Figure 78), there are two domains clearly visible on the cation: a charged head region with the aromatic imidazole group, and a non-polar decyl chain. The effect of this ionic and non-polar structure is to create different domains which can be described as “cage” and “jump” regions, this terminology was introduced to ionic liquid research by Araque *et al.* in 2015.²⁶⁵

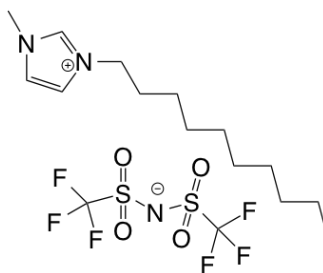


Figure 78. The structure of the room temperature ionic liquid $[\text{C}_{10}\text{mim}][\text{NTf}_2]$.

Whilst in a polar region diffusion is reported to be slower, owing to greater friction in the solute-solvent interactions, meaning solute movement is slower. This is not a consequence of greater attraction between the solute and the polar region, but it is caused by slower diffusion in this region, analogous to congestion in traffic. Conversely, in the non-polar region the diffusion is much faster, causing solutes to jump through this domain. This leads to a structural duality in the ionic liquid solvent leading to slow and fast diffusion.²⁶⁵ The movement of solutes through ionic liquids was visualised by Araque *et al.* (Figure 79). From these plots, the different trajectories of the solute molecule, methane, in the ionic liquid solvent, 1-butyl-1-

methylypyrrolidinium bistriflimide, can be seen, with the radius of gyration, R_g , significantly smaller in the cage domains ($R_g < 0.100$ nm) than in the jump domains ($R_g > 0.375$ nm).²⁶⁵

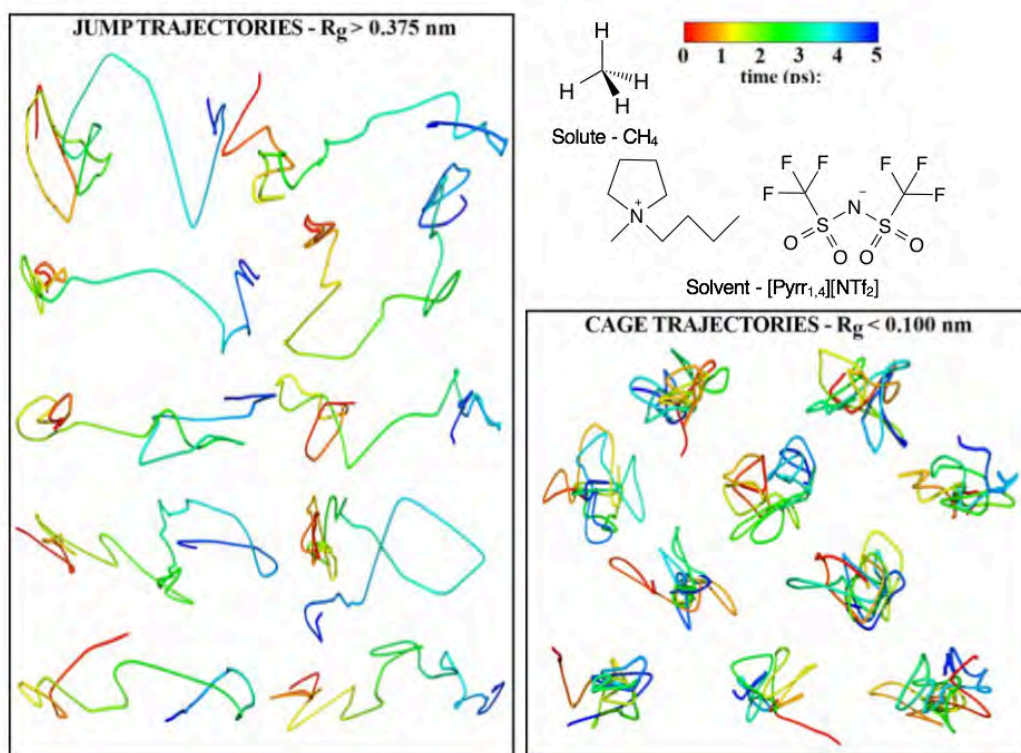


Figure 79. Representations of cage and jump movements for the solute methane in the ionic liquid 1-butyl-1-methylpyrrolidinium bistriflimide, illustrating the different movements through each domain of the ionic liquid.²⁶⁵

The results suggested by the computational studies described above help explain the observations that the FLP in ionic liquid diffuses less quickly and thus that the encounter complex is longer lived. This gives the promise that FLP reactions in ionic liquids will have increased kinetics over those in molecular solvents. Neutron scattering has been demonstrated as a technique capable of providing empirical evidence of B-P distances in FLP encounter complexes and the relative concentration of these encounter complexes (Section 4.4). The outcomes have been recognised as crucial by the precursor of FLP chemistry in his authoritative review in *Trends in Chemistry*.²⁰⁹

To expand this methodology to other systems, neutron scattering data was collected for the BCF/ P^tBu₃ FLP in [C₁₀mim][NTf₂] at 160 mmol to provide a direct comparison to the system in benzene, however owing to the long decyl chain on the ionic liquid solvent it was not possible to model the system using EPSR. New modelling software, DISSOLVE, is currently under development by beamline scientists at the ISIS Neutron and Muon Source and it is expected that this will be capable of modelling the system in [C₁₀mim][NTf₂]. Concurrently,

the shorter chained $[\text{C}_2\text{mim}][\text{NTf}_2]$ was also used as a solvent for BCF/ P^tBu_3 FLP 160 mmol and neutron scattering data for this system was collected as it is easier to model using EPSR and this is currently waiting analysis. Computational modelling of these systems is also being undertaken through a collaboration with the Pas group.

5.3 Hydrogenation of FLPs in inert ionic liquids

The results demonstrating enhanced stabilisation of the encounter complex were extremely encouraging, but the observation would have been worthless should this assembly not catalyse H_2 splitting. To probe the activity of the BCF/ P^tBu_3 FLP in ionic liquid, a simple study was designed to observe whether the capacity for hydrogen splitting has been retained, in analogy to what was reported for molecular solvents.²¹⁴ In this a simple experiment, pure H_2 was flowed overnight over a vigorously stirred 160 mmol solution of BCF/ P^tBu_3 , both in benzene and in $[\text{C}_{10}\text{mim}][\text{NTf}_2]$. The set-up depicted in Figure 80 was used.



Figure 80. Setup for H_2 saturation experiments.

Firstly, the BCF/ P^tBu_3 in benzene was tested. Although the experiment of the splitting of H_2 by the FLP combination BCF/ P^tBu_3 in benzene was previously reported by Welch *et al.*, it was important to confirm the experimental setup designed here for their system would have delivered the same result. Indeed, in benzene solution after the experiment, expected ^1H NMR signals signifying the H_2 splitting were found (Figure 81).²¹⁴ They had the expected 1:1 integration, corresponding to two new hydrogen atoms attached to both boron and phosphine.

Following this, an identical experiment in $[\text{C}_{10}\text{mim}][\text{NTf}_2]$ was conducted. In the ionic liquid two new peaks with equal integration are also observed, downfield from the signals recorded in the less polar benzene solution.

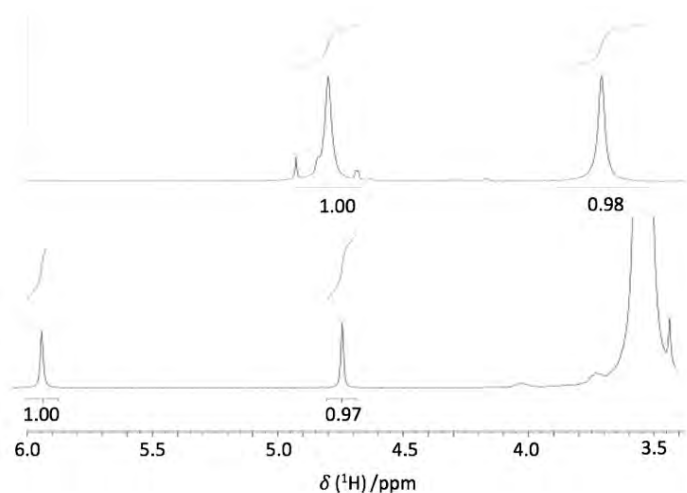


Figure 81. Fragments of ^1H NMR spectra of the FLP solutions in benzene (top) and $[\text{C}_{10}\text{mim}][\text{NTf}_2]$ (bottom) after saturation with H_2 , showing signals from split H_2 molecule.

In agreement with the literature,²¹⁴ hydrogen split by the $\text{BCF}/\text{P}^t\text{Bu}_3$ pair could not be released from the benzene solution upon heating to $60\text{ }^\circ\text{C}$ under ambient pressure. Taking advantage of higher thermal stability of $[\text{C}_{10}\text{mim}][\text{NTf}_2]$ compared to benzene, the sample was heated higher than in the literature, and under reduced pressure (1.0^{-3} mbar). However, hydrogen was only released at $150\text{ }^\circ\text{C}$, which was accompanied by decomposition of the FLP components.

Although this particular system did not offer reversible H_2 capture, this work opened a very interesting area of FLP chemistry in ionic liquids. This offers the opportunity to introduce some of the functionality of ionic liquids to the burgeoning main-group FLP community. For example by creating FLP catalysts in the supported ionic liquid phase (SILPs), immobilising a film of ionic liquid on a solid phase to create a heterogeneous catalyst. The future target of this work would be to use FLP systems with established catalytic reactivity and observe this activity in ionic liquids. This would look to expand the range of FLP in ionic liquid activity beyond H_2 splitting and to ambitious reactions such as N_2 splitting and the formation of methane from CO_2 .^{274,275}

5.4 Development of Ionic Liquid FLPs

5.4.1 First Generation Borenium Ionic Liquids as FLP Components

The family of borenium ionic liquids with the general structure $\text{L-BCl}_3\text{-nMCl}_3$ were trialled as potential Lewis acidic component in FLPs. The crucial aspect of FLP design was that the Lewis acid and base components cannot form an adduct, as this precludes their interaction with substrate molecules. Therefore, preliminary experiments were carried out using reasonably hindered, readily available bases (Figure 82). Initially, these were amines, because a nitrogen centre was speculated to be preferable over phosphorus: as a smaller atom, nitrogen

has less disperse orbitals, and therefore disfavours adduct formation in a sterically hindered system. The amines initially selected for investigation were N,N-diisopropyl ethyl amine, 2,2,4,6-tetramethyl piperidine and the Proton Sponge (1,8-bis(dimethylamino)naphthalene). Since phosphines have been widely used in FLP chemistry, triphenyl phosphine was also included in these experiments.

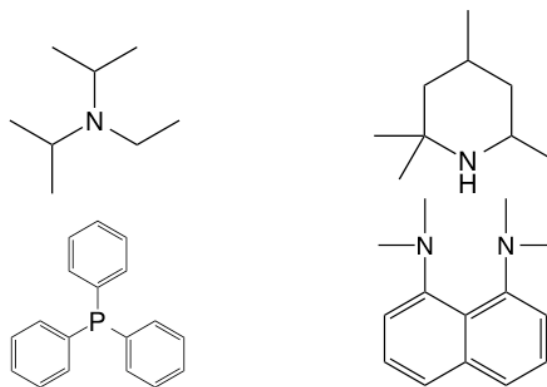


Figure 82. Structures of (clockwise from top right): N,N diisopropyl ethyl amine; 2,2,4,6 tetramethyl piperidine; proton sponge (1,8-bis(dimethylamino)naphthalene) and triphenyl phosphine.

Unfortunately, in each case, an interaction of these bases and the Lewis acidic ionic liquids was observed, which resulted in the formation of a solid, suggesting that a reaction between acid and base had occurred. The ^{11}B NMR spectra of the reaction products indicated a change to the boron environment. In all cases, a broad peak centred around 45 ppm for $[\text{BCl}_2(\text{mim})][\text{Al}_2\text{Cl}_7]$ (Figure 83a), indicating a tricoordinate boron centre, was replaced by a narrow peak at around 0-10 ppm suggesting coordination at the boron centre to the basic group and a tetrahedral species forming (Figure 83 b-e).

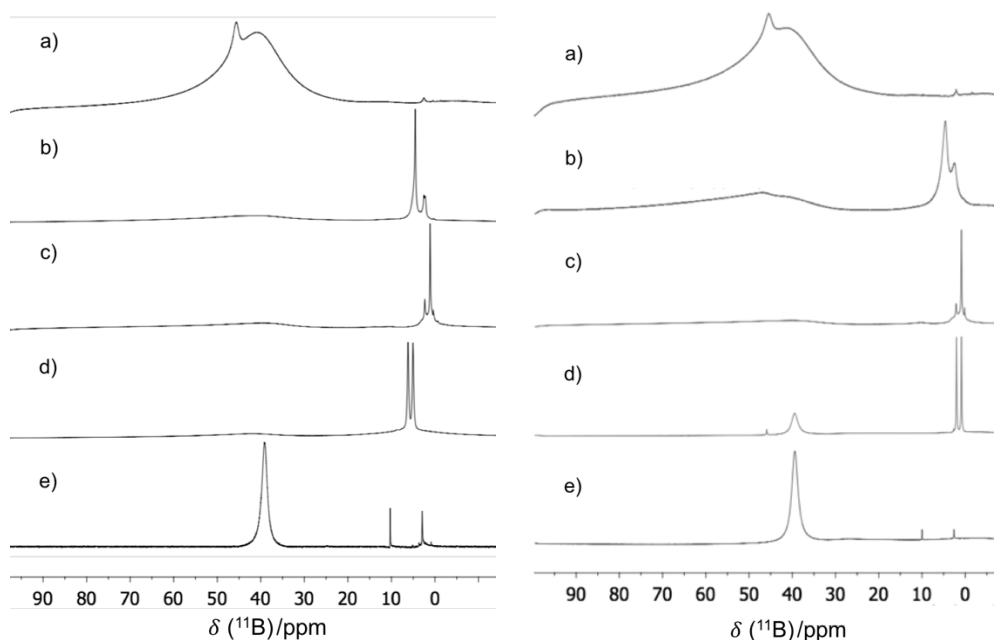


Figure 83. Comparison of ^{11}B NMR spectra illustrating the change of boron environment from a) $[\text{BCl}_2(\text{mim})][\text{M}_2\text{Cl}_7]$ on the addition of a 0.5 mol equivalents of a base b) diisopropyl ethylamine, c) tetramethyl piperidine, d) triphenyl phosphine and e) 0.1 mol equivalents of proton sponge. (left $\text{M} = \text{Al}$; right $\text{M} = \text{Ga}$)

In addition to the highly acidic borenium cations, dinuclear chlorometallate anions, $[\text{M}_2\text{Cl}_7]^-$ are strong Lewis acids in their own right. The interaction between a base and a chloroaluminate anion were monitored by ^{27}Al NMR spectroscopy (Figure 84).

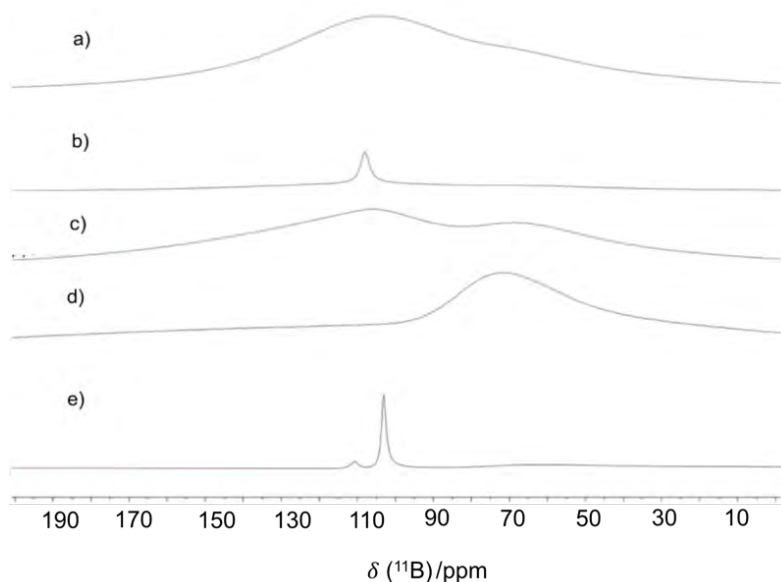


Figure 84. Comparison of ^{27}Al NMR spectra illustrating the change of boron environment from a) neat $[\text{BCl}_2(\text{mim})][\text{Al}_2\text{Cl}_7]$ upon the addition of a 0.5 mol equivalents of a base b) diisopropyl ethylamine, c) tetramethyl piperidine, d) triphenyl phosphine and e) 0.1 mol equivalents of proton sponge.

The starting material, $[\text{BCl}_2(\text{mim})][\text{Al}_2\text{Cl}_7]$, was represented by a broad peak centred around 107.4 ppm, which represents equilibrated species $[\text{AlCl}_4]^-$, $[\text{Al}_2\text{Cl}_7]^-$ and $[\text{AlCl}_3(\text{mim})]$, with a shoulder at 74.5 ppm, which represents the pentacoordinate complexes $[\text{AlCl}_3\text{L}_2]$ and $[\text{AlCl}_2\text{L}_2]^+$ (Figure 84a).⁴ The emergence of sharp peaks in the spectra at around 105 ppm, for the samples containing the proton sponge and the diisopropyl ethylamine (Figure 84b and e), indicated higher symmetry, which likely implies an increase in $[\text{AlCl}_4]^-$ concentration, and therefore that the Lewis base is reacting with the Lewis acidic anion. For the spectra arising from combination with tetramethyl piperidine and triphenyl phosphine (Figure 84c and d) a shift from the starting material is evident with an increase in both spectra of the peak centred around 75 ppm. This indicates a decrease in the concentration of the Lewis acidic anion $[\text{Al}_2\text{Cl}_7]^-$, suggesting that it reacts with the basic N-donors.

For the system containing triphenyl phosphine more data is available from ^{31}P NMR spectrum, which showed a quartet from the interaction between the phosphorus centre and the ^{11}B nucleus, where $I = 3/2$ (Figure 85). This has a coupling constant of $^2J_{\text{P-B}} = 147.2$ Hz, which corresponds to the doublet in the ^{11}B NMR spectrum, this frequency is in the region expected for a boron-phosphine interaction.¹⁹⁹

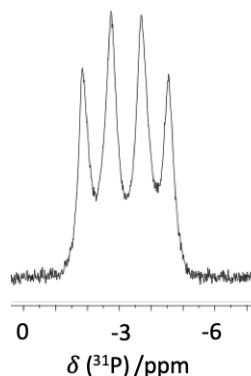
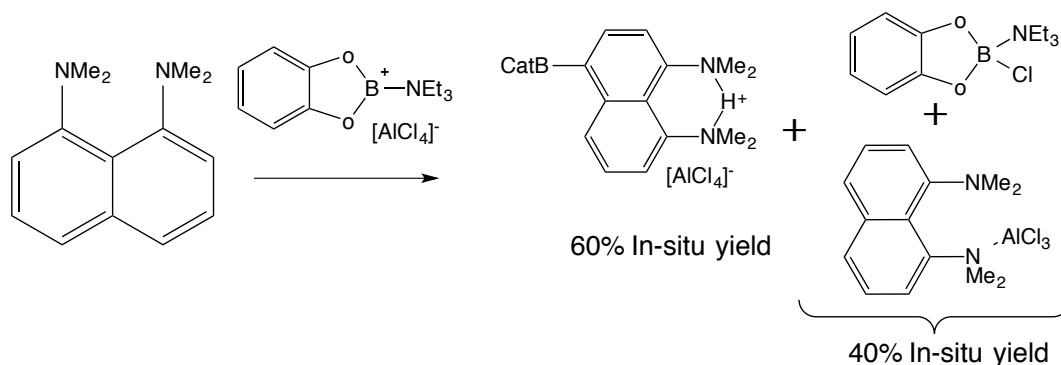


Figure 85. The ^{31}P spectrum of $[\text{BCl}_2(\text{mim})][\text{Al}_2\text{Cl}_7]$ with PPh_3 .

Unlike the other bases trialled, the combination of $[\text{BCl}_2(\text{mim})][\text{M}_2\text{Cl}_7]$ to the proton sponge did not dissolve easily into the ionic liquid, as such the concentration of base was reduced to 0.1 molar equivalents. Interestingly, the ^{11}B NMR spectrum from this reaction shows a sharp peak at 45 ppm, indicating a tricoordinate boron species (Figure 83e). The nature of the interaction is likely to result from aryl borylation. In a similar work, Solomon *et al.* have demonstrated that the para-carbon on the proton sponge is a site of electrophilic attack by boron and that aluminium trichloride coordinates to an amine on the proton sponge (Scheme 28).⁷²

Scheme 28. The products observed in-situ from the reaction of 1,8-Bis(dimethylamino)naphthalene with a catechol borenium (Bcat) with a triethyl amine adduct.(Adapted from ⁷²)



This work helps to explain our observations that 1,8-bis(dimethylamino)naphthalene, marketed as a base reactive only to protons, reacted with [BCl₂mim][Al₂Cl₇], which was observed by a narrowing of the ²⁷Al spectrum indicating a symmetrical environment representing [AlCl₄]⁻. The borenium cation [BCl₂(mim)]⁺ in these reactions is significantly less hindered than the catechol borenium which suggests that the boron may be able to attack both the para-carbon and coordinate to the amine group (Scheme 28). This is supported by the presence of two tetracoordinate peaks in the ¹¹B NMR spectrum. This is an interesting finding because the proton sponge is an incredibly hindered base, in fact it is so named because only protons are expected to be able small enough to interact with the lone pair on the nitrogen (Figure 82 bottom right).

In conclusion, these initial studies into the potential for using the reported borenium ionic liquids in frustrated Lewis pair chemistry have demonstrated that they are not suitable as the Lewis acidic components of FLPs. Owing to the equilibrium between different species in the ionic liquid and a lack of steric hindrance around the boron centre triethylamine, tri-tert-butylphosphine and N,N-diisopropylethylamine reacted with both the anion and cation of borenium ionic liquids; even the sterically hindered proton sponge reacted with the borenium ionic liquid. This provided a strong motivation to develop more sterically hindered systems, combining components which are known to be FLPs capable of H₂ activation, and modify them to form ionic liquids.

5.4.2 Second Generation Borenium Ionic Liquids as FLP Components

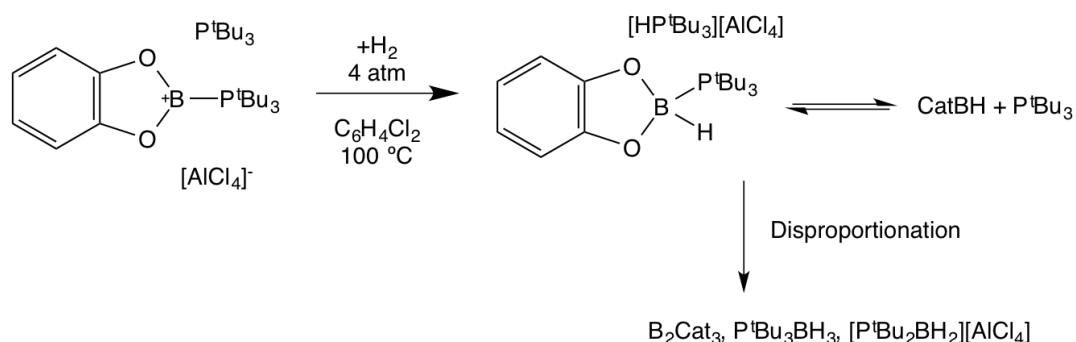
5.4.2.1 Ionic Liquids with Chlorometallate Anions as FLP Components

Development of the second generation borenium ionic liquids (Chapter 3) was targeting compounds without halometallate anions, minimised degree to which dynamic equilibria

could form, and increased control to limit the number of non-equivalent Lewis acidic species. These were designed with the view to an application as components of FLP catalysts. Work by Dureen *et al.* in 2008 first postulated the use of a catechol borenium with a bulky phosphine in FLP chemistry, with the bulky phosphine activating the B-H bond of the catechol borane, with the anion $[\text{HB}(\text{C}_6\text{F}_5)_3]^-$ forming along with a boron-phosphorus cation.¹⁸⁸ In this work they also investigated the nature of the boron-phosphorus interaction in the context of the formal positioning of the positive charge suggesting that while it can be viewed as a borenium cation, DFT data suggests there is a significant boryl-phosphonium nature to the interaction.

Despite this boryl-phosphonium nature, these species are described as borenium cations in work by Del Grosso *et al.*¹⁸⁹ Subsequently, Solomon *et al.* broadened the scope of catechol borenium cations to include trimethyl phosphine and tri-*tert*-butyl phosphine with $[\text{AlCl}_4]^-$ anions.⁷² The target of these papers was to generate new catalysts for arene borylation. However, the potential of these borenium catalysts as bulky Lewis acids in FLP did not go unnoticed and subsequent work from Clark *et al.* used the previously characterised $[\text{Bcat}(\text{P}^t\text{Bu}_3)][\text{AlCl}_4]$, in combination with an additional molar equivalent of tri-*tert*-butyl phosphine to activate H_2 .¹⁹⁰ This demonstrates the successful cleavage of the H-H bond (Scheme 29). This reaction proceeds at 100 °C under 4 atmospheres of H_2 . Under these relatively harsh conditions, after 72 h the products disproportionate (Scheme 29).

Scheme 29. The activation of H_2 by $[\text{CatB}(\text{P}^t\text{Bu}_3)][\text{AlCl}_4]/\text{P}^t\text{Bu}_3$ and the subsequent equilibrium which forms and the products of disproportionation. (Adapted from¹⁹⁰)



As a bridge between creating FLP systems with the ionic liquids synthesised in Chapter 3, this work began by combining the cation from the work by Clark *et al.* with higher molar ratio of metal chlorides, to form oligomeric anions.¹⁹⁰ The intention behind this development was to form a liquid Lewis acid to which P^tBu_3 could be added, in order to form an ionic liquid FLP. The cation precursor was synthesised as described in Section 3.1.5. Subsequently, the precursor was reacted, under solventless conditions, with aluminium chloride. Initially one equivalent of AlCl_3 was used, in line with the literature report, before synthesising a second

sample with 2 mol eq. of AlCl_3 . Both the starting materials and the product were analysed by multinuclear NMR spectroscopy.

In the ^{11}B NMR spectra, the spectrum of $[\text{BcatCl}(\text{P}^t\text{Bu}_3)]$ featured one signal at 12.88 ppm, corresponding to the tetracoordinate adduct (Figure 86a). Following the addition of equimolar amount of AlCl_3 , two major peaks were recorded (Figure 86b), at 29 ppm, which represents $[\text{Bcat}(\text{P}^t\text{Bu}_3)]^+$ and 21 ppm, which may represent $[\text{Bcat}(\text{AlCl}_3)]$. Finally, when two equivalents of AlCl_3 were added, the ^{11}B NMR spectrum featured just one major peak at 29 ppm, which represents $[\text{Bcat}(\text{P}^t\text{Bu}_3)]^+$ (Figure 86c).

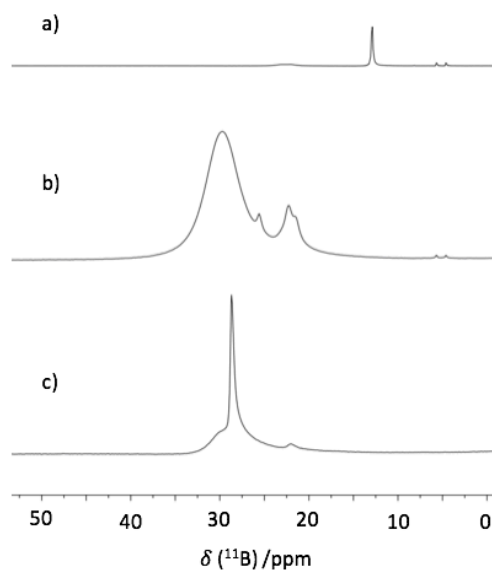


Figure 86. ^{11}B NMR spectra (in benzene) showing the effect of increasing concentration of metal halide on the system $[\text{BcatCl}(\text{P}^t\text{Bu}_3)]$ where a) $\chi_{\text{AlCl}_3} = 0$, b) $\chi_{\text{AlCl}_3} = 0.5$ and a) $\chi_{\text{AlCl}_3} = 0.67$.

In corroborating results, ^{31}P NMR spectrum of $[\text{BcatCl}(\text{P}^t\text{Bu}_3)]$ featured one signal at 19.7 ppm, corresponding to the adduct (Figure 87a). Upon the addition of either quantity of aluminium chloride, the only additional peak to appear was at 58 ppm, which represents free P^tBu_3 (Figure 87b and c), suggesting that there is no adduct formation between $[\text{Al}_2\text{Cl}_7]^-$ and P^tBu_3 .

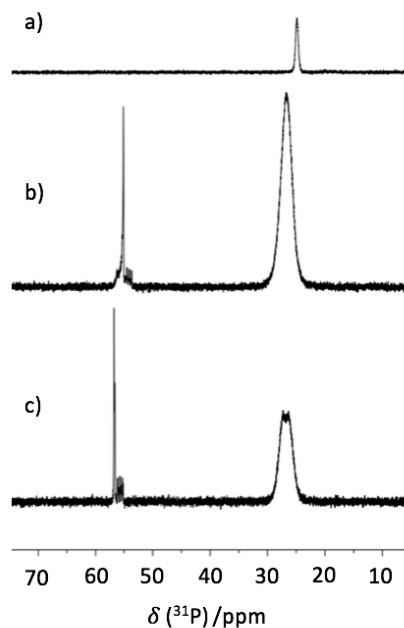
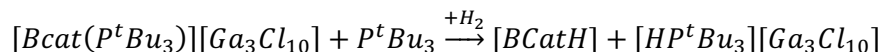


Figure 87. ^{31}P NMR spectra (in benzene) showing the effect of increasing concentration of metal halide on the system $[\text{BcatCl}(\text{P}^t\text{Bu}_3)]$ where a) $\chi_{\text{AlCl}_3} = 0$, b) $\chi_{\text{AlCl}_3} = 0.5$ and a) $\chi_{\text{AlCl}_3} = 0.67$.

Although NMR spectroscopy showed the formation of ionic species, the melting point of the compositions was not low enough to measure them as neat liquids, nor use them as liquid catalysts.

As outlined in Section 3.3.1 the system with three equivalents of gallium trichloride generated a room temperature liquid, featuring the oligomeric anion $[\text{Ga}_3\text{Cl}_{10}]^-$. To this liquid the addition of an additional equivalent of P^tBu_3 resulted in a more viscous homogeneous liquid forming (Scheme 30 left). This system $[\text{BCat}(\text{P}^t\text{Bu}_3)][\text{Ga}_3\text{Cl}_{10}]/\text{P}^t\text{Bu}_3$ represents the ionic liquid equivalent of the previously reported $[\text{BCat}(\text{P}^t\text{Bu}_3)][\text{AlCl}_4]/\text{P}^t\text{Bu}_3$ FLP. This ionic liquid was reacted with hydrogen, following the procedure described in Section 5.3. Rather than heating to $100\text{ }^\circ\text{C}$, a temperature at which was reported to result in disproportionation, the reaction mixture was maintained at $60\text{ }^\circ\text{C}$ overnight (Equation 62).

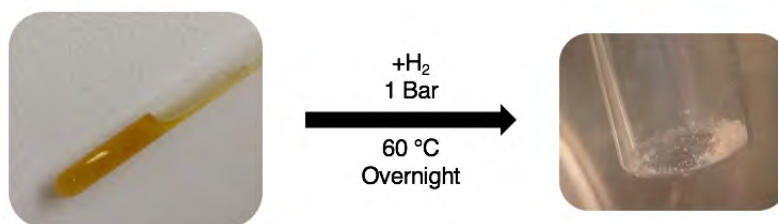


Equation 62

The reduced temperature was used to minimise the risk of disproportionation, which results from high temperatures as described in Section 3.2 with the formation of B_2Cat_3 . The influence of the ionic liquid on this activity at lower temperatures has not been established as the reaction is only reported as run at room temperature, where there was no reactivity, and at $100\text{ }^\circ\text{C}$, which induced disproportionation.¹⁹⁰

The appearance of the product before and after reaction with H₂ changed from a golden, viscous liquid, to a solid crystalline material (Scheme 30), which was assumed to be the result of salt formation, as outlined in (Equation 62). As confirmation that this change was the result of H₂ activation the same composition was heated overnight at 60 °C and no change in physical appearance was observed.

Scheme 30. The appearance before and after hydrogen activation of [Bcat(P^tBu₃)] [Ga₃Cl₁₀]/ P^tBu₃.



NMR spectra of the product were recorded as benzene solutions, rather than as a neat ionic liquid. From the ¹H NMR spectrum (Figure 88), two prominent additional peaks are observed which represent the splitting of H₂, these peaks at 5.2 ppm and 4.1 ppm correspond well to the peaks which appeared in the original work by Clark *et al.* at 5.4 ppm and 4.3 ppm.¹⁹⁰

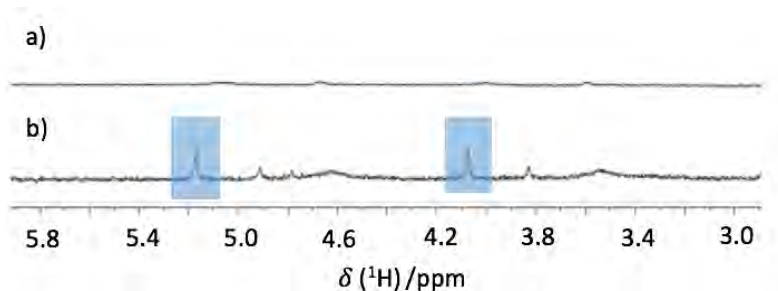


Figure 88. ¹H NMR spectra showing the effect of adding H₂ to [Bcat(P^tBu₃)] [Ga₃Cl₁₀]/ P^tBu₃, where a) is before exposure to H₂ and b) is following H₂ exposure.

This preliminary work provided the confirmation that a borenium ionic liquid is capable of acting as neat, liquid frustrated Lewis pair. It was the first known example of an ionic liquid acting as an FLP in H₂ activation.

5.4.2.2 Ionic Liquids with Chloride-Free Anions as FLP Components

In line with the arguments presented in Chapter 3, the next stage was developing ionic liquid FLPs which did not contain any chloride anions. The ionic liquid [Bcat(P₈₈₈)] [NTf₂], synthesised as described in Section 3.3.2.2.5, was investigated as an ionic liquid FLP for the activation of H₂. This ionic liquid was selected because it was a room temperature liquid, with

the long chained octyl groups suppressing its melting point, and the borenium species were present even at room temperature.

The combination of $[\text{Bcat}(\text{P}_{888})][\text{NTf}_2]$ with an equivalent of P^tBu_3 produced a viscous liquid (Figure 89).



Figure 89. The liquid $[\text{Bcat}(\text{P}_{888})][\text{NTf}_2]$ with one equivalent of P^tBu_3

The ^{11}B NMR spectrum of this mixture (Figure 90a and b) suggested that the additional phosphine formed a tetracoordinate, cationic adduct with boron. This is seen in the loss of the tri-coordinate $[\text{Bcat}(\text{P}_{888})]^+$ peak at 23 ppm and a growth in the tetracoordinate peak at 9.93 ppm and another at 1.69 ppm (Figure 90b), resulting in only two peaks, both of which are doublets with coupling constants of 166 and 152 Hz respectively which are consistent with boron-phosphine interactions.¹⁹⁹ Therefore, any reactivity of this system may be regarded as a masked frustrated Lewis pair, which is to say that the acidic and basic components form a complex which is weakly bound and was expected to readily react with H_2 . From the ^{31}P NMR spectra (Figure 90c and d) the P^tBu_3 is represented by a broad peak around 49.7 ppm which suggests that some phosphine is interacting with the catechol borane species. This broad peak has a shoulder at 54.0 ppm which represents free phosphine. The peaks at 30.6, -12.5 and -3.7 ppm represent trioctylphosphine (Section 3.3.2.2.5), the sharp peak at 30.6 ppm has been assigned to the complex $[\text{BcatP}_{888}]^+$, while a tricoordinate peak is not visible in the ^{11}B NMR spectrum it has been seen through Section 3.3.2 that these species can be visible in the ^{31}P NMR spectrum while not so easily resolved from the baseline in the ^{11}B NMR spectrum and only revealed by increasing temperatures VT NMR spectroscopy. The peak at -12.5 ppm represents $[\text{Bcat}(\text{NTf}_2)(\text{P}_{888})]$ (Section 3.3.2.2.5) and the additional peak at -3.7 ppm is assigned to $[\text{Bcat}(\text{P}_{888})(\text{P}^t\text{Bu}_3)]$ with this additionally accounting for the peak at 49.7 ppm.

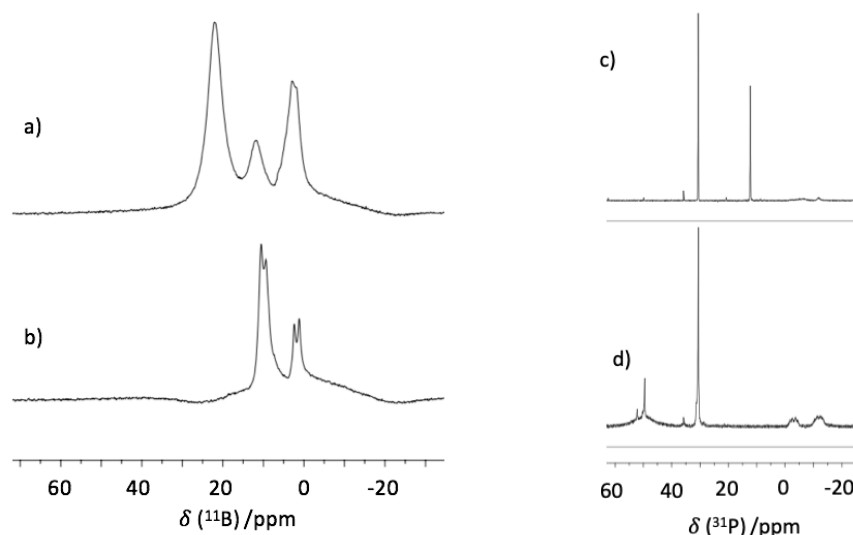
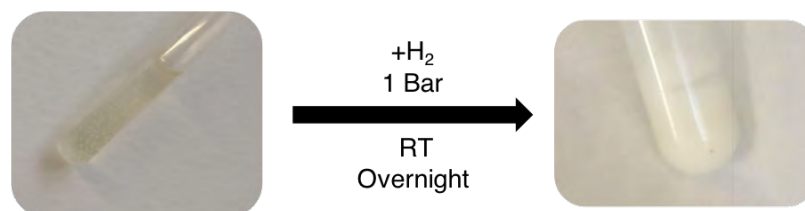


Figure 90. ^{11}B NMR spectra of a) the Lewis acidic ionic liquid $[\text{Bcat}(\text{P}_{888})][\text{NTf}_2]$ and b) $[\text{Bcat}(\text{P}_{888})][\text{NTf}_2]$ with 1 eq. of P^tBu_3 and ^{31}P NMR spectra of c) the Lewis acidic ionic liquid $[\text{Bcat}(\text{P}_{888})][\text{NTf}_2]$ and d) $[\text{Bcat}(\text{P}_{888})][\text{NTf}_2]$ with 1 eq. of P^tBu_3

The sample of $[\text{Bcat}(\text{NTf}_2)(\text{P}_{888})]/\text{P}^t\text{Bu}_3$ was reacted with H_2 in the same manner as the previous samples, described in Section 5.3, but at room temperature (Scheme 31).

Scheme 31. The appearance before and after hydrogen activation of $[\text{Bcat}(\text{P}_{888})(\text{P}^t\text{Bu}_3)][\text{NTf}_2]$



The product was very viscous and it was not possible to record neat NMR spectra. Instead, multinuclear NMR studies were carried out on benzene solutions. Therefore, in the subsequent spectra of the ionic liquid and salt (Figure 91), both samples were dissolved in benzene to make comparison clearer and to illustrate the lack of interaction between benzene and the ionic liquid. The ^1H NMR spectrum illustrates the splitting of H_2 through the emergence of two new peaks with equal splitting in at 5.6 ppm and 6.4 ppm which are reasonably more deshielded than those peaks reported for the system $[\text{Bcat}(\text{P}^t\text{Bu}_3)][\text{Ga}_3\text{Cl}_{10}]/\text{P}^t\text{Bu}_3$.

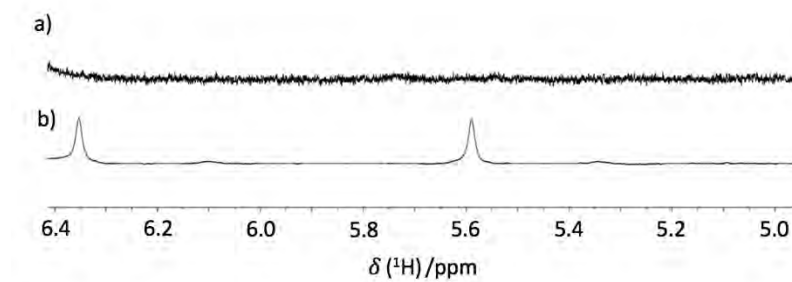


Figure 91. ^1H NMR spectra in C_6D_6 of a) the Lewis acidic ionic liquid $[\text{Bcat}(\text{P}_{888})][\text{NTf}_2]$ with 1 eq. of P^tBu_3 and b) the sample following exposure the 1 bar of H_2 overnight.

The presence of these ^1H NMR peaks demonstrates the capability of the $[\text{Bcat}(\text{P}_{888})][\text{NTf}_2]/\text{P}^t\text{Bu}_3$ system to split H_2 . This can also be determined from the ^{31}P NMR spectra of the solutions, the coordination of both phosphines to boron were previously reported in this thesis at 31 ppm and 49 ppm (Section 3.3.2.2) and these are both observed in the spectra before it is introduced to hydrogen (Figure 92). However, following the addition of hydrogen, an additional peak appeared at 53 ppm, which has been previously described by Clark *et al.* to correspond to $[\text{HP}^t\text{Bu}_3]^+$.¹⁹⁰

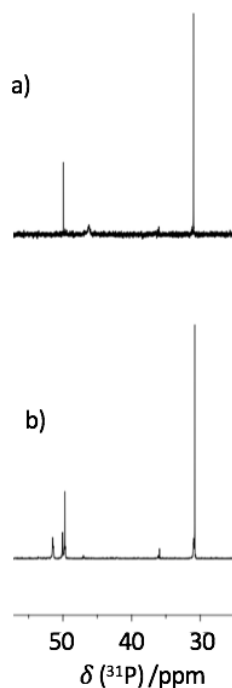


Figure 92. ^{31}P NMR spectra in C_6D_6 showing a) the Lewis acidic ionic liquid $[\text{Bcat}(\text{P}_{888})][\text{NTf}_2]$ with 1 eq. of P^tBu_3 and b) the sample following exposure the 1 bar of H_2 overnight.

It would be worthwhile attempting in future work whether the H_2 can be removed from the system under vacuum with or without heating to establish the reversibility of this reaction. If the H_2 is removable that would suggest that there is potential for this ionic liquid FLP to act as a catalyst to reduction reactions

5.5 Conclusions

This chapter outlined the first report of ionic liquid used as a frustrated Lewis pair to split H_2 molecule. Their function as a solvent has been illustrated by using an off-the-shelf ionic liquid, $[C_{10}mim][NTf_2]$, and finding that concentrations of 160 mmol, greater than those typically used in the literature in molecular solvents, could be achieved. Further to this, through heteronuclear NMR spectroscopy additional, unexpected peaks were observed and assigned to the elusive encounter complex.⁵ In molecular solvents interactions between BCF and P^tBu_3 have not been observed in 1D NMR spectroscopy, however the multidomain network of ionic liquids on a molecular scale means that the lifetime of encounter complexes is extended. This work was concluded by demonstrating the identical capability of hydrogen splitting by the BCF/ P^tBu_3 FLP in benzene and $[C_{10}mim][NTf_2]$.

The borenium family of ionic liquids with a general formula of $[BX_2L][M_2Cl_7]$ were combined with soluble and sterically hindered bases to test their suitability as liquid Lewis acids for FLP chemistry. It was determined that the boron centre was not hindered enough to avoid adduct formation and in addition the presence of a Lewis acidic anion offered a secondary route to adduct formation.

Further work then aimed at taking a known FLP system, $[Bcat(P^tBu_3)][AlCl_4]/P^tBu_3$, and converting it into an ionic liquid. This was achieved by using the $[Ga_3Cl_{10}]^-$ anion and splitting of H_2 identical to that in $C_6H_4Cl_2$ was observed using the system $[Bcat(P^tBu_3)][Ga_3Cl_{10}]/P^tBu_3$. This demonstrated an ionic liquid with a dual role as a liquid Lewis acid and solvent in an FLP mediated H_2 activation.

The final step of this work was to use the borenium ionic liquids generated in Chapter 3 which have a non-Lewis acidic anion and a bidentate ligand to avoid dynamic equilibria. The ionic liquid $[Bcat(P_{888})][NTf_2]$ was combined with one equivalent of P^tBu_3 and it was observed to activate hydrogen. This demonstrates the potential of designer ionic liquids in FLP catalysis and potentially paves the way for their application in catalytic reactions.

6 SUMMARY AND CONCLUSIONS

The work discussed in this thesis has covered synthesising new liquid Lewis acids and their characterisation, a study on the fundamental behaviour of FLP systems in molecular solvents and ionic liquids and the development of borenium ionic liquid FLPs.

The work on LCCs investigated the potential of using different metal halides aluminium chloride, gallium chloride, indium chloride, antimony chloride, tin(II) chloride, tin(IV) chloride, titanium chloride, zinc chloride in combination with the ligands trioctylphosphine and trioctylphosphine oxide. These ligands allowed for the comparison of species present in each composition through ^{31}P NMR spectroscopy where the metal nucleus could not be studied by NMR spectroscopy. Compositions were synthesised with increasing concentrations of metal halide until the liquid was no longer heterogeneous and comparing results to previously reported crystal structures dimeric and oligomeric metal halide species were identified. The Lewis acidities of metal halides were measured and was found to decrease in the order $\text{TiCl}_4 > \text{SbCl}_5 > \text{AlCl}_3 > \text{SnCl}_4 > \text{GaCl}_3 \approx \text{InCl}_3 \approx \text{SnCl}_2 > \text{ZnCl}_2 > \text{SbCl}_3$. The Lewis acidities of LCCs were also measured and they gave equal or greater ANs than their equivalent metal halide. The Gutmann ANs recorded showed a range of values between 60 – 110 with compositions where oligomeric $[\text{Ga}_3\text{Cl}_{10}]^-$ formed, where $\chi_{\text{GaCl}_3} > 0.60$, and TiCl_4 compositions being superacidic.

Borenium ionic liquids were synthesised with chloride-free anions, triflate and bistriflimide, to make less corrosive Lewis acidic catalysts. These liquids showed an increase in tricoordinate species on heating the samples in heteronuclear NMR spectroscopy. These products remained in a dynamic equilibrium with tri-coordinate species where either the ligand, triflate or bistriflimide was coordinated to the boron centre, however unlike chlorometallate ionic liquids none of the additional species were volatile or Lewis acidic. Gutmann acceptor number measurements confirmed the high acidity of these liquids with values around 100.

The synthesis of deuterated trimesityl phosphine and tri-*tert*-butyl phosphine *via* Grignard intermediates was detailed, with moderate yields reported for both products. These were synthesised for use in neutron scattering experiments on FLP systems to increase contrast to improve the quality of the data. The neutron scattering data from mixtures of BCF/ P^tBu_3 at a high concentration demonstrated the formation of a solvent separated encounter complex which had been previously observed in DFT studies. This suggested that approximately 5% of molecules were in the encounter complex with a B-P distance of 8 Å.

The final section of this work addressed the combination of ionic liquids and FLPs. Firstly the FLP system BCF/ P^tBu_3 at a high concentration in $[C_{10}mim][NTf_2]$ was demonstrated to promote the lifetime of encounter complexes. The complexes were detectable in heteronuclear NMR spectroscopy which suggested that up to 20% of molecules were in the reactive encounter complex formation at any one time. The reactivity of the FLP system in $[C_{10}mim][NTf_2]$ was found to be identical to that in benzene. Having demonstrated the strengths of ionic liquids as solvents for FLPs the next phase of work focused on developing Lewis acidic ionic liquids for use as solvent and FLP component. In this work it was demonstrated that by forming an IL based upon $[Bcat(P^tBu_3)][AlCl_4]/P^tBu_3$, by exchanging the anion for three equivalents of gallium trichloride, reactivity was maintained and a lower temperature was required. Following work from Chapter 3, this system was modified to be chloride free with the use of a bistriflimide anion. The ionic liquid $[Bcat(P_{888})][NTf_2]$ was combined with P^tBu_3 and was demonstrated to activate H_2 . This is the first known example of an ionic liquid acting as a solvent and Lewis acid in FLP mediated H_2 activation.

7 BIBLIOGRAPHY

- 1 L. C. Brown, J. M. Hogg and M. Swadźba-Kwaśny, *Topics in Current Chemistry*, 2017, **375**, 1–40.
- 2 F. Coleman, G. Srinivasan and M. Swadźba-Kwaśny, *Angew. Chem. Int. Ed.*, 2013, **52**, 12582–12586.
- 3 J. M. Hogg, L. C. Brown, K. Matuszek, P. Latos, A. Chrobok and M. Swadźba-Kwaśny, *Dalton Transactions*, 2017, **46**, 11561–11574.
- 4 S. Coffie, J. M. Hogg, L. Cailler, A. Ferrer-Ugalde, R. W. Murphy, J. D. Holbrey, F. Coleman and M. Swadźba-Kwaśny, *Angew. Chem.*, 2015, **127**, 15183–15186.
- 5 L. C. Brown, J. M. Hogg, M. Gilmore, L. Moura, S. Imberti, S. Gärtner, H. Q. N. Gunaratne, R. J. O'Donnell, N. Artioli, J. D. Holbrey and M. Swadźba-Kwaśny, *Chem. Commun.*, 2018, **54**, 8689–8692.
- 6 I. Bakó, A. Stirling, S. Bálint and I. Pápai, *Dalton Trans.*, 2012, **41**, 9029–4.
- 7 R. M. Pagni, *Foundations of Chemistry*, 2009, **11**, 43–50.
- 8 N. Hall, *J. Chem. Educ.*, 1940, **17**, 124–128.
- 9 A. F. O. Germann, *J. Am. Chem. Soc.*, 1925, **47**, 2461–2468.
- 10 S.-H. Paik, *J. Chem. Educ.*, 2015, **92**, 1484–1489.
- 11 G. N. Lewis, *Valence and the Structure of Atoms and Molecules*, Chemical Catalog Company, Incorporated, 1923.
- 12 G. N. Lewis, *Journal of the Franklin Institute*, 1938, **226**, 293–313.
- 13 R. G. Pearson, *J. Am. Chem. Soc.*, 1963, **85**, 3533–3539.
- 14 R. G. Pearson, *J. Chem. Educ.*, 1968, **45**, 581–587.
- 15 R. G. Pearson, *J. Chem. Educ.*, 1968, **45**, 643–648.
- 16 B. D. Rowsell, R. J. Gillespie and G. L. Heard, *Inorg. Chem.*, 1999, **38**, 4659–4662.
- 17 V. Gutmann, *Electrochimica Acta*, 1976, **21**, 661.
- 18 V. Gutmann, *Pure and Applied Chemistry*, 1979, **51**, 21987–22210.
- 19 T. A. Zawodzinski and R. A. Osteryoung, *Inorg. Chem.*, 1989, **28**, 1710–1715.
- 20 I. C. Quarmby and R. A. Osteryoung, *J. Am. Chem. Soc.*, 1994, **116**, 2649–2650.
- 21 J. Estager, A. A. Oliferenko, K. R. Seddon and M. Swadźba-Kwaśny, *Dalton Trans.*, 2010, **39**, 11375–8.
- 22 V. Gutmann, *Pure and Applied Chemistry*, 1971, **27**, 73–88.
- 23 M. H. Holthausen, M. Mehta and D. W. Stephan, *Angew. Chem. Int. Ed.*, 2014, **53**, 6538–6541.
- 24 G. J. P. Britovsek, J. Ugoletti and A. J. P. White, *Organometallics*, 2005, **24**, 1685–1691.

- 25 M. A. Beckett, G. C. Strickland, J. R. Holland and K. Sukumar Varma, *Polymer*, 1996, **37**, 4629–4631.
- 26 I. B. Sivaev and V. I. Bregadze, *Coordination Chemistry Reviews*, 2013, 1–14.
- 27 G. C. Welch, L. Cabrera, P. A. Chase, E. Hollink, J. D. Masuda, P. Wei and D. W. Stephan, *Dalton Trans.*, 2007, **75**, 3407–9.
- 28 H. Großekappenberg, M. Reißmann, M. Schmidtman and T. Müller, *Organometallics*, 2015, **34**, 4952–4958.
- 29 R. F. Childs, D. L. Mulholland and A. Nixon, *Canadian Journal of Chemistry*, 1982, **60**, 801–808.
- 30 Y.-L. Yang and Y. Kou, *Chem. Commun.*, 2004, 226–2.
- 31 C. Morterra, G. Cerrato, V. Bolis, S. Di Ciero and M. Signoretto, *Faraday Trans.*, 1997, **93**, 1179–1184.
- 32 E. P. Parry, *Journal of Catalysis*, 1963, **2**, 371–379.
- 33 J. C. Haartz and D. H. McDaniel, *J. Am. Chem. Soc.*, 1973, **95**, 8562–8565.
- 34 J. L. Bills and F. A. Cotton, *J. Phys. Chem.*, 1960, **64**, 1477–1479.
- 35 T. E. Mallouk, G. L. Rosenthal, G. Müller, R. Brusasco and N. Bartlett, *Inorg. Chem.*, 1984, **23**, 3167–3173.
- 36 L. O. Müller, D. Himmel, J. Stauffer, G. Steinfeld, J. Slattery, G. Santiso-Quiñones, V. Brecht and I. Krossing, *Angew. Chem. Int. Ed.*, 2008, **47**, 7659–7663.
- 37 M. J. Frisch, G. W. Trucks, H. B. Schlegel, P. Gill, B. G. Johnson, M. A. Robb, J. R. Cheeseman, T. Keith, G. A. Petersson and J. A. Montgomery, *Gaussian*, 1995, Revision B. 2.
- 38 M. J. Frisch, G. W. Trucks, H. B. Schlegel, G. E. Scuseria, M. A. Robb, J. R. Cheeseman, V. G. Zakrzewski, J. A. Montgomery Jr, R. E. Stratmann and J. C. Burant, *Gaussian*, 1998, Revision A.7.
- 39 C. G. Krespan and D. A. Dixon, *Journal of Fluorine Chemistry*, 1996, **77**, 117–126.
- 40 K. O. Christe, D. A. Dixon, D. McLemore, W. W. Wilson, J. A. Sheehy and J. A. Boatz, *Journal of Fluorine Chemistry*, 2000, **101**, 151–153.
- 41 C. H. Rochester, *Acidity functions*, Academic Press, 1970, vol. 17.
- 42 G. A. Olah, G. K. S. Prakash and J. Sommer, *Science*, 1979, **206**, 13–20.
- 43 Y. Hayashi, J. J. Rohde and E. J. Corey, *J. Am. Chem. Soc.*, 1996, **118**, 5502–5503.
- 44 A. Hasegawa, K. Ishihara and H. Yamamoto, *Angew. Chem. Int. Ed.*, 2003, **42**, 5731–5733.
- 45 S. Antonietti, V. Dalla and E. Duñach, *Angew. Chem. Int. Ed.*, 2010, **49**, 7860–7888.
- 46 U. Mayer, W. Gerger and V. Gutmann, *Monatshefte Fur Chemie*, 1975, **106**, 1235–1257.

- 47 D. C. Apperley, C. Hardacre, P. Licence, R. W. Murphy, N. V. Plechkova, K. R. Seddon, G. Srinivasan, M. Swadźba-Kwaśny and I. J. Villar-Garcia, *Dalton Trans.*, 2010, **39**, 8679–9.
- 48 N. N. Greenwood and A. Earnshaw, in *Chemistry of the Elements (Second Edition)*, Butterworth-Heinemann, Oxford, 1997, pp. 216–267.
- 49 N. N. Greenwood and A. Earnshaw, in *Chemistry of the Elements (Second Edition)*, Butterworth-Heinemann, Oxford, 1997, pp. 139–215.
- 50 E. L. Muetterties, *The Chemistry of Boron and Its Compounds*, Wiley, New York, 1967.
- 51 H. C. Brown and R. R. Holmes, *J. Am. Chem. Soc.*, 1956, **78**, 2173–2176.
- 52 T. Brinck, J. S. Murray and P. Politzer, *Inorg. Chem.*, 1993, **32**, 2622–2625.
- 53 P. Politzer, J. Huheey, J. S. Murray and M. Grodzicki, *J. Mol. Struct. Thermochem.*, 1992, **259**, 99–120.
- 54 W. Dilthey, F. Eduardoff and F. J. Schumacher, *Justus Liebigs Ann. Chem.*, 1906, **344**, 300–313.
- 55 P. Koelle, P. Kölle, H. Noeth and H. Nöth, *Chem. Rev.*, 1985, **85**, 399–418.
- 56 O. P. Shitov, S. L. Ioffe, V. A. Tartakovskii and S. S. Novikov, *Russ. Chem. Rev.*, 1970, **39**, 905–922.
- 57 W. E. Piers, S. C. Bourke and K. D. Conroy, *Angew. Chem. Int. Ed.*, 2005, **44**, 5016–5036.
- 58 J. Higashi, A. Eastman and R. W. Parry, *Inorg. Chem.*, 1982, **21**, 716–720.
- 59 C. J. Major, K. L. Bamford, Z.-W. Qu and D. W. Stephan, *Chem. Commun.*, 2019, **117**, 5142–4.
- 60 Y. Shoji, N. Tanaka, K. Mikami, M. Uchiyama and T. Fukushima, *Nature Chemistry*, 2014, **6**, 498–503.
- 61 C.-W. Chiu and F. P. Gabbaï, *Organometallics*, 2008, **27**, 1657–1659.
- 62 T. Matsumoto and F. P. Gabbaï, *Organometallics*, 2009, **28**, 4252–4253.
- 63 S. Courtenay, J. Mutus, R. Schurko and D. W. Stephan, *Angew. Chem. Int. Ed. Engl.*, 2002, **41**, 498–501.
- 64 Y. Shoji, N. Tanaka, D. Hashizume and T. Fukushima, *Chem. Commun.*, 2015, **51**, 13342–13345.
- 65 M. J. Ingleson, in *Synthesis and Application of Organoboron Compounds*, Springer International Publishing, Cham, 2015, vol. 49, pp. 39–71.
- 66 P. A. Fox, S. T. Griffin, W. M. Reichert, E. A. Salter, A. B. Smith, M. D. Tickell, B. F. Wicker, E. A. Cioffi, J. H. Davis Jr, R. D. Rogers and A. Wierzbicki, *Chem. Commun.*, 2005, 3679–3.
- 67 *US Pat.*, US7,709,635B2, 2010

- 68 W. F. Schneider, C. K. Narula, H. Noeth and B. E. Bursten, *Inorg. Chem.*, 1991, **30**, 3919–3927.
- 69 G. E. Ryschkewitsch and J. W. Wiggins, *J. Am. Chem. Soc.*, 1970, **92**, 1790–1791.
- 70 V. Bagutski, A. Del Grosso, J. A. Carrillo, I. A. Cade, M. D. Helm, J. R. Lawson, P. J. Singleton, S. A. Solomon, T. Marcelli and M. J. Ingleson, *J. Am. Chem. Soc.*, 2012, **135**, 474–487.
- 71 H. Nöth, S. Weber, B. Rasthofer, C. K. Narula and A. Konstantinov, *Pure and Applied Chemistry*, 1983, **55**, 1453–1461.
- 72 S. A. Solomon, A. Del Grosso, E. R. Clark, V. Bagutski, J. J. W. McDouall and M. J. Ingleson, *Organometallics*, 2012, **31**, 1908–1916.
- 73 P. Eisenberger, A. M. Bailey and C. M. Crudden, *J. Am. Chem. Soc.*, 2012, **134**, 17384–17387.
- 74 T. S. De Vries, A. Prokofjevs and E. Vedejs, *Chem. Rev.*, 2012, **112**, 4246–4282.
- 75 E. J. Corey, *Angew. Chem. Int. Ed.*, 2009, **48**, 2100–2117.
- 76 C. K. Narula, H. Noeth and H. Nöth, *Inorg. Chem.*, 1985, **24**, 2532–2539.
- 77 A. Cowley, M. Cushner, R. Davis and P. Riley, *Inorg. Chem.*, 1981, **20**, 1179–1181.
- 78 D. P. Gates, R. Ziembinski, A. L. Rheingold, B. S. Haggerty and I. Manners, *Angew. Chem. Int. Ed. Engl.*, 2003, **33**, 2277–2279.
- 79 I. Ghesner, W. E. Piers, M. Parvez and R. McDonald, *Chem. Commun.*, 2005, **85**, 2480–3.
- 80 D. P. Gates, A. R. McWilliams, R. Ziembinski, L. M. Liable-Sands, I. A. Guzei, G. P. A. Yap, A. L. Rheingold and I. Manners, *Chem. Eur. J.*, 1998, **4**, 1489–1503.
- 81 E. Vedejs, T. Nguyen, D. R. Powell and M. R. Schrimpf, *Chem. Commun.*, 1996, 2721–2.
- 82 B. Bentivegna, C. I. Mariani, J. R. Smith, S. Ma, A. L. Rheingold and T. J. Brunker, *Organometallics*, 2014, **33**, 2820–2830.
- 83 M. Brahmi, M. Malacria, D. Curran, L. Fensterbank and E. Lacôte, *Synlett*, 2013, **24**, 1260–1262.
- 84 T. Scherpf, K.-S. Feichtner and V. H. Gessner, *Angew. Chem. Int. Ed.*, 2017, **56**, 3275–3279.
- 85 S. Muthaiah, D. C. H. Do, R. Ganguly and D. Vidović, *Organometallics*, 2013, **32**, 6718–6724.
- 86 P. Walden, *Bull. Russian Acad Sci*, 1914, **8**, 405–422.
- 87 J. Estager, J. D. Holbrey and M. Swadźba-Kwaśny, *Chem. Soc. Rev.*, 2014, **43**, 847–886.
- 88 J. S. Wilkes, *Green Chemistry*, 2002, **4**, 73–80.
- 89 H. C. Brown and H. W. Pearsall, *J. Am. Chem. Soc.*, 1952, **74**, 191–195.

- 90 J. A. Boon, J. A. Levisky, J. L. Pflug and J. S. Wilkes, *J. Org. Chem.*, 1986, **51**, 480–483.
- 91 C. L. Hussey, *Advances in Molten Salt Chemistry*, 1983, **5**, 185–230.
- 92 T. Welton, *Chem. Rev.*, 1999, **99**, 2071–2084.
- 93 P. Nockemann, M. Pellens, K. Van Hecke, L. Van Meervelt, J. Wouters, B. Thijs, E. Vanecht, T. N. Parac-Vogt, H. Mehdi, S. Schaltin, J. Fransaer, S. Zahn, B. Kirchner and K. Binnemans, *Chem. Eur. J.*, 2010, **16**, 1849–1858.
- 94 A. Fannin, D. Floreani, L. King, B. Piersma, D. Stech, R. Vaughn, J. S. Wilkes and J. Williams, *J. Phys. Chem.*, 1984, **88**, 2614–2621.
- 95 R. Gale, B. Gilbert and R. A. Osteryoung, *Inorg. Chem.*, 1978, **17**, 2728–2729.
- 96 S. Takahashi, M.-L. Saboungi, R. J. Klingler, M. J. Chen and J. W. Rathke, *Faraday Trans.*, 1993, **89**, 3591–5.
- 97 M. Schmeisser, P. Illner, R. Puchta, A. Zahl and R. van Eldik, *Chem. Eur. J.*, 2012, **18**, 10969–10982.
- 98 A. W. Taylor, S. Men, C. J. Clarke and P. Licence, *RSC Adv.*, 2013, **3**, 9436–10.
- 99 X. Xing, G. Zhao and J. Cui, *Sci. China Chem.*, 2012, **55**, 1542–1547.
- 100 S. P. Wicelinski, R. Gale, S. D. Williams and G. Mamantov, *Spectrochim Acta Part A*, 1989, **45A**, 759–762.
- 101 C. Hardacre, R. W. Murphy, K. R. Seddon, G. Srinivasan and M. Swadźba-Kwaśny, *Aust. J. Chem.*, 2010, **63**, 845–4.
- 102 J.-Z. Yang, P. Tian, L.-L. He and W.-G. Xu, *Fluid Phase Equilibria*, 2003, **204**, 295–302.
- 103 H. Q. N. Gunaratne, T. J. Lotz and K. R. Seddon, *New J. Chem.*, 2010, **34**, 1821–4.
- 104 R. A. Mantz, P. C. Trulove, R. T. Carlin, T. L. Theim and R. A. Osteryoung, *Inorg. Chem.*, 1997, **36**, 1227–1232.
- 105 J. Estager, P. Nockemann, K. R. Seddon, M. Swadźba-Kwaśny and S. Tyrrell, *Inorg. Chem.*, 2011, **50**, 5258–5271.
- 106 M. Currie, J. Estager, P. Licence, S. Men, P. Nockemann, K. R. Seddon, M. Swadźba-Kwaśny and C. Terrade, *Inorg. Chem.*, 2013, **52**, 1710–1721.
- 107 H. Olivier-Bourbigou, L. Magna and D. Morvan, *Applied Catalysis A: General*, 2010, **373**, 1–56.
- 108 N. V. Plechkova and K. R. Seddon, *Chem. Soc. Rev.*, 2008, **37**, 123–150.
- 109 Z.C. Liu, R. Zhang, C.M. Xu and R.G. Xia, *Oil Gas J.*, 2006, **104**, 52–56.
- 110 Y. Liu, R. Hu, C. Xu and H. Su, *Applied Catalysis A: General*, 2008, **346**, 189–193.
- 111 H. Ma, R. Zhang, X. Meng, Z. Liu, H. Liu, C. Xu, R. Chen, P. A. A. Klusener and J. de With, *Energy Fuels*, 2014, **28**, 5389–5395.

- 112 J. Simley, 2016, Honeywell UOP, https://www.uop.com/?press_release=honeywell-uop-introduces-ionic-liquids. (accessed 12 April 2019).
- 113 J. Simley, 2017, Honeywell UOP, https://www.uop.com/?press_release=honeywell-uop-and-chevron-win-2017-platts-breakthrough-solution-award-for-ionic-liquids-alkylation-technology. (accessed 12 April 2019).
- 114 Gasoline, 2016, Honeywell UOP, <https://www.uop.com/processing-solutions/refining/gasoline/#alkylation>. (accessed 12 April 2019).
- 115 A. Wang, G. Zhao, F. Liu, L. Ullah, S. Zhang and A. Zheng, *Ind. Eng. Chem. Res.*, 2016, **55**, 8271–8280.
- 116 Y. Chauvin, A. Hirschauer and H. Olivier, *J. Mol Cat*, 1994, **92**, 155–165.
- 117 T. L. T. Bui, W. Korth, S. Aschauer and A. Jess, *Green Chem.*, 2009, **11**, 1961–8.
- 118 S. Aschauer, L. Schilder, W. Korth, S. Fritschi and A. Jess, *Catal Lett*, 2011, **141**, 1405–1419.
- 119 T. L. T. Bui, W. Korth and A. Jess, *Catalysis Communications*, 2012, **25**, 118–124.
- 120 L. Schilder, S. Maaß and A. Jess, *Ind. Eng. Chem. Res.*, 2013, **52**, 1877–1885.
- 121 F. Pöhlmann, L. Schilder, W. Korth and A. Jess, *ChemPlusChem*, 2013, **78**, 570–577.
- 122 K. Yoo, V. Namboodiri, R. Varma and P. Smirniotis, *Journal of Catalysis*, 2004, **222**, 511–519.
- 123 S. Yous, J. Poupaert, I. Lesieur, P. Depreux and D. Lesueur, *J. Org. Chem.*, 1994, **59**, 1574–1576.
- 124 F. Guenadil and H. Aichaoui, *Phosphorus, Sulfur, and Silicon and the Related Elements*, 2002, **177**, 2633–2638.
- 125 F. Fringuelli, R. Girotti, F. Pizzo and L. Vaccaro, *Org. Lett.*, 2006, **8**, 2487–2489.
- 126 N. C. Means, C. M. Means, S. G. Bott and J. L. Atwood, *Inorg. Chem.*, 1987, **26**, 1466–1468.
- 127 O. Han and E. Oldfield, *Inorg. Chem.*, 1990, **29**, 3666–3669.
- 128 A. P. Abbott, J. C. Barron, K. S. Ryder and D. Wilson, *Chem. Eur. J.*, 2007, **13**, 6495–6501.
- 129 H. M. A. Abood, A. P. Abbott, A. D. Ballantyne and K. S. Ryder, *Chem. Commun.*, 2011, **47**, 3523–3.
- 130 K. Yoshii, X. Jiang, X.-G. Sun, T. Tsuda, N. Mehio and S. Dai, *Electrochimica Acta*, 2015, **160**, 82–88.
- 131 Y. Fang, X. Jiang, X.-G. Sun and S. Dai, *Chem. Commun.*, 2015, **51**, 13286–13289.
- 132 P. Hu, R. Zhang, X. Meng, H. Liu, C. Xu and Z. Liu, *Inorg. Chem.*, 2016, **55**, 2374–2380.
- 133 M. Hog, M. Schneider, G. Studer, M. Bäuerle, S. A. Föhrenbacher, H. Scherer and I. Krossing, *Chem. Eur. J.*, 2017, **23**, 11054–11066.

- 134 M. Hog, M. Schneider and I. Krossing, *Chem. Eur. J.*, 2017, **23**, 9821–9830.
- 135 P. Hu, W. Jiang, L. Zhong and S.-F. Zhou, *RSC Adv.*, 2018, **8**, 13248–13252.
- 136 K. Matuszek, A. Chrobok, J. M. Hogg, F. Coleman and M. Swadźba-Kwaśny, *Green Chem.*, 2015, **17**, 4255–4262.
- 137 P. Hu, Y. Wang, X. Meng, R. Zhang, H. Liu, C. Xu and Z. Liu, *Fuel*, 2017, **189**, 203–209.
- 138 M. Lijewski, J. M. Hogg, M. Swadźba-Kwaśny, P. Wasserscheid and M. Haumann, *RSC Adv.*, 2017, **7**, 27558–27563.
- 139 J. Shen, F. Wang, T. Wang, H. Li, G. Wang and X. Zhang, *Molecular Catalysis*, 2019, **462**, 56–60.
- 140 T. Tamura, K. Yoshida, T. Hachida, M. Tsuchiya, M. Nakamura, Y. Kazue, N. Tachikawa, K. Dokko and M. Watanabe, *Chem. Lett.*, 2010, **39**, 753–755.
- 141 D. J. Eyckens and L. C. Henderson, *Front. Chem.*, 2019, **7**, 1978–15.
- 142 T. Mandai, K. Yoshida, K. Ueno, K. Dokko and M. Watanabe, *Phys. Chem. Chem. Phys.*, 2014, **16**, 8761–12.
- 143 Y. Kitazawa, K. Iwata, S. Imaizumi, H. Ahn, S. Y. Kim, K. Ueno, M. J. Park and M. Watanabe, *Macromolecules*, 2014, **47**, 6009–6016.
- 144 D. J. Eyckens, M. E. Champion, B. L. Fox, P. Yoganantharajah, Y. Gibert, T. Welton and L. C. Henderson, *Eur. J. Org. Chem.*, 2016, **2016**, 913–917.
- 145 D. J. Eyckens and L. C. Henderson, *RSC Adv.*, 2017, **7**, 27900–27904.
- 146 K. Matuszek, S. Coffie, A. Chrobok and M. Swadźba-Kwaśny, *Catalysis Science & Technology*, 2017, **7**, 1045–1049.
- 147 J. M. Hogg, A. Ferrer-Ugalde, F. Coleman and M. Swadźba-Kwaśny, *ACS Sustainable Chem. Eng.*, 2019, **7**, 15044–15052.
- 148 I. López-Martin, E. Burello, P. N. Davey, K. R. Seddon and G. Rothenberg, *ChemPhysChem*, 2007, **8**, 690–695.
- 149 K. R. Dixon, *Multinuclear NMR*, Plenum Press, New York, 1987.
- 150 J. Burt, W. Levason and G. Reid, *Coordination Chemistry Reviews*, 2014, **260**, 65–115.
- 151 J. Burt, W. Levason, M. E. Light and G. Reid, *Dalton Trans.*, 2014, **43**, 14600–14611.
- 152 W. Levason, G. Reid and W. Zhang, *Dalton Transactions*, 2011, **40**, 8491–16.
- 153 F. Cheng, H. L. Codgbrook, A. L. Hector, W. Levason, G. Reid, M. Webster and W. Zhang, *Polyhedron*, 2007, **26**, 4147–4155.
- 154 F. Cheng, A. L. Hector, W. Levason, G. Reid, M. Webster and W. Zhang, *Inorg. Chem.*, 2007, **46**, 7215–7223.
- 155 A. El-Hellani, J. Monot, R. Guillot, C. Bour and V. Gandon, *Inorg. Chem.*, 2012, **52**, 506–514.

- 156 W. T. Robinson, C. J. Wilkins and Z. Zeying, *J. Chem. Soc., Dalton Trans.*, 1990, **1**, 219–227.
- 157 F. W. B. Einstein and D. G. Tuck, *Chem Commun*, 1970, 1182–1183.
- 158 S. S. Chitnis, N. Burford, R. McDonald and M. J. Ferguson, *Inorg. Chem.*, 2014, **53**, 5359–5372.
- 159 C. A. Tolman, *Chem. Rev.*, 1977, **77**, 313–348.
- 160 R. M. Denton, J. An, B. Adeniran, A. J. Blake, W. Lewis and A. M. Poulton, *J. Org. Chem.*, 2011, **76**, 6749–6767.
- 161 K. L. Bamford, A. P. M. Robertson, H. A. Jenkins, B. O. Patrick and N. Burford, *Canadian Journal of Chemistry*, 2015, **93**, 375–379.
- 162 S. S. Chitnis and N. Burford, *Dalton Trans.*, 2015, **44**, 17–29.
- 163 H. Arp, C. Marschner, J. Baumgartner, P. Zark and T. Müller, *J. Am. Chem. Soc.*, 2013, **135**, 7949–7959.
- 164 C. Gurnani, A. L. Hector, E. Jager, W. Levason, D. Pugh and G. Reid, *Dalton Trans.*, 2013, **42**, 8364–11.
- 165 E. MacDonald, L. Doyle, S. S. Chitnis, U. Werner-Zwanziger, N. Burford and A. Decken, *Chem. Commun.*, 2012, **48**, 7922–4.
- 166 S. E. Denmark and J. Fu, *J. Am. Chem. Soc.*, 2003, **125**, 2208–2216.
- 167 F. Calderazzo, S. Losi and B. Susz, *Helvetica Chimica Acta*, 1971, **54**, 1156–1175.
- 168 A. Vogler and H. Kunkely, *Coordination Chemistry Reviews*, 2002, **230**, 243–251.
- 169 F. Calderazzo, S. Losi and B. Susz, *Inorganical Chimica Acta*, 1969, **3**, 329–330.
- 170 D. Gordon and M. Wallbridge, *Inorganica Chimica Acta*, 1986, **111**, 77–81.
- 171 M. Li and Y. Shan, *Zeitschrift für Kristallographie*, 2006, **211**, 41–42.
- 172 Z. Zhu, W. Zhang and C. Y. Cheng, *Hydrometallurgy*, 2011, **105**, 304–313.
- 173 M. Cargnello, T. R. Gordon and C. B. Murray, *Chem. Rev.*, 2014, **114**, 9319–9345.
- 174 M. B. Alves, V. O. Santos Jr, V. C. D. Soares, P. A. Z. Suarez and J. C. Rubim, *J. Raman Spectrosc.*, 2008, **39**, 1388–1395.
- 175 A. D. Finke, D. L. Gray and J. S. Moore, *Acta Cryst*, 2016, **72**, 35–39.
- 176 S. Martinez and F. Alguacil, *J Chem Research*, 2000, 188–189.
- 177 J. Burgess and R. H. Prince, *Zinc: Inorganic & Coordination*, John Wiley & Sons, Ltd, Chichester, UK, 31st edn. 2006.
- 178 S. I. Troyanov, G. N. Mazo, V. B. Rybakov and K. V. Budkina, *Koordinatsionnaya Khimya*, 1990, **16**, 466–476.
- 179 L. Hubener, H.-W. Lerner and M. Bolte, *Acta Cryst. E*, 2003, **59**, 929–930.
- 180 S. Kobayashi, T. Busujima and S. Nagayama, *Chem. Eur. J.*, 2000, **6**, 3491–3494.
- 181 J. M. Hogg, F. Coleman, A. Ferrer-Ugalde, M. P. Atkins and M. Swadźba-Kwaśny, *Green Chemistry*, 2015, **17**, 1831–1841.

- 182 G. Hilt and A. Nödling, *Eur. J. Org. Chem.*, 2011, **2011**, 7071–7075.
- 183 S. A. Westcott, H. P. Blom, T. B. Marder, R. T. Baker and J. C. Calabrese, *Inorg. Chem.*, 1993, **32**, 2175–2182.
- 184 A. Del Grosso, R. G. Pritchard, C. A. Muryn and M. J. Ingleson, *Organometallics*, 2010, **29**, 241–249.
- 185 R. B. Coapes, F. E. S. Souza, M. A. Fox, A. S. Batsanov, A. E. Goeta, D. S. Yufit, M. A. Leech, J. A. K. Howard, A. J. Scott, W. Clegg and T. B. Marder, *J. Chem. Soc., Dalton Trans.*, 2001, 1201–1209.
- 186 S. Dagorne and D. A. Atwood, *Chem. Rev.*, 2008, **108**, 4037–4071.
- 187 A. R. Shaffer, N. Deligonul, D. A. Scherson and J. D. Protasiewicz, *Inorg. Chem.*, 2010, **49**, 10756–10758.
- 188 M. A. Dureen, A. Lough, T. M. Gilbert and D. W. Stephan, *Chem. Commun.*, 2008, **6**, 4303–3.
- 189 A. Del Grosso, P. J. Singleton, C. A. Muryn and M. J. Ingleson, *Angew. Chem. Int. Ed.*, 2011, **50**, 2102–2106.
- 190 E. R. Clark, A. Del Grosso and M. J. Ingleson, *Chem. Eur. J.*, 2013, **19**, 2462–2466.
- 191 T. Umemoto and Y. Gotoh, *BCSJ*, 1991, **64**, 2008–2010.
- 192 E. I. Cooper and E. O'Sullivan, *Proceedings of the 8th International Symposium on Molten Salts*, The Electrochemical Society INC, Pennington, NJ, 1992.
- 193 V. Koch, C. Nanjundiah, G. B. Appetecchi and B. Scrosati, *J. Electrochem. Soc.*, 1995, **142**, 116–118.
- 194 P. Bonhôte, A.-P. Dias, N. Papageorgiou, K. Kalyanasundaram and M. Grätzel, *Inorg. Chem.*, 1996, **35**, 1168–1178.
- 195 S. Coffie, PhD Thesis, The Queen's University of Belfast, 2018
- 196 E. J. Corey, T. Shibata and T. W. Lee, *J. Am. Chem. Soc.*, 2002, **124**, 3808–3809.
- 197 P. Wei and D. A. Atwood, *Inorg. Chem.*, 1998, **37**, 4934–4938.
- 198 N. V. Ignat'ev, P. Barthen, A. Kucheryna, H. Willner and P. Sartori, *Molecules*, 2012, **17**, 5319–5338.
- 199 R. W. Rudolph and C. W. Schultz, *J. Am. Chem. Soc.*, 1971, **93**, 6821–6822.
- 200 D. H. Ryu and E. J. Corey, *J. Am. Chem. Soc.*, 2003, **125**, 6388–6390.
- 201 K. Fumino, T. Peppel, M. Geppert-Rybczyńska, D. H. Zaitsau, J. K. Lehmann, S. P. Verevkin, M. Köckerling and R. Ludwig, *Phys. Chem. Chem. Phys.*, 2011, **13**, 14064–14075.
- 202 A. Prokofjevs, J. W. Kampf and E. Vedejs, *Angew. Chem. Int. Ed.*, 2011, **50**, 2098–2101.
- 203 S. M. Cornet, I. May, M. P. Redmond, A. J. Selvage, C. A. Sharrad and O. Rosnel, *Polyhedron*, 2009, **28**, 363–369.

- 204 S. O. Grim and W. McFarlane, *Nature*, 1965, **208**, 995–996.
- 205 S. O. Grim, W. McFarlane and E. F. Davidoff, *J. Org. Chem.*, 1967, **32**, 781–784.
- 206 V. H. Paschoal, L. F. O. Faria and M. C. C. Ribeiro, *Chem. Rev.*, 2017, **117**, 7053–7112.
- 207 P. Kebarle, *J. Mass Spectrom.*, 2000, **35**, 804–817.
- 208 K. R. J. Lovelock, C. Kolbeck, T. Cremer, N. Paape, P. S. Schulz, P. Wasserscheid, F. Maier and H. P. Steinrück, *J. Phys. Chem. B*, 2009, **113**, 2854–2864.
- 209 A. R. Jupp and D. W. Stephan, *Trends in Cognitive Sciences*, 2019, **1**, 35–48.
- 210 D. W. Stephan, G. C. Welch, R. San Juan and J. D. Masuda, *Science*, 2006, **314**, 1121–1124.
- 211 H. C. Brown, H. I. Schlesinger and S. Z. Cardon, *J. Am. Chem. Soc.*, 1942, **64**, 325–329.
- 212 S. Bontemps, G. Bouhadir, K. Miqueu and D. Bourissou, *J. Am. Chem. Soc.*, 2006, **128**, 12056–12057.
- 213 R. Roesler, W. E. Piers and M. Parvez, *Journal of Organometallic Chemistry*, 2003, **680**, 218–222.
- 214 G. C. Welch and D. W. Stephan, *J. Am. Chem. Soc.*, 2007, **129**, 1880–1881.
- 215 T. A. Rokob, A. Hamza, A. Stirling, T. Soós and I. Pápai, *Angew. Chem. Int. Ed.*, 2008, **47**, 2435–2438.
- 216 H. W. Kim and Y. M. Rhee, *Chem. Eur. J.*, 2009, **15**, 13348–13355.
- 217 J. Daru, I. Bakó, A. Stirling and I. Pápai, *ACS Catal.*, 2019, **9**, 6049–6057.
- 218 S. Grimme, H. Kruse, L. Goerigk and G. Erker, *Angew. Chem. Int. Ed.*, 2010, **49**, 1402–1405.
- 219 T. A. Rokob, I. Bakó, A. Stirling, A. Hamza and I. Pápai, *J. Am. Chem. Soc.*, 2013, **135**, 4425–4437.
- 220 G. Erker and D. W. Stephan, *Angew. Chem. Int. Ed.*, 2015, **54**, 6400–6441.
- 221 L. L. Zeonjuk, P. St Petkov, T. Heine, G.-V. Röschenthaler, J. Eicher and N. Vankova, *Physical Chemistry Chemical Physics*, 2015, **17**, 10687–10698.
- 222 S. Das, S. Mondal and S. K. Pati, *Chem. Eur. J.*, 2018, **24**, 2575–2579.
- 223 L. Rocchigiani, G. Ciancaleoni, C. Zuccaccia and A. Macchioni, *J. Am. Chem. Soc.*, 2014, **136**, 112–115.
- 224 A. Y. Houghton and T. Autrey, *J. Phys. Chem. A*, 2017, **121**, 8785–8790.
- 225 R. Leberman and A. K. Soper, *Nature*, 1995, **378**, 364–366.
- 226 J. J. Towey, A. K. Soper and L. Dougan, *J. Phys. Chem. B*, 2016, **120**, 4439–4448.
- 227 M. Falkowska, D. T. Bowron, H. G. Manyar, C. Hardacre and T. G. A. Youngs, *ChemPhysChem*, 2016, **17**, 2043–2055.

- 228 S. Lenton, N. H. Rhys, J. J. Towey, A. K. Soper and L. Dougan, *Nature Communications*, 2017, **8**, 1–5.
- 229 Y. M. Delavoux, M. Gilmore, M. P. Atkins, M. Swadźba-Kwaśny and J. D. Holbrey, *Phys. Chem. Chem. Phys.*, 2017, **19**, 2867–2876.
- 230 D. T. Bowron, C. D’Agostino, L. F. Gladden, C. Hardacre, J. D. Holbrey, M. C. Lagunas, J. McGregor, M. D. Mantle, C. L. Mullan and T. G. A. Youngs, *J. Phys. Chem. B*, 2010, **114**, 7760–7768.
- 231 R. Hayes, S. Imberti, G. G. Warr and R. Atkin, *Phys. Chem. Chem. Phys.*, 2011, **13**, 3237–3247.
- 232 R. Hayes, S. Imberti, G. G. Warr and R. Atkin, *Angew. Chem. Int. Ed.*, 2012, **51**, 7468–7471.
- 233 J. A. McCune, A. H. Turner, F. Coleman, C. M. White, S. K. Callear, T. G. A. Youngs, M. Swadźba-Kwaśny and J. D. Holbrey, *Phys. Chem. Chem. Phys.*, 2015, **17**, 6767–6777.
- 234 S. Norman, A. H. Turner, J. D. Holbrey and T. G. A. Youngs, *ChemPhysChem*, 2016, **17**, 3923–3931.
- 235 A. H. Turner, S. Imberti, M. Swadźba-Kwaśny and J. D. Holbrey, *Faraday Discuss.*, 2018, **206**, 247–263.
- 236 V. F. Sears, *Neutron News*, 1992, **3**, 26–37.
- 237 L. M. Pignolet, *Homogeneous Catalysis with Metal Phosphine Complexes*, Springer, New York, 2013.
- 238 J. P. Stambuli, S. R. Stauffer, K. H. Shaughnessy and J. F. Hartwig, *J. Am. Chem. Soc.*, 2001, **123**, 2677–2678.
- 239 F. H. Westheimer, *Chem. Rev.*, 1961, **61**, 265–273.
- 240 M. Miyashita, M. Sasaki, I. Hattori, M. Sakai and K. Tanino, *Science*, 2004, **305**, 495.
- 241 C. Liu, Z. Chen, C. Su, X. Zhao, Q. Gao, G.-H. Ning, H. Zhu, W. Tang, K. Leng, W. Fu, B. Tian, X. Peng, J. Li, Q.-H. Xu, W. Zhou and K. P. Loh, *Nature Communications*, 2018, **9**, 1–9.
- 242 K. Hiruma-Shimizu, H. Shimizu, G. S. Thompson, A. P. Kalverda and S. G. Patching, *Molecular Membrane Biology*, 2016, **32**, 139–155.
- 243 L. L. Liu, L. L. Cao, Y. Shao, G. Menard and D. W. Stephan, *Chem*, 2017, **3**, 259–267.
- 244 M. Reißmann, A. Schäfer, S. Jung and T. Müller, *Organometallics*, 2013, **32**, 6736–6744.
- 245 S. Yasui, Y. Ogawa, K. Shioji and S. Yamazaki, *Chem. Lett.*, 2013, **42**, 1478–1480.
- 246 R. S. Davidson, R. A. Sheldon and S. Trippett, *J. Chem. Soc., C*, 1966, 722–3.
- 247 T. Bartik and T. Himmler, *Journal of Organometallic Chemistry*, 1985, **293**, 343–351.

- 248 K. Shaughnessy, F. Pinsonneault and A. Gagnon, in *Encyclopedia of Reagents for Organic Synthesis*, 2015, pp. 1–10.
- 249 A. F. Littke and G. C. Fu, *J. Org. Chem.*, 1999, **64**, 10–11.
- 250 H. Hoffmann and P. Schellenbeck, *Chem. Ber.*, 1967, **100**, 692–693.
- 251 R. C. Srivastava, *J Chem Res S*, 1985, 330–331.
- 252 US Pat 2003/0229240 A1, 2003
- 253 US Pat 7,250,535 B2, 2007
- 254 C. A. Fleckenstein and H. Plenio, *Chem. Soc. Rev.*, 2010, **39**, 694–711.
- 255 S. Ley and C. Low, in *Ultrasound in Synthesis. Reactivity and Structure Concepts in Organic Chemistry*, Berlin, 1989, vol. 27, pp. 33–38.
- 256 M. Baudler K. Glinka, A. H. Cowley and M. Pakulski Main Group Ring Systems and Related Compounds, H. R. Allcock, Wiley, New York, 1989, vol. 25, ch. 1, pp 1-5
- 257 H. Goldwhite, J. Kaminski, G. Millhauser, J. Ortiz, M. Vargas, L. Vertal, M. F. Lappert and S. J. Smith, *Journal of Organometallic Chemistry*, 1986, **310**, 21–25.
- 258 A. A. Prishchenko, A. V. Gromov, M. I. Kadyko and I. F. Lutsenko, *Chemischer Informationsdienst*, 1985, **16**, 2517–2532.
- 259 A. K. Soper, *Chemical Physics*, 1996, **202**, 295–306.
- 260 A. K. Soper, *Molecular Physics*, 2001, **99**, 1503–1516.
- 261 A. K. Soper, *RAL Technical Report No*, RAL-TR-201, 2011.
- 262 T. F. Headen, C. A. Howard, N. T. Skipper, M. A. Wilkinson, D. T. Bowron and A. K. Soper, *J. Am. Chem. Soc.*, 2010, **132**, 5735–5742.
- 263 A. J. V. Marwitz, J. L. Dutton, L. G. Mercier and W. E. Piers, *J. Am. Chem. Soc.*, 2011, **133**, 10026–10029.
- 264 S. R. Ghanta, M. H. Rao and K. Muralidharan, *Dalton Trans.*, 2013, **42**, 8420–6.
- 265 J. C. Araque, S. K. Yadav, M. Shadeck, M. Maroncelli and C. J. Margulis, *J. Phys. Chem. B*, 2015, **119**, 7015–7029.
- 266 J. C. Araque, J. J. Hettige and C. J. Margulis, *J. Phys. Chem. B*, 2015, **119**, 12727–12740.
- 267 Y. Marcus, *Chem. Rev.*, 2013, **113**, 6536–6551.
- 268 A. Noda, K. Hayamizu and M. Watanabe, *J. Phys. Chem. B*, 2001, **105**, 4603–4610.
- 269 H. Tokuda, K. Hayamizu, K. Ishii, M. A. B. H. Susan and M. Watanabe, *J. Phys. Chem. B*, 2005, **109**, 6103–6110.
- 270 H. K. Kashyap, J. J. Hettige, H. V. R. Annapureddy and C. J. Margulis, *Chem. Commun.*, 2012, **48**, 5103–4.
- 271 H. K. Kashyap, C. S. Santos, R. P. Daly, J. J. Hettige, N. S. Murthy, H. Shiota, E. W. Castner Jr. and C. J. Margulis, *J. Phys. Chem. B*, 2013, **117**, 1130–1135.

- 272 J. J. Hettige, H. K. Kashyap, H. V. R. Annapureddy and C. J. Margulis, *J. Phys. Chem. Lett.*, 2012, **4**, 105–110.
- 273 H. K. Kashyap, C. S. Santos, H. V. R. Annapureddy, N. S. Murthy, C. J. Margulis and E. W. Castner Jr., *Faraday Discuss.*, 2012, **154**, 133–143.
- 274 A. Simonneau, R. Turrel, L. Vendier and M. Etienne, *Angew. Chem. Int. Ed.*, 2017, **56**, 12268–12272.
- 275 J. Chen, L. Falivene, L. Caporaso, L. Cavallo and E. Y. X. Chen, *J. Am. Chem. Soc.*, 2016, **138**, 5321–5333.

APPENDIX A

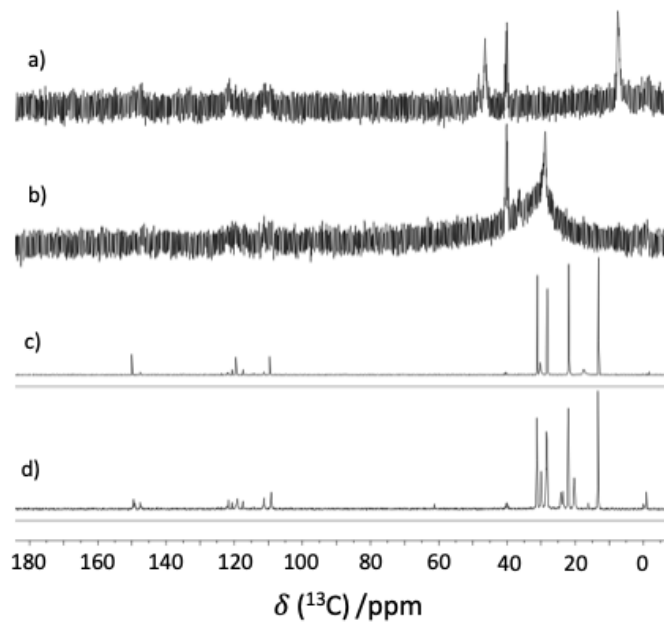


Figure 93. The ^{13}C NMR spectrum of $[\text{Bcat}(\text{OTf})\text{L}]$ adducts, where L is: a), triethylamine b) tri-*tert*-butyl phosphine c) trioctylphosphine d) trioctylphosphine oxide (samples recorded neat at 300 K with a DMSO-d_6 capillary).

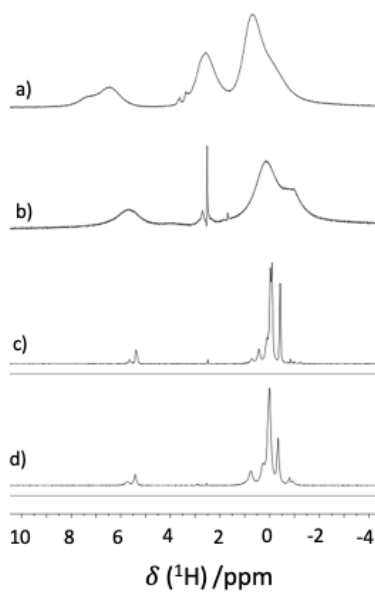


Figure 94. The ^1H NMR spectrum of $[\text{Bcat}(\text{OTf})\text{L}]$ adducts, where L is: a), triethylamine b) tri-*tert*-butyl phosphine c) trioctylphosphine d) trioctylphosphine oxide (samples recorded neat at 300 K with a DMSO-d_6 capillary).

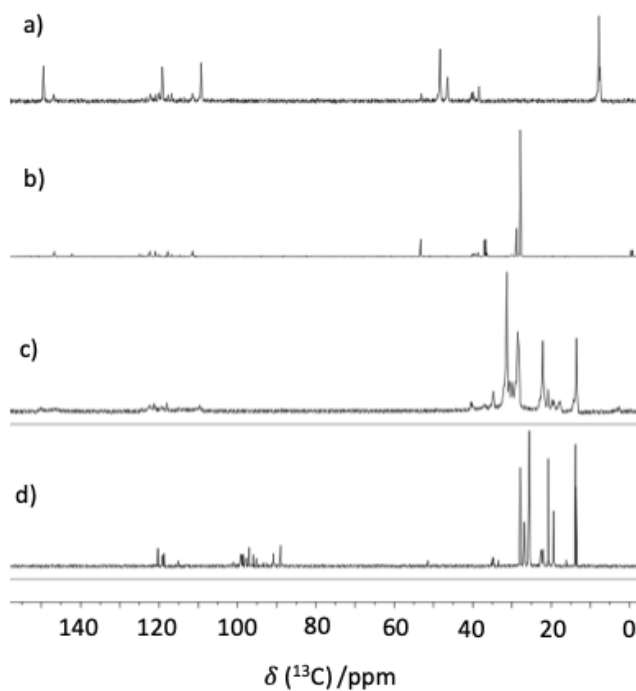


Figure 95. The ^{13}C NMR spectrum of $[\text{Bcat}(\text{NTf}_2)\text{L}]$ adducts, where L is: a), triethylamine b) tri-*tert*-butyl phosphine c) trioctylphosphine d) trioctylphosphine oxide (samples recorded neat at 300 K with a DMSO-d_6 capillary).

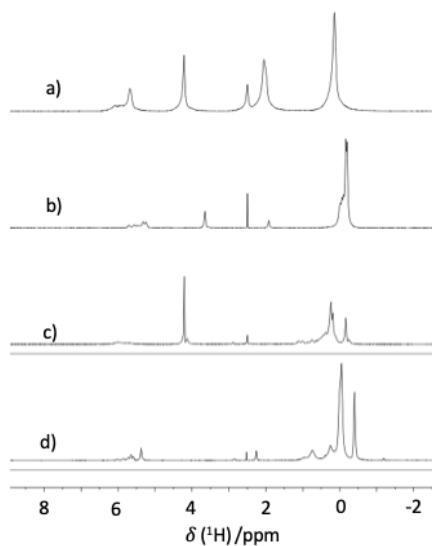


Figure 96. The ^1H NMR spectrum of $[\text{Bcat}(\text{NTf}_2)\text{L}]$ adducts, where L is: a), triethylamine b) tri-*tert*-butyl phosphine c) trioctylphosphine d) trioctylphosphine oxide (samples recorded neat at 300 K with a DMSO-d_6 capillary).

APPENDIX B

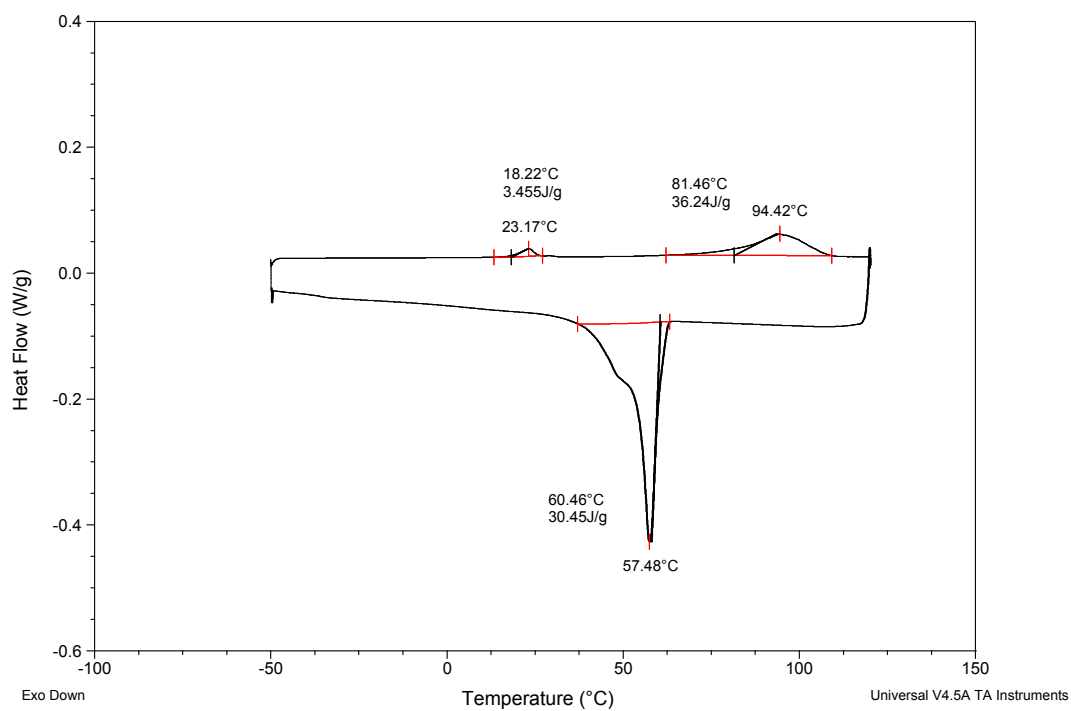


Figure 97. DSC plot for [Bcat(OTf)(N₂₂₂)]

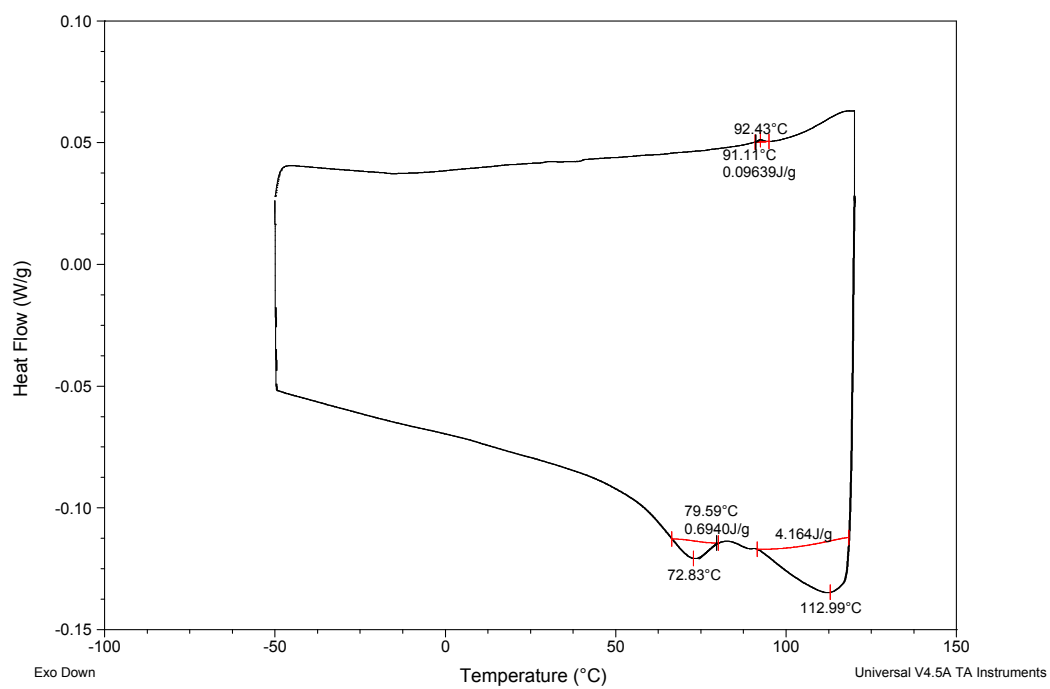


Figure 98. DSC plot for [Bcat(OTf)(P^tBu₃)]

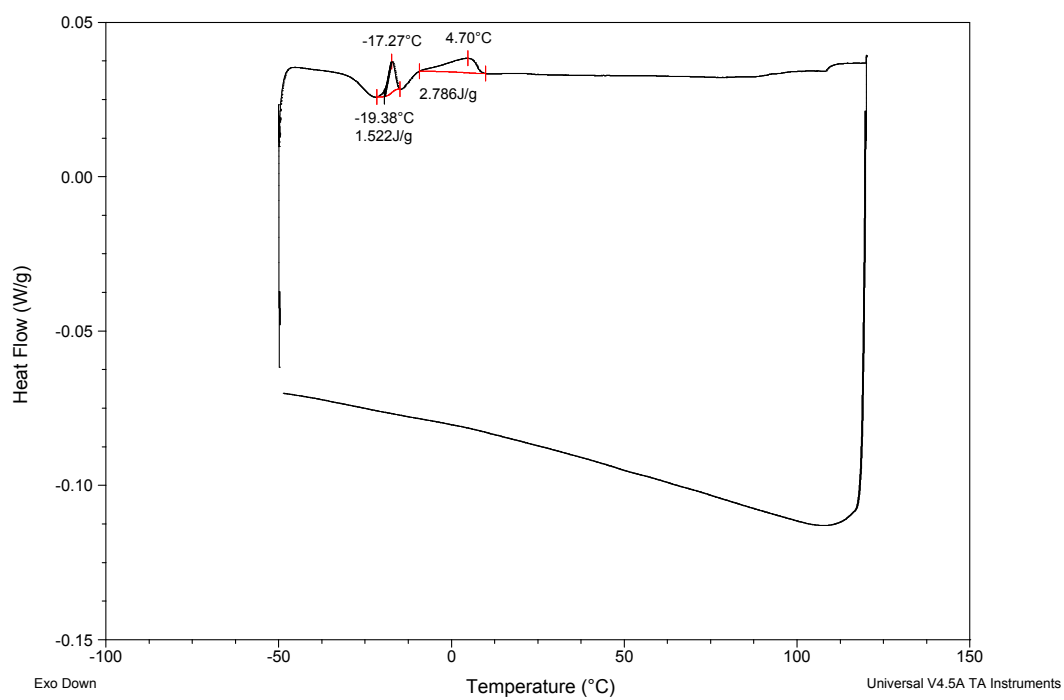


Figure 99. DSC plot for [Bcat(OTf)(P₈₈₈)]

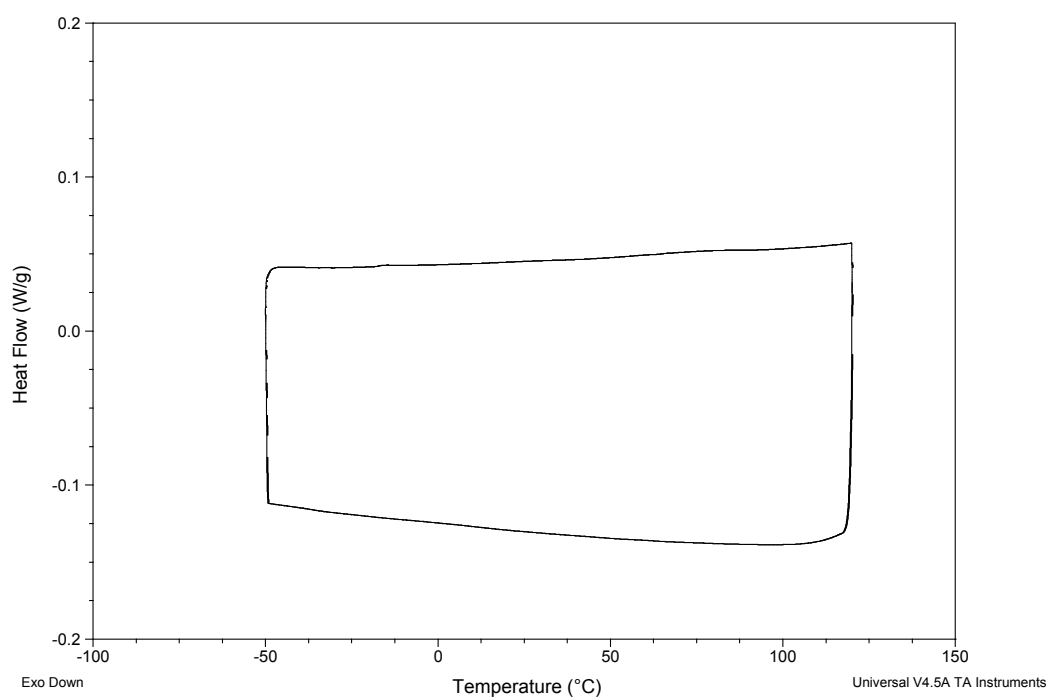


Figure 100. DSC plot for [Bcat(OTf)(P₈₈₈O)]

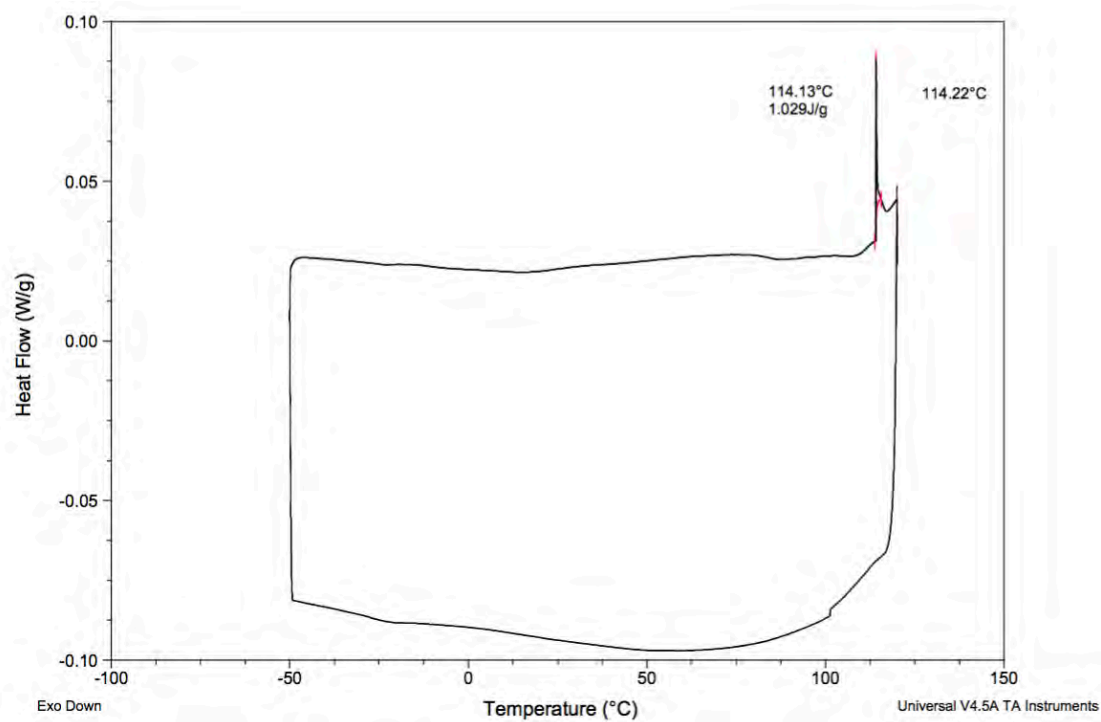


Figure 101. DSC plot for [Bcat(NTf₂)(N₂₂₂)]

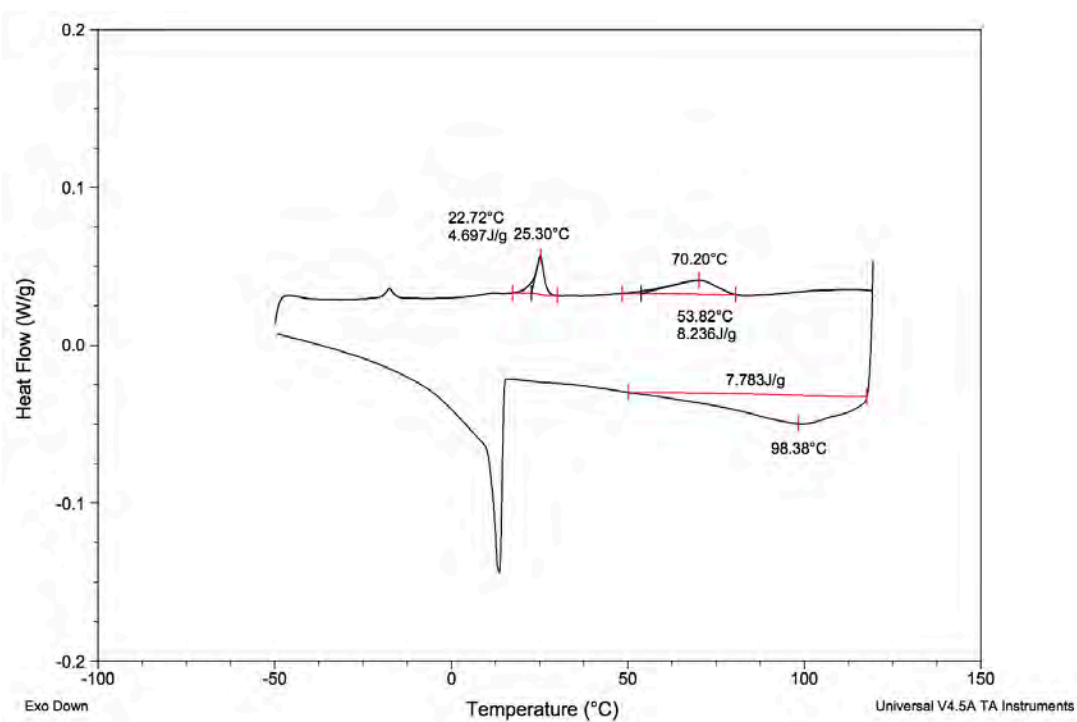


Figure 102. DSC plot for [Bcat(NTf₂)(P'Bu₃)]

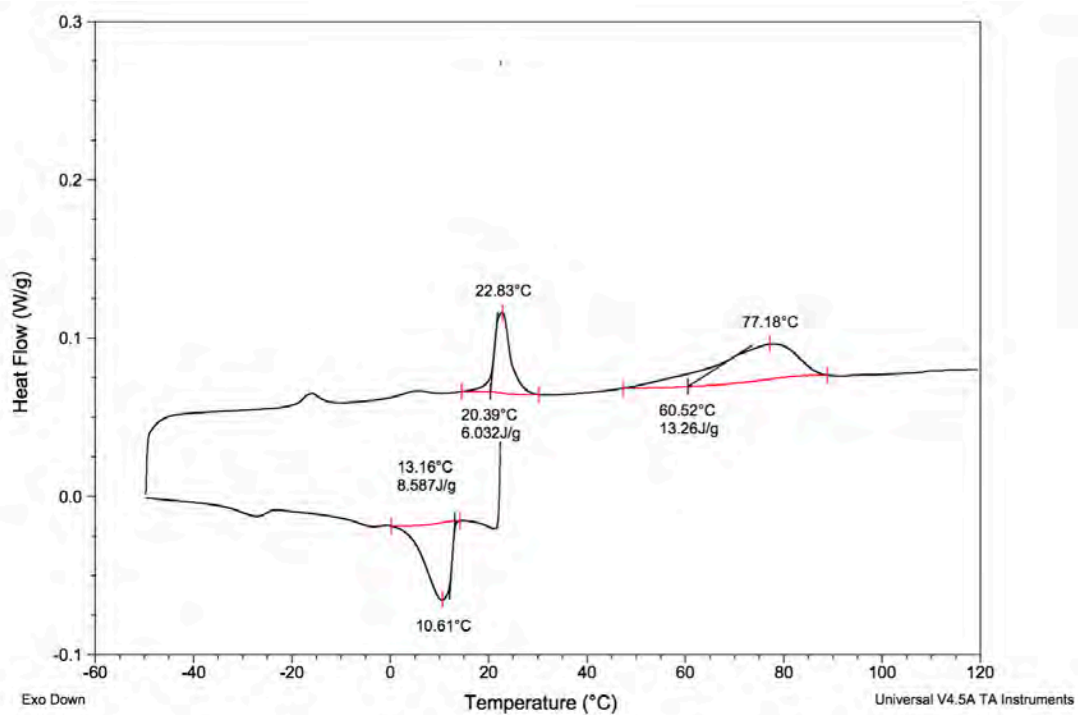


Figure 103. DSC plot for [Bcat(NTf₂)(P₈₈₈)

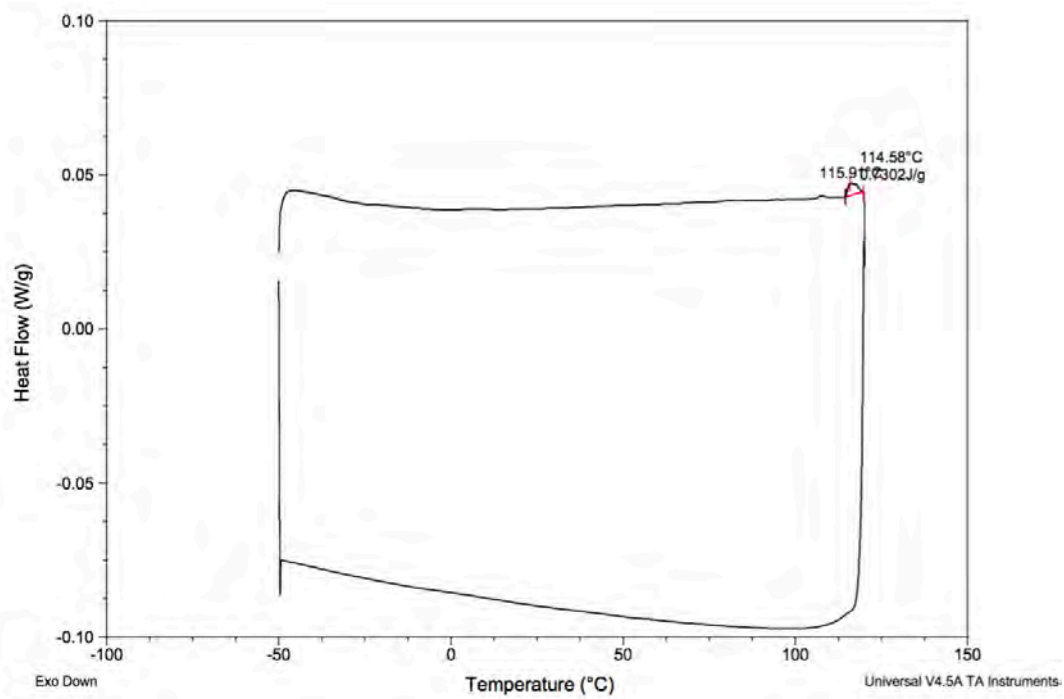


Figure 104. DSC plot for [Bcat(NTf₂)(P₈₈₈O)